42/448

3 8006 10104 7085

90E

CRANFIELD INSTITUTE OF TECHNOLOGY

SCHOOL OF MECHANICAL ENGINEERING

PhD THESIS

Academic Year 1988-89

C E ORAM

Aerodynamic surface pressure measurement in atmosphere and wind tunnel on a vertical axis wind turbine blade using pressure transducers.

Supervisors: A J Garside R L Hales J B Moss

September 1989

This thesis is submitted in partial submission for the degree of Doctor of Philosophy

ProQuest Number: 10832231

All rights reserved

INFORMATION TO ALL USERS
The quality of this reproduction is dependent upon the quality of the copy submitted.

In the unlikely event that the author did not send a complete manuscript
and there are missing pages, these will be noted. Also, if material had to be removed,
a note will indicate the deletion.

ProQuest 10832231

Published by ProQuest LLC (2018). Copyright of the Dissertation is held by Cranfield University.

All rights reserved.
This work is protected against unauthorized copying under Title 17, United States Code
Microform Edition © ProQuest LLC.

ProQuest LLC.
789 East Eisenhower Parkway
P.O. Box 1346
Ann Arbor, MI 48106 – 1346

ABSTRACT

Blade aerodynamic loads during operation of a wind turbine are poorly understood. Better measurements of these forces are needed for the design of more cost effective turbines. Existing estimates have been inferred from strain gauges in the blade structure, but such measurements are confused by the complexity of the blade's structural response. This present work has pressure tapped the blade surface and recorded at high speed, giving a highly detailed picture of dynamic events and blade loads.

A modular blade was constructed for the 6m diameter Rutherford Appleton Vertical Axis Wind Turbine and instrumented with 32 semiconductor pressure transducers. A flow probe using a further three transducers projected ahead of the blade during some of the tests. The instrumented module was also operated in the oscillating mounting of the University of Glasgow's 1.6m by 2.4m wind tunnel.

1760 revolutions of data were collected in atmosphere with blade speed ratios down to about 2.0 and with a variety of blade leanout angles. Some 118 runs of a variety of waveform types and Reynolds numbers from 0.3 to 1.1 million, were collected from the blade in tunnel.

Analysis of transducer calibrations concluded that the novel temperature correction technique used allowed pressure readings to 40Pa or better with 95% confidence. Confidence in measured pressures has allowed use of leading edge stagnation point pressure and position as a measure of wind in the rotor flowfield and as a surrogate measure of blade angle of attack.

Blade surface pressures and integrated forces show the progression of dynamic stall with increase in wind speed, the dominance of the upstream blade pass in usefulness at low and moderate windspeeds and the rough equality at high windspeeds. Comparisons of wind tunnel and on-rotor data show much lower force and moment coefficients in atmosphere. Rotor 'goodness' ratios of average blade tangential force to maximum blade and rotor force coefficients peak at a blade speed ratio of about 2.8. Goodness ratios show a mixed pattern with blade leanout. Analysis of pressure coefficient traces through stall indicate a mixed stall type starting at mid chord, moving to leading edge and thence to trailing edge.

ACKNOWLEDGEMENTS

I would like to thank those people who have helped so much to guide me through the difficulties of this project.

Firstly my thanks go to my supervisor, Barrie Moss, who as my invaluable link with the academic establishment, attempted to keep me on a timetable and refused to allow panic when things went awry.

Next must come the two research staff John Garside and Richard Hales whose enthusiasm and willingness to work all hours of the day and night were an inspiration. Additionally Martin Bellia helped greatly by writing some of the early software and by much other assistance and general encouragement.

I would like pay special thanks too to Brian Moffitt, electronics expert and mentor for the four years. Without his advice there is no doubt that the project would have foundered.

Other staff at Cranfield were most helpful too principally John Dawe and Frank Walker who respectively built lots of electronics and put up with my unusual purchasing methods.

I owe considerable debts to the staff at the Rutherford Appleton Laboratory, Mike Percival, David Infield, Peter Goodyer, John White, Jerry Brewer, Jeremy Bass, John Gardner, Hans Bleijs and Jim Halliday many of whom were willing to assist well after normal working hours to accommodate the random nature of the wind.

Staff at the wind tunnel in Glasgow were also willingly prepared to go beyond normal working hours to get the work done. Of these Roddy Galbraith, Mark Gracy, David Herring and Tony Smedley are to be warmly thanked.

I would like to have it recorded that my family too put in considerable sacrifice, particularly my wife Wendy, enduring several years as a 'windmill widow'.

Finally I must thank the SERC for the funding to carry out the work under contracts GR/C50038 and GR/D99249.

LIST OF CONTENTS

		Page
CHAPTER 1	INTRODUCTION	
1.1.0	Current status of windpower in the UK.	1.1
1.2.0	Machine configuration, advantages of the VAWT.	1.3
1.2.1	Difficulties with the use of vertical axis.	1.4
1.3.0	Aerodynamics.	1.6
1.3.1	Stall regulation.	1.8
1.3.2	Blade sections.	1.9
1.4.0	Pressure transducer measurements.	1.9
1.5.0	Aerodynamic scope of the present work.	1.10
CHAPTER 2	REVIEW OF EXISTING LITERATURE	
2.0.0	Introduction.	2.1
2.1.0	Pressure transducer temperature compensation.	2.3
2.1.1	Pressure transducer temp compensation at MIT.	2.3
2.1.2	Pressure transducer temperature compensation at RAE Bedford.	2.4
2.2.0	Dynamic stall.	2.5
2.2.1	Dynamic stall investigation methods.	2.7
2.3.0	VAWT rotor flow field work.	2.8
2.3.2	Previous work using the RAL 6 metre machine.	2.9
2.3.3	NASA Sandia work.	2.10
2.3.4	Canadian and French work.	2.11
2.3.5	VAWT Ltd and ETSU/Department of Energy.	2.12

2.4.0	Summary.	2.13
CHAPTER 3	PRESSURE TRANSDUCERS	
3.0.0	Introduction.	3.1
3.1.0	Transducer construction.	3.2
3.2.0	Early transducer scheme.	3.4
3.3.4	Cranfield Kulite scheme.	3.5
3.3.5	Early experience with the Kulite transducer.	3.6
3.3.6	Transducer temperature by drawn current.	3.7
3.3.7	Compensation module temperature coefficient.	3.7
3.3.8	Transducer cooldown tests.	3.7
3.3.9	Flatpack mechanical strain tests.	3.8
3.3.10	Transducer temperature effect and consistency tests.	3.9
3.3.11	Results and conclusions of consistency tests.	3.10
3.3.12	Subjective comments on transducer performance.	3.12
3.3.13	Absolute versus differential transducers.	3.13
3.3.14	Method of transducer use.	3.15
3.3.15	Zero offset resistor.	3.15
3.3.16	Sensym transducer installation.	3.16
3.3.17	Ducts.	3.17
3.4.0	Software temperature correction.	3.18
CHAPTER 4	OTHER EXPERIMENTAL EQUIPMENT	
4.1.0	Blade design and manufacture: general module scheme.	4.1
4.1.1	Basic structural design.	4.2

4.1.2	Blade geometrical tolerances.	4.4
4.1.3	Sensym blade.	4.4
4.1.4	Sensym blade: structural design.	4.4
4.1.5	Aerodynamic surface pressure tappings.	4.5
4.2.0	First probe using Kulite transducers.	4.7
4.2.1	Second probe using Sensym transducers.	4.8
4.3.0	Anemometers and towers.	4.9
4.4.0	Rotor torque measurement.	4.10
4.5.0	Rotor drive system.	4.11
4.6.0	Signal conditioning and data logging scheme and equipment.	4.11
4.6.1	Analogue scheme.	4.12
4.6.2	Final signal logging scheme: general outline.	4.13
4.6.3	Rotating instrument rack.	4.16
4.6.4	RAL system earthing.	4.17
4.6.5	Signal conditioning equipment.	4.17
4.6.6	Optical disc signal conditioning.	4.19
4.6.7	On-rotor low voltage power supplies.	4.19
4.6.8	Control cabin signal conditioning box.	4.20
4.6.9	Data logging process.	4.20
CHAPTER 5	TUNNEL EQUIPMENT AND METHOD	
5.0.0	Introduction.	5.1
5.1.0	Hardware.	5.2
5.2.0	Transducer calibration and temperature compensation.	5.4
CHAPTER 6	DATA TRANSFER, PROCESSING AND REDUCTION	

6.0.0	Introduction.	6.1
6.1.0	BBC micro computer software.	6.1
6.1.1	Data logging software, W/24/10.	6.1
6.1.2	Parallel data downloading program, P/24/10.	6.2
6.1.3	Transducer calibration software, 'C/24'.	6.2
6.1.4	Hardware debugger, RDADR++.	6.3
6.1.5	Other BBC code.	6.3
6.2.0	Archimedes data reduction code.	6.4
6.2.1	Supply voltage correction.	6.4
6.2.2	Sets.	6.4
6.2.3	Coefficient fitting.	6.5
6.2.4	Constraint to RDADR data.	6.5
6.2.5	Azimuth handling and the 'display frame'.	6.6
6.2.6	Aerodynamic and ground based start of revolution.	6.7
6.2.7	Stagnation point fitting.	6.7
6.2.8	Stagnation point position based turbulence.	6.7
6.2.9	Stagnation pressure based turbulence.	6.8
6.2.10	Stagnation pressure based wind speed.	6.8
6.2.11	Summary building.	6.8
6.2.12	Average revolution building.	6.9
6.2.13	Glasgow data frames per cycle.	6.9

CHAPTER 7 WIND TUNNEL TESTING

7.0.0	Introduction.	7.1
7.1.0	Test schedule and parameter selection.	7.3
7.2.0	Standard graphical and tabular presentation of results.	7.3

7.3.0	Tunnel pitot /blade stagnation pressure discrepancies.	7.8
7.4.0	Asymmetry of tunnel flow.	7.10
7.5.0	Static test results.	7.11
7.6.0	Ramp wave test results.	7.13
7.7.0	Sine wave test results.	7.15
7.7.1	Sine waves: effect of reduced frequency.	7.15
7.7.2	Sine waves: effect of Reynolds number.	7.17
7.7.3	Sine waves: effect of change in maximum amplitude.	7.18
7.7.4	Sine waves below static stall incidence.	7.18
7.7.5	Sine waveform runs above static stall angle.	7.19
7.8.0	Vawt wave test results.	7.20
7.8.1	Vawt waveform runs: differences from sine input.	7.21
7.9.0	Pressure signal measurement of incidence.	7.22
7.9.1	Comparison of blade incidence measures.	7.23
7.10.0	Dynamic stall type.	7.25
7.11.0	Stall delay analysis.	7.27
7.12.0	Summary of wind tunnel results.	7.28
CHAPTER 8	ATMOSPHERIC TESTING	
8.0.0	Introduction.	8.1
8.1.0	Wind data and runs.	8.1
8.1.1	Anemometer siting and rotor interference.	8.2
8.1.2	In-rotor wind turbulence.	8.2
8.2.0	Dynamic pressure versus anemometer based windspeed.	8.3
8.3.0	Averaged run data.	8.5

8.3.1	Averaged runs without stall.	8.6
8.3.2	Averaged runs with stall.	8.8
8.3.3	Fourier transforms of blade forces.	8.10
8.3.4	Summary of trends over the decreasing blade speed.	8.11
8.4.1	Comparison of RAL with Sandia Labs data.	8.12
8.5.0	Comparison of atmospheric with wind tunnel data.	8.13
8.5.1	Maximum normal force coefficients.	8.13
8.5.3	Blade tangential force.	8.14
8.5.4	Blade force and moment coefficients in tunnel and atmosphere.	8.14
8.6.0	Rotor coefficient data.	8.16
8.6.1	Rotor torque coefficient.	8.16
8.6.2	Rotor power coefficient.	8.17
8.6.3	Rotor thrust coefficient.	8.17
8.6.3	Maximum/ average tangential forces and rotor torque.	8.18
8.6.4	Average tangential/ maximum normal forces.	8.18
8.6.5	Average tangential forces/ rotor thrust.	8.19
8.7.0	Summary.	8.19
CHAPTER 9	CONCLUSIONS	
9.0.0	Introduction.	9.1
9.1.0	Aerodynamic conclusions.	9.1
9.2.0	Software temperature compensation of transducer output.	9.4
9.3.0	General conclusions regarding site suitability.	9.5
9.4.0	Further work.	9.5

9.5.0	Conclusion.	9.6
CHAPTER 10	REFERENCES	10.1
CHAPTER 11	APPENDICES	
APPENDIX 1	Compensation Module Resistance TempCo.	
11.1.0	Introduction	11.1
11.1.1	Method of tests	11.1
11.1.2	Calc. of sensitivity of output to temp.	11.1
APPENDIX 2	Centrifugal Effect on Blade Reference Pressure.	
11.2.0	Introduction and analysis.	11.3
APPENDIX 3	Duct Experiments.	
11.3.0	Introduction.	11.5
11.3.1	Experiment.	11.5
APPENDIX 4	Proof for incidence /azimuth formulae.	11.8
CHAPTER 12	TABLES	
CHAPTER 13	FIGURES	

SCHEDULE OF TABLES

1 Transducer consistency: Kulite 1066-4-71

2 Transducer calibration drift.

3 Transducer calibration number 20411B11

4 Transducer calibration number 21832B11

5 Blade to amplifier connection schedule

6 Wind tunnel connection schedule

7 Blade pressure tappings positions

8 Static wind tunnel run schedule

9 Ramp wind tunnel run schedule

10 Sine wave wind tunnel run schedule

11 Vawt function wind tunnel run schedule

12 Maximum aerodynamic coeffs in static tunnel runs

13 Maximum aerodynamic coeffs in ramp tunnel runs

14 Reduced frequency and sine wave runs: max coeffs

15 Reynolds number and sine wave runs: max coeffs

16 Maximum amplitude and sine wave runs; max coeffs

17 Vawt function runs: increasing max ampl: coeffs

18 Schedule of tunnel statistics including time delays

19 Wind and rotor statistics during atmospheric runs.

20 Atmospheric run blade aerodynamic coefficients

SCHEDULE OF FIGURES

1 Overview of Rutherford Appleton Wind Research Site

2 Wind turbine in operation at RAL

3 Wind tunnel and rotor blade configurations

4 Design drawing of first blade

5 Drawing of first flow probe

6 Transducers tested in consistency programme

7 Kulite mounting techniques

8 Kulite temperature compensation module temp effect

9 Cool down of Kulite transducer on-rotor

10 Strain effect on transducer output

11 Transducer electrical connection schematic.

12 Consistency of Kulite output.

13 Consistency of Sensym SPX50D output.

14 Transducer pneumatic connection and mounting.

15 Fourier transforms of single transducer waveforms

16 Rotating instrument rack and data downloading

17 Spanwise and chordwise pressure tapping positions.

18 Drilling of pressure tapping hole position setting

19 Photograph of second probe with Sensym transducers.

20 Anemometer position with respect to rotor and wind

21 Lowne anemometer heads and setting with template.

22 Digital data logging scheme

23 Amplifier and sample and hold circuits

24 Mounting of blade in wind tunnel

25 Turbulence measures and comparisons

26 Principal aerodynamic coefficients over Re range

27 Static series run 125

28 Static series run 126

29 Static series run 127

30 Static series run 128

31 Two vector model of vawt flowfield.

32 Aerodynamic coeffs for vawt runs 171, 172 and 173

33 Aerodynamic coeffs for vawt runs 174, 175 and 176

34 Ramp run 173 pressure coefficient plot

35 Aerodyn coeffs over range of reduced frequencies

36 Sine run 142 pressure coefficient plot

37 Sine run 92 pressure coefficient plot

38 Aerodyn coeffs over range of Renolds numbers

39 Sine waveform run 62

40 Sine waveform run 149

41 Aerodyn coeffs over range of maximum α sine waves

42 Sine waveform: run 76

43 Sine waveform: run 77

44 Sine waveform: run 79

45 Sine waveform: run 147

46 Aerodyn coeffs over range of maximum α vawt waves

47 Vawt waveform: run 110

48 Vawt waveform: run 166

49 Comparison of coefficients from runs 162 and 137

50 Comparison of 3 measures of incidence with α

51 Stagnation point position superimposed for 4 runs

52 Stagnation point offset and incidence maxima

53 Aerodynamic coeffs against stagnation point offset
54 Pressure coefficients during stall 'Carta plot'.
55 Three stall indicators against reduced time.
56 Incoming wind for run 200
57 Incoming wind for run 210
58 Fourier transform of distant and close anem signal.
59 Wind: anemometer & stagn pressure 0° to 45° leanout
60 Torque power and thrust coeffs /stagn press wind
61 Torque power and thrust coeffs /anemometer wind
62 Averaged data for blade speed ratio 7.83
63 Averaged data for blade speed ratio 5.74
64 Averaged data for blade speed ratio 4.65
65 Averaged data for blade speed ratio 3.85
66 Averaged data for blade speed ratio 3.36
67 Averaged data for blade speed ratio 2.94
68 Averaged data for blade speed ratio 2.66
69 Averaged data for blade speed ratio 2.34
70 Averaged data for blade speed ratio 2.19
71 Averaged data for strong downwind stall: bsr 2.50
72 Pitching moment against bsr: 0° blade leanout
73 Fourier transform of normal force
74 Fourier transform of tangential force
75 Fourier transform of pitching moment
76 Fourier transform of forces and moments single rev
77 Comparison of Sandia and RAL Cn data
78 Comparison of Cn and Ct maxima with 2 incidences
79 Comparison RAL and tunnel coeff traces ß=3.36

80 Comparison RAL and tunnel coeff traces ß=2.19

81 Measures of rotor force 'efficiencies'

82 Duct frequency response

83 Passive temp compensation module circuit

84 Wind tunnel layout

SCHEDULE OF APPENDICES

1 Temperature coefficient of compensation module

2 Centrifugal effect on reference pressure duct

3 Effects of ducts in pressure transmission

4 Proof of incidence with azimuth relationship etc

CHAPTER 1

INTRODUCTION

1.1.0 Current Status of Windpower in the UK

Since the oil crisis of the 70's many of the major industrialised countries have looked afresh at the potential of windpower as a source of electrical energy and have begun to invest in it as a means of supplementing their electricity supplies. The status of windpower and its perceived potential has grown very rapidly since then. In 1985 the UK Government's Energy Technology Support Unit ETSU described windpower as 'the most promising of the renewable energy sources'. In 1987 the British Wind Energy Association in its position paper 'Wind Power for the UK' reference(16), claimed that windpower, when installed on the best sites, was the cheapest form of energy supply available in the UK today, at £800 per kW installed or 2.1p/kWh. This was using figures agreed by the CEGB and based on prices and costs at which major UK manufacturers were prepared to enter into contracts. Wind power is proposed as a means of generation which is highly modular and quick to install, requiring no large capital outlay and interest charges before useful production begins.

Nevertheless it is early days and only about thirty medium and large machines are turning in the UK, the largest a 3MW machine having been commissioned recently on Orkney. However in the spring of 1988 the CEGB, in concert with the UK Department of Energy, announced a programme of three wind parks to be built on sites in the South West, in Wales and in the Pennines. Additionally and more immediately, there are several individual machines on order, including the first to be erected offshore.

The UK manufacturing scene has recently been disrupted by the news that James Howden & Co Ltd is to quit windpower and is to honour only its existing contracts. Since this leaves only WEG and VAWT as UK manufacturers with substantial backing, the windparks mentioned above are likely to contain vertical axis machines where previously they might well not. There is thus a reiterated pressing need for research into the aerodynamics of the VAWT

rotor.

In the US several thousand machines have been erected, particularly because of a favourable tax system. This system has now lapsed, slowing but not stopping wind turbine installation there where over 2000MW is currently installed, equivalent to a large conventional power station. Jaras reference(42) quoted by Milborrow, shows that the world market peaked at about 550MW in 1985 but has now settled to about 350MW with North America continuing to account for about half world sales.

The public perception of windpower as one of an unreliable nature has been successfully challenged. Various studies have shown that wind energy conversion systems WECS, have availability better than conventional supplies 'Beaufort' reference(8) and can make a significant contribution to 'firm' power without special problems to the existing electricity supply network. This fact too is recognised by the CEGB. No consensus as to the level of penetration of WECS into the UK scene has however been reached, with estimates of the ultimate level varying widely between 2% from the Department of Energy early in the modern interest in wind power, to 50% from some correspondents in the press. Grubb reference(37) suggests that at the 15% penetration level, wind power could supply 88% of its average power as firm power being, in this respect, entirely comparable with conventional sources. Recognised, is the large size of the resource, with the whole of the UK supply being theoretically possible by wind power, if realistic estimates are made of the shallow water sites around our coast, Grubb *ibid*.

Predominant in research and development of wind turbines is the requirement to reduce the cost per unit of delivered electricity. Early work in the field, tended to concentrate on the aerodynamic efficiency of the turbine, but more recently it has been recognised that whilst this aspect is undoubtedly important, the cost of manufacture of a machine and its maintenance costs together with its reliability and availability are much more important, Migliore reference(55).

1.2.0 Machine Configuration, Advantages of the VAWT.

Another aspect very much open to debate is the configuration of the machine. Most wind turbines operating today are of the HAWT (horizontal axis wind turbine) configuration, where the rotational axis is nominally parallel with the wind direction. There is however, a strong school of thought that the alternative cross wind configuration, usually manifest in the vertical axis wind turbine, will ultimately prove more successful, particularly with increase in turbine size.

At small scale the dominant forces on the horizontal axis wind turbine are aerodynamic in nature, but with increase in size, and much larger machines will be needed for economic operation on offshore sites, the cyclic loading and stress caused by the self weight of the blades themselves, becomes very significant and, it is thought, will constitute a barrier to the operation of machines above about 150m diameter.

Small VAWT rotor design is dominated by the large centrifugal loads experienced by the blades at the high rotational speeds necessary. At large size however, perhaps 100m and above, the necessary blade air speed is obtained at modest rotational speed and centrifugal loads become much less significant. VAWT gravitational loads are constant and so the only loads of concern are those of aerodynamic origin. Again at small size these are important design loads, but at large size they become of lesser significance compared to the self weight of the structure and centrifugal loads.

Nevertheless airloads remain important because of their strongly periodic nature and the impact that this has on the fatigue life of the structure and drive train. All loads of a periodic nature are important in wind turbine design because, for economic reasons, design lives will be very long, of order 25 years, in which time hundreds of millions of stress cycles could occur.

Further advantages of VAWTS are seen as the potential to keep the heavy and expensive machinery, brake gearbox and electrical machine, at or near ground level and on the V VAWT proposed by Derek Taylor of the Open University, the potential for easy access to the blades because of the ease with which they may be lowered to near ground level. Benefits of this low level machinery siting are sometimes of an unexpected nature. For example

the HAWT nacelle, for aerodynamic and cost reasons, tends to be a small cramped and unpleasant place for a maintenance technician, a place to avoid. By contrast ground based or low level machinery enclosures are less constrained, with likely improvements in maintenance quality and safety.

Additionally the VAWT of whatever type, does not need aiming into the wind and does not lose power because of alignment or yaw errors. Yaw control remains an area of concern in the research community and much effort is expended on it. Yaw manoeuvres and consequent gyroscopic moments give rise to substantial complication in the design of the rotor hub and teeter freedom. Yaw drive error or failure is usually about third in the league table of causes of machine outage after control system failure and loss of grid. There is a certain elegance in an essentially one moving part machine such as the latest VAWT Ltd 500 kW design proposal Morgan reference(56), which must be recognised.

Vertical axis machines are conventionally thought of as being inferior to horizontal axis in aerodynamic efficiency but Maydew and Klimas reference(51) have rebutted this allegation by comparing the Sandia 17 metre machine performance with that of the MOD-1 and MOD-0A machines. The evidence suggests that there is very little to choose between the two configurations and indeed that the VAWT may even have the edge in some situations.

1.2.1 Difficulties with the use of Vertical Axis.

The above factors are attractive, but there are also problems and disbenefits associated with wind power and with vertical axis machines in particular. At the solidities (ratio of blade area to rotor projected area) proposed and used at medium to large scale, the cross wind turbine does not reliably self start and so must be driven up to speed using the electrical machine as a motor. Recently however VAWT Ltd have claimed that their Scilly Isles 100kW machine will self start, Morgan *et al* reference(56). Nevertheless there is here the potential undesirability of starting many machines at once because of the large inrush currents that would then flow. Large electrical machines can draw five or more times their rated current in such start situations. Simultaneous starting appears unlikely however, because of the

distributed nature of proposed turbine arrays.

More serious difficulties are connected with the cyclic nature of the aerodynamic loads and the control problems associated with constant or variable speed operation.

At low levels of penetration into a power system, perhaps up to 15% to 20%, WECS (wind energy conversion systems) can be left to generate power up to their maximum rating using the other grid connected prime movers for regulation. There is of course a cost associated with this in that conventional thermal plant will be operating at below conventional or ideal rating in order that there be capacity at short notice to meet shortfall in the wind component. Fuel costs are likely to be a few percent higher pro rata over the whole system from this cause. At higher penetrations however, some self regulation of wind plant output may be necessary.

Many current machines are being designed with the ability to regulate their power on a seconds time scale by means of aerodynamic control, usually with controllable blade tips, sometimes together with some compliance or speed adjustment in the drive train. Cheaper machines can probably be made however, if the stall control technique is used, whereby blade stall in high winds limits torque and hence power. Techniques of power control in such systems are then probably limited to patterns of machine shut down with inevitably much slower speed of response.

Connected with the problem of control, but more particularly with the maximisation of energy capture per unit of swept area is rotor speed and its control. Two strategies are commonly proposed, either rotor speed is varied to maintain optimum aerodynamic efficiency maximising energy capture, or a fixed speed is used with some sort of control device to limit power production. Some intermediate options are currently under trial.

In the WEG 3MW Orkney machine, small changes in rotor speed are permitted to absorb short term changes in wind power. A low power auxiliary shaft connects a differential element within the main gearbox to a small variable speed electrical machine; the main electrical generator runing at fixed speed. Speed changes in the small machine, electronically controlled, allow small changes in rotor speed. Such small changes in rotational speed

in a rotating system of such large mass (about 60 tonnes) can absorb sufficient energy to ease the very variable wind power input smoothing problem.

Another approach is to use a two speed PAM electrical machine allowing an additional low speed for quieter operation in low wind speeds and this system is also currently promoted by WEG in its MS3 machines.

Variable speed approaches, while initially attractive because of their higher maximum power rating and higher energy capture over an operating period, in fact have disadvantages. The mechanical power train between rotor and electrical machine must be capable of variable speed, the electrical engineering used to transform rotor power to grid quality power is complicated (current research machines using ac-dc-ac links involving expensive power electronics), the grid will be fed an even more variable power, and variable speed increases turbine weight generally since a stiffer structure is required to avoid problems with resonance. The present feeling is that infinitely variable speed over a wide range is a useful second option but that it is unlikely to prove sufficiently attractive to warrant adoption in the near to medium future.

Thus most large machines operating today are fixed speed, having either a simple induction electrical machine when operating into a stiff grid, or a synchronous machine in conjunction with a weak one. Strong grids can tolerate relatively robust rotor torque control methods such as stall limiting, whilst control surface methods are needed for much finer regulation in areas with weak grids.

1.3.0 Aerodynamics.

Two areas in particular appear to be important and remain badly understood in the aerodynamics of wind turbines; air loads and stall regulation; and these are crucial to the whole question of the economics of wind power as outlined in the sections above. Air loads are cyclic in nature, particularly in the vertical axis machine and give rise to most of the fatigue damage sustained by such a machine. Stall regulation holds the promise of successful control of rotor torque to a design maximum without the use of a moveable control surface and this clearly has benefits in terms of first cost, maintenance and reliability.

At low wind speed, the rotor blade of a constant speed machine sees essentially a zero incidence as it moves upwind at the start of the first quadrant. Imagining a clock face with the rotor rotating anticlockwise, the first quadrant would be from 3 o'clock to 12 o'clock; the second quadrant from 12 o'clock to 9 and so on. Incidence increases to a maximum at about the end of the first quadrant and with it rise the blade normal and tangential forces, giving the first force peak on the structure and the first drive train and electrical torque peak.

The second quadrant sees a decay to nominally zero loadings before the third quadrant produces a qualitative repeat of the first. Tangential force and driving torque again rise as does blade normal force, but this time although the tower load is in the same sense as before, blade load with respect to the rotor is reversed. The forth quadrant manifests a repeat of the second, a reduction to zero forces. There are thus two tower load and two rotor torque peaks, plus one complete stress reversal cycle per revolution of the rotor. However on the downwind side of the rotor flow field wind speeds tend to be lower as suggested by Baker reference(7) and various double disc multiple streamtube theories and documented in this present work in Chapter 8, reducing the importance of the secondary peaks.

In winds higher than a critical level, a more complicated blade loading pattern occurs and the work of Brochier *et al* reference(18), illustrates the flow pattern. As the blade traverses the first quadrant, a point is reached when the static stall angle for the blade section at the local Reynolds number, is exceeded. This phenomenon occurs typically at a blade speed to windspeed ratio (termed the blade speed ratio bsr or ß in the present work) of about three or four. A more familiar term, usually used in the context of the horizontal axis wind turbine, is the nearly analogous 'tipspeed ratio'. Dynamic stall occurs after a further period of time and may take place in the first or second quadrant. In the period before stall takes place, blade normal forces reach higher values than would be expected from measurements made under constant incidence conditions. Associated with the stall event there is an abrupt change in pitching moment as the aerodynamic pressure centre moves backwards along the chord. As will be seen, these force overheads

are less pronounced than had been feared in the early days of modern wind turbine design.

Flow around the blade in the rest of the rotor flowfield is very confused and vortices generated by the upstream pass will be convected downstream, so that stall recovery may potentially be delayed or even prevented over a substantial portion of the downwind pass in the third and fourth quadrants, Brochier *ibid*. In the present study there is little evidence that this in fact takes place. There is evidence of tower shadow, but most significant is the relative importance of the upstream to downstream blade forces and the relative energy capture by the two passes, the upstream contributing a very disproportionate share. There are important implications here for such things as blade section design and blade alignment or 'toe out'. Interestingly Stacey reference(88) shows details of work carried out on a high solidity turbine with a chord to diameter ratio of 0.4/3.0 where a toe out of 3.5° markedly improved the rotor performance over the entire speed range.

It is the events associated with the dynamic stall, namely the large normal force and its collapse and the pitching moment divergence, that are of major structural importance and hence of economic interest since these are of almost an impulsive nature and as such are capable of exciting any structural resonance. It is these blade forces which are the main subject of the present work.

1.3.1 Stall regulation

Rotor torque control using moving elements and control surfaces, represents a significant proportion of the cost of wind turbines and furthermore represents a potential risk to the reliability of the machine. The possibility of control by careful choice of rotor geometry is an attractive prospect. VAWT Ltd have now abandoned the concept of the variable geometry or 'Musgrove' VAWT in favour of stall control, but have not finally ruled out the need for aerodynamic control surfaces on large machines.

Stall control of a VAWT would appear, at first sight, to be potentially more gradual on the troposkein or 'eggbeater' machines, where the blade sections at small radius are likely to be stalled even at high tip speed ratios. It would appear however, that this analysis fails to consider the

three dimensional aspects of the flow field and the high level of turbulence here. Under these 3D and turbulent conditions stall becomes a gradual event (even on straight upright blades) in the sense that it starts at isolated points over the blade surface and only becomes complete at yet higher windspeeds

1.3.2 Blade sections

Some authors such as Klimas reference(43) and Zervos *et al* reference(102) have looked at alternatives to standard blade sections either by making modification to camber to account for flow curvature; or by more comprehensive modifications to enhance laminar flow and hence lower drag or to promote stall at higher incidence (in order to control blade thrust and hence rotor torque).

Also established is research into thicker blade sections, for considerable economies in the rotor structure may be possible if increases are made in the second moment of area of the cross section. Progress in this direction has already been made. The NACA-0012 was used in some of the very early model and wind tunnel VAWT experiments following its use in the helicopter industry. Early practical machines including the NASA Sandia Laboratories Darrieus, the Carmarthen Bay VAWT Ltd machine and the Rutherford VAWT of the present work have opted for NACA-0015. Canadian workers have used NACA-0018 for Project Eoli as has VAWT Ltd for the Scilly Isles machine and there is currently substantial research effort into the NACA-0020 Harris *et al* reference(38).

1.4.0 Pressure transducer measurements

Using pressure transducers to measure changing airloads on operating wind turbine blades has, in the past, been difficult because such transducers are fiercely temperature dependant. Moreover the pressures typical of those on the surface of operating blades are low compared to the full scale pressure of commercially available transducers. Any temperature effect, usually described in terms of this full scale pressure, is thus very significant indeed.

Temperature effect is conventionally handled by means of passive resistor circuits, one for each transducer, and tuned to the individual transducer's peculiar characteristics. The cost of

this approach is high and is reflected in the high purchase cost of the transducers. The present project has used a novel technique of monitoring and recording transducer temperature throughout the course of all experiments together with the data from the transducer outputs and has used this temperature data to correct for temperature effect at the data reduction stage. The author is confident that the data provided in the present work by this method is of a good quality and that the present method of use of integrated semiconductor strain gauge pressure transducers merits attention.

1.5.0 Aerodynamic scope of the present work

As is discussed elsewhere the recent changes in the UK manufacturing base make the need for research into VAWT aerodynamics more pressing. The present work has arisen out of the need to provide firm data of blade aerodynamic forces and moments over a wide variety of operating conditions on a blade of known characteristics and performance.

Primarily in the wind tunnel, normal and chordwise force and pitching moment behaviour is required against incidence under a variety of incidence time histories. Such data is required to enable further progress to be made in the characterisation and modelling of VAWT rotor output performance and blade loading. As will be discussed in the next chapter, current performance and loading models for VAWT rotors leave something to be desired particularly in higher winds, when stalled conditions pertain over part or all of the blade and part or all of the revolution.

Various authors, for example Paraschiviou reference(69), have included dynamic stall effects in streamtube models and have improved model performance by so doing, but the dynamic stall models *per se* are those optimised for helicopter work where incidence is characterised by oscillations about static stall incidence. In contrast the VAWT blade is experiencing reversing incidence to values somewhat higher than those on the helicopter blade and thus existing models need tuning to the new regime or indeed may need reformulating for the new conditions. Detailed examination of individual pressure traces is necessary to time the various events of dynamic stall for use in these models.

In addressing the needs outlined above, the project has been successful.

A vertical axis wind turbine blade has been calibrated in a wind tunnel under conditions of dynamically varying incidence and then exposed, with nearly identical instrumentation, to real life atmospheric loading on an operating VAWT rotor. A wind tunnel programme consisting of 118 runs was made in the University of Glasgow Oscillating Aerofoil Wind Tunnel Facility and some 1760 revolutions of atmospheric data were gained with the same blade mounted on the 6 metre Rutherford Appleton Laboratory machine. Figure(1) gives an overall view of the machine situation on site and figure(2) shows the machine in operation. Figure(3) shows the five possible configurations for the instrumented module, one in the wind tunnel and four on-rotor. The blade was run under a wide variety of wind conditions, rotor speeds and blade leanout angles. Chapter 7 details the wind tunnel programme and results and Chapter 8 the programme and results arising from the atmospheric experiments.

Data obtained in this experimental programme has been analysed in a variety of ways to address the questions set out above. Blade performance in wind tunnel has been examined in terms of stall type, normal force gradient against incidence and maximum normal and tangential forces and pitching moments. Flow probe signals have been examined in conjunction with those from single pressure tappings and blade stagnation point position to investigate various surrogate blade incidence measures. Throughout the present work the stagnation point position has been used as a common measure of incidence. Correlation exercises have also been carried out to determine the various delays in the dynamic stall process.

Atmospheric run data has been analysed for the same forces and moments as well as for trends in rotor thrust and maximum to mean rotor torque. Frequency content of the various forces and moments has also been examined as has the relative effectiveness of the front and back pass of a blade during a revolution. Throughout the analysis of the atmospheric data a windspeed based on the stagnation pressure and blade speed, rather than a windspeed from anemometers, has been used because of time of flight correction problems.

The reader may be tempted to ask why the present

work was carried out in addition to the Sandia work of Akins reference(3). In fact the present work was well under way by the time the Sandia work was presented and it was immediately obvious that temperature compensation problems were present, furthermore the American work was concerned with Darrieus configuration machines and so there was seen to be only limited overlap and thus no reason to abandon the present work.

To reiterate then, the present project has been able to gather a data base from both wind tunnel and on-rotor experiments using the same blade and the same instrumentation and to compare the performance of the blade in the two environments. Because of the extent of this data base only a subset has been presented in this thesis, but it is hoped that some of the main conclusions have been drawn from the data.

CHAPTER 2

REVIEW OF EXISTING LITERATURE

2.0.0 Introduction.

Aerodynamics is, compared to many scientific and engineering disciplines, a well developed science, arguably better advanced than any other in terms of the wealth of analytical theory and experimental data. However, significant advances over the amateur efforts of the early pioneers have largely been driven by the military and civil needs of the aero industry for better aircraft performance. Research has, as a consequence, concentrated on steady state aerodynamics with attached flows at high Reynolds numbers. Drag reduction at ever higher speed has concentrated research work in the transonic and supersonic domains and understanding of structural stability has enabled progressively lighter machines made of very sophisticated and expensive materials.

It might be assumed that this sophistication has generated a pool of knowledge which has only to be tapped to provide all the data that is required for the design of modern wind turbines. However the requirements of the wind turbine industry are very different from those of the aircraft manufacturer. Flow is essentially subsonic and incompressible, Reynolds numbers are much lower, efficiency and drag reduction are less crucial and structural weight less important.

Moreover turbulence levels are considerably higher and the likelihood of high angles of attack or incidence together with associated stall, certain. Indeed as discussed in the introduction in the previous chapter, blades may be deliberately stalled as a control technique, an anathema to the aircraft designer and pilot. Even reliability is, compared to that required of aircraft, less significant, the machine can always be stopped. What is required is cheap power that is controllable, and a somewhat more 'agricultural' approach is required in which simplicity, reliability and low cost, rather than efficiency, is emphasised, Migliore reference(55). Thus existing conventional aerodynamic research has only limited relevance.

Aerodynamic research of consequence to the present work comes from two sources: from the helicopter industry, notwithstanding the comments above, and from the wind turbine industry itself and its academic contacts.

In the helicopter field, the need for progressively higher over ground speed and consequent smaller rotor diameter has pushed disc loadings to high levels and with them angles of attack. This translates into excursions into the stalled domain. For current helicopters with very flexible blades and simple control systems this domain has to be treated with considerable caution, for most blade section generate considerable negative pitching moment post stall and this generates severe control loads and vibration. High harmonic control systems may however be available before long which will allow blades to be taken further into stall and advantage taken of the substantial increases in lift available. Even were this not so, considerable effort is required to exploit the phenomenon as far as possible and so much research effort has been expended by the helicopter industry into dynamic stall. Some of this research is relevant.

Research specifically for the vertical axis machine conducted by the industry itself is very limited. Only a few research teams have attempted to investigate the flow field in and around an operating rotor and to look at blade loads during operation. Even fewer have attempted to measure airloads directly by means of pressure readings to separate or isolate the effects of structural deflection, these latter normally measured by resistive strain gauge. The use of alternative techniques to handle pressure transducer temperature effects has received only limited attention.

One group of workers has concentrated on the use of laser velocity measurement of water through a model rotor to pick up data on rotor loads and flowfield patterns. Another group has recently produced pressure data from rotating rotor blades in wind tunnel where consistency and repeatability of input conditions ease the transducer temperature effect problem.

2.1.0 Pressure transducer temperature compensation: conventional method.

Semiconductor resistive strain gauge bridge pressure transducers were first developed in the mid sixties and have gradually become more reliable and consistent since then. Further, their price has fallen significantly and their use become common. The main difficulty with their use is their considerable thermal sensitivity and this is dealt with conventionally by the use of a network of, usually three, thermally stable resistors. Mallon and Bernstein reference(50) and Kulite reference(46) detail the fairly simple theory of the technique.

Two thermal effects are apparent. So called span effect changes the sensitivity of the simple bridge when excited at constant voltage to pressure, so that signal will change with temperature even when exposed to a constant pressure. Zero pressure offset relates to the change in signal with temperature, present even when the span or sensitivity effect described above has been corrected. Span effect is corrected by slugging the exciting power supply so that it behaves as one whose voltage falls with increased current demand and zero pressure offset is corrected by means of diluting an appropriate arm of the bridge with a stable shunt resistor. Modern compensation networks supplied with the transducer are trimmed using computer controlled laser equipment in the factory.

2.1.1 Pressure transducer temp compensation at MIT.

Kerrebrock *et al* reference(45) have continued a line of research into gas turbine cascade aerodynamics using a miniature flow probe only 5mm in diameter and containing five surface mounted pressure transducers. The transducers are of the semiconductor resistive strain gauge type as in the present project, but they are of a different make. Flow angles and speeds in a running gas turbine compressor model in a blow down wind tunnel are measured using the probe. Gas velocities and frequencies of significant events are very high and the duration of experiments very short. Transducer output is strongly affected by differential thermal movement between the transducers and their mechanical supports and the temperature gradients within transducer diaphragms, as well as gross diaphragm temperature.

Temperature compensation was effected by a combination of techniques including insulating the transducer diaphragms from the air blast, mounting on materials having similar thermal expansion coefficients, using the conventional passive resistor network technique, and making empirical corrections to zero pressure offset after a run, on the basis of much experience of the zero offset behaviour. Calibration of the transducers was effected at the beginning of the blow down tunnel run and at its end, less than 200 milliseconds later.

2.1.2 Pressure transducer temperature compensation at RAE Bedford.

Two groups of workers at RAE Bedford have occasion to use miniature pressure transducers and require some form of temperature compensation.

Much work is currently being undertaken to increase helicopter rotor disc loading and more particularly to increase tolerable blade tip speeds. To this end blade tip planforms and sections are being modified and performance is monitored during flight manoeuvers by the use of many pressure transducers mounted within the blade fairing. This group of workers are less interested in mean levels of pressure signal than fast changes and so have dispensed with any attempt to correct for dc drift Moulang reference(58). Instead they place great store in very careful matching of each span correction resistor to its transducer. Span correction refers to the required constant relationship between output signal and input pressure. Such matching work is of course carried out within the facility. Thermal drift is catered for in data logging by the use of 16 bit recorders, thus having wide range as well as high resolution. All transducers are set up to respond in the same electrical sense and are additionally sealed so that they have no reference connection. It is thus possible to ensure that all signals are on scale by changes in aircraft altitude.

Welsh and Pyne reference(97), working with wind tunnel models, are interested however in both mean levels and rapid fluctuations. Miniature pressure transducers mounted within models can experience large changes in tunnel air temperature, perhaps as much as 50° Celcius during a run as a result of the kinetic heating of the air. Specialist amplifier techniques are used by this team wherein transducer

drawn current is used as a measure of temperature and this signal is used to adjust amplifier gain and zero pressure offset.

The technique is reasonably effective, improving accuracy by as much as an order of magnitude, but it is time consuming and tedious to set up. As will be noted in the sections of this thesis dealing with transducer appraisal, output response to thermal change is not necessarily monotonic and further has a long time period, implying the possibility of only a few thermal cycles in a working day and thus only a few chances to iterate towards the best compromise settings. The problem is compounded by the fact that transducers drift over time in addition to their other characteristics and so much effort is required simultaneously to get settings correct for all transducers in a model at the same time. It should be clear that each transducer has to be treated individually and has to be matched only to its own amplifier board.

2.2.0 Dynamic stall.

Dynamic stall concerns the process whereby flow patterns and aerofoil forces and moments change in a sudden and almost discontinuous manner at relatively high angles of incidence or attack, from large values of lift to small and from small values of drag and pitching moment, to large. Conventionally expressed, airflow over the upper surface of a wing or aerofoil ceases to flow in an orderly and attached manner after stall and breaks away, leaving a volume of stagnant or only weakly moving air over most of the surface.

Flow velocities over the suction surface in the pre stall or attached case are normally elevated over the freestream value and this implies the low pressures that provide aerodynamic lift. If incidence is changed at a significant rate, so that only a finite number of blade chords of air flow past during the manoeuvre, that is motion is at a significant reduced frequency, flow breakdown or stall is hampered by natural inertia and takes a significant time to occur. As a consequence a large angle of attack may be reached before the point of stall and with it larger forces and moments than are experienced during slow manoeuvres.

It is now clear that part of the dynamic stall event consists of the formation of a strong vortex

over the suction surface. This vortex is energised by the highly accelerated flow in the region of maximum suction just before stall and is the reason why many aerofoils exhibit increased lift or normal force coefficient against angle of attack slopes. After a delay the vortex breaks away from the surface and is convected downstream at somewhat less than half the freestream velocity - this probably being the mean of the reversed flow boundary layer and freestream velocities. In doing so and in moving away from the blade surface, the vortex effect is spread more widely, so that normal force may not immediately fall. Rearward movement of suction will however, already have caused the classical pitching moment break or divergence associated with stall.

Position of vortex formation on the suction surface appears to be geometry dependant, McCroskey reference(54). Relatively thin sections for example the NACA 0012 and thinner, are prone to promote the forward positioning of the vortex centre even to within the first few percent of chord. Thicker sections, perhaps those over 16% thickness to chord ratio, appear to favour positioning as far back as 30% of chord. Forward positioning results in strong vortex activity and consequently strong dynamic stall effect, rearward activity is relatively weak.

Vortex initiation position is influenced by the behaviour of the boundary layer and this must be the reason for geometric influence. Trailing edge dynamic stall appears to be triggered when, at high incidence and boundary layer flow reversal, boundary layer disturbances move forward from the trailing edge. The leading edge dynamic stall trigger is less clear and McCroskey *ibid* cites conflicting evidence about whether it is, or is not, related to any leading edge bubble collapse. In the case of the thin (8.6% x/c) NLR-1 aerofoil, for example, stall was not influenced significantly by leading edge trips, whereas in reference(52) a connection is recognised, in some circumstances, for the NACA-0012.

McCroskey reference(54) has categorised four dynamic stall types: leading edge, trailing edge and two forms of mixed stall. In the present work, evidence as to the stall category is not always clear, but where strong activity is present it would appear to start from about midchord, progress to the leading edge and then on to the trailing edge again. It would therefore be classed as of the

mixed type. In fact Beddoes reference(11) 1982 suggests that trailing edge separation is suppressed by significant pitch rate and therefore it might be hazarded that trailing edge separation only penetrates to the 30% x/c region before vortex initiation.

Various authors, for example Gangwani reference(34) and Boeing-Vertol following Gormont and Beddoes reference(10), have provided empirical rules to enable reasonable prediction of dynamic stall behaviour from a combination of thin aerofoil theory, static behaviour and some geometric attribute of the aerofoil section. Beddoes reference(9) early models are based on the modelling of two reduced time delays after the achievement of static stall incidence: moment stall or divergence (when the quarter chord pitching moment diverges from a nominally zero value) and normal force collapse when the suction surface vortex has essentially ceased to exert significant influence. Other authors have preferred to express these delays in terms of incidence.

Computational solutions to the Navier Stokes equations are unlikely to be usable for practical blade loading prediction for some time, for example Shida *et al* required about 6 hours of cpu time to generate realistic representation of dynamic stall on a NACA 0012 going through a sinisoidal incidence manoeuvre.

2.2.1 Dynamic stall investigation methods.

Dynamic stall has been investigated in a variety of ways usually by driving the test aerofoil through a regular motion in pitch in the wind tunnel. Pitching motion has usually been on a centre through the quarter chord point and has normally had a sinisoidal form. Alternatives have involved the use of water tow tanks normally used for ship model research and water tunnels. Use of water enables high Reynolds numbers at modest linear speed and so is particularly useful where any element of flow visualisation is required. Alternatives to the regular sinisoidal motion have included ramp motions in pitch and attempts to more closely model the characteristics of helicopter and wind turbine conditions by motions which change airspeed as well as incidence.

Some groups notably Favier *et al* reference(29)

and Francis and Keesee reference(30), oscillate the whole aerofoil, set at a geometric angle of incidence, axially or at an angle in the tunnel working section. These motions can be arranged simultaneously to modulate airspeed and effective incidence in a variety of in and out of phase combinations.

Another group Clayton and Morsi reference(21), moves the whole aerofoil on a circular path but maintains alignment between aerofoil chord and tunnel airflow. Incidence is achieved as the blade moves transversely.

Moss and Murdin reference(57) provide one of the first pieces of modern work on this subject, though the history of dynamic stall investigation reportedly goes back to the work of Kramer in 1932, Daley and Jumper reference(22). Primarily driven by problems with the operation of helicopters, Moss and Murdin oscillated a NACA-0012 aerofoil attached to a modified force balance, in a wind tunnel. The experiments covered a range of reduced frequency at two tunnel speeds with and without laminar boundary layer trip.

Ericson and Reding reference(27) have provided reviews of various dynamic stall studies and suggested reconciliations between the results of those studies using plunge or heave to provide dynamic incidence variation, and those using pitch change (usually about the quarter chord point). It might be pointed out that there are significant differences between the two methods in terms of their results, both in the amount of hysteresis experienced and in the level of the achieved force coefficients. From the point of view of the vertical axis wind turbine, from vector considerations, the pitching method would seem the most appropriate.

2.3.0 VAWT rotor flow field work.

Theoretical models of rotor power, flowfields and blade load have sprung out of the work done on propeller modelling for the aircraft industry. Stacey reference(88) and now Eggleston and Stoddard reference(24) provide succinct accounts of the various theories and model types and their strengths and weaknesses - although the latter does not deal with the vertical axis case. The problem is essentially one of providing adequate and useful accuracy whilst at the same

time avoiding long and impractical computer run times. Substantial progress has been made and practical multiple streamtube double actuator disc models appear to give good modelling of low to moderate windspeed conditions. At high winds however, power estimation is somewhat unreliable and estimates of instantaneous blade loads may not only be fairly seriously in error, they also may miss qualitative details: modelling of the effects of dynamic stall and its recovery is the problem here. Secondary flows in the boundary layer as a result of centrifugal effect and the effect of fences, struts and hinges and other auxiliaries may play an important role in modifying dynamic stall behaviour.

Experimental work in the area is sparse. Perhaps due to the difficulty of mounting such experiments and their cost only a very few vertical axis machines have been fitted with pressure transducers and data taken. Akins reference(3) and Anderson reference(5) have both used conventionally compensated transducers and both have reported substantial difficulty in reducing the data. Some wind tunnel studies have been made, for example Zervos reference(102), and useful water tunnel flow visualisations have been made by Brochier *et al* reference(18). An important and comprehensive study Willmer reference(99) has tunnel tested a turbine blade to obtain its conventional static characteristics and then tunnel tested a rotor using the same blades. As far as the author is aware, no work other than the present, contains pressure data from a blade both in tunnel and in atmosphere. None has produced data nearly all of which is immediately usable without processing to correct or eliminate errant transducer signals.

2.3.1 Previous work using the RAL 6 metre machine.

Stacey reference(88) carried out a programme of work on VAWT dynamics and aerodynamics and looked at blade and tower loads by means of strain gauged blade and cross arm, and by means of an instrumented tower head bearing carrier. Rotor torque and hence power were logged.

In general maximum measured power coefficients were of order 0.3 at a blade speed ratio of about 4.5, but considerable scatter was present. These results compared reasonably with the theoretical expectations of the machine as estimated by means

of Stacey's double actuator disc model. Blade forces suffered from extensive ringing but peak mean values were in reasonable agreement with predicted peak values. Noise was such however as to obscure virtually all features of the data within a revolution.

2.3.2 NASA Sandia work.

Akins *et al* reference(3) have produced the work most relevant to the present project. The 17 metre Sandia troposkein bladed VAWT was equipped with 29 pressure transducers one quarter chord below the equatorial position and a flow angularity probe mounted an equal distance above the equator and projecting 0.375 blade chords forward of the leading edge. A large number of runs of data was collected and analysed using the method of bins whereby revolutions of similar blade speed ratio were aggregated together. Significant temperature drift problems were encountered to the point where the transducers were encapsulated in silicone rubber and covered overall with mylar film to provide some thermal insulation. Interpolation was used to fill gaps in data left by errant transducers or else runs were rejected.

Published data shows normal force coefficient data plotted against two estimates of incidence: that from the flow probe and that obtained from a two vector model. This latter simply uses the vector addition of the wind vector and instantaneous blade velocity arising from blade tangential speed. The authors have rejected incidence data obtained from the flow probe because of hysteresis in normal force data plotted against this incidence signal for runs of low wind speed where stall effects were not expected. They suspect errors in the unsteady potential flow corrections necessary because of the aerodynamic interference to probe signal resulting from the proximity of the blade.

At higher windspeeds aerofoil stall will grossly affect the flowfield in the vicinity of the blade and this will strongly affect the flow angle seen by the probe. This effect is seen in data from the wind tunnel testing of the present blade and probe. Akins *et al* present the two measures of blade incidence for a tip speed ratio of 2.6 where stalling would be expected. Early peaking of the probe signal compared to the two vector model is symptomatic of blade stall effect on flowfield. Significantly this blade speed ratio is one where

the up and the downstream maximum incidences would be comparable on the basis of the present work see Chapter 8.

Results are shown for averaged runs of blade speed ratios 4.6 to 2.6 using the two vector incidence model. In traces from runs of blade speed ratio less than 3.9 significant hysteresis is noted in the upstream normal force coefficient whilst there is very little downstream. At the Reynolds numbers of the Sandia machine viz about 1.5 to 2 million static stall would be expected at about 16.5° from the Jacobs and Sherman correlation $alpha_{stall} = 1.79 * ln(Re/202)$ as quoted in Strickland and Graham reference(89) and this angle or something near it would appear consistent with the displayed figures for the upstream half cycle, at least as far as normal force divergence is concerned. Perhaps strange is the non linear nature of normal force against the measure of incidence.

Downstream this effect of curvilinear Cn/alpha characteristic is also present. It is tempting to suppose that these incidence measures are poor and that actual incidence is markedly less, particularly for the downstream pass and this would be consistent with the results of the present work. An additional difficulty with this quoted work is that of the dynamic pressure used to compute normal force coefficients, the maxima of which are all low for the Reynolds number particularly under dynamic conditions.

2.3.3 Canadian and French work.

Rangi and South working in Canada reinvented the Darrieus turbine aerodynamic operating principle in the late '60s and Canada has sponsored this form of turbine in preference to other configurations. Templin of the Canadian National Research Council has research this area and published many papers on the subject developing one of the early single streamtube prediction methods. More recently Paraschivoiu from Montreal and colleagues from institutions in France, have carried out theoretical and experimental studies of the Darrieus rotor flow field, including flow visualisation of dynamic stall in a rig kinematically similar to that of Clayton and flow field studies through model rotors. Additionally a study by Wickens reference(98) at NRC Canada subjected a NACA-0018 to vawt function incidence waveforms at a reduced frequency and tunnel speed

comparable with the conditions experienced by the blades on the Canadian Eole Darrieus machine.

2.3.4 VAWT Ltd and ETSU/Department of Energy.

Anderson reference(5) has recently presented data from three blade speed ratio aggregate runs taken from the 25 metre Carmarthen Bay machine. As with the Sandia Laboratories experience, transducer thermal drift was serious to the point where no absolute or mean pressure levels were obtainable and a correction scheme based on selected transducers and the pressure profile suggested by Riegels reference(74) at zero incidence was used. Since no absolute signals were available no measured incident air velocity was available and both incidence angle and velocity were obtained from a multiple stream tube double actuator disc model of the flowfield. Data are available only from transducers located in the region of tower shadow and effects from the supporting strut arrangements.

Presented are traces of normal and tangential force and pitching moment and the respective coefficients for an upright blade case at a 2.04 blade speed ratio. Two figures are provided showing pressure coefficients against chord over two aggregate revolutions at 4.1 and 1.6 blade speed ratio. Also shown are maxima and minima of normal force coefficient and normal force coefficient slope with incidence.

Qualitatively, the forces and moments are not remarkable in the light of the present work except that the downstream results show the effect of considerable tower shadow - indicated by localised depressions in the magnitude of blade forces mid way through the downstream pass. Normal force coefficients are also of an expected shape although they are of a slightly low value at this blade speed ratio. Pitching moment and to a lesser extent tangential force coefficients are however distorted, the latter showing a very strong positive going ramp during recovery from the upwind pass. Too much should perhaps not be made of these differences which may be attributable to transducer errors, these coefficients being particularly susceptible to small errors.

Harris reference(38) presents example data from the current Department of Energy contract with VAWT Ltd, University College, Rutherford Appleton

Laboratory, Glasgow University, Reading University and Cranfield Institute of Technology. Several blade sections are being investigated in wind tunnels and in atmosphere in an attempt to assess thicker and hence structurally more beneficial sections. Shown in the paper are comparisons of normal and tangential force coefficient for tunnel and atmospheric situations.

2.4.0 Summary.

Literature in the areas of instrumentation and dynamic stall exists in useful measure, but there is little regarding experimental work in the rotor flow field. Almost all work in the dynamic stall area has been carried out for the benefit of the helicopter and military aircraft and missile community and therefore has not concentrated on the particular problems of the VAWT, namely reversing incidence to moderately high values at relatively modest pitch rates. The above users are primarily interested in the use of the dynamic stall phenomenon pre lift stall to enhance maximum lift. In contrast the wind turbine community wishes to use stall to limit power and desires to limit the high values of normal force normally encountered in dynamic stall. Wind turbines operate well into the deeply stalled domain in high wind and therefore the wind turbine designer is interested in the behaviour post-stall as well as pre-stall. Moreover there is interest in the frequency content of the forces arising from the stall event since stall will take place every revolution in high wind and must constitute a major component of the stress and fatigue history of a turbine.

Many points thus arise from the literature reviewed above. Blade force data exists for full size machines and for models but this data is derived, with only a very few exceptions, from strain gauges in the blade structure and is thus complicated by structural response, making accurate estimation difficult. A method which does not suffer this difficulty is that of pressure tapping a representative blade section to provide pressure data which may be integrated to provide blade force information or histories. However those few studies which have tried to pressure tap a blade on-rotor have encountered the temperature effect in the pressure transducers used and have had severe difficulties reducing the data to sensible conclusions.

On the theoretical prediction and modelling side the considerable complexity of the flow field and the many different operating regimes of the rotor prevent the use of a full stepwise analysis based on the Navier Stokes equations because of the extreme amount of computing power required. Many models such as prescribed wake models have been proposed which economise on computing but which inevitably involve compromise and are thus less confidence inspiring. At this level the models require considerable validation against experimental data. Most models are unable to give completely convincing prediction of all the features of force pattern around the cycle and are frequently significantly in error in a quantitative sense also.

The present work is thus manifestly necessary.

CHAPTER 3

PRESSURE TRANSDUCERS

3.0.0 Introduction.

Central to this study is the pressure transducer. Selection of the particular transducer finally used in the study was the result of a long and unexpected test programme. During project planning, consultations had been made with both wind tunnel experts and helicopter people, particularly those at RAE Bedford, as to the best choice of transducer for our purpose. At that time choice was very restricted. Miniature semiconductor piezo-resistive bridge pressure transducers for scientific use were, and remain, the only real choice for this application. They were made in small numbers and considerable effort was expended by the manufacturers to fit them into as small a package as possible to aid incorporation into, for example, research helicopter blades and wind tunnel models.

Subsequently semiconductor technology has advanced and commercial requirements for measuring pressure have become much more common in, for example, road vehicle fuel and emission control equipment. The result has been a considerable price reduction in semiconductor transducers intended for the commercial market. There has not however, been the same incentive to reduce package bulk in this market and there is indeed a need to keep package size large enough to provide good mechanical robustness. This has resulted in package dimensions typically of about 10mm or larger.

This project started with the intention of using transducers of the small scientific package type: a blade figure(4) and probe figure(5) were made and part instrumented and some data was taken as a backup to the subsequent programme using them. But, as will be described below, because of severe delays in the delivery of both the transducers and this blade and a desire to use some existing transducers, a programme of tests extending over several months and involving the recording and analysis of several hundred test cases was run. This concluded that conventional methods of use with existing transducers could not give data to an adequate accuracy and confidence level.

The project then elected to change transducer to the commercial type, which had come onto the market after the start of the project. Figure(6) shows some of the transducers tested. There was a considerable cost in terms of time and effort associated with this move, but there were also felt to be benefits associated with the maintainability and reliability of the equipment. Atmospheric testing relies on equipment working perfectly whenever weather conditions permit and equipment must behave consistently: calibrations must not change significantly over the time period between calm and windy conditions.

This chapter describes the construction of piezoresistive semiconductor pressure transducers, the initial transducer scheme, the problems which led to the transducer test programme, the programme itself, the new transducers and the method of their use.

3.1.0 Transducer construction.

All the transducers discussed in this study, with the exception of the Tinsley type 156, are of the piezo resistive type. Here fluid pressure is sensed by the deflection of a silicon diaphragm etched into a silicon chip about 3mm square. Integral with the diaphragm is a full four arm resistive bridge formed by tracks of doping element diffused into the silicon. With diaphragm deflection shear strains are set up in the diaphragm with the result that two opposite resistors in the bridge increase in value whilst the two remaining decrease and this results in an imbalance in the bridge and an output voltage. Transducers examined in this study produce of order 1mV/kPa at rated excitation voltage. A box of plastic and metal is used to mount the silicon chip, isolate it from mechanical strain, prevent light from reaching the silicon, and provide mechanically robust electrical termination.

Unfortunately, because of manufacturing realities it is not possible to make the four arms of the resistance bridge equal either in absolute value, or in temperature coefficient. So called 'zero pressure offset', an output signal present with zero input pressure, results from the simple imbalance: a change in this offset with temperature change is the manifestation of the temperature coefficient effect. A second temperature effect is also inherent in the device: decrease in sensitivity with rise in temperature.

To ameliorate these effects the standard technique is to equip the transducer with a network of three resistors tailored to the individual silicon transducer element. These resistors may be incorporated into the transducer body or may be packaged in a separate temperature compensation module. Where such compensation is provided, the resistors are normally executed in thick film metal resistor technology and the exact values are obtained by laser trimming under computer control in the factory.

References(50) and (46) give a full explanation of this temperature compensation technique, but briefly, offset temperature effect is corrected by 'diluting' one of the high coefficient bridge arms with a zero coefficient resistance shunted across it. A second resistance is connected either in series with this pair, or in series with the other bridge arm on the same side to correct for simple offset. The third resistance is in series with the whole bridge, across a constant voltage power supply. With temperature rise, bridge input resistance rises and thus applied bridge voltage voltage rises. This effect is arranged to compensate for the effect of loss of sensitivity with temperature.

It is important to stress that success in temperature compensation relies on zero temperature coefficient compensation resistors fully isolated from mechanical strain. Most of the trouble associated with the use of transducers formed as described above springs from two effects: inadequate performance of the temperature compensation mechanism and strain effect. Manufacturers specifications normally give the maximum allowed temperature effects in terms of the full scale ratings of the transducer and they normally do not quote figures for the strain effect. Until recently the most sensitive transducer readily available has been rated at 5psi (35kPa) full scale.

This project has used as its benchmark a pressure of 1kPa, this being based on the dynamic pressure seen by the wind turbine blade due to its rotational speed. Suctions around the blade's leading edge may reach an order of magnitude or more greater than this, but towards the trailing edge they will be less and 1kPa may then be perhaps regarded as a kind of 'average'. Indeed there would be considerable interest in resolving to a few

percent of the dynamic pressure in order to pick out events of significance during a revolution. Hence the rule of thumb pressure is only about 3% of the typical transducer's full scale rating. It may be appreciated that any temperature effect specified in terms of the full scale ratings of a 35kPa transducer has the potential to be severe. 1kPa is also about 1% of atmospheric pressure and so barometric movement is unfortunately likely to be very significant if absolute transducers are used.

3.2.0 Early transducer scheme.

As mentioned above, during the planning of the project it was envisaged that blade surface pressure data would be obtained in a way as close as possible to that used by the helicopter research industry. The method used at RAE Bedford is based on the use of the Kulite 'Flatpack' transducer, a package about 1.7mm thick, 6mm wide and 20mm long. Up to one hundred of these devices have been fitted to one helicopter blade by this organisation. Two methods of mounting are used: either a shallow pocket is machined into the metal surface of the blade and the transducer cemented into this, or more commonly, the transducer is used to investigate the aerodynamics of modified blade sections and blade planform shapes, particularly at the blade tip. Such modified tips are effected by building up the surface of the blade with a balsa wood 'glove' shaped to the aerofoil section of interest. Pockets are cut into this wood, the transducers cemented in with their wires being accommodated in grooves also in the wood and the glove covered with a skin of glassfibre. Holes left by moulding the glassfibre around a fine rod such as a small drill, communicate the pressure to the transducer. Considerable care is needed to avoid debris falling into the hole. Once in, the transducer cannot be removed without destroying the glove. The process is time consuming, but is clearly satisfactory for helicopter research. Not wishing to 'pioneer', the project decided to follow this method as closely as possible.

3.3.4 Cranfield Kulite scheme.

Transducers were cemented into pockets moulded into the aerodynamic surface of the blade module. Wiring was of 24swg enamelled copper wire, four conductors per transducer, set into grooves or channels also moulded into the blade surface. Figure(4), a drawing used in the manufacture of the blades, shows this. The wiring ran back to a terminal board mounted in a hatch stationed at mid module. A second hatch was provided at the flow probe mounting position to facilitate connection of the probe: again wires were run from a small terminal board, back through further grooves to the main terminal board. The grooves were rectilinear in cross section to facilitate moulding and were arranged in such a pattern on the blade surface as to facilitate preparation of the final blade surface: a 300mm straight edge arranged spanwise, can bridge all the depressions. Since the transducers were of the absolute type no reference pressure tubing or manifolding was necessary.

The transducer mounting scheme was, as shown in figure(7), to use cylindrical Kulite transducers left over from earlier work at Cranfield for the leading edge positions and to use 'flatpack' transducers elsewhere. Aerodynamic pressures at the leading edge were to be communicated to the transducers by means of aluminium blocks drilled appropriately, to provide passages or ducts of minimal volume. These blocks were to be cemented into pockets in the blade with the transducers already fitted to them. The aerodynamic surface would then be built up and over them with car body filler. Because of the difficulties over the use of the cylindrical transducers however, in particular the difficulty with the temperature compensation modules discussed elsewhere, these transducers were never fitted. Some Kulite cylindrical transducers of a slightly different size however, were fitted to a five hole flow probe as described below.

The Kulite flatpack transducers were fitted as had been originally planned, but their positions were changed so that some were fitted to leading edge positions. Figure(7) shows the mounting arrangement used and also shows the unused method of cylindrical transducer mounting. Aerodynamic surface on top of the transducer and wiring channels was produced by filler as intended but this was of the pva/marble dust (exterior 'Polyfiller') type because of the incompatability

of the polyester adhesives used in car body fillers with the adhesive tapes used to block the entry of debris into the transducer.

3.3.5 Early experience with the Kulite transducer.

Some cylindrical package Kulite transducers had been recovered from previous experimental work at CIT and it was considered appropriate that experience be obtained in operation of the devices at as early a stage as possible. It was hoped that enough experience might be gained to enable new compensation modules to be made for those transducers without them and thus increase the stocks of transducers available. In addition to these transducers, others complete with temperature compensation modules were available. Preliminary looks at these latter were not encouraging however because of the overwhelming thermal effect compared with that of pressure. In one early test with the first flow probe, it was impossible to measure any pressure effect due to incident flow, without using ac coupling - the probe having been mounted on the RAL machine rotor for this test.

There was hope that the poor performance mentioned above might be improved by careful tinkering with compensation resistance values. A BASIC program was therefore written to generate required resistance values for thermal effect correction and zero offset reduction using as input the measured transducer arm resistance values at two temperatures. Resulting resistor values were implemented using precision laboratory resistor boxes and temperatures were varied by the use of Dewar flasks containing water at different temperatures, typically in the range 5degC to 35degC.

Attempts to make progress along these lines were frustrated by the difficulty of making sensible, repeatable and accurate readings of transducer resistance values. It was quickly realised that ohmic heating of the bridge at rated excitation voltages (allowing for the fact that the span resistor was absent) was the dominant thermal input and that resistance values taken without excitation power were irrelevant. At this point insufficient confidence existed to lower excitation voltage in view of the effect that this might have on signal to electrical noise ratios and so this option was not followed. Instead attempts were made to arrive at suitable resistor values by the use of trial and

error, but this too failed - significantly because it was not possible to replicate any previous state or reading. Moreover in moving from one temperature to another, transducer output signal did not change monotonically to a new value, but moved in a seemingly unpredictable fashion. Efforts along the lines described were therefore quickly abandoned and with them went hope of easily using the cylindrical transducers.

3.3.6 Transducer temperature by drawn current.

Welsh and Pyne reference(97) describe a method used to correct for the thermal effects on transducers used in wind tunnels by the use of variable gain and offset amplification. Both gain and offset were arranged to be functions of a single control parameter: the current drawn by the transducer from a constant voltage supply. As is described above, bridge input resistance increases with temperature and tests undertaken in this project confirmed the reliability of this parameter as a measure of bridge temperature. From an early stage in the project, transducer temperatures have been determined by inserting 10 ohm precision resistors in series with the power supply, this value being judged the smallest giving an adequate signal.

3.3.7 Compensation module temperature coefficient.

An experiment was conducted to determine the temperature coefficient of resistance of one element of a compensation module. Figure(8) shows the the change in resistance against temperature equivalent to a coefficient of 230 ppm/^{o}C. Appendix(1) shows that the effect of a change in temperature of 20^{o}C on the compensation module is comparable with the signal expected from one dynamic head of pressure. The effect is thus very serious.

3.3.8 Transducer cooldown tests.

Tests on the flatpack transducer were started upon receipt of the first batch of 17 of the ordered 32 in September 1984. One of the early tests was designed to gauge the effect of air blast on the transducer temperature and thus its output signal. At the specified excitation of 20 volts the transducer absorbs about 50mW making it quite warm

to the touch when in still air. Akins *et al* reference(3) indicate that transducer cooldown was a major problem in tests on a wind turbine in the USA and that attempts at insulation using mylar film were made to combat the problem. Klimas reference(44) indicates that this effect has been the main impediment to successful reduction of the data in these tests.

In the on-rotor cooldown tests at RAL, transducers were mounted on the inside surface of one of the existing blades and faired over with 'Blutac'. Transducer temperature was allowed to stabilise, as judged by output and drawn current signals and the drawn current signal then monitored as the rotor was taken up to speed. The data taken, one example of which is shown in figure(9), is not of adequate extent because of the limitations of the recording voltmeter used and the very limited number of starts that the RAL machine could make in a day on the old battery starter system, but the effect on output was and must be considered significant.

3.3.9 Flatpack mechanical strain tests.

Two flatpack transducers were mounted in a 250mm chord blade model equipped with full size pockets in the surface as described elsewhere. The transducers were cemented in with a variety of adhesives including 'blutack' and silicone rubber. Attempts were made to produce aerodynamically fair surfaces over the transducer, whilst maintaining clean tapping holes to communicate pressure, but this turned out to be a difficult and time consuming activity. More worrying was the signal output produced by any mechanical load on the transducer case and its only partial recovery on release. No satisfactory solution to the problem of isolating for strain, in the space available, whilst providing smooth aerodynamic surface, readily emerged.

Delivery was later taken of the first 'to be instrumented' blade module. A flatpack transducer was mounted in one of the surface pockets at about 70% chord using 'blutack' and was faired into the surface with this material leaving a communicating hole to the pressure port. Figure(10) shows the transducer output signal, taken with a recording digital voltmeter, during the imposition of a 700N load at the blade centre whilst being simply supported at its ends. This is equivalent to about

one quarter of the centrifugal load imposed on the blade and about equal to the air load. It will be seen that the strain effect might reach about 10% of the signal due to dynamic head. It is suspected that the strain effect on the temperature compensation section of the package is every bit as important as its effect on the transducer element proper. It must be expected that, when covered with a more permanent filler material, strain sensitivity would be worse. McCroskey and Fisher reference(53) describe similar strain effect problems occurring in a wind tunnel model rotor model.

3.3.10 Transducer temperature effect and consistency tests.

Earlier tests (above) had shown that temperature effects could not be ignored and that a change in strategy would be necessary to deal with the problem. One signal alone could not be used to record pressure on the transducer, but it was conceivable that an adaptation of the method of Welsh and Pyne reference(97) would work, whereby two signals per transducer would be recorded: a 'pressure' signal and a 'current drawn' signal. Correction for thermal effects could then be made in software afterwards with considerable savings in hardware over the method of Welsh *ibid*. There was of course an increase in hardware over the requirements of the initial method, ie as manufactured passive thermal compensation, but it was judged that this was acceptable and that the additional hardware requirement would then 'just be more of the same'. It was then necessary to see if such a two signal system was likely to work adequately and a programme of tests, to measure temperature effect and consistency of output, was undertaken to find out.

A time scale of one or two weeks was judged necessary for the tests, since this would probably be typical of the time interval between wind (and hence experiment) and calm (and hence calibration of the transducers).

The opportunity was taken to look at the performance of other transducers, by then also available, in addition to the Kulite flatpack. Other transducers tested were the Tinsley model 156 and the Sensym LX015A, LX01D, SPX100A and SPX50D models. The Tinsley being attractive because of small size comparable with the Kulite and the

others because of their very low cost and almost immediate availability.

Transducers were excited with a high quality laboratory proportional power supply and transducer power supply voltage, drawn current and output were measured with a Thulby model 1905a 5½ digit voltmeter. The electrical circuit used during the tests was very like that shown in figure(11) except that the matched shunt resistor was omitted. To avoid problems and uncertainties over instrument warm up, all the equipment was left powered up all the time. Readings were taken always in the same order and care was taken to minimise hand contact with the probes of the digital voltmeter to minimise thermoelectric effect, this having been identified as an earlier problem. Earlier tests too, had shown inconsistency problems with a wafer switch used to change the dvm reading points. Barometric pressure was noted immediately before each set of absolute transducer readings from a Fortin barometer and this reading temperature corrected. A separate exercise had earlier confirmed agreement between this barometer and that of the Cranfield aerodrome control tower, about 400m away.

The test method was then to expose transducers to changes of temperature and pressure over a period of ten or fifteen days. A particular condition having been set, the transducer was allowed to settle, judged by insignificant change of output with time and the barometric reading, temperature, excitation voltage, drawn current signal, and output signal noted, plus any other relevant parameter. Both drawn current and output signal were then corrected to the nominal excitation voltage on a simple proportionality basis and the results plotted. In the case of absolute transducers, where barometric effects are very significant, a correction to output signal was made on the basis of the sensitivity of the transducer as measured by the manufacturer and stated on the specification document supplied with each transducer.

3.3.11 Results and conclusions of consistency tests.

As has been stated above, the programme of transducer testing was extensive and altogether about forty transducers were tested to a greater or lesser degree. Of these interest focussed on the Kulite flatpack and the Sensym SPX100A and SPX50D.

Early experience had shown that all transducers had a pronounced temperature effect and so the consistency test investigated primarily the repeatability of the devices

Table(1) presents an example of the data taken from the main body of tests for the Kulite transducers. It shows the primary and derived data for transducer excitation voltage, current drawn and output signal, barometric pressure, barometer and room temperature and transducer output corrected to 1 bar and 20 volts excitation. Similar data for another Kulite transducer is shown in figure(12). Here the horizontal axis is the current drawn signal and hence a measure of transducer temperature, and the vertical axis is output signal. If no temperature effect were present then clearly fitted curves would have zero gradient. Consistency requires only that all measured points lie on one characteristic line, which need not be straight and can have any gradient. This figure shows the typical temperature effect combined with drifts and random effects which, as can be seen from the arrow length showing the approximate signal expected from 1kPa, are very serious for the present project.

A similar graph for one of the Sensym SPX50D transducer is plotted in figure(13). There is a marked improvement in the consistency of the output with only one spot grossly off the line and this was the result of a transient test where the transducer was deliberately not allowed to settle thermally before readings were taken.

Other transducers tested fell into a general pattern, where any passive compensation was included severe (in terms of the low pressures of interest in the present project) unrepeatability problems were present. Where no such elements were included severe thermal effect was present but it was repeatable over a reasonable time span such as two or four weeks. The odd transducer of the set, the Tinsley 156 metal strain gauge device, was so pressure insensitive and so temperature sensitive as to be useless for the present purpose.

Thus none of the transducers could claim to have adequate temperature immunity and therefore the less stringent test of repeatability was used as the arbiter of goodness. On this criterion the Sensym SPX series and in particular the SPX50D transducer appeared adequate and was therefore the preferred choice.

3.3.12 Subjective comments on transducer performance.

In addition to the quantified results presented it may be useful to pass on something of the 'feel' of each transducer. Changes in ambient temperature or bias resistor voltage for example were frequently made with the dvm connected throughout the manoeuvre . It was possible therefore to judge how quickly settling took place after the change, how stable the new value appeared to be and perhaps most telling, how monotonic was the approach to the new value. All the absolute transducers eroded confidence here, particularly when relatively low value resistors had been shunted across them to reduce gross zero pressure offset. The differential transducers required relatively small amounts of offset correction and inspired confidence.

Selected because of its small size, the Tinsley 156 was the only transducer tested which used metal strain gauges to detect diaphragm deflection. Sensitivity was therefore very low, only about 140 µV/kPa at the maximum allowed excitation of 1.5v in air. Furthermore hysteresis was also found to be large. The device is further unusual in having the half bridge configuration and is supplied with a high value compensation resistor to be shunted across one of the arms. This supplied resistor was of poor quality with a high temperature coefficient. Use of these transducers in this project would perhaps have required a dummy half bridge for each transducer and might have required amplification in the blade to reduce the potential noise problem. It was decided that this transducer was not the one for this job.

Sensym LX06015A transducers have integral temperature compensation networks in thick film resistor technology on a ceramic substrate section of the package. The inconsistency in output shown by these transducers is suspected to arise from flexure of this substrate under its own weight combined with a thermal effect on this network. The transducer appears to be acceleration or weight sensitive, which would be explained by this flexure and the LX01D would appear more sensitive in this regard.

3.3.13 Absolute versus differential transducers.

Debate had existed within the personnel of the project over the relative merits of absolute versus differential pressure transducers. The perceived advantages of using differential transducers were mainly concerned with easier calibration. It is possible to be sure of applying a zero pressure to a differential transducer, whereas an absolute device always has barometric pressure acting on it. The difficulty here, is of accurate and reliable measurement of this barometric pressure. Taking our unit of one dynamic head, about 1kPa, one might reasonably wish to resolve to 1% of this, that is about 10Pa, equivalent to about 0.076mmHg. This must be compared with a resolution of about 0.05mmHg, just possible with most Fortin barometers using the vernier facility. Calibrations require either elaborate equipment to isolate the transducer from the environment, or must be done quickly and out of doors in still conditions in order to avoid the effects of natural and/or man-made air pressure changes, for example, those produced by building ventilation equipment, doors opening and closing etc.

Secondly, advantage can be taken of the reference pressure manifold system to provide a very quick and convenient calibration technique. At RAL the reference pressure tubes are brought back to the hub of the rotor and thence down into the hut. All the transducers may be calibrated at once, except the two in the probe sensing blade incidence and sweep, by applying a pressure to the two reference lines, one to each blade module half. The probe thus requires an additional tube to be applied to two of its ports for calibration, but since it was calibrated before being mounted in the blade, there was not felt the same need to calibrate it as often as was felt necessary for the blade transducers. Provided that there was little wind, calibration could thus be carried out quickly and easily. This made for rapid checking that all was well, adding to confidence.

In fact the above faith in 'ground based calibration' for the probe can now be seen as perhaps misplaced, for some difficulty has been experienced in extracting probe calibrations for the atmospheric experiments.

A third argument for differential transducers is that, in order to use a pressure measured with an absolute transducer, the barometric pressure must

be subtracted. This leads to the problem of the signal of interest being the difference between two very large numbers, at worst three or four orders of magnitude greater.

Fourthly, barometric changes do not use up any of the system's dynamic range. To the absolute transducer barometric changes are just another component of air pressure and produce output signals which must be conditioned and logged like any other. Using the benchmark of the dynamic head of 1kPa, perhaps ten units of dynamic head would have to be allowed for this effect. 'Barometric noise' would oblige system gain to be cut by a half and thus halve the overall signal to noise ratio.

The penalty with the use of the differential transducer, is the need for the provision of reference pressure. Air in the reference lines leading out along the cross arm, experiences a centrifugal acceleration, thereby generating a reference pressure in the blade, above atmospheric. The magnitude of this increase is dependant on rotational speed, effective radius of transducers from axis of rotation and air density. For the present work, this magnitude is about 1kPa, as shown in appendix(2). Potential for error from this source must not therefore be ignored, but its magnitude is estimated to be small. Rotational speed is measured 256 times per revolution with a quartz controlled clock in the data logger, geometry has been measured to a few millimetres in a few metres with a steel tape, barometric pressure is measured with an aneroid barometer calibrated against the barometer at CIT, and air temperature is read just after data taking with an alcohol in glass thermometer.

A more significant problem is likely to be the error introduced by the effect of terminating the reference pressure tubes inside the rotor hut, rather than outside at a static pressure probe. Dynamic pressure at a wind speed of 10 m/s is of order 50Pa, about 5% of dynamic head and what proportion of this pressure is present inside the hut is unknown. It may be pointed out however, that reduced data, that is the result of pressure integration around the aerofoil, is not subject to reference pressure error, since all transducers are affected equally and all in the same sense. Leaks in the reference manifold system have been checked for regularly, using a transducer configured as a flow meter as described below. On one occasion, with an early method of tube jointing, leaks

approaching a magnitude potentially able to give a reference pressure error, were detected: the blade was removed and the fault corrected.

3.3.14 Method of transducer use.

From the above considerations and the consistency tests, the Sensym SPX50D was selected as the transducer most likely to produce useful data. The method of use has been to accept that both zero offset and sensitivity vary with temperature and that each transducer has its own individual characteristics. A measure of transducer temperature has then been used to calibrate these effects and this measure is, as has been described elsewhere, a drawn current signal.

Figure(11) shows the circuit used in the blade to connect the transducers. A 5ppm/degC precision 10 ohm resistor drains current from each transducer into the negative bus bar in each half of the blade module. As with reference pressure, each blade half is independent with its own separate terminal board in the module and its own separate wiring. Typically, 62mV exists across a current drawn resistor and over a temperature range of 30°C, this changes by perhaps 1mV. To give a signal suitable for amplification, the output from the top of a resistor is compared with that from a similar resistor draining a 460 ohm dummy transducer: another precision resistor. Only one of these dummy half bridges is provided per blade half, since amplification by instrumentation amplifiers imposes negligible load on such a circuit.

Transducer excitation voltage is defined, for the purposes of this project, as the voltage between the negative bus bar already mentioned and the positive, supplying current. The two transducer excitation voltages, one for each module half, are conditioned in the amplifier box and digitised at every azimuthal station ie 256 times per rev.

3.3.15 Zero offset resistor.

As supplied, the Sensym transducers have a zero offset signal of typically 20mV when excited at their rated 3V. A maximum expected aerodynamic signal is of order 10mV and so this zero offset would use up a large part of the dynamic range of the conditioning and logging equipment. To avoid this problem a very high stability 5ppm/degC

resistor, was selected for each individual transducer and connected, on the blade terminal board, as a shunt across one arm of the transducer bridge. Usually the zero offset, as supplied, was positive and so the resistors, ranging from 39kohm to 100kohm, were arranged between the negative power pin and the positive signal pin, this having the effect of bringing down the offset. In fact, because of the limited range of these precision resistors, two were used in parallel in some cases, to achieve the required offset value. This latter was not zero, but slightly positive, since the transducers were connected electrically and pneumatically so that aerodynamic surface suction, the dominant sense, produced a negative going transducer signal. The arrangement therefore allowed the use of higher amplifier gain than could have been accommodated had a zero value of initial offset been used.

A calibration programme, facilitated by the convenience of the reference pressure system, has been used to determine the characteristics of each transducer. Calibrations have taken place throughout a span of temperatures, covering the range experienced during both atmospheric and wind tunnel testing and a surface generated in the data reduction software, for each transducer. Going into the surface with both the recorded pressure and temperature signals, both corrected to the nominal excitation voltage, produces a true pressure.

3.3.16 Sensym transducer installation.

The method of mechanically mounting the transducer in the blade module and effecting pneumatic connection to it from a pressure tapping in the aerodynamic surface, is shown in figure(14). The pneumatic seals of double sided sponge tape were checked both with immersion tests in water and with helium gas and detector equipment. Some failures have been discovered during the project, but the method has proved adequate. In fact the transducer is now available in an alternative package with integral tube connections, so that the above method is now redundant. More trouble was experienced however, with the method of sealing into the aluminium blocks stuck to each transducer and with those blocks used to provide the manifolding system. The design was adopted, over a soldered brass system, because of considerable time pressure and its use has proved to be a false economy, although it has worked adequately

throughout the experimental programme.

Leak detection was effected by the use of a flow meter consisting of a 3m length of 1mm diameter bore tubing and a spare transducer. This latter was arranged to measure the pressure across the two ends of the tube, whilst it supplied air to the reference pressure manifold system. Air was obtained from the same aquarium aeration pump used to provide air for transducer calibration purposes and was used at the pump's full output pressure of about 10kPa. Readings of transducer output down to 1 μV were possible, equivalent to a leak of 0.4 mm^3/s. Leak position and magnitude could be discovered during setting with the blade open by pinching the silicone rubber of the reference system with narrow nose pliers and observing the resulting difference in transducer output.

Transducer mounting, effected with more double sided sponge tape, has appeared to be reliable and isolates the transducer from the worst of mechanical shock. Figure(14) also shows the transducer layout inside the blade, including the reference pressure manifold system. Advantage was taken of the space inside the blade to arrange that, with the blade mounted on the rotor at any angle of leanout, the planes of the transducer diaphragms were approximately radial. This was done to minimise the potential effect of centrifugal acceleration on transducer output signal although tests during the transducer selection phase had shown these to be unmeasurable.

3.3.17 Ducts.

Some work was carried out in this project to determine the effect of a duct communicating a pressure of interest to a remote transducer. Because of the physical bulk of the Sensym transducer, ducts of approximately 50mm length have been used in all cases, except in the case of the flow probe incidence pressure ports, where the length was about 20mm. Of primary concern was the effect of bends in a duct, since no reference on their effect was forthcoming and no experience was available in house, except that concerned with oil in ducts. In fact bends were found to have a negligible effect unless they were so tight that they constituted a substantial constriction. It was confirmed that a 50mm length of 1mm bore tubing had negligible effect on pressure signal fidelity, up to a frequency of 100Hz or so.

Vittecoq and Laneville reference(95) suggest that it is necessary to capture frequencies up to the eighth harmonic of rotor frequency for adequate fidelity which would be equivalent to only 16 Hz in the present work. Turbomachinery specialists at CIT use the 50th harmonic as a rule of thumb. Thus a frequency response up to 100Hz appeared acceptable.

Figure(15) shows a fourier transform of some signals taken from an atmospheric run and shows clearly the low frequency content of the signal where the highest harmonic of any significance would appear to be about the fifteenth or twentieth confirming the conclusion of Vittecoq above.

Experimental results and discussion on the duct work are given in appendix(3).

3.4.0 Software temperature correction.

As has been described above conventional temperature correction of semiconductor piezoresistive pressure transducers is effected in hardware in the form of passive resistive networks connected both to the electrical supply to each transducer and to its output. Each transducer is different and requires individual matching of resistive elements, a process that is normally carried out under computer control. The time constants of temperature change within the transducer package ensure that this process of matching is slow and that transducers compensated by this technique are expensive. As has been shown the technique is not very effective at small proportions of the transducer's span.

The present project has used the novel technique of software temperature compensation. A temperature signal for each transducer has been recorded once per revolution and has been used to allow characterisation of both zero pressure offset (the zero shift) and sensitivity, with temperature. The technique makes no assumption as to the future behaviour of the transducer nor does it assume any behaviour with temperature. Provided calibration exercises are carried out frequently enough, temperature correction algorithms can be tried out after the event, in order to select the best.

This section presents the results of the analysis of two calibrations carried out during July and August 1987. The calibration coefficient fitting

method used for all the data shown in this report has been that of the code DATPROC described in Chapter 6. Here a 'set' of calibration spots is decided upon after eliminating rogues, and a fit is made to the zero pressure spots. This is the 'offset' fit. Sensitivity coefficients are determined by predicting transducer output signals on the basis of these offset coefficients together with the recorded temperature signal and then deriving a 'sensitivity' for each non zero pressure spot. Coefficients can then be fitted to these sensitivities against temperature.

Thus:

$$offset = off_0 + off_1 * vi_{corr}$$

and

$$sensit = sensit_0 + sensit_1 * vi_{corr}$$

where off_0 and off_1 are the offset coefficients and $sensit_0$ and $sensit_1$ those of the sensitivity and vi_{corr} is the temperature signal that is the current drawn derived voltage corrected for variation in transducer power supply voltage.

The analysis has attempted to answer five questions:

1) with frequent calibration, how good is the technique

2) how much better is accuracy if correction is used

3) how much better is the present method than that using resistive elements.

4) how much better is the present method than that of Welsh reference(97)

5) how quickly do the present transducers' calibrations change?

Results suggest that the average error would be less than 30 Pa for a device capable of measuring 50kPa or about 0.06% of full scale.

Over an interval of approximately one month the transducers' characteristics changed so that the average zero pressure offset moved by an amount equivalent to about 95 Pa and the sensitivity changed by about 1.6 percent.

Table(2) shows the derivation of the drift figures. To compare the two calibrations a representative temperature signal for each transducer is required for both calibrations. This has been derived from the mean of the extremes recorded in the two calibrations for zero pressure. This representative temperature signal (column 'mean for 0Pa appld') has been used to generate zero pressure offsets and sensitivities (column 'mean offset or sensit')to represent the two calibrations. Throughout the table, pairs of rows represent each transducer, the upper showing the offset related parameters and the lower the sensitivity.

Full details of the two calibrations are shown individually in tables(3) and (4).
These tables show the recorded calibration pressures for each calibration spot, the pressures predicted from the fitted calibration coefficients and the recorded signals for each transducer, the standard deviation of the predictions and the errors expressed both as simple differences and as percentages. Where the calibration pressure was zero the percentage error has been calculated using 1kPa as the denominator.

Notable in the two tables above are the cases where the residual is much larger than the standard deviation. Standard deviations larger than 3 have only a small likelihood of being correct (less than 1 in 200) and it seems probable that these spots have incorrectly recorded applied pressures. Such a conclusion would imply that accuracies and consistencies suggested above would be conservative.

A further source of error present in some of the calibrations, was that due to the manometer.
It was noted that even after the manometer (shown in the background of figure(16) had been allowed to settle and achieve thermal equilibrium, it would read non zero with zero imposed pressure. Despite trials with detergent and soaking of the tube to eliminate differences in surface tension effects, this effect could not be eliminated. Recourse to large bore tube (12mm diameter) did not help. Discrepancies were of order 2mm.

It is noticeable that zero pressure calibration spots have much lower residuals than those where the manometer was used: refer to tables(3) and (4) where the standard deviations of the

zero and non zero residuals are in the ratio 3 or 4 to one. It might be fairer to the the temperature compensation scheme if the data relating to the zero pressure calibrations were more heavily emphasised. As far as the transducers and the other components of the system are concerned there is nothing unique about zero pressure and consistencies shown in such data spots should be available at other pressures. At the head of each transducer's column in the tables above, are shown the standard deviations of the calibration's zero pressure spots; 20.4 Pa and 14.8 Pa for the two tables respectively. These figures would suggest that the average transducer has an accuracy of about 40 Pa or better at 95% confidence level over the limited temperature range of these calibrations.

Better consistency could be obtained by better modelling of the transducers' characteristics, for example by using second order fits to the calibration data. It might be noted that with the amplifier gain and excitation voltage used, the available resolution of the data acquisition system is of order 9 Pa. Electronic noise during the course of these calibration spots was of order ±2.5mV corresponding to about 9 Pa.

The accuracy figures suggested above can be compared with those obtained by the work of Welsh and Pyne reference(97). These authors suggested a tenfold improvement in transducer temperature stability resulting in a maximum error of about 0.05% of full scale. The present work would suggest that errors with the present equipment might be twice this, that is 40Pa/50kPa or about 0.08%, over a smaller temperature range but in field conditions. Perhaps it is worth pointing out that software correction after the fact is as good as is possible: other errors may arise from hysteresis and other effects, but these are not correctable under any scheme.

An exercise has been carried out to show the effect of not using the temperature correction signal ie simply taking the mean sensitivity and offset for each transducer. Even over the very restricted temperature range of the calibrations, 12 to 18°C, accuracy is improved on average over fourfold.

CHAPTER 4

OTHER EXPERIMENTAL EQUIPMENT

4.1.0 Blade design and manufacture: general module scheme.

The existing blades on the RAL machine were considered unsuitable for use in this project for a number of reasons including inadequate structural stiffness and uncertain cross sectional profile - blade deflection would, for example, introduce spurious signals as it deviated from its nominal position on the rotor. New blades were therefore required and since it was wished that a representative section be wind tunnel tested, it was decided to make each of the two blades of the machine from two modules, each of a length that would fit into the tunnel. If the fixing point of each module to the machine, were at mid module, no bending moment need be transferred across the joint. Making each blade in two pieces would require smaller and cheaper moulds, allow more learning time with less commitment of expensive material and be more convenient for transport.

The initial scheme was then to have made, five blade modules, four of them plain, whilst the fifth would contain the instrumentation, including the flow probe. Four plain modules would allow the turbine to be run without instrumentation for initial commissioning and the spare plain module could also be used in situations where it would be undesirable to place the instrumentation, for example in flow visualisation experiments, where an oily dye is used.

Advantage could be taken of the symmetry of the blade section, since a blade module could be inverted top to bottom, without changing the aerodynamics at all: arranging the instrumentation asymmetrically about mid module, would allow it to be placed in any one of four spanwise positions in the blade. It would be a simple matter to change configuration and move the instrumentation from one position to another, giving substantial increase in data capture without increase in instrumentation. It would perhaps, be a unique opportunity to test exactly the same blade in the wind tunnel as in atmosphere. Figure(3) shows the five possible mounting configurations possible with the

instrumented blade module.

As has been described elsewhere, the aerodynamic surface of the first instrumented blade module to be fitted with Kulite transducers, was especially moulded with rectilinear pockets and tracks to provide accommodation for the pressure transducer instrumentation and its associated wiring. Two hatches were provided on each side of this module, to allow access to two terminal boards, to which all surface wiring and cables going to the rotor hub and thus the outside world, were connected.

4.1.1 Basic structural design.

The wind tunnel model length was 1500mm and this allowed a total blade length of 3m. Blade chord was already determined as 300mm because solidity, blade chord*number blades/rotor diameter, was required to be the same as that of the VAWT Ltd 25m machine. Tie up with this machine also decided the blade section, NACA 0015. Blade cantilever at top and bottom was then 750mm and this considerably eased the structural design. Since the present work is an experiment in aerodynamics, it was required that blade deflection under all working loads be minimised and investigation of various structures to replicate the 1600mm cantilever of the existing blade format, showed large deflections of the order of 100mm, to be likely. With a 750mm cantilever, deflections of a few millimetres could be achieved, with simple structural designs.

All the structural schemes employed carbon fibre composites as the preferred option, providing the best combination of ease of manufacture and minimal deflection under centrifugal and aerodynamic loading; but it was noted that a steel/glass reinforced resin structure was almost good enough to provide the necessary stiffness. An epoxy resin was decided upon as the most appropriate for the requirements of maximum strength and good stability during service.

An arrangement of seven layers of carbon was decided upon, the outside skin was a woven cloth with its fibres disposed at 45° to the spanwise direction, two layers of unidirectional tape arranged spanwise followed, then a further cloth, again at 45° then two more tapes and finally another cloth also at 45°. The lay up was then symmetrical in its thickness, the better to resist distortion after moulding. Cloth was used to 'tie

in' the other fibres and provide a better surface inside upon which transducers and other equipment could more readily be mounted.

The fibres disposed at 45° were present to resist the substantial torsional loads that arise in the blade just above the rotor cross arm. This latter is responsible for restraining five of the six degrees of freedom of the blade with respect to the rotor, the sixth being controlled by the top tie bars. Thus torsional loads arising from aerodynamic pitching moment divergence (aerodynamic centre of pressure movement during stall), are taken from the upper blade, down through its structure and out into the cross arm. Structural calculations for a number of trial blade designs showed that the structural problem is of providing stiffness rather than strength, the latter being easily satisfied. In fact the blade is about an order of magnitude stronger than necessary.

Module internal structure was very simple and consisted of a centre module block to accept the blade mounting fixings, a block at each end, again to accept fixings, leading and trailing edge spars and two spars/shear webs, one at maximum thickness and the other at about 70% chord. This position would allow it to pick up the rear edge of a suitable fish plate, reckoned to be the best way to join two modules together. In the instrumented module, between the leading edge spar and the shear web, a fourth block was provided to carry the flow probe. All these blocks were of dough moulding compound, pre cast in suitable moulds. The fish plate was sized to allow it to pick up the existing pattern of bolt fixings of the RAL blade hinge piece. Space between the rear shear web and the trailing edge spar, was kept clear throughout the length of the module, to provide a cable duct.

Over provision of fixings, some debate took place regarding the relative merits of through bolt holes and tapped inserts moulded into the module, but there was concern over the possibility of corrosion in such a fitting and a through bolt system was used. Here nuts were made from the heads of M12 countersunk socket head bolts and provided fixings for the M8 bolts used to fix the hinge, top tie bar and fish plates, bolts here needing countersunk washers. Bolt countersunk head and other blade surface holes were successfully filled with beeswax.

4.1.2 Blade geometrical tolerances.

Blade surface finish was required to have no touch detectable bumps or steps and to have a fine matt or gloss finish. Waviness of up to 0.05mm in 50mm and gross profile errors of up to 0.25mm, provided the other conditions were met, were stated to be acceptable.

Unfortunately the bought in blade modules did not meet these tolerances by a considerable margin, particularly around the leading edge, but it was felt that time pressure allowed no choice as to their acceptability.

4.1.3 Sensym blade.

The adoption of the new transducer, with its much greater bulk, necessitated the manufacture of a new instrumented blade module. Instead of working only on the outside of the blade, as with the module fitted with Kulite transducers, it was now necessary to provide access to the inside. It was decided to split the instrumented blade module along the plane of its chord line, into two halves, to be bolted together. This would provide complete access to the transducer instrumentation inside the blade, for manufacture and maintenance.

Advantage was again taken of the section symmetry, to ease manufacture. The new module was this time constructed in house by the author. A new mould was built in wood particle board, by copy routing about ninety sections of board directly to a negative of the blade cross section. These sections were then stacked next to each other on a suitable chassis, thus forming a female mould directly. The aluminium plate template for the routing operation, was produced by coordinate drilling using a cutter in a milling machine, on about 400 centres. The technique can be recommended, for after moulding, the raw module halves were found to be within about 0.2mm of required size.

4.1.4 Sensym blade: structural design.

The new blade module was similar to the old one, but there were some changes. Basic internal layout and structure remained the same, but this structure was formed of natural fibre material in a polyester resin matrix. Layers of hessian were stippled in resin and built up to the required level. After

curing, all the surfaces of this material were machined to tolerances of about 0.1mm with a router carried on a carriage over the mould. Machining in this way facilitated accurate positioning of the internal features of the module including the fish plate socket, a source of trouble to the first manufacturer and provided a means of effecting gross changes to the module thickness, without necessitating work on the aerodynamic surface.

Skin structure was of six layers, a layer of glass fibre surface tissue, two layers of unidirectional carbon fibre tape arranged at 45° to the span, two layers of tape parallel to the span and one layer of bidirectional carbon fibre cloth, again at 45°. Polyester resin was used for this module, because of time pressure and the new learning time required: no experience of epoxy composites was adequately to hand.

The two halves of the module were held together with 4mm socket countersunk head stainless steel machine screws. Each screw was tightened into a brass cylinder 5.5mm in diameter and length appropriate to the space available, that spanned the chord line, these can be seen in figure(14). Thus, showing in each module surface, are about eighty screw heads. Beeswax was used here to provide an aerodynamic surface, though it must be said that the result was not perfect, due to the slight inaccuracies in the resin surface around each hole preventing perfect cleaning up.

The two halves having been bolted together for the first time, the resulting module was hand scraped to a tolerance of better than 0.05mm of true section from the leading edge to maximum thickness and to 0.1mm elsewhere, using feeler gauges together with templates made on a numerically controlled machine at RAL.

4.1.5 Aerodynamic surface pressure tappings.

It was reckoned that 32 transducers around the chord was about the maximum that could be accommodated in the space available. An even number was decided upon because of a reluctance to having a tapping at exactly the leading edge. This, because of the risk of damage to any equipment projecting above the chord line, with the module open.

Exact position of the tappings in the surface was,

in the spanwise sense, similar to that of the old blade, that is, the transducers were stationed one quarter module span from one end. Unlike the old module, however, there were no secondary or part instrumented stations and figure(17) shows the spanwise positions of the tappings and the flow probe.

In the chordwise sense positioning was a compromise between the need to measure accurately the leading edge suction peak and the need to obtain information about stall events as they convected down the suction surface. For want of a better method, a single parameter was used to select the relative weighting given to the leading and trailing edges. It was first decided how close to the leading and trailing edges it was possible to site transducer tappings. The chordwise position quotients of these two stations were then raised to a power and fourteen intermediate values of raised power evenly interpolated between them, from which the stations themselves were reduced. A power of 0.45 was selected as giving the best compromise of the factors mentioned above, together with a convenient transducer disposition relative to the module's internal structure. Figure(17) shows the transducer tapping positions on a blade section.

The blade surface tappings were effected, using brass tubing of 1mm bore, pressed and cemented into holes drilled or machined into the module's composite skin. Supported by the work of Rayle described in Dean reference(23), the axes of the tapping tubes were either normal or parallel, to the chord line. The first two tappings on each side, back from the leading edge, were effected by cutting a groove parallel to the chord, and of an appropriate depth, and pressing in the tapping tube. Resin and hessian fibre were then used to backfill the hole. Figure(18) shows a hole being drilled normal to the chord line.

Positioning of the machining was effected using a steel tape for the spanwise sense and a vernier caliper gauge for the chordwise coordinate and this can be seen in the previous figure. The adhesive having gone off, the brass tube was cleaned back to the aerodynamic surface and the hole deburred with a very light countersink, as suggested by Rayle. About 3mm of tubing was left projecting on the inside of the blade, so that the tapping could be connected to the pressure transducer. Where necessary on the inside, the internal structure was

cut away, to allow the connecting tubing space. Duct tests described elsewhere, had confirmed that the bends necessary to effect connection, introduced no noticeable effect.

4.2.0 First probe using Kulite transducers.

A practical way to obtain incident flow data is by means of a flow probe. This means was adopted at the earliest stage in the project, since the most common form of probe, that using pressure differences around a suitably shaped body, would fit in well with the pressure measuring equipment to be used on the turbine blade. As with most other parts of the equipment, the difficulties experienced with the early transducers and the change to a different type of transducer forced changes in this area also so that two probes were designed and made.

Figure(5) shows the first probe, fitted with five cylindrical Kulite transducers each of which was just over 3mm diameter. The transducers fitted were, as has been explained elsewhere, recovered from previous work at Cranfield. Unfortunately they were of the differential type, but had had their reference pressure tubes cut short and filled with solder to seal them. No doubt the thermal effect of Charles law contributed to the problems experienced in the early stage of this project and described elsewhere.

The transducers were mounted in silicone rubber adhesive and polythene gaskets were used between the various sections of the probe to effect gas tight seals. In fact it proved difficult to achieve sealing and the probe was stripped down and rebuilt several times before an adequate performance was achieved. This unexpected work on the probe had the effect of producing wear and tear on the very fine wire used to connect to the transducers and some breakages occurred. The resulting repairs were unexpectedly difficult, due to the ptfe insulation and the silver wire, neither of which proved easy to work with.

Overall design of the probe was an attempt to strike an acceptable compromise between disturbance to the air flow around the blade, particularly at non zero values of incidence and distortion of the high frequency content of any change in incident flow signal. The former requires a small probe body, ideally having the transducers inside the

blade, whilst the latter needs them as close as possible to the probe head. In the design of the first probe, a duct length of about 75mm was considered acceptable and so the waisted head probe design was adopted. Other constraints on the design were the need to provide space for fixings, to leave enough material in the body for adequate mechanical strength bearing in mind the centrifugal and angular acceleration that the test programme would impose and the need to provide adequately for wiring. It is felt, with the benefit of hindsight, that proper cable clamp facilities and more attention to wire run considerations, would have saved rather than cost time.

4.2.1 Second probe using Sensym transducers.

The same considerations of duct length versus flow disturbance, mechanical strength, ease of sealing, provision for wire run and ease of manufacture, applied to this probe design. More consideration was given to access and maintainability and is felt to be adequately catered for in this design. Regrettably, it was not felt possible to keep 75mm ducts and these were reduced to the standard 50mm. This obliged the transducers to be immediately behind the probe head and required an unwaisted design of 19mm outside diameter.

It was envisaged that the flow disturbance problem would be avoided by initially using the flow probe to 'calibrate' the leading edge transducers for flow angularity, in other words, a correlation would be established between incidence and leading edge transducer output, and the probe would then be removed. In fact runs up to number 203 were taken with the probe in place and runs thereafter taken with it removed.

Probe head design is an amalgam of designs from references(19), (86), (77) and (66). Whilst these designs are all intended for wind tunnel work, with the implication that they will have small dimensions, the literature claims that they are Reynolds number insensitive.

Ideally for the flow angles experienced in this project, up to 30° of angularity, each pressure tapping in the probe head should have its own transducer, to provide an independent data stream. Because of the tight space constraints and the fact that duct lengths could not then be held to 50mm, only three transducers have been included. Five

transducers would have facilitated data reduction, in particular the provision of a pressure with which to non dimensionalise the flow angularity signals. Without this arrangement a unique solution still exists, but it must be arrived at through an iterative algorithm.

Transducer mounting performance and accessibility has proved to be very adequate: after an early strip down, transducer offsets, a good measure of mechanical abuse and likely to be the first parameter to change after a refit, were unaffected. It is felt however that the new transducer package now available would have considerably simplified design and manufacture. A photograph of the design used is shown in figure(19).

4.3.0 Anemometers and towers.

To supply data on the incoming wind two anemometer towers were built to give wind vectors at two points in the rotor flowfield, upwind of the rotor, as shown in figure(20). Two vectors were used rather than one, to allow assessment of the degree of rotor scale turbulence present in the incident wind. The separation of the two towers from the rotor was the subject of debate, and investigation of the best distance was desired. In the time available however, this has not been possible and the separation used has been decided by considerations of convenience: the boundary fence to the RAL site frustrates attempts to achieve a separation, uniform with azimuth. Described elsewhere in this thesis is a comparison of two runs, one made with anemometer towers one diameter distant from the rotor axis and the other three diameters. There is no noticeable influence by the near passage of rotor blades on the anemometer signals.

Each anemometer tower carried two ducted turbine type, Leda 1000 anemometer heads, manufactured by the Lowne Instrument Co. Ltd of London. The heads, shown in figure(21), were equipped with mica vaned rotors with a distance constant of about 0.3m. On each tower, the heads were mounted 350mm apart, with an included angle between their axes, of 90° and figure(21) also shows this angle being set using a template. Since the response of a head is almost perfectly cosinusoidal, Hobbs reference(83), the wind strength and direction can be obtained from the two signals from each tower, by vector arithmetic.

Tower height was arranged such that the anemometers were positioned level with mid blade. The two towers could be fitted with wheels to facilitate movement between the various required anemometer sites. These latter being surveyed with steel tape and marked with paint on the sealed surfaces around the tower, or with stakes in the ground elsewhere. The towers were designed and made in house by the author to withstand 25m/s winds without ballasting.

Output from the anemometer heads was communicated to the rotor slipring ground terminal box, described below, via a screened cable. The output was in the form of a TTL pulse train whose frequency was directly proportional to the axial component of wind strength at the tower. The two pulse trains were, for convenience, converted into analogue voltages by a signal conditioning box on the rotating instrumentation rack described below. A counter, fed an anemometer pulse train, was reset to zero every 0.1 seconds. Its count was fed to an eight bit digital to analogue converter, sample and hold chip and amplifier combination, set to give 4.500V with an input pulse frequency of 1000Hz corresponding to a wind speed of 25m/s. The sample and hold circuit was enabled just before the counter reset and so held a constant value of wind analogue relevant to the preceding 0.1 seconds, (in fact the time average wind over that period).

4.4.0 Rotor torque measurement.

Measurement of rotor torque is one of the few checks that are available on the aerodynamic data coming from the blade. The chordwise component of blade force should appear as rotor torque, allowing for the effects of aerodynamic drag on the blade and rotor and frictional torque loss in the rotor drive system. It was considered important then to attempt to measure rotor torque and record it.

Torque measurement was accomplished by using the force block already installed in the drive system belt wheel at the bottom of the rotor shaft and described by Stacey reference(88). The rim of this wheel was connected to the centre by ball races for location and by the force block transmitting torque. The block was a strain gauge device requiring excitation and amplification. Excitation power was obtained from the 5V supply on the sample and hold boards described below, this being a stabilised supply, and amplification was

achieved using one of the fast amplification channels as described in the signal conditioning section below. A non standard amplification factor of approximately 2000 was required for this.

Calibration of this torque transducer was accomplished by jamming the rotor drive motor pulley with a sash cramp and pulling tangentially on one blade with a spring balance. Positive torque was defined as that tending to increase rotor speed.

In fact during the experimental phase time pressure prevented adequate monitoring of the torque transducer status with the result that the signal was unreliable and prone to go out of range of the data logging system and has not therefore been included in the present work.

4.5.0 Rotor drive system.

Originally an automotive starter motor was used to start the machine and wind power to run it, but this was found to be inadequate and was improved. A 4kW induction motor was already present on the machine and this was mounted properly and a suitable belt ratio fitted to drive the machine at the required speed of about 120rpm, once it had been established that the motor was adequately powerful by tests at a lower speed. The battery start system was found to unreliable and a star delta switch system was fitted, that could be operated remotely from the turbine control cabin.

An improvement was also made to the rotor tachometer system to allow measurement at the new high speeds.

4.6.0 Signal conditioning and data logging scheme and equipment.

Analysis of the rotor blade load pattern and flowfield aerodynamics, demands considerable detail in the recorded data. The implication is that a large number of transducers will be needed and that the many data streams that they generate, will need to be recorded either continuously, or at least often enough to discern sub chord scale detail. For this project, of order forty transducers were considered necessary, with the signal being recorded at least 250 times per revolution.

With the large number of transducers and data streams required, it would be very expensive to record data simultaneously and continuously. Initially, it was decided to tackle the problem by having two schemes of recording. In general, signals from all transducers would be recorded by sampling them and recording the samples. The samples would be taken using sample and hold circuits, triggered simultaneously, from an optical disc on the rotor. Thus they would be at regular intervals of azimuth, allowing better binning and averaging techniques to be applied.

Two data logging schemes were investigated, an analogue scheme using an FM tape recorder and a digital using a micro computer driven intelligent data logger. In the former scheme there was facility for both the multiplexed recording of sampled data at regular intervals of azimuth, at 256 stations per revolution, and continuous recording of eight signals of interest. Digital techniques, by their nature, are only capable of sampling signals of interest and in the latter scheme only provision for azimuth locked data sampling was made, again at the rate of 256 samples per revolution. However the logger was very versatile and should it have proved necessary, could have been configured to record a smaller number of data streams at a higher rate.

4.6.1 Analogue scheme.

The initial intention of this project was to use a two stage process to obtain digitised data for final computerised reduction and analysis. An fm tape recorder was to be used to take data in an analogue format and the recordings were then to be processed by the Signal Processing and Analysis Group at CIT, to generate digital data for transfer to mainframe computer.

The signals from the transducers were to be amplified, anti-alias filtered, sampled and held, and then multiplexed on-rotor. They were then to pass through slip rings, to the tape recorder on the ground. The multiplexers were to reduce 48 on-rotor data streams to 8, including two spares. A complicated spaghetti of logic, multiplexers and digital to analogue converters, dealt with other signals, including anemometers, rotor torque and the number of rotor revolutions from the beginning of testing. The fourteenth tape recorder channel was to be used as a voice channel for verbal

comments, in addition to which, a continuous tone was to be recorded when the experimenter considered the wind to be of the required condition.

The anticipated problem with this scheme was concerned with the signal to noise ratio which could be expected from the tape recorder. The industry standard for such machines was 48dB, or about one part in 150. As has been outlined in the section on transducers, the pressures that are of interest to this project, span a range of perhaps 1000 to one. Therefore it would have been necessary to have amplifier gains tailored to each transducer, if the strong signals were not to swamp the recorder whilst the weak signals were not to be so noisy as to be useless. This would have introduced an element of uniqueness to each channel, which we would have preferred to have avoided.

One further effect would have had a more serious implication in connection with signal to noise ratio, barometric effect on transducer output signal. As has been stated in the transducer section, barometric pressure varies by several percent, perhaps 3kPa and does so especially in times of high wind. This is then several times the benchmark pressure of one dynamic head, based on blade air speed. To accommodate this, the amplifier gains on the low pressure signal channels, from the trailing forward to the 30% chord position and for the probe transducers, would have had to have been cut by a factor of three. This would have eroded the signal to noise ratio.

This discussion has so far ignored the effect of temperature on transducer output. From the results of the temperature and consistency tests, further large signal excursions were to be expected. These would have required further cuts in amplification and hence further erosions of signal to noise ratio. The inevitable conclusion was that the analogue system would have given an inadequate quality of data and further interest in this method therefore lapsed.

4.6.2 Final signal logging scheme: general outline.

Because of the difficulties over the signal to noise ratio outlined above, the reliability of the analogue scheme in general and the cumbersomeness of the scheme for recording and digitising the episodes of good wind it was decided to seek a

digital recording technique, the price of these having come down dramatically since the start of the project.

Three systems were examined, from which one was selected, manufactured by Cambridge Electronic Design, of Cambridge, UK. Their '1401' model was supplied with custom software on ROMs and floppy discs, together with a 96 channel single ended input multiplexer (the '1605') and BBC micro computer with second processor, double disc drive and other peripherals. Two interface boxes were also supplied, one to communicate with the BBC via the RS423 serial port and the other through the 1MHz parallel bus also on the micro. The 1401 was equipped with a 2 Mbyte mass RAM enabling it to store one million readings, about 40 seconds of recording, at the rate used in the project.

Advantage was taken of the vertical axis configuration of the wind turbine, which facilitated mounting the data logger on an instrument rack at ground level and rotating with the rotor. The rack is shown in figure(16). On this rack also, was mounted all the signal conditioning equipment, resulting in a neat self contained arrangement, as detailed below and shown schematically in figure(22).

In the data logging mode the incoming wind was measured by the anemometers, as described elsewhere. Signals from these anemometers were brought to the ground based signal slipring terminal box, passed in pulse train format through the sliprings to the anemometer signal conditioning box described elsewhere. Here it was converted to analogue format and the signal split into two. One path led up to the main amplifier box on the rotating rack, to be fed into the data logging system, whilst the other was passed, in analogue format, back to the sliprings and then through a cable, down to the turbine control cabin, about 150m distant, from where the experiment was controlled by the BBC micro computer.

In the control cabin the analogue signals were conditioned in another box to a voltage suitable for reading by the BBC micro's analogue to digital converter, suitably modified. Running in the micro, was a program, again described elsewhere, included within which was a loop which looked at intervals at its A/Ds and hence the instantaneous wind strength. A simple window test was used wherein if the instantaneous wind were within a previously set

window, the 1401 data logger could be enabled by a signal, the 'GONOGO', from the micro's user port. The micro's VDU displayed all the current relevant parameters, including the instantaneous wind speeds from the four anemometer heads, the set window and the 1401's status.

Thus having started the turbine with the required configuration of blade leanout etc, and having set an appropriate wind speed window for the current wind, the system would be armed and would then wait for wind inside the target window. On receipt of such wind, the 1401 would automatically start taking data for a pre determined number of revolutions, eight normally, irrespective of the subsequent wind pattern. At the end of this period the wind would be examined again until it again met the criterion, whereupon logging would start again. This process was repeated until the 1401 RAM was full.

To download data, two schemes were available, the original serial method and a faster parallel method. The former method used the RS423 protocol used to communicate commands and responses between the BBC and the 1401, and was convenient in that the micro did not have to be moved, but was very slow, some three hours being required to download the 2 Mbyte RAM. The normally used alternative was to move the micro after having stopped the turbine, to the rotor hut and establish the parallel link, which worked from the micro's 1MHz bus. Using this route, data down loading could be accomplished in about half an hour. One RAM full, about 40s or 80 revolutions of data, required six double sided single density 5.25" floppy discs.

The 1401 was arranged to take data, as has already been indicated, in 256 samples per revolution format. However, as has been indicated in the transducer section, two signals are required to be recorded per transducer, one the quickly changing pressure signal and the other the current drawn or temperature signal. This latter changes relatively slowly and so to economise on the quantity of data recorded, two rates of recording were used 'fast' and 'slow'. The fast streams were taken at the 256 per revolution rate and the slow at one per revolution. The logger had the capability of accepting 48 fast and 48 slow data streams. Both were controlled by the optical disc signal. The 256 pulse train was also fed to the amplifier box and there drove the sample and hold circuits.

4.6.3 Rotating instrument rack.

Most signals of interest in this project originated on-rotor. In early tests with on-rotor mounted transducers trouble had been experienced with cross talk between channels occurring because of very low (2kohm) resistance between slipring channels. These latter were designed for high speed operation with air blast cooling and without this debris from brush wear had built up, leading to the loss of performance. Because of these factors it was decided to mount the signal conditioning and data logger equipment on-rotor. This would allow unbroken connection right through the data chain right up to the logging equipment, all moving as one.

Figure(16) shows the final arrangement. A stub shaft was mounted just off the floor on a cross beam from the existing machine chassis. On this sat a bearing which carried the instrumentation rack made of 80mm square steel tubing and 18mm plywood. Connection with the rotor shaft was effected with a flexible joint just under the rotor bottom bearing. In use the arrangement has worked perfectly, though it must be said that observation of the machine when working is not for the faint hearted!

At the top of the rack is the main signal conditioning box arranged so that access to each and every contact pin and solder joint is extremely easy, something that has proved invaluable. Below this is the multiplexer box and the data logger and below again the signal and power sliprings for communication with the outside world. Below these is the optical disc mounted stationary on the stub shaft and its sensor mounted on the rack. Around the slip rings and optical disc equipment are, a terminal box for the signal slipring channels, the transducer power supply and power supplies for the main amplifiers, a conditioning box for the anemometer and optical disc signals, 240v ac sockets for the on-rotor equipment, and a step up transformer for this mains power supply. Mounted on the stationary support of the stub shaft were two boxes servicing the rotating rack, these were a step down transformer for the mains power supply and a terminal box for the signal sliprings, arranged exactly like that on the rotor.

Low voltage was used in the power sliprings for safety since they were made in house, but the isolation arising from this allowed the on-rotor

power to be center tapped to earth, further providing safety and reducing mains noise slightly. On-rotor power demand was about 100W.

4.6.4 RAL system earthing.

Substantial effort was expended to eliminate loops in earth and other system cables and was very successful at providing a low level of measured noise. On most signals, noise was of order 5 mV or less, about 0.5% or less of the voltage typically developed by the benchmark dynamic pressure. Briefly the outer instrument cases were earthed locally whilst the signal ground was earthed by the micro computer. Blade transducer power supply was grounded to the amplifier ground.

4.6.5 Signal conditioning equipment.

Signals from the transducers are derived as has been described in Chapter 3. They were transmitted to the amplifier box via nine 18 way screened cables. The wires passed from instrumented blade, through the trailing edge cable ducts, the rotor cross arm, the rotor shaft, and the bottom bearing, to the amplifier box, a distance of about 10m. Constrictions were very tight in several places en route, preventing any cable connectors being used anywhere and so the cables were soldered directly to the amplifier boards. Also the smallest available cable was used, ten by 0.1mm cores. The inconvenience caused by these constrictions, was considered to be unsatisfactory.

The amplifier box contained conditioning equipment for 80 data streams, of which 77 were used. As has been described above, signals were classified into and handled in two ways, those digitised 256 times per rev and those digitised once. There was amplifier capacity for 48 fast channels and 32 slow on a total of five amplifier and five sample and hold boards and table(5) shows the wiring and amplifier schedule. Signals arose from the 32 pressure transducers inside the blade, three transducers inside the flow probe, the two module half's transducer excitation voltages, four anemometers and the rotor torque.

An Analogue Devices AD524 instrumentation amplifier was set to a gain of ten for all data streams except the anemometers and the blade excitation voltages, where unity was used. Output from here

went to an OP07 operational amplifier with gain resistors set to a nominal gain of 50, except in the case of the anemometers, blade excitation voltages and the torque stream, where the gains were unity, unity and 200 respectively. Figure(23) shows the circuit diagram for the amplification, anti-alias filter and sample and hold chain.

Up to this point all data streams have been handled in the same way, but with the transfer from the amplifier boards to the anti-alias and sample-and-hold boards, the fast and slow streams were processed differently. Slow channels were fed into 741 operational amplifiers configured as first order low pass filters with a corner frequency of 500Hz, whose purpose was to provide some resistance to aliasing and a reduction in rf noise. The outputs of this stage then went directly via twist and flat ribbon cable to the 1605 multiplexer just below the amplifier box. Fast channels had the same treatment, but before going to the multiplexer, were fed into Matra Harris HA2425 sample and hold chips.

Sample-and-hold or track modes of these latter chips were controlled by OR gates on each board. One input to the OR gate was obtained from the optical disc conditioning box and the other from a DIL relay, also on each board. This relay was controlled, via the sliprings, cable and control cabin conditioning box, by a line on the BBC user port, the SAMPLE HOLD/TRACK signal. Thus the micro could control the sample-and-hold mode; this was felt to be a safer and more versatile method than a switch on the rotor in that a line in the control program, running in the micro, dictated the state of the sample-and-hold circuits.

For the two transducer excitation voltage conditioning amplifier chains it was necessary to calibrate their characteristics by applying sequentially a zero voltage and then a known voltage, about 3V to the amplifier inputs. The calibration program C/24 was run to record the resulting readings appearing at the 1401.

4.6.6 Optical disc signal conditioning.

The 1401 data logger required two pulse trains for operation, a once per rev and a 256/rev pulse and it was sensitive to the negative edges of these. Additionally, at the once per rev position, the two edges were required to be synchronous and so the two raw pulses were gated together to ensure this condition. Trouble had been experienced earlier with circuits employing monostables to give short pulses and so these were avoided after having ascertained that the 1401 had enough time to finish its logging, before the sample and hold circuits were re-enabled.

Calibration of the optical disc position, that is the position of the once per rev pulse (1ppr) relative to the anemometer reference direction, was effected by first inserting the rotor shaft locking dog fully into its slot, this being taken as the rotor's 'home' position. The optical disc was then rotated on its mounting until the once per rev signal line was on the point of its negative going transition, this being then the standard position of the disc. The dog was then removed and the rotor rotated until its cross arm was parallel with the RAL site fence, the anemometer reference direction, this being done using surveyed anemometer marks on the ground. Output from the 256ppr line was then fed to a resistor ladder, the output from which in turn went to the BBC analogue input. A short BASIC program then counted line transitions as the rotor was turned back to its home position.

4.6.7 On-rotor low voltage power supplies.

Three Farnell model 144-010 adjustable regulated power supplies were fitted to the rotating instrument rack and drew power from the on-rotor mains supply. One unit provided the pressure transducer excitation and was set either to nominally 3.0 or 1.5V. The other two supplies were used for positive and negative amplifier power. Initially these had been set to +7.5V and -7.5V, because of the sensitivity of the 1605 to overvoltage, but after having proved the system, this was increased to +10V and -10V.

Trouble was experienced with these supplies when the rotor mains voltage dropped to around 210Vac. In such conditions the PSU internal supply was inadequate and large ripple was observed on power output which resulted in much poor data early in

the programme. This shortcoming was cured by changing the resistor supplying the band gap reference. The supplies were also reluctant to give more than 800mA and another resistor in the current sense circuit needed to be changed to correct this.

4.6.8 Control cabin signal conditioning box.

A box was fitted at the end of the 150m cable to provide suitable connection with the BBC micro. The RS423 connection was straightforward, but the user port required the circuit and power supply (which was fitted inside the box) to isolate and buffer the lines controlling the 1401 GONOGO signal and the SAMPLE HOLD/ TRACK signal. The micro A/D input, used for anemometer monitoring, also required a change of circuit of to improve the stability of reading and to suitably scale the anemometer signal conditioning box output.

4.6.9 Data logging process.

Data logging with the 1401 was controlled by a set of commands which could be sent via either the serial or the parallel interfaces. The commands included the existing standard 1401 commands plus six new ones able to arm WNDML, the special logging command, disarm it, interrogate as to status, download data via the serial interface and run a special calibration routine. This latter read all 96 inputs a number of times, set by a parameter in the command and recorded the average, the maximum and the minimum for each of the channels. The routine took about 1/80 second to execute once and was usually executed 80 times to give an idea of the noise present on the system.

The WNDML command was stored on ROM in the 1401 and was written in assembler code for speed.

The sequence of events which took place for a logging sequence was complicated but was briefly as follows. A WNDML,G command would be received from the BBC which would arm the 1401 and start the ROM based code running. At the next once per rev pulse applied to the EVENT0 input, the 1401 would check the status of bit15 of its digital input port, the 'GONOGO' signal and if low, no further action would take place. However, if high, the logger would note the time on a 500kHz clock and digitise the first six analogue channels, storing the results in order in the mass-RAM. A new address would then be sent to

the 1605 multiplexer, presenting six new channels to the 1401 and these would then be dealt with in the same way. this would go on until the first 48, the fast channels, had been recorded, the first slow channel was then digitised by setting an appropriate address on the 1401 digital output port for the 1605 as above, the result being stored as before, in order.

The next pulse received from the optical disc conditioning box would be on the EVENT1 input and would trigger a very similar procedure, except that no check would be made of the GONOGO signal before again reading the 48 fast channels. The time would again be read and the interval between this and the last event pulse recorded in mass-RAM and the second slow channel would then be read on this the second event pulse.

After 48 event pulses no more slow analogue inputs were read, but on the 49th pulse, the time would be read from a 1Hz clock, reading from the time of the issue of the WNDML,G command, enabling a 'date stamp'to be associated with a particular rev of data.

Logging of fast data would be repeated until 256 snapshots of data had been recorded and the next pulse would be a once per rev pulse again, with or without a GO signal on BIT15. Each snapshot required 100bytes for 50 readings: 48 fast channels, 1 slow channel and the time interval since the last snapshot as a record of nearly instantaneous rotor speed.

Timing of the sample and hold circuits, came from the 256 pulse per rev line of the optical disc signal conditioning box. The sample and hold chips were arranged to sample with this line high and hold with it low, by using an inversion stage on the circuit boards, since the chips themselves show the opposite characteristic. The 1401, connected to the 256ppr line through its EVENT1 input was sensitive to negative going transitions of the line. Thus as the line went low, samples would be held and the 1401 triggered to take a snapshot. A scan through the 96 channels took 870 µsec and so it was necessary for the 256ppr line to stay low for at least this time, to ensure that the recorded data was all from the same pulse. This was determined by examining the voltage present on the line when in the low and the high states and when running, the latter voltage being a time weighted average, from which the mark space ratio could be

determined. It was found to give ample time for uncorrupted data to be taken.

CHAPTER 5

WIND TUNNEL TESTING EQUIPMENT AND METHOD

5.0.0 Introduction.

Wind tunnel testing of a representative blade section from the project test turbine, was considered to be an important part of the whole programme. Little surface pressure data for the NACA 0015 section exists at the Reynolds numbers experienced in the atmospheric experiments and less yet exists for 0015 under dynamic stall conditions. The object of the present series of tests was to establish data for the section of interest under known and controlled conditions of dynamically varying incidence. The ability to test the actual blade module itself in both atmosphere and tunnel, has been a unique opportunity to examine the correlation between the unsteady aerodynamics of the two environments.

As will be described below, the tests consisted of mounting the instrumented blade module from RAL, in the Glasgow University 'Handley Page' wind tunnel. References(32) and (81) describe the mechanical and data logging arrangements of the Glasgow facility in more detail. The blade mounting in this facility has the power to change blade incidence rapidly by the use of a servo hydraulic system, this in turn controlled by a Commadore PET micro computer running a machine code program.

Tunnel working section speed was measured by means of a pitot static tube positioned about one chord upstream of the blade and towards the side and floor of the tunnel.

Transducer output was conditioned by the same amplifier and signal conditioning array as used at RAL and recorded both by the same 1401 data logger system used at RAL and the usual resident system at Glasgow. The latter was used to record the rapidly changing signals of aerodynamic interest for later analysis, whilst the former recorded the transducer temperature or drawn current signals. This approach was required because the Glasgow system had signal handling capacity for only 30 data streams whilst the RAL blade generated 72.

The different data handling method and the different conditions in which the transducers were used, required a different approach to the method of interpreting transducer signal output and effecting temperature compensation from that which had been used at RAL. Fortunately the compensation problems were substantially easier to solve because of the very much shorter time scale and the much more controlled conditions, involved in these tests.

Four waveforms of blade incidence versus time, static, sinusoidal, vawt and ramp, were used in the tests and, combined with variations of tunnel speed, swept angles of incidence and frequencies of oscillation, made for a programme of some 120 test runs.

Data from the experiments was reduced by the standard Glasgow system, into a preliminary form for checking and later with revised coefficients and offsets, into its standard Glasgow format. It was later transferred to the system used for the atmospheric data, so that comparison between the two data sets, ie the tunnel and the atmospheric, was facilitated.

5.1.0 Hardware.

The wind tunnel working section is approximately 1608mm from floor to ceiling and is thus slightly bigger than the length of the 1500mm long blade. To fill this gap, two cuffs or extension pieces were made of glass fibre material. Special fish plates were made up to connect with the blade, using the sockets in the blade ends. These finished at the ends of the cuffs to make the correct length blade. The ends of the fish plates were equipped with discs, suitably shaped and drilled to mate with the Glasgow standard fittings. Felt was used on the ends of the cuffs, to effect an air tight seal with the wind tunnel floor and ceiling. The gap between the instrumented module proper and the cuffs, was filled with beeswax, but it was suspected that the severe shaking that the blade experienced during setting up may have reduced the effectiveness of this fill. Other holes in the blade surface were filled with beeswax also. Figure(24) shows the blade being mounted in the wind tunnel.

The cables connected to the blade instrumentation, were led out through the the bottom cuff and then down through the lower support tube to the outside

of the tunnel. The silicone rubber tubes conveying blade reference pressure, were also led out by this route. Throughout the wind tunnel tests, the ends of the reference tubes were left open to the atmosphere in the tunnel building. A ring of holes is present in the tunnel walls, floor and ceiling at the downstream end of the working section, to ensure that the pressure in the tunnel is the same as that outside, in the tunnel building.

As has been stated above, the same amplification and signal conditioning arrangement was used at Glasgow as at RAL and so the connecting cables were soldered to the amplifier boards in exactly the same pattern. Power supplies and voltages were also left untouched for all tests, except those on the last day of testing, when the blade excitation voltages were lowered to approximately 1.5 Volts to avoid problems of overranging. Only one other change was made in the connection schedule and concerned the connections of the screening of the blade connection cables mentioned above. Connection as at RAL produced so much electrical noise on all channels in the amplifier box, that the signals were unusable and several days were wasted discovering that disconnection of all but two of these screen connections, resulted in lower noise levels than were present at RAL.

Optimisation of the earth connection scheme was also very time consuming (~2 weeks) and during the setting up period some damage was done both to the BBC micro and the 1401, requiring adaptation of software and finally repair at CED. The final scheme involved an unavoidable earth loop, but as has been stated, the final electrical noise level was very acceptable.

A special harness connected to the Glasgow system to enable the required signals to be tapped off from the back of the 1605 multiplexer box. Table(6) shows the connection schedule and the arrangement of the transducers and blade surface tappings used. Signals fed to the Glasgow sample and hold box, the first in the Glasgow system, were thus at a 5 Volt full scale level and no further amplification was necessary.

5.2.0 Transducer calibration and temperature compensation.

Calibration of the transducers, the establishment of their characteristics (ideally the same as at RAL), was carried out in exactly the same way as for the atmospheric experiments. Pressure was applied to the reference lines and to a line connected to the usual flow probe incidence port and the code C/24 run. Additionally the code RDADR++ was run at intervals to check on the health of the system.

As has been stated above transducer signal output required new handling. The Glasgow system assumes a constant transducer sensitivity, that is voltage output for a given pressure input, whereas the Sensym transducer as here used, has a variable characteristic with temperature, though the change is only a fraction of a percent per ^{o}Celcius. Progress was made by running the tunnel for a period of 45 minutes or so, until tunnel air temperature had reached a typical experiment value of about 29^{o}C. The tunnel was then stopped and either the code RDADR++ run with two different pressures, giving two sets of output voltages from which the sensitivities were calculated, or the code SENS run, which automated the process.

Zero pressure offsets were dealt with by the standard Glasgow method: the offset was logged immediately before a run with the wind off and the resulting offset values then subtracted by the Glasgow reduction software. This then allowed preliminary results to be produced. However records of the pre run offsets and transducer temperatures were also taken before every run, using the C/24 program. Final data produced from the Glasgow tests has been produced using the raw data as taken, together with the sensitivities and offsets derived from the computerised characteristics routines as used for the RAL data. Checks were made of the temperature drift during a run by using C/24. Changes in temperature and thus sensitivity and offset were usually insignificant, though during runs at the highest tunnel speed, some drift did occur.

CHAPTER 6

DATA TRANSFER, PROCESSING AND REDUCTION

6.0.0 Introduction.

Data presented in this thesis has all been reduced and presented using microcomputers, despite the initial intention that mainframe computing be used. This chapter describes the significant details of the various codes that have been used in data taking and reduction.

6.1.0 BBC micro computer software.

Several pieces of code were written in 'HI BASIC', for use on the BBC micro computer, to log and download data and to calibrate and debug the system hardware.

A self documenting program was supplied by the logger manufacturer CED, as an example program of how to use the especially written WNDML commands. The program was able to arm the 1401, take data as described elsewhere and download via the serial link, onto floppy discs. It was very slow however and there were other shortcomings.

6.1.1 Data logging software, W/24/10.

As had been intended, an enhanced program was developed in house, which extended the power and control of the original CED example program.

The BBC VDU display was developed to carry all the main parameters important whilst running the turbine. The 'good wind' testing procedure was written in and the necessary commands for the user port and second processor researched and applied. Serial downloading was improved and ways found of efficiently combining all data streams into one, to allow packing onto a reduced number of discs. The format of these files was made compatible with the KERMIT software used to transfer data to the RAL VAX and with the VAX itself. Considerable familiarity was required with both the BBC micro and the 1401, to allow these developments.

An interactive section was inserted into the program, which enquired of the operator many parameters of importance, not automatically recorded. These were all bundled into a text file, which also allowed experimenter's comments. Thus only two files carried 8 revolutions of data, this filling one disc side. In this scheme, data was arranged as one concatenation of the data stream files, first the slow in order, then the fast and finally the text file. Downloading was still slow however, taking about three hours to transfer 80 revolutions.

6.1.2 Parallel data downloading program, P/24/10.

A second enhancement phase developed a code for data transfer by the parallel interface and this required about 30 minutes to complete the task. The disadvantage of this approach was that the BBC micro had to be disconnected from its station in the turbine control cabin and placed close to the rotating instrument rack in the rotor hut, the rotor having been stopped for the downloading procedure. At the end of downloading it had to be replaced in the control cabin and the many connections remade. The continual making and breaking of the connectors was a source of concern, but the process was eased by the construction of a portable rack to house the micro and its peripherals.

Using this software, only seven revolutions of data would fit onto a disc side, because of the way in which the 1401 stored data in the mass-RAM and the way it could conveniently be written to disc. A direct copy of the mass-RAM was transferred to disc, working in blocks of 12800 bytes at a time, in this method. A means, was devised, of transfer of the 'GO' date and time from the BBC to the 1401, before the former 'forgot' it due to being moved to the rotor hut.

6.1.3 Transducer calibration software, 'C/24'.

A second writing and development phase, in parallel with the above, was used to generate a program for the calibration of the pressure transducers. The program was also used to calibrate rotor torque, anemometer signal conditioning, and transducer excitation voltage signal conditioning.

The program, written in house, essentially issued

the WNDML,C command, and wrote the results to disc. It had a similar interactive enquiry section to that in the data logging program, in that a section of text containing otherwise unrecorded information, including experimenter's comments, was written to disc. The two sections did however, form only one disc file.

Contained in the disc file name was the identifying 'run' number, calibration procedures occupying the same sequence of run numbers as the main experiments. Also present was a sub number, identifying the particular data stream scan concerned.

The program had two modes of operation: an automatic scan of all data streams and recording of results, at a regular interval of time, and an interactive mode, in which scans were taken after the experimenter had set up a particular condition of input pressure or some other parameter, the scan being initiated manually. Automatic scanning was provided to facilitate the establishment of the transducer zero offset characteristic for each transducer. It was required that this characteristic be known with considerable confidence, implying that the scan be repeated a large number of times throughout a wide range of temperatures. In practice, in order to capture the range of temperatures required, calibration scans were executed from morning through to late at night.

6.1.4 Hardware debugger, RDADR++.

One other, very short program, has been used a great deal, a program which runs a data stream scan as above, but only prints the results on paper. This has normally been run before any other to check on system health and to facilitate repair and debugging of the hardware. A record of these has been kept as a back up to the C/24 program above.

6.1.5 Other BBC code.

Some other programs were written to perform special tasks, the largest was a program written for use at Glasgow to produce a list of transducer sensitivities from the results of a series of data stream or calibration scans. Other codes were produced and used to check particular aspects of the data transfer process, for instance that the

C/24 program faithfully reproduced calibration data on the disc.

6.2.0 Archimedes data reduction code.

The coding DATPROC was used to reduce and present the results shown in this thesis and runs to nearly 3500 lines in BBC BASIC V5.

Routines are provided to plot out wind data. The program allows raw calibration data to be compiled into appropriate sections, calibration fits to be applied to this data both for temperature and pressure effects, fit quality to be assessed on screen, and the calibrations to be used on the atmospheric run data. All atmospheric run data has been analysed and about 40 parameters summarising each revolution of data have been compiled. These have been used to allow ensemble averages of revolution data to be produced. Wind tunnel data has gone through an abridged process wherein pressure coefficient data has been produced using a mainframe computer at Glasgow and the present code is used to convert this data into standard atmospheric format by interpolation ready for plotting by the same routines as used for the atmospheric data.

6.2.1 Supply voltage correction.

As detailed elsewhere, available in the data from the aerodynamic tests, are records of the in blade transducer power supply voltages: these are used in the present code to correct all signals coming from the transducers on a linear basis. Two power supply systems were used in the present blade for reasons of reliability and convenience xiteP and xiteN. Since these signals themselves pass through a stage of amplification to isolate and buffer them from the data logger, they have corrections in the form of gain and offset coefficients, which were determined in a 'once and for all' calibration.

6.2.2 Sets

This term is used to label the set of calibration spots that are used in the calibration coefficient fitting routines. The concept allows for the possibility of rogue spots by permitting these to be omitted from a set used for calibration purposes. The present code does not facilitate the

omission of existing spots, omission can only be achieved by non inclusion during set building. During the present study no spots were omitted from the calibration data.

6.2.3 Coefficient fitting.

Coefficient fitting in the present code is performed in two stages. The set is scanned to produce an array of spots of zero applied calibration pressure and these have coefficients of 'offset' fitted to them; there are individual coefficients for each transducer. In the present work only first order fits have been applied to these data after difficulties were experienced in early reduction with calibrations of inadequate temperature span, leading to extrapolation errors.

Using the above offset coefficients, the program goes on to predict the offset for each of the non zero applied calibration pressures using 'vicorr' the corrected transducer temperature signal. Subtracting this prediction from the actual corrected transducer output 'vocorr' leaves the effect of the applied calibration pressure, which in turn can be used to derive an expression of transducer sensitivity [volts per Pascal]. Finally these sensitivities are fitted against the transducer temperature signal to produce the sensitivity coefficients, one set per transducer. Again in the present work, only first order fits have been used for sensitivity.

6.2.4 Constraint to RDADR data.

Lack of funding at one stage prevented adequate calibration of the transducers over a period during which several experimental runs were made. Existing calibrations made several months later were found to be inadequate and so an additional routine has been included into DATPROC to allow data recorded by the RDADR++ routine, described above, to be used. The assumption has been made here that transducer zero pressure offset is volatile for present purposes, whereas sensitivity is not. The routines therefore take the RDADR++ data as a good record of transducer offset on the day of the experimental run, determine the expected offset from the best available calibration coefficients and then adjust these latter to give agreement with the RDADR++ data.

The polynomial fitting routine used in the present code, has been taken from Lee and Lee reference(47) and can be recommended.

6.2.5 Azimuth handling and the 'display frame'.

Determination of the azimuthal position of the rotor relative to the wind is complicated because of the turbulent nature of the wind. The present code uses a two stage process to establish several estimates of the wind direction at three points during a rotor revolution.

An initial estimate is made from the recorded anemometer configuration and the anemometer data recorded during the revolution being reduced. Figure(20) shows the anemometer configurations used. The convention used to describe rotor position relative to the wind was that zero aerodynamic azimuth occurs when the blade is moving exactly upwind.

Having obtained a preliminary estimate of wind direction from the anemometer data the array of 321 by 32 (or 35 if the flow probe data were processed) transducer measured pressures is calculated. Here the reduction process is carried out on data starting from a position 45° or 32 data frames before the anemometer wind direction, in order to ensure that the true aerodynamic start of the revolution is captured, whatever the angular wind turbulence (within reason).

Leading edge pressures are then tested to find crossings where stagnation point crosses chord line. Starting the 'display frames' 32 before the anemometer expected start of revolution position, implies that the wind will be blowing onto the inside of the blade, so the code is set to detect the display frame number when this case no longer holds then noting the rotor azimuth. After a further revolution the same geometry will apply and a second note of start of revolution display frame is made. In between, the blade has experienced a reversal of incidence and this crossing point is also noted giving three stagnation point crossing wind direction estimates.

6.2.6 Aerodynamic and ground based start of revolution positions.

Data recording was based on a flag wheel fixed to the ground and so recorded revolutions of data started at random positions relative to the wind direction. The convention which has been used in the present reduction code is that the display revolution is started somewhere between the start of the second half of the ground based revolution preceding the revolution number of interest and the end of the first half of the ground based revolution of interest bearing the same revolution number. This is done so that the majority of a revolution of aerodynamic data comes from the ground based revolution of the same number.

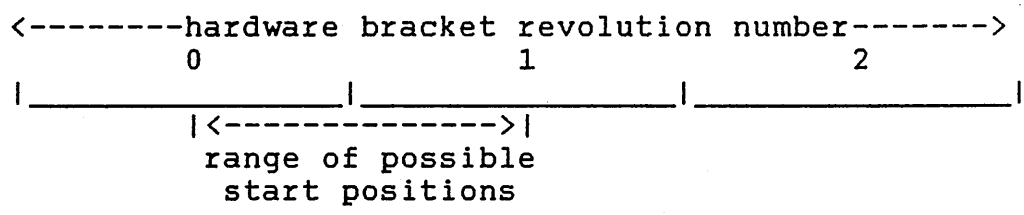

6.2.7 Stagnation point fitting.

For each azimuthal data taking station or data frame, the code fits a fourth order polynomial through the observed pressures of the three tappings on either side of the maximum. The method of bisection is then used to establish the fitted maximum and its position.

A second stage of curve fitting is used to provide smoothing of both the fitted maxima and their positions, by fitting tenth order curves to the arrays of both for each revolution. Figure(25) shows an example of data for an average turbulence revolution. The data is used in several ways as descibed below.

6.2.8 Stagnation point position based turbulence.

Stagnation point position is used to provide a measure of the rotor flowfield turbulence by summing the difference between the smoothed values and the fourth order fit derived stagnation point position described above and calculating an average value.

6.2.9 Stagnation pressure based turbulence.

Stagnation pressure is used to provide a measure of the rotor flowfield turbulence by summing the difference between the smoothed values and the fourth order fit derived stagnation pressure and calculating an average value in a similar way to the position based turbulence.

6.2.10 Stagnation pressure based wind speed.

Anemometers distanced two or three rotor diameters upstream inevitably measure wind a time interval equivalent to perhaps four rotor revolutions ahead. Determination of the time of flight correction that is necessary, in order to look at the correct section of anemometer record, is a daunting task and has not been attempted in the present project. It would appear further, that because of the high turbulence in wind at ground level especially at this site, low correlation in wind speed exists between two points one upwind of the other, at any supposed delay.

To overcome these time of flight problems the present code uses a wind speed based on the maximum and minimum dynamic pressure experienced by the instrumented section of the blade as it moves through a revolution plus its knowledge of the barometric pressure and air temperature.

To prevent turbulence unduly affecting these maxima and minima, the fitted smoothed data described in section 6.2.7 is used.

6.2.11 Summary building.

To facilitate the analysis of the atmospheric data DATPROC calculates about 35 parameters related to windspeed and angle, maxima and minima of blade forces and when they occur, turbulence levels, anemometer readings, rotor speed and air temperature and pressure.

These parameters are recorded onto disc and are available for plotting using the graphics drivers. Additionally they are used to sort revolution data into refined classes for analysis. Sorting may be on any combination of parameters of any values.

6.2.12 Average revolution building.

Using the summary data detailed above, the program is able to access sorted sets of revolutions and to produce ensemble averages of all the revolutions in each class.

6.2.13 Glasgow data frames per cycle.

Consistency with atmospheric data presentation requires lead in and lead out data. To provide this data, data corresponding to the same cyclic position has been used, justified because the data is ensemble averaged. To avoid discontinuity in the traces it has been necessary to interpolate data for some traces on the basis that 127 data frames constitute a data gathering cycle.

CHAPTER 7

WIND TUNNEL RESULTS

7.0.0 Introduction

Wind tunnel testing is a useful and convenient way of applying known and tightly controlled flow conditions around an object. In the present work tunnel testing was used to provide performance data of the particular blade used in the atmospheric testing. The opportunity to do this at a Reynolds number identical with that of atmospheric tests was considered to be very unusual. Indeed detailed pressure data around an aerofoil chord both in tunnel and atmosphere is probably almost unique. The University of Glasgow 2.4m by 1.6m closed circuit wind tunnel, shown in figure(84), is equipped with a mounting able to oscillate a blade in pitch dynamically and this facility was used in the present work as described below.

This chapter defines the four types of run used in the present tests, describes and defines terms used in the presentation of the results and then examines subsets of runs making up significant sequences such as changes in tunnel speed or reduced frequency. Descriptions of the pressure coefficient behaviour over the chord are given, together with the maximum and minimum force coefficients and other data, for each of these runs. Altogether some 120 useful runs were taken in the wind tunnel.

No correction for tunnel blockage in any of the data presented has been made. This is in line with the policy of the Glasgow team and follows from the lack of a coherent understanding of blockage correction in the dynamic case. In order to be consistent no correction are therefore made to the static data either. Blade chord is 0.3m and compares with 2.4m tunnel width ie a maximum geometric blockage of about 12.5%.

Wind tunnel runs were of four types:

1) STATIC. Blade incidence was incremented in 64 steps from the start at a small negative value, to the maximum positive value approaching 30°. Each measurement sweep occurred after a settling

interval of about 0.5 second. Incidence was then decremented in the same way back to the start value. Figures(27) to (30) show this.

Static runs were made for all four tunnel speeds or Reynolds number conditions, nominally 0.4, 0.6, 0.8 and 1.1 million, based on blade chord. This output was available real time from the Glasgow system and was used as a system health check.

2) RAMP. Incidence, starting at a small negative value, was increased at a finite and constant rate, up to a maximum of nearly 30°. The rate of increase measured in degrees of motion per second together with the tunnel speed, were the important parameters. Tests started at 15° per second and ended at ramps of 370° per second. Five ramps were executed for each test run and the results averaged as for the other tests.

3) SINUSOID. Here incidence was changed dynamically in a sinusoidal pattern of waveform with time. Frequencies of motion and their relationship with tunnel speed, plus amplitudes of motion and mean angles were the important parameters. Swept angles ranged up to ±30° and frequencies up to 5.25Hz. Data was taken from ten cycles of waveform for these tests and the results ensemble averaged to produce typical cycles.

4) VAWT. Incidence varied in a pattern generated by a simple vector model of the airflow through a vawt rotor. Figure 31 shows the derivation of this function. Waveform is sinusoidal at infinite blade speed ratio, but becomes distorted at windspeeds of interest, towards a saw tooth pattern. A slow increase in incidence, corresponds to the first quadrant of the rotation of the rotor. This is followed by a rapid excursion to a negative incidence, corresponding to the downstream pass of the blade, followed in turn by a slow return to the start condition. Also implied is a change in airspeed over the blade and these variations are shown in figure(31) for a blade speed ratio of 2.0 No attempt was made to produce this change in airspeed in the wind tunnel.

For this waveform tunnel speed, frequency of oscillation and sweep amplitude were used as controlling parameters. Again sweeps of ±30° and

frequencies up to 3Hz were used. As with the sinusoidal tests, ten cycles of motion were recorded for each run and only averaged data from the ten cycles is presented here.

7.1.0 Test Schedule and Parameter Selection.

Tables(8) to (11) show the main parameters of each tunnel run. Particular values of the various parameters controlling the run were decided by the need for comparability with existing work in the area of dynamic stall and the need to investigate the area around the operating point of the atmospheric experiments. Comparability with the work of published data in terms of maximum amplitudes, reduced frequencies and so on, decided some of the sine waveform schedule. The remainder of the sine waves were chosen to allow comparison of the effects of similar instantaneous incidence change rates obtained from the combination of different frequencies and different swept angles.

Vawt waves were chosen to replicate as closely as possible some of the sine waves and to allow further comparison of the effects of instantaneous incidence change rates. Thus the different waveform types were used to produce similar waveform shapes over a limited range of incidence. Ramp tests are essentially a simple more analysable motion and are increasingly seen as a better method of determining the parameters of interest in empirical and semi-empirical models of dynamic stall such as that due to Beddoes reference(9). An analysis of the two time delays of interest, namely that from static stall to moment stall and that from static to normal force stall, is given below. Ramp tests are however severe on the blade mechanically, exerting a considerable torsional impulse. For this reason their use in the present tests was restricted.

7.2.0 Standard graphical and tabular presentations of tunnel results.

A standard layout, as in figure(27) above, is used to present tunnel runs. Over a single cycle in the case of 'static' runs, ten cycles for the 'sine' and 'vawt' wave runs and five cycles for the 'ramp' runs, this layout shows the averaged pattern of pressure coefficient over the blade's two surfaces.

Presentation conforms to the standard layout used in the present work of 256 'data frames' per cycle together with 32 frames of lead in and out at the beginning and end of the traces, to aid the eye. Every fourth of these frames is shown in the plots. A cycle thus starts at frame 0 and ends at 256 and proceeds from left to right in time. Leading edges for the two surfaces are towards the bottom of the figures, trailing edges towards the top. Pressure coefficient is plotted positive upwards. 'Outside surface' is the pressure surface during positive incidence excursions and the suction surface with negative incidence. Table(7) shows the tapping positions as a percentage of blade chord both along (x/c) and normal to the chord (y/c) and also the colour coding used in the standard plots for these positions.

Pressure coefficient is based, in this present work, on the stagnation pressure as determined by the transducers around the blade's leading edge. As described elsewhere, this pressure is derived from a fourth order curve fit to the six most positive tapping pressures at each data frame. The fit yields the stagnation pressure and the stagnation point position.

At the bottom of the standard plots are traces of the tunnel pitot pressure and the blade stagnation pressure as outlined above. In some cases the tunnel trace will be seen to be perfectly straight as the result of a data loss: here the tunnel pressure has been taken from the single manual record taken during the run.

Stagnation point position is also plotted and has been used in this work as a crude measure of incidence. The normal distance from the chord line has been normalised by the blade chord throughout this work. Because of the sign conventions used, positive stagnation point position corresponds with positive incidence.

Shown in the second set of graphs are the integrated pressure forces. A simple trapezoidal routine has been used to generate these traces. Pitching moment is taken about the quarter chord point. Sign conventions are such as to generate negative pitching moments during positive incidence manoeuvres. Again from the sign convention, positive incidence generates negative lift and normal force.

The third set of graphs show the force and moment

coefficients: normal force Cn, tangential or chordwise force Ct and pitching moment Cm, plotted against stagnation point position. Coefficients are based on blade chord c, moment Pm about the quarter chord position and instantaneous stagnation or dynamic pressure dp. That is:

$$Cn = \frac{N}{dp.c}$$

$$Ct = \frac{T}{dp.c}$$

$$Cm = \frac{Pm}{dp.c^2}$$

where forces and moments are per unit length of blade span.

Tunnel speed shown is the speed derived from the tunnel instrumentation.

Reynolds number is derived from the blade stagnation pressure and the kinematic viscosity of air derived from the formula:

kinvisc=(temp*0.09+13.2)/1E6 m^2/s

and based on the tunnel air temperature as measured in the tunnel settling chamber. This formula adequately represents the kinematic viscosity of air over the range 0°C to 30°C.

Stated turbulence intensity is obtained in a way consistent with that used for the atmospheric data. A tenth order polynomial is fitted to the blade leading edge stagnation pressure data for each run. The value of this smoothed function 'smdp', is subtracted from the instantaneous reading dp, at each data frame. Turbulence intensity dpturb is then evaluated from the formula:

$$dpturb = \left[\frac{((dp-smdp)/smdp)^2}{321} \right]^{\frac{1}{2}}$$

since there are actually 321 data frames in one display rev.

Reduced frequency k, used to express the angular frequency of oscillation of blade incidence Ω,

related to the incident airspeed V, is derived from the formula:

$$k = \frac{\Omega.c}{2.V}$$

In the case of the ramp runs, the reduced frequency is derived from:

$$k = \frac{pitchrate.c}{2.V}$$

In this case the reduced frequency is one half of the reduced ramp rate presented in the tables defined below. Reduced ramp or pitch rate is defined as

$$\alpha\hat{} = \frac{pitchrate.c}{V.2}$$

Reduced time is derived from

$$tau = \frac{t.V}{c}$$

and one unit is equivalent to the time taken for the passage of the freestream over distance equal to one chord.

Calculation of the ramp rates at the point of static stall for the sine and vawt function waveforms is set out below.

Sine wave:

the instantaneous incidence α is conventionally given by

$$\alpha=\alpha_0+\alpha_1*\sin(\Omega*t)$$

where α_0 is the mean angle and α_1 the amplitude of the motion

differentiating this expression with respect to time gives simply

$$\alpha'=\alpha_1*\Omega*\cos(\Omega*t)$$

where α' is the pitch rate per unit time

In nearly all runs in the present work α_o was set to zero so that

$\alpha=\alpha_i * \sin(\Omega * t)$

Rearranging this expression

$\sin(\Omega * t)=\alpha/\alpha_i$

so that for example: with static stall at 12° and a maximum incidence of 30°, stall occurs at

$\sin(\Omega * t)=12/30$

$\Omega * t=23.6°$ or 0.4115 rads of 'azimuth'

now if for example $\Omega=2.2$ Hz or $2.2*2*\pi$ rads/s and maximum incidence is 0.5236 rads (30°) then

$\alpha'=0.52*2.2*2*\pi*\cos(0.4115) = 6.634$rads/sec

or = 6.634*0.3/42 = 0.047rads/unit reduced time

at static stall incidence if the tunnel speed is 42m/s.

Vawt wave: the proof is somewhat more complicated and is shown in appendix 4 for completeness. The VAWT wave is defined as:

$$\alpha = \arctan\left[\frac{\sin(\Psi)}{\beta+\cos(\Psi)}\right]$$

differentiating using standard form and quotient rule yields:

$$\frac{d(\alpha)}{d(\Psi)} = \frac{\beta*\cos(\Psi)+1}{\beta^2+2*\beta*\cos(\Psi)+1}$$

where

Ψ = 'azimuth' ie $\Psi = \Omega * t$

β = blade speed ratio

For the azimuth at which the static stall incidence is achieved

$$\alpha = \arctan\left[\frac{\sin(\Psi)}{\beta+\cos(\Psi)}\right]$$

substituting expanding and rearranging this gives a quadratic in $\sin(\Psi)$ and solving this yields:

$$\Psi = \arcsin\left[\frac{\beta\pm\mathrm{sqr}[(1-\beta^2)*\tan^2(\alpha)+1]}{\tan(\alpha)+1/\tan(\alpha)}\right]$$

Again the derivation of this formula is shown in appendix 4.

There are four solutions possible per cycle of Ψ, two positive going and two negative going, but only two absolute numerical values; for the present purpose these two different numerical values are required.

The above expressions can now be combined and evaluated to determine the reduced pitch rate at static stall. This data is shown where appropriate in the the tables showing results of aerodynamic coefficient maxima for series of runs of interest such as table(13).

7.3.0 Tunnel pitot /blade stagnation pressure discrepancy.

For all runs there is a substantial difference of up to 20% between the blade stagnation pressure as outlined above and the tunnel pitot pressure with the pitot pressure being the higher. This might suggest:

a) calibration errors with the transducers: a systematic error would be necessary to explain this result since any derived pressure is the result of six transducers' outputs due to the curve fitting method used

b) transducer reference pressure is taken to be tunnel building pressure and equalisation between this and the tunnel working section is assumed because of the array of slots in the

working section walls, floor and ceiling

c) significant non uniformity of flow caused by the blockage of the blade.
Of note is
the nearly constant blade measured stagnation pressure compared to the pitot probe's undulating trace. There is a clear phase relationship between blade geometric incidence shown by the black traces and the pitot pressure, with the latter lagging the former by about 30°.

In the case of the static runs, the blade stagnation pressure does show a pronounced dip during stall and the tunnel instrumentation similarly shows a slowing of tunnel wind. This suggests that a two phase behaviour of the air in the tunnel occurs. A stalled blade definitely slows the tunnel speed: this is very audible when operating the tunnel in these circumstances. However the slow down occurs over a time scale of several seconds. Under the circumstances of the rapidly oscillating blade this effect is too slow and the evidence suggests that air is diverted and accelerated around the obstruction of the blade instead.

Further evidence against the suggestion of transducer error *per se* is afforded by the effects of gross changes of tunnel speed such as those shown in the static run discussions below. Here the roughly 20% error between the two estimates of stagnation pressure is preserved across speed change: transducer error would result in constant pressure error. To be added to these observations is the good correspondence of the two measures post stall in the ramp runs such as run 173. The error here is only a few percent.

Of the three suggestions above it seems likely then that the last, the flow non uniformity, plays the major part in the discrepancy. There is here no questioning of Bernoulli's equation and energy loss, for the pitot tube is here using its own static pressure some distance from the tunnel wall slots mentioned above. The probe can just be seen projecting form the right hand tunnel wall in the photograph of the installation of the blade into the wind tunnel figure(24).

Use of the blade derived stagnation pressure has been maintained despite the above question, in order to maintain consistency with atmospheric

practice.

7.4.0 Asymmetry of tunnel flow

Examination of the results given in the figures below, particularly the plots of pressure coefficients and forces shows some evidence of asymmetry between the positive and negative incidence half cycles see for instance run 79 figure(44). Pitching moment traces of runs around the stall point suggest that as much as 1.5° of asymmetry might exist. This phenomena may perhaps be attributed to several causes:

a) flow asymmetry in the tunnel: there is some documented evidence of this feature in this tunnel

b) blade misalignment in the tunnel: considerable effort was made to align the blade accurately, as described elsewhere in this thesis, but errors of order 1° cannot be ruled out.

c) in the case of VAWT wave runs, ramp rates of incidence to the maximum amplitude are asymmetrical: going positive is slower than going negative. In an isolated instance this might be expected to increase forces in the negative going half cycle, because of the greater incidence delay before stall. However it may be that the flow does not have time, because of the rapid transition, to establish fully and lower forces result. Cp trace evidence would suggest that this reason is not supported.

d) restricted numbers of data acquisition channels in the tunnel setup necessitated some transducer signals being unused. To provide good coverage of the 'suction' surface data all transducers here were sampled, but on the 'pressure' surface alternate transducers were omitted from the data gathering scheme over a section of the surface from about 25% x/c rearwards as detailed in table 6. To fill in the missing data for this thesis only linear interpolation has been used and this could introduce errors. However inspection of the Cp traces in any of the figures shows that departures from the linear in the areas in question on the 'outside surface' are small and that therefore this category of error is of small magnitude.

It must be concluded that asymmetry in the observed

result is most likely to have arisen from errors in alignment between the flow and the geometrical incidence in addition to the errors arising from the differences in maximum geometric amplitude in some runs.

7.5.0 Static Test Results

Figure 26 shows graphically the principal aerodynamic coefficients for a series of static runs at four Reynolds numbers in the range 0.322 million to 0.960 million and figures(27) and (29) show typical runs at Reynolds numbers of about 0.32 and 0.75 million. Table(12) charts the maxima of the aerodynamic coefficients and the moment stall break points.

From the table it will be seen that there is a very modest increase in the normal and tangential force stall angle with Reynolds number, whilst that of moment stall is essentially constant. This allows a small increase in normal force coefficient over the range.

Most noticeable in figure(26), is the behaviour of the normal force coefficient through the Reynolds number range. At the two lowest Reynolds numbers the curve shows the effects of various separations around the profile including the Cn/α slope change at about 5^{o} of incidence discussed by Willmer reference(100). This latter effect arises from a separation bubble on the pressure surface of the aerofoil causing effective camber which eventually collapses with increase in incidence. At stall, normal force shows a pronounced trend with Reynolds number: at low Re there is a significant drop in value in a sudden manner whilst at high Re this effect is much less marked.

In general the agreement in the normal force coefficient with the coefficient obtained from the data of Willmer reference(100) and of Sheldahl and Klimas reference(84) is good. But there is little evidence of a pronounced Reynolds number effect on maximum normal force coefficient as the two references above suggest. Willmer suggests that maximum lift coefficient rises from 0.95 to 1.17 between 0.32 and 1.0 million Reynolds number. Sheldahl and Blackwell suggest that lift coefficient rises from 0.96 to 1.1 over a similar range. This compares with figures of about 1.15 to 1.23 over the same range for the present data.

Regarding static stall incidence, Strickland and Graham reference(89) correlate the data of Jacobs an Sherman reference(41) to the relationship

$\alpha_{static\ stall} = 1.79 * \ln(Re/202)$

which would evaluate to 13.2° for the lowest Re of the present tests and 15.3° for the highest and these figures compare with 11.9° to 12.9° for the present work.

Stall in the present tests is about halfway in character between the step change of Willmer and the gradual stall of Sheldahl *ibid* as quoted in Stacey reference(88) and occurs at about the incidence indicated by these authors. Inspection of the Cn/α curves of figure(26) in conjunction with Gault reference(35) would then suggest that the stall was of a mixed type as is consistent with the latter's correlation work.

Examination of the Cp traces of individual runs such as figures() and (27) over the Reynolds number range shows a number of features. Away from the leading edge and pre stall, surface pressure coefficients show very little trend with Reynolds number. At low Reynolds numbers however, leading edge pressure coefficients show evidence of laminar separation bubbles in the 6.5% x/c traces starting at about 7° of incidence and moving forward to the 4% trace by the time 11° is reached, just before stall. At the high Reynolds numbers the separation bubble occurs only at higher incidences of perhaps 12° at the 4% x/c position. These bubbles are evidenced by divergence of particular leading edge traces, from the general pattern, over time.

At low Reynolds numbers during stall, pressure coefficient traces show the sudden fall to base pressure expected from inspection of figure 26. Normal force and particularly tangential force show a very sudden collapse as a consequence. At higher Reynolds numbers the transitions are much less sudden. Further, the behaviour of the leading edge traces explains the relative maintenance of the tangential force component to higher incidence at higher Reynolds numbers. Figure(29) shows the minor effect that stall has on the magnitudes of the first three tapping traces, ie those back to about 2% x/c, at these higher speeds. Leading edge pressure does not collapse until 26° of incidence is reached at 0.76 million and does not collapse at all at the highest tunnel speed and maximum

incidence of nearly 30°. The effects of these maintained suctions on tangential or chordwise force is pronounced in figure(26).

Stagnation point position over the Reynolds number range shows a trend for substantial reverse movement during stall at low numbers, but a much less severe change at high numbers.

From these four runs it must be concluded that there exists a moderately important transition Reynolds number for this aerofoil between about 0.32 and 0.56 million based on chord. Reynolds numbers as low as this are experienced by the blade when run in atmosphere but usually at times of low incidence. As incidence mounts in the atmospheric runs so too does Reynolds number and so it is likely that the atmospheric runs take place above this critical Reynolds number.

7.6.0 RAMP wave test results

Six ramp wave tests were conducted in the present series of tests to provide an alternative motion to the cyclic tests described below. Ramp tests are useful in providing a simpler test condition than oscillatory motions, uncluttered by the reattachment process. Ramp down tests in which incidence is rapidly decreased, provide a comparable and additional insight into the reattachment process.

Figures(32) and (33) show the principal aerodynamic coefficients for all the ramp runs, figure(34) shows run 173 in standard Cp format and table(13) details the maximum force coefficients for the runs. Five runs were carried out at a nominal Reynolds number of 0.75 million based on chord and stagnation pressure and the last was carried out at an Re of 0.96 million. To provide some basis of comparison for run 176, a set of coefficients has been interpolated between two appropriate runs in the main series.

Considering figures(32) and (33) and the tabular data, there is a marked increase in the magnitudes of the force and moment coefficients with increase in pitch rate. The normal force trace for run 172 shows the start of a roll off at about the static stall point but then the appearance of a second increment of coefficient to bring the level up to expected levels. Run 174 shows the classical short duration change in Cn/α gradient and

the strong peak of dynamic stall. Most notable of the traces are perhaps those of pitching moment where in run 175 a value of -0.48 is attained. This value is approaching that equivalent to a movement of the aerodynamic centre from the quarter chord to the mid chord point (Cn/4).

Maximum normal force coefficients show augmentation compared to static values for even the most modest of ramp rates. This is in agreement with the results of Moss and Murdin reference(57) for sine wave motions. A reduced frequency of only 0.005 is shown in this latter work to have increased Cl_{max} values by about 8%, but an increase in reduced frequency to 0.05 is necessary for an equal increment in Cl_{max}. Values are also substantially higher than those of comparable reduced ramp rate at static stall.

Strickland and Graham reference(90) detail water tow tank results for the NACA-0015 aerofoil at Reynolds numbers of approximately 100 000, incidences up to 90° and reduced pitch rates up to 0.99. The authors suggest that lift coefficients may be obtained from the following empirical expression

$$Cl(\alpha)=2a_L*\sin(\alpha)*\cos(\alpha)$$

where

$$a_L=7.1*k+2.25$$

k being the reduced frequency as defined above for ramp rates.

Applying this relationship, for example to run 173 at the maximum normal force incidence of 20.9°, gives a maximum lift coefficient of 1.55 compared to the figure of 1.87 for the present work at the substantially higher Reynolds number of 0.75 million. At the highest pitch rate of the present tests run 175, the corresponding maximum normal force coefficients are 1.61 and 2.32. A difference between the two data sets is not too surprising for not only are the Reynolds numbers different but the blade in the water tank work did not extend to the bottom of the tank and therefore the test environment cannot be considered 2D. Under the circumstances it seems reasonable to conclude that the present blade conforms reasonably well to established data.

7.7.0 Sine wave test results

Most data gathered to date on the phenomena of dynamic stall has used the sine wave oscillation as the wave shape and the research, carried out for helicopter interests, has used a non zero incidence as the mean angle. Furthermore the section used has primarily been the NACA-0012 or derivatives and so there is not much relevant data for the 0015 section, particularly since the work has been carried out for the relatively high reduced frequencies arising from the elastic torsion of helicopter blades. However Angel reference(6) has recently carried out a programme of tests on the 0015 and thicker sections, although only a little of the data has been published to date. In the present work some non zero mean angle runs were carried out in the present wind tunnel tests for purposes of comparison, but the main body of tests has used zero mean incidence. The present programme has attempted to quantify the the effects of change in Reynolds number, reduced frequency and maximum achieved incidence. The simple analysis below attempts to describe the main features of stall for the current blade and to this end three series of sine wave runs are presented.

7.7.1 SINE waves: effect of reduced frequency

Figure(35) shows the principal aerodynamic force and moment coefficients for four runs over a range of reduced frequencies from 0.023 to 0.079 and reduced pitch rates from 0.008 to 0.026. Reynolds numbers for these runs were all about 0.75 million and maximum amplitude was maintained at 22.5°. Reduced pitch rate has here been calculated at the position corresponding to static stall on the upstroke ie incidence increasing, since the rate of increase changes with position in the cycle or incidence. Table(14) shows the changes that occurred in the values of the three main aerodynamic coefficients over this range and figure(36) and figure(37) show runs at the low and high reduced frequencies.

All coefficients show the expected rise, with the exception of the normal force coefficient for the highest reduced frequency, where the peak value was disrupted. Most striking of the trends in the coefficient values is that of pitching moment where a doubling in this coefficient has resulted from a three fold increase in reduced frequency. Along with the rise in coefficients, the pitching moment

break, usually taken as the best indicator of stall, is progressively delayed with rise in reduced frequency.

Figure 35 shows clearly the trend of pitching moment with increase in reduced frequency and shows also, as cross hatched, the regions where negative pitch moment damping exists, that is regions where pitching moment is aiding motion rather than hindering it as is usual. All coefficients are of a substantially higher value than those obtained during static tests. The values at the present Reynolds number are a little lower than those of Angel reference(6) as would be expected because of t lower values of Reynolds numbers of the present tests.

Most noticeable in the normal force traces is the relative recovery period from stalled values to attached. At the lowest three reduced rates reattachment is complete before zero incidence is reached in the down stroke but at the highest frequency insufficient time is available and significant reverse incidence is achieved before reattachment occurs.

Regarding the tangential or chordwise coefficients; in tandem with the rise in maximum values is a lowering of the values in the stalled domain. That is, post stall some positive force still exists over most of the cycle, however at the higher frequencies significant negative chordwise force exists. Clearly this could have implications for the blade on a wind turbine rotor.

Inspection of figures(36) and (37) shows the trend that a leading edge bubble is clearly apparent for all reduced frequencies shown here but that in the last plot this is less marked. The classical features of dynamic stall can also be clearly seen; rapid loss of suction at the leading edge and depression of the suction surface pressure coefficients below base pressure, indicating the passage of the leading edge vortex rolling away. This latter effect is suggested in the first figure, but very marked by the last having a strength of about Cp=2 by this stage. Stall type in this series would appear to be of the mixed type.

The effect of increased reduced frequency on the movement of the stagnation point is to reduce the reverse movement mentioned below. Standard plots using stagnation point position as an incidence surrogate have shape differences compared with the

traces plotted against geometric incidence as can be seen by comparing the equivalent pitching moment traces of figure(35) with those of figures(36) and (37).

From the above discussion it must be concluded that reduced frequency has an important effect on the quantitative behaviour of the aerofoil.

7.7.2 Sine waves: effect of Reynolds number

Figures(38), (39) and (40) and table(15) present a series of runs taken at a constant nominal reduced frequency of 0.05 over a range of Reynolds number from 0.395 to 0.961 million.

Compared to the differences experienced over the range of reduced frequency discussed above, differences due to change in Reynolds number in the principal force and moment coefficients are modest. Table(15) lists these changes over the range: normal force coefficient increases by approximately 7% and chordwise or tangential force coefficient by only 5%. However the pitching moment coefficient does change more significantly - by about 27%.

Considering the normal force coefficient traces in figure(38): change appears most marked between the first two runs with respect to width of hysteresis loop. This implies greater difference between the attached and the unattached normal force versus angle of attack slopes, which agrees with the results of the static tests. Tangential force coefficients post stall appear significantly more negative at low Reynolds numbers - to be expected from the lower degree of attachment around the leading edge at low Re.

Behaviour of the pressure coefficient traces at the leading edge post stall reflect those in the static tests: at the lowest Re suction collapses completely right up to the leading edge, whereas at higher Re suction is maintained over the first 2% of chord. Passage of the leading edge vortex backward over the suction surface is much more pronounced at higher Re but is still discernible at lower values. The leading edge bubble is very evident at the lowest Re but becomes less pronounced with rise in this parameter. Reattachment of the flow from the leading edge with reduction of incidence is clearly visible.

Thus the effect of Reynolds number is modest and most significant at values below those encountered in the majority of the atmospheric tests, certainly at times of significant incidence.

7.7.3 Sine waves: effect of change in maximum amplitude.

A series of runs figures(42) to (45) show the effects of change in the maximum amplitude of motion of a sinusoidal waveform over the range ±13° to ±26°. Reynolds number has been maintained at a figure representative of tangential velocity of the blade on the wind turbine, that is at about 0.8 million, and so too has the reduced frequency at about 0.05. Maximum force and moment coefficients are detailed in table 16 together with reduced pitch rates at static stall and figure(41) shows the coefficients plotted against tunnel incidence. The runs in the series have been chosen to include one with a maximum incidence approximately equal to static stall, one somewhat past this so that light dynamic stall occurs, another where stall is of a severity comparable with that experienced in atmosphere in the present project and finally a run of extreme severity such as might be seen at the very low blade speed ratios currently proposed for new machines operating in the strongest winds.

7.7.4 Sine Waves Below Static Stall Incidence

Static moment stall occurs at about 12° for the blade under the nominal conditions of this series of runs and the first column of graphs in figure(41) shows the coefficient traces of a wind tunnel run of maximum incidence just above this angle. The looped nature of all the traces reflects the inertia of the aerodynamic system in the tunnel.

Figure(42) shows the pressure coefficient pattern of the above run, and reveals only a modest area of loss of trailing edge pressure recovery at maximum incidence. At the leading edge the 4% x/c Cp trace diverges at an incidence of about 10° geometric and persists until this angle is regained on the downstroke. The 6.5% trace on the other surface shows evidence of separation bubble also.

7.7.5 SINE waveform runs above static stall angle

Pitching moment is the coefficient most strongly affected in exceeding the static stall angle. A divergence occurs at about maximum incidence in run 77 and a crossover in the hysteresis loop is evident. Pitching moment here aids motion: negative pitch moment damping appears soon after the static stall angle is exceeded.

In run 79 with a maximum amplitude of 17.5°, the small increase in incidence over run 77 produces a 160% increase in blade pitching moment during positive incidence. Pitching moment here shows a clear positive going divergence over the negative incidence half cycle- indicating stall and the pitching moment trace has crossed on the return from negative incidence, implying negative pitch moment damping here also.

Both the normal and tangential force traces show marked evidence of stall also at this incidence. The smooth rise in forces is followed by abrupt collapse to a fraction of the peak value and a ragged return to zero.

Referring to the Cp traces: in run 77 a pronounced moment stall occurs just before maximum incidence. Trailing edge pressure coefficients go negative from about 13° and spread forward perhaps reaching the 60% chord position just past maximum incidence. The 4% transducer trace has collapsed at an incidence of 12°, but the general leading edge suction is maintained throughout the cycle. Back from the leading edge however at about x/c=15%, suction does show the first hint of partial collapse.

In run 79, pitching moment divergence during the negative incidence half cycle is reflected in the collapse of trailing edge pressure recovery. At the leading edge the 4% x/c trace shows the expected separation bubble behaviour and the other traces have started to show the characteristic shape of post stall behaviour above the critical Reynolds number. Here substantial suction of about 4 times dynamic pressure is maintained regardless of incidence, but only over the first 4% of chord, with base pressure to the rear. Forward movement of the base pressure domain is clearly visible on the suction surface and evidence of vortex suction starts at perhaps the 25% to 35% x/c area.

Stagnation pressure position has now taken on the

'broken hill' feature which becomes more pronounced with yet higher incidence. The tendency towards reverse movement of the stagnation point with rising incidence during stall, has been discussed above. This centripetal tendency is expressed in the trace losing its correlation with incidence. The trace peaks early and never reaches a magnitude consistent with the achieved incidence. The issue of stagnation point position is discussed more fully in section 7.9.0 and onward below. The general pattern of Cp trace has taken on an asymmetric pattern with incidence.

Run 147, the last of the series, shows a deeply stalled situation with a pronounced primary vortex passage from very close to the leading edge rearwards, taking about 3 periods of reduced time to reach the trailing edge. Pitching moments have reached about the maximum possible.

The issue of pitching moment has been of major importance to the helicopter industry because of the torsional flexibility of the helicopter blade and the consequent possibilities for instability. For the vertical axis wind turbine pitching moment is of secondary importance since blades are of much lower aspect ratio and hence torsionally much stiffer. However if control surfaces are to be fitted to vertical axis machines and there have been suggestions that they might constitute all moving tips in the case of one of the American straight bladed Darrieus designs and of the Open University V vawt machine, then these surfaces will experience these pitching moment impulses every revolution in stall conditions. Such exposure would probably dominate the design of such surfaces.

7.8.0 VAWT Wave Test Results

Figure(46) shows a series of vawt wave aerodynamic coefficient results over a range of nominal maximum incidence of ±12.5° to ±25° taken at a Reynolds number comparable with that of the blade run on rotor ie 0.8 million, and at a reduced frequency close to the nominal atmospheric value of 0.05. Table 17 shows the main aerodynamic coefficient maxima and minima for both the positive and the negative half cycles separately. Oscillation amplitude was symmetrical about zero for this waveform.

At small amplitudes the difference between the vawt and sine waveforms is very minor and performance in

the two regimes is correspondingly very similar as may be seen by comparing the traces of figure(46) with those of figure(41). No attempt is therefore made in this thesis to describe performance in this low maximum amplitude domain.

7.8.1 VAWT waveform runs: differences from sine input

No significant difference between the two waveform results is detectable in the present tests until motion amplitudes in excess of 22.5° or 25° are present. Figure(48) run 166 with a maximum amplitude of ±25°, may be compared with figure(45) run 147, the equivalent sine wave run of similar maximum incidence. Both runs had Reynolds numbers of about 0.75 million. As may be seen the general pattern of the pressure coefficient traces is almost identical and the only differences are those associated with the negative incidence peak where the suction collapse is more sudden than in the case of the sine wave test and of the initiation of the vortex suction peaks.

Comparison of sine and vawt waveform runs is pursued further in figure(49) by comparing run 162 (vawt) with run 137 (sine) in terms of force and moment coefficients plotted against tunnel geometric incidence. These two runs have a nominal maximum amplitude of ±30° and a Reynolds number of approximately 0.56 million: unfortunately comparable runs to high incidence and high Reynolds number together are not available.

Most noticeable is the closeness of the two results. At static stall incidence the reduced pitch rates on the up and down strokes are respectively 0.012 and 0.032 for the vawt wave and 0.025 for the sine wave which is symmetrical, yet maximum force and moment coefficients are essentially symmetrical over positive and negative half cycles. In the case of the sine wave run, the reduced time interval static stall to incidence maxima is of order 10.6 and for the vawt waveform this interval is 13.4 for positive and 7.8 for negative incidence half cycles. Thus for all but the last situation there is no question but that maximum possible forces and moments were developed since these reduced delays are greater than the delays normally expected between attainment of static stall incidence and dynamic stall. Analysis of this stall delay is covered in section 7.11.0 below where results regarding the latter stall

delay were obtained from table(18).

Speed of stall recovery appears to be the main factor differentiating the blade's performance under the two waveforms. The rate of return to the attached condition in terms of incidence is identical between the two regimes. However the possible time available for reattachment is not and so in the case of the sine waveform, flow reattaches at about zero incidence whereas in the vawt waveform case on the slow positive going stroke, reattachment occurs before zero incidence. On the negative going stroke however time is not available and flow does not reattach until significant negative angle of attack (about 6°) is attained.

Thus it would appear that even in the extreme case represented by the comparison above, where angles of attack are well over anything experienced in the present on rotor or atmospheric tests, little is to gained by tests with this waveform except perhaps that in a sense, two test reduced pitch rate tests are carried out at the same time. As will be seen in the next chapter, incidence waveform shapes on-rotor bear little relationship to the vawt waveshape, so that if a closer input waveform shape is to be proposed it might be better formulated than the vawt waveform.

7.9.0 Pressure Signal Measurement of Incidence.

Some effort has been expended in the present work to determine some measurement of incidence from the various pressure signals available. As described elsewhere, a flowprobe was fitted to the blade during the tunnel runs described in this chapter and full data is available from it. Whilst run in atmosphere however, the probe was present on the blade in only a very limited number of runs and only very poor calibrations are available for it during this period. Since incident airstream conditions are the normal link between the modelled airfoil response and predicted blade and rotor response there is some interest in measuring incidence on rotor.

There are however some philosophical difficulties here, for the normal concepts of aerofoil behaviour are based on the ideas of flow at infinity. That is, flow at such a separation from the aerofoil, that the latter has insignificant effect. It is thus meaningful to discuss geometric incidence as

being the angle between this freestream flow and the aerofoil chord. In the present context of atmospheric work however, one might ask 'what is the freestream incident velocity?' The combined effects of very high turbulence levels compared to those of conventional aerodynamics and flow curvature due to the circular path of the blade and its implied incidence, necessarily introduce some difficulty into these simple concepts. For instance flowfield curvature for the RAL vawt as set up for the present tests is of order 2.4° at leading edge and 3.4° at trailing and is furthermore of opposite sense for leading and trailing edge.

Use of a short probe as in the present project follows the example of Akins *et al* reference(3). In the present tests the projection of the probe in front of the leading edge was one half chord compared to the 0.375 chord used in the Sandia Labs experiments. In the analysis below it is suggested that at this proximity, usefulness of probe output is limited by the heavy influence of the aerofoil behind it. In such conditions the probe may be little better than blade stagnation point position as a measure of incidence in the dynamic case, although it is significantly better in the static. Stagnation pressure at probe tip and at blade surface is unlikely to be very different and therefore this pressure has been accepted as a reasonable measure of incident airspeed.

7.9.1 Comparison of blade incidence measure.

Helicopter researchers have used the pressure signal from a single tapping close to the leading edge as a convenient measure of incidence Riley reference(75), when a measure of incident airspeed has been available. Figure(50) shows this measure (the pressure coefficient at 1.9% chord) along with that of stagnation point position and probe pressure coefficient all plotted against tunnel geometric incidence, for a static run (127) and three vawt function runs of 0.05 reduced frequency and ±10°, ±15° and ±20° maximum incidence, runs 110, 112 and 114 respectively.

Probe signal is the pressure across two faces of the probe head each cut at 45° to the probe axis. Reference to Dean reference(23) shows that large Cp of the order shown in the figures can only be obtained at very large flow angles of order 60°, demonstrating the extremely powerful effect of upwash in this region. This apparent upwash is much

larger than either Butterfield reference(20) or Oler *et al* reference(65) suggest and may result from the significant blockage which is evidenced by the difference between the blade measured stagnation pressure and the tunnel pitot probe signal discussed above.

The first column of graphs in figure(50) shows the situation in the static case and demonstrates the superiority of the probe over stagnation point position in this situation as an incidence measuring tool. Single tapping readings clearly have the double disadvantage of being non linear in the attached regime and of possessing a complicated post stall behaviour.

Further columns in the figure chart the behaviour at the progressively larger maximum incidences stated above and show that, in the dynamic case, the stagnation point position is not very much if at all worse than probe output up to a maximum incidence of about 20° for these runs, at least in so far as the width of the hysteresis loop is concerned. Examination of the width of the stagnation point position loop shows that this is commonly less than about 4° of incidence so that a mean line or best fit would give an error or uncertainty of about 2° of incidence. Such a best fit line to the plot pertaining to run 114 has a gradient of 2.31E-3c/° or 434°/c, remembering that stagnation point thickness position has been expressed in terms of chord. Fits to the linear region of stagnation point/alpha plots from static tests have gradients of order 2.86E-3c/° or 350°/c.

Referring to figure(51) showing a static and three vawt waves up to a maximum amplitude of 30°, shows that at this maximum amplitude stagnation point behaviour is a poor measure of incidence. Sufficient time has been available for the stagnation point to move well away from the attached flow position. It happens however that the divergence from the linear relationship is delayed almost until normal force stall, that is well past moment stall, so that this incidence measure is useful more or less until normal force stall.

Figure(52) shows stagnation point position results of all wind tunnel tests of the present work plotted to show the effects of Reynolds number, reduced frequency and waveform type. The last plot of the set shows maximum achieved normal force coefficient plotted against maximum achieved stagnation point position. From these and other

plots it is reasonable to conclude that stagnation point position is a reasonable guide to incidence up to an incidence approaching 20° and that this measure is insensitive to Reynolds number, reduced frequency and waveform type other than static, over this incidence range.

Figure(53) shows the normal, tangential or chordwise force and pitching moment coefficients plotted against stagnation point position for the same runs as figure(46). There is clear sympathy between the figures but good agreement is spoilt both by lack of fidelity in representing hysteresis throughout the range and in the distortion caused by the nonlinear behaviour of stagnation point position at higher incidence. It is conceivable that more sophisticated modelling of stagnation point position would allow more convincing rendition of incidence.

7.10.0 Dynamic Stall Type

Dynamic stall control is likely to develop to become a major issue in the wind turbine engineering field as the industry matures and seeks to cut the production cost of new machines. The possibility of stall tailoring so that stall occurs in a predictable and designed manner with change in wind speed, holds the attraction of major cost cutting potential. Stall controlled wind turbines are well established in the medium scale horizontal axis market and there is substantial interest in designing in this control technique into vertical axis machines as well. Klimas reference(43) reports work on a modified NACA-0015 section on the 17m Sandia machine intended to investigate this aspect and others of blade section design.

Stall type is important not only in regard to the possibilities for control but also in its possible implications on the structure of the machine since sudden or abrupt changes in blade load are more able to excite comprehensive structural response. Stall type and its morphosis has been studied extensively for helicopter rotor blades and as with static stall, dynamic stall has been classified into a number of types somewhat parallel to the static cases. McCroskey *et al* reference(54) provides a useful review of three stall types.

Leading edge stall is normally associated with the

thinner airfoils, the NACA-0012 being perhaps the thickest regarded as performing this stall type. Leading edge stall is indicated by sudden collapse of suction over the whole suction surface commencing from very near the leading edge and progressing towards the trailing edge. The collapse at any point is associated with and follows the passage of a strong vortex which travels rearward at somewhat less than half the free air stream velocity. Secondary vortices may subsequently traverse the surface and generate similar though smaller suction waves.

Trailing edge stall is recognised in thicker sections, the example given in McCroskey *ibid* being the NLR-7301 a 16.5% thick section. Here reversed boundary layer flow occurs over a longer period commencing at the trailing edge. When the reversed flow reaches a point in the leading edge region a vortex, like that in the leading edge stall but somewhat weaker, forms at around the 30% chord region and rolls back in a similar manner to that in the leading edge stall case. McCroskey further describes two cases of *mixed stall* type where initial disturbances and separation starts at some point mid chord. Unfortunately the diagnosis of the various stall types tends to rely on hot film detection of boundary layer behaviour, which is beyond the scope of the present experiment.

Notwithstanding the comments of the previous paragraph some evidence is presented figure(54) of the pressure coefficient traces of two ramp runs 173 and 174. There is evidence of forward movement of pressure disturbance starting between the 32% and 40% x/c positions at perhaps +4 units of reduced time. The arrival of this disturbance at the leading edge coincides with the partial collapse of the leading edge suction and there is then a pause before a rearward movement of disturbance starts from about the 25% x/c point. Reporting work on the NACA-0018 Wickens reference(98) shows similar pressure disturbances emanating from mid chord and travelling forward followed by the passage aft of the main vortex behaviour.

Using the guidance of McCroskey *ibid*, stall on the present blade is probably of the mixed variety, indicated by the pattern of movement referred to in the paragraphs above. At the higher ramp rate of run 174 in figure(54), a similar pattern of disturbance at mid chord spreading forward can be seen as can a secondary suction wave.

Gault's work reference(35) dealing with the static behaviour of airfoils based on a geometric parameter, the ordinate at 1.25% chord, suggests that stall type on the 15% section would be of the trailing edge variety and that thicker sections would progress more surely into this domain. Comparing the traces of normal force against α for the NACA-0018 of Wickens *ibid* with the present results shows the 0018 to have much more protracted and more gentle behaviour after the maximum value has been reached. The trend towards thicker sections on proposed vertical axis designs, with their greater tendency towards trailing edge stall usually a more gradual process, will imply lower impulsive loading and thus help doubly in lowering loads and in catering more readily for them.

7.11.0 Stall delay analysis

Table(18) shows an analysis of the two time delays normally used in the empirical modelling of dynamic stall. Beddoes reference(9) suggests that to first order, the delays between achievement of static stall incidence and moment and normal force or lift stall are independent of pitch rate, aerofoil profile, Mach number and maximum incidence. Measuring the delays in terms of reduced time resulted in figures of 2.44 and 5.41 with standard deviations of 0.49 and 0.61 for the two events respectively. This data pertained to an analysis of some 150 test cases on four aerofoils. The present analysis deals with 78 test cases and three motion types and yields corresponding results of 2.48 and 7.29 with standard deviations of 0.63 and 1.07. The moment stall delay is thus highly compatible with Beddoes' work, but the normal force stall delay correlation poor.

The latter disparate result may arise from difficulty over the definition of the exact point at which the three stall events take place. Because of the ragged nature of the force and pressure traces, despite the averaged nature of the data, stall point has been taken as that point at which there is no doubt that divergence has occurred. For the purposes of this analysis no Reynolds number effect has been incorporated and the static stall angle has been taken as constant at 12.5°. This assumption of constancy in static stall behaviour has already been examined above.

Galbraith *et al* reference(31), in the analysis

of data from NACA 23012 tests, use a variety of stall indicators including the 34% x/c pressure coefficient as a marker for the inception of stall; that is the point at which pitching moment divergence might occur. Inspection of figure(55) of the present data shows that there is indeed a correlation between divergence of the pitching moment and that of the 32.6% x/c Cp traces, but that this is by no means clear cut and that errors of one or more units of reduced time might readily be made. Galbraith *ibid* tabulates only the delay between the two stalls and suggest that this might be of order 3.8. For the present work a figure of 4.8 is apparent.

The data has also been analysed using the tunnel instrumentation velocity as the measure of air speed but as will be seen the use of this measure makes very little difference to the outcome, essentially only increasing the standard deviation of the results.

7.12.0 Summary of wind tunnel results

This chapter has detailed some of the runs taken in the wind tunnel in terms of the effect of Reynolds number, reduced frequency and maximum amplitude of motion for four classes of wind tunnel run: static, ramp, sinusoidal and vawt. Leading edge separation bubble appearance, pressure coefficient behaviour over the whole chord and stall have been examined and discussed. Stagnation point position as a measure of incidence has been looked at and a rough calibration and measure of accuracy decided. In comparison with available data the blade appears to perform as expected in terms of maximum blade force coefficients, stall angles and blade surface pressure coefficients. More conclusions are given in Chapter 9.

CHAPTER 8

ATMOSPHERIC RESULTS

8.0.0 Introduction

Atmospheric testing of the blade on-rotor comprised the main experimental effort of the present project. Previous chapters have described the design and construction of the experimental equipment, the software used to control it and the methods used to run the experiments and gather the data. This chapter describes the data gathered and presents some analyses of the data. It gives primary and reduced results for 22 runs numbered between 200 to 231 recorded over the period 1st May to 14th September 1987. Data is presented in an individual run, averaged run and parametric basis. Blade leanout effects, turbulence levels and Reynolds numbers effects are all discussed. Most data is for a Reynolds number (based on chord) of about 0.75 million.

8.1.0 Wind data and runs

Table(19) shows some details of the runs which are presented in this thesis and figures(56) and (71) show graphs typical of the wind record during a strong wind run and an average wind run. It will be remembered that two anemometer towers were used throughout this project, in order that some data be available on the spatial distribution of turbulence in the wind. The graphs show the signals from the two towers separately and combined to provide an average windspeed. Two further curves show the absolute windspeed difference between the two towers. Angular data is treated similarly.

Reduced speed running was accomplished by controlling rotor speed by manual switching of the electrical machine and application of the brake. Attempts were made to switch the electrical machine on or off only whilst the logger was not operating, but this was not always possible and some of the records of runs at reduced speed have been digitally filtered to eliminate spikes due to the electrical interference arising from this cause.

8.1.1 Anemometer siting and rotor interference

Fidelity of measurement of wind at a turbine rotor by a distant anemometer is a compromise between time of flight and turbulence generated errors and distortion arising from induced velocity or inflow effects. There is also the possibility of periodicity from closely passing blades. As described elsewhere, anemometer positioning was dictated by considerations of obstruction around the turbine and so anemometers were placed upstream between one and three diameters of the rotor centre. Run data has been analysed for interference as described below.

Figure(58) shows Fourier transforms of two windspeed traces into the frequency domain. The data stream analysed was the wind speed from one tower closest to the rotor centre and was the result of the addition of the signals from the two anemometer heads on that tower. Because data logging was tied to equal intervals of rotor azimuth rather than time, the 'frequency' axis is based on harmonics of rotor rotation period, usually about 0.5 sec. The first figure shows the transform for the case where the anemometers were transform of data from a run with towers 18m or 3 rotor diameters upstream of the rotor centre whilst the second shows a run where the anemometer towers were only 6m upstream. In this latter situation the anemometer heads were within 3m of the blades. There is no evidence of periodicity at the blade passing frequency in the transforms, that is at 2.0 on the harmonic scale (for the two bladed rotor).

8.1.2 In-rotor wind turbulence

Atmospheric wind data presented in figures(56) and (71) shows the high level of turbulence on this site. Standard deviations of wind speed over the runs can be as high as 30% of the corresponding windspeed means. Turbulence has long been known to affect the performance of aerofoils both in a beneficial and a deleterious manner and so a measure of turbulence as seen by the blade on-rotor has been used in the present analysis. In particular no understanding of the effect of turbulence on the dynamic stall of an aerofoil is available.

As a measure of the local turbulence at the blade instrumented station, two methods based respectively on the magnitude of the stagnation

pressure and on the position of the stagnation point have been used. As described elsewhere, a fourth order polynomial has been fitted to the blade tapping pressures around the maximum pressure position for each data frame or azimuthal position of each revolution of data presented here. A tenth order curve has then been fitted to the stagnation pressures and positions for each revolution. The measures of turbulence are then the root mean square differences between the smooth fitted curves and the raw data for both the magnitude and the position of stagnation point methods.

Figure(25) shows an example of the two methods for a single revolution (200.2) of average turbulence levels where the blade speed ratio was 5.23 based on the stagnation pressure and the two measures of turbulence were 0.039 for the pressure method and 2.00E-3 for the position method. A comparison of the two methods one plotted against the other for all 0° blade leanout revolutions is also shown.

The example in the figure shows that incident velocities seen by the blade vary by 2% or so and peak at 6%. In the highest turbulence revolutions in the data gathered in the present work, this rises to 6% with a 12% peak. Blade incidence or angle of attack in the example shown is changing by about ±1.5° as a rough maximum, if stagnation point position is converted into incidence. In the highest turbulence revolutions the stagnation point movement is equivalent to about ±3° of incidence.

Run data has been analysed on the basis of these turbulence measures, but no clear effect is shown and no distinction has been made between data at different turbulence levels in the bulk of the data presented in this thesis.

8.2.0 Dynamic pressure versus anemometer based windspeed

Stagnation pressures provide a useful means of in and near rotor wind speed measure. Present data has been analysed on the basis of stagnation pressure derived windspeed and shows a useful reduction in scatter as described below.

The rational for the use of this method is essentially that the leading edge of the aerofoil at zero incidence is little different to the tip of a flow or pitot probe and that therefore the instantaneous stagnation pressure measured with the

blade at low or zero incidence should provide a more representative windspeed for that revolution than an anemometer positioned effectively several revolutions away. It is not suggested that this method of windspeed should supplant anemometer methods, merely that with the limited time and resources available and with the limited data set available to the present project, this method avoids the need for time of flight corrections. It is recognised that inflow and blade wake effects will compromise the accuracy of the method, but it is argued that the method at least allows a less noisy picture of the wind even if a distorted one.

In this method instantaneous maximum and minimum pressures are obtained from the tenth order fitted curves to the frame by frame stagnation pressures described above. These pressures, combined with a knowledge of local radius of rotation, angular velocity and air temperature and barometric pressure, enable estimates of wind speed at the advancing and retreating blade positions. An average of the three estimates, two advancing and a single retreating, added in the proportions ¼+¼+½ respectively, is used as the dynamic pressure wind speed for each revolution.

Figure(59) shows scatter graphs of the two estimates of windspeed for the four blade leanout angles. The figures show the average from the two anemometer towers and the estimate derived from the maximum and minimum dynamic pressures experienced by the blade in the same revolution. Turbulence aside, there is clear agreement between the two methods and a first order regression fit forced through the origin for the four blade leanout angles, suggests that in-rotor flowfield windspeeds are about 86% of freestream and independent of blade speed ratio.

The reduction in scatter referred to above can be seen for example by comparing figures(60) and (61). The figures show in mean ±1 standard deviation format, torque, power and thrust coefficients over each revolution of the rotor for atmospheric runs: a very clear improvement is apparent particularly at the lower windspeeds, ie lower windspeed ratios (windspeed/blade speed). The use here of windspeed ratio follows that of van_Bussel reference(93) where the author has attempted to reduce rotor torque data from a horizontal axis wind turbine. Most published data of power coefficient is of averages taken over relatively long periods, for example one or ten

minutes, when following IEA guidelines for the performance measurement of wind turbines in the field and power curves published on this basis contain a very great deal more data than the present work has at its disposal. Averaging of such data generates the apparent good quality lines.

8.3.0 Averaged run data

The data reduction software DATPROC, discussed in Chapter 6, enables a summary of statistics to be produced automatically for each of the 1760 revolutions of data gathered in this thesis. Sorting on any combination of these statistics is possible and has been carried out primarily on the basis of blade leanout angle, blade speed ratio, wind turbulence and Reynolds number. Series of average runs have been generated on the basis of 'refined' files or lists of revolutions conforming to a required specification.

Figures(62) to (71) show a series of such average revolutions wherein the wind strength, as measured by the stagnation pressure method mentioned above, is increased so that blade speed ratio and hence maximum incidence as implied by the two vector vawt model, steps up in line with the wind tunnel series of increasing maximum incidence vawt runs. Table(20) shows some statistics of these average revolutions including the main aerodynamic coefficients, the pitching moment break point and the reduced pitch rate as the blade passes through static stall incidence. The latter ramp rates have been calculated on the basis of stagnation point position movement using data from the wind tunnel runs. A second order curve was fitted to the data points immediately around that corresponding to 12.5º of incidence to avoid local noise generating spurious results and a factor of 350 has been used to convert stagnation point position into incidence. As with the vawt runs described in the wind tunnel results chapter, the upstream and downstream passes of the blade are treated separately: positive incidence corresponds to the upstream and negative to the downstream pass. Also shown in Table(20) is the ratio of upstream to downstream tangential force integrated over the half revolution.

8.3.1 Averaged runs without stall

At low wind speed perhaps the most striking feature is the difference between the upstream and the downstream passes. Referring to Table(20), maximum normal force coefficient for the revolution at a blade speed ratio of 7.83 is close to eight times larger over the upstream pass. Apparent incidence as set out in the table does not show this same degree of disparity, but incidence entries in this table do not take account of the built in incidence arising from the curved flow field around the blade. Normal intersection between blade chordline and rotor crossarm radius occurs approximately 124mm behind the leading edge of the 300mm chord blade. Projection forward of the crossarm radius results in the leading edge having an effective built in negative incidence under the present
coordinate system of:

$$\text{incidence} = \arctan\left[\frac{\text{projection}}{\text{crossarm radius}}\right]$$

For the present configuration this evaluates to -2.37°. Likewise the trailing edge sees an effective positive incidence of approximately 3.36° as already discussed in the previous Chapter.

Nose out of the leading edge is, however, likely to be more significant than trailing edge tail out since the leading edge and airflow around it tend to contribute a major portion of the normal force and tend also to control stall behaviour. Applying a correction of perhaps 1.5° on this basis might largely explain the apparent discrepancy between tabulated values of incidence and normal force coefficient. When the blade is set with leanout, that is span is no longer parallel with rotor rotational axis, this built in incidence will be reduced and will furthermore vary along the blade.

This first figure reveals an important conclusion: at low wind speed or high blade speed ratio the upwind blade is much more effective.

Cp traces show little of significance apart perhaps from the significant differences between the pressures at the trailing edge. On the outside surface there is substantially higher pressure than on the inside and this supports the conclusions drawn above with regard to trailing edge geometric tail out.

Also noticeable throughout the series is the lack of hysteresis loops in the force coefficient traces which were always present in the wind tunnel results even for runs of the smallest amplitude of motion.

At a blade speed ratio of 5.74 the flow curvature effect is relatively less significant ie leading and trailing edge effective toe out are smaller compared to maximum achieved incidence and, as shown in Table(20), there is less difference between maximum normal force coefficient and apparent incidence as determined by stagnation point position. Again outside trailing edge surfaces show higher pressure coefficients and leading edge behaviour is unremarkable, no evidence of a separation bubble being apparent. On the traces of normal and tangential force during the downstream pass there is, however, clear evidence of tower shadow, with the centre of the disturbance appearing late, that is after the blade has passed the geometrical downwind position. This latter is to be expected since the wake from the upstream pass should be convected trailing edgewards from the upstream pass from momentum considerations. No significant loops are apparent in the pitching moment traces.

Comparison of results with those of the vawt wave wind tunnel run 110 show lower incidence and lower main aerodynamic coefficients in atmosphere at stall. However no significant differences in normal force coefficient slope with respect to incidence can be reliably inferred. A lift coefficient slope correction would be about 20%, based on the aspect ratio of the present blade 10.0 and the relationship first due to Prandtl and quoted in Anderson reference (4) as shown below, where a is lift coefficient slope, a_o the 2D slope, AR the aspect ratio and tau a function of aspect ratio and equal to about 0.25 for a rectangular planform wing.

$$a = \frac{a_o}{1+(a_o/\pi.AR)(1+tau)}$$

However previous work by Willmer reference(99) has suggested that there is little spanwise change in lift coefficient and it is tempting therefore to compare directly 3D atmospheric data with that from 2D tunnel work. The conventional lift slope corrections relate to steady state behaviour and it

may be that the constant reversal of lift sense of the blade on-rotor does not allow time for the build up of the flow patterns that distinguish 3D from 2D flow.

Increasing wind further to a blade speed ratio of 4.65 results in the first sign of leading edge separation at the 6.5% tapping. Outside trailing edge pressure coefficients are depressed and on the inside surface they go negative for the first time. Stagnation point position indicates that static stall incidence has been exceeded during the upwind pass and the first hint of a loop in the pitching moment trace is apparent here also, but there is no divergence. Maximum normal force coefficient and incidence over this average revolution are now similar to those during the static wind tunnel run 127 shown at the head of Table(20). There remains, however about 10% difference between tunnel and atmospheric results at the equivalent blade speed ratio for the upstream pass. Downstream coefficients are here much less than one half of the upstream equivalents. A blade speed ratio of 4.65 is equivalent, using the two vector model, to a maximum incidence of 12.5° and so this plot may also be compared with the sine waveform wind tunnel run 76 figure(42).

At a blade speed ratio of 3.85 the pitching moment trace shows the first evidence of stall with a hint of divergence on the force trace and a loop on the coefficient versus stagnation point position graph, as the flow reattaches to the suction surface. There is however no negative movement of this coefficient during the cycle. Downwind coefficients are half or more of upstream, but there is much greater endurance of significant forces downstream so that the downstream pass is more effective at providing average torque for example, than its maximum value would imply.

8.3.2 Averaged runs with stall

Figure(66) at ß=3.35 shows the development of light stall during the upwind pass. Cp traces show the forward movement of a separated area of base pressure, but there is not yet evidence of vortex activity. Separation bubbles are apparent on both surfaces and pressure recovery at the trailing edge has collapsed even on the outer surface during upstream stall. Stagnation point position is now clearly affected by stall. Additionally significant hysteresis loops have opened up in the main

aerodynamic coefficient traces, significant particularly in the case of the pitching moment coefficient where the loop crosses, implying negative damping of pitching moment.

By ß=2.95 vortex behaviour is beginning to be apparent on the suction surface. Further, there is time for the base pressure area to reach nearly over the entire suction surface before incidence is reduced towards the end of the half cycle. The leading edge separation bubble appears to have moved forward to the 4% x/c position. From table(20) the up and downstream blade passes are providing here the same useful energy (neglecting of course skin friction drag). Tower shadow is now earlier, being exactly downwind.

At an average blade speed ratio of 2.66 hysteresis loops in the main force coefficients have opened up during the downwind pass and there is the first hint of downwind pitching moment break, but this latter does appear to be related to the tower shadow rather than a stall as such. Figure(69) at 2.34 ß shows these trends clearly. In contrast, the downwind stall of figure(70) at a blade speed ratio of 2.19 is fully developed and shows a stall generating vortices which move backwards over the outer surface from the leading edge. There is then a lengthy period of fully separated flow before reattachment. During reattachment there is little evidence of the pitching moment behaviour associated with suction being regained from the leading edge, as occurs during upwind recovery.

The last figure in this series figure(71) is formed of an average of revolutions which exhibited significant downwind stall as determined by pitching moment coefficient. They have been selected regardless of stagnation pressure blade speed ratio. The appearance of the traces and reduced forces is little different from the preceding figure except of course for the enhanced downwind pitching moment.

Figure(72) shows a scatter plot of pitching moment against blade speed ratio for the up and the downstream passes separately. The sudden divergence at ß=3 for the upstream pass is clear as is that for the downstream pass, but also evident is that this behaviour at these speed ratios is by no means universal and that divergence has not occurred in the majority of the revolutions downwind.

8.3.3 Fourier transforms of blade forces

Figures(73) to (75) show the Fourier transforms of normal force, tangential force and pitching moment over another series of blade speed ratios. The transforms are of average single revolutions and so the horizontal axis is effectively of rotor harmonic. No preconditioning or windowing has been carried out on the input signals.

Normal force transforms show the predominant importance of the fundamental with a falling importance of the mean level with wind speed in line with observations above regarding balance between up and downstream forces. Second harmonic initially rises with windspeed but then, above a blade speed ratio of about three, it begins to fall. Little energy is present in the third harmonic and above.

With regard to tangential force, the mean value is predominant but there is more energy available in the higher harmonics. The fundamental peaks in importance at about ß=5 and falls to only about 5% of the mean or 'dc' level at ß=2.5. The second harmonic remains high across the wind speed range averaging about 50% of mean strength whilst the third harmonic maintains a 20% to 30% strength. Higher harmonics are weak except at the highest wind strength represented here (ß=2.5) where a signal strength of nearly 30% of mean is shown.

Pitching moment transforms show little interest until ß=3 and below whereupon even harmonics up to 14 contain signals to nearly 10%, and harmonics up to three nearly 30%, of mean value.

The plots above pertain to average revolutions which tend to contain less high frequency excitation. The last plot of the series figure(76) shows a result for a single revolution at a blade speed ratio of 2.47. The picture described above holds roughly true here but the fourth harmonic of tangential force is quite strong at over 30% of mean value. The fundamental is dominant in the case of pitching moment and the third harmonic of are very strong at nearly 90% of this. Harmonics 5,6,8 and 10 are also strong.

8.3.4 Summary of trends over the decreasing blade speed ratio series

Most marked in the series is the difference in the behaviour of the blade during the upstream pass compared with the downstream. In low wind conditions at a blade speed ratio of 8 the upstream pass accounts for nearly all the energy extracted from the wind. If due account were taken of skin friction drag it is feasible that no net power is obtained downwind indeed it may be absorbed. At higher wind speeds the imbalance in usefulness becomes less marked as the aerofoil is loaded more fully and drag rises. At a blade speed ratio of about 3 the effectiveness of the upstream pass has decayed sufficiently to make equal to the downstream and this trend is continued becoming most marked at β=2.7 where upstream contributes only 3/4 of upstream power. With further increase in wind, downstream performance deteriorates further due to increased separation and greater tendency to stall. This is enough to reverse the trend and at the highest winds encountered in the present study (β = 2.2) the upwind pass has regained its dominance, with a ratio of upstream to downstream power extraction of about 1.2

Power imbalance up and downwind is not reflected in the ratios of peak forces, where downwind values never equal those of upstream. At low winds there is a factor of eight between up and downstream and this ratio never falls below about 1.3 over the full wind speed range encountered in the present work.

Gross differences such as these are in sympathy with the patterns of forces predicted by the double actuator disc multiple streamtube models of authors such as Sharpe references(73) and (83), Paraschiviou reference(68) and Stacey reference(88). Comparison of the integrated pressure forces with those of this latter author and also with those of Willmer reference(99) show the improvement of this technique over that of strain gauging rotor structural components.

In the frequency domain normal force is well behaved but both tangential force and pitching moment have significant excitation at high harmonics.

8.4.1 Comparison of RAL with Sandia Labs data

Figure(77) presents data from the present work and from the paper by Akins *et al* reference(3), showing probe incidence and normal force data for the 17m Sandia machine. The figure is arranged in columns.

Top of the first column is a graph of Sandia data showing the two vector vawt function model incidence compared to incidence derived from the flow probe projecting 0.375 chord before the blade leading edge. As noted by Akins there is a significant disparity.

The second graph in the figure is of stagnation point position derived incidence from the present experimental work plotted together with the probe data from the previous figure ie Sandia data. A factor of 350 has been used as the conversion between stagnation point position and incidence as was suggested by the wind analysis and discussed elsewhere. Agreement in the region of reasonable stagnation point fidelity ie below about 20° of incidence is good and demonstrates the deleterious effect on probe fidelity caused by blade presence. Both graphs discussed pertain to blade speed ratios of 2.6.

Five subsequent graphs compare normal force data from the RAL and the Sandia machines over a range of blade speed ratios. Incidence measure in both cases is two vector model or vawt function. Throughout the range there is remarkably good agreement between the two data sets although there is a measure of absolute level shift perhaps due to a difference in the 'toe in or out' of the blades. This latter effect may explain too the lower relative coefficient maxima towards and at the positive incidence extreme, that is the Sandia data shows less extreme positive coefficient excursions than does the RAL data.

The penultimate graph shows that too much emphasis should not be placed on any loops that may be present in the plots described above. In this present graph the relative phasing of the vawt function ie the incidence and the normal force coefficient data has been shifted by +6° and -6°, 6° being the interval between data frames in the Sandia data.

The last graph shows data from RAL selected on the basis of strong downwind stall pitching moment and

is included to show that using the method of Akins hysteresis loops over the downwind pass are possible but that they do not occur over the blade speed ratio range of the Sandia data.

8.5.0 Comparison of atmospheric with wind tunnel data

The present data set offers a unique chance to compare the performance of the same blade in tunnel and in atmosphere on-rotor. The following sections compare the tunnel and on-rotor data sets in terms of achieved blade force coefficient maxima and by comparing coefficient traces taken during the two phases of the experiment.

8.5.1 Maximum normal force coefficients

Figure(78) shows the maximum normal and tangential force coefficients achieved during both wind tunnel and atmospheric testing of the blade, against two measures of maximum incidence. In the top left of the figure are shown results for normal force coefficient against, in the case of the wind tunnel tests, the geometric incidence. For atmospheric data a supposed maximum incidence has been used based on the blade speed ratio and the two vector model so that

$$\text{alpha}_{max} = \arcsin(1/\beta)$$

Bladespeed ratio (β) has here been determined using stagnation pressure and no inflow effect has been allowed for. Manifest is a substantial difference in the normal force coefficient maxima, the largest atmospheric coefficients being about 1.5 (taking the mean line) whilst in tunnel coefficients reach 2.4 In doubt here is the accuracy of the relationship above overestimating incidence in atmosphere. Stagnation point offset evidence is used in the companion graphs at top right, where stagnation point position has been used for both data sets. At large incidence this is inadequate, as has been discussed elsewhere, but its use is retained here because interest is primarily at less than extreme stagnation point position.

Irrespective of the incidence method, maximum normal force coefficients during atmospheric running are clearly much less than those experienced during tunnel testing. Moreover the gradients of the two data sets are significantly different by a factor of perhaps 70%. Aspect ratio

effects might be of order 17% as suggested above, but it is clear that the change from two dimensional flow to three dimensional flow and the differences in spanwise constraint plus flow curvature and radically different turbulence levels are major contributors to the effect. Galbraith reference(33) suggests that progress in the understanding of the present differences can only be made by the use of flow visualisation techniques. Manifest is that structural design of wind turbines based on simple wind tunnel studies of oscillating blades is likely to be very conservative.

A point which should not be overlooked is that although the reduced pitch rates at static stall have been listed they are not necessarily a good measure of the incidence achieved between static stall incidence and the expiry of the stall delays discussed in the previous chapter. It is the pitch rate and by implication the maximum incidence achieved before the expiry of the delays that, to a first approximation, decides the maximum achieved normal force coefficients. This point deserves further investigation.

8.5.3 Blade tangential force

Tangential force coefficient comparisons in the same format as above are shown in the bottom two graphs in figure(78). Coefficients are based, as above, on instantaneous stagnation pressure and integrated pressures around the aerofoil.

Again, as with normal force coefficient, the two data sets are different by a large factor and again a modest improvement is made when the data is compared on the equal footing of maximum achieved stagnation point position, but there remains a substantial difference which must be explained by 3D effects.

8.5.4 Blade force and moment coefficients in tunnel and atmosphere

Figures(79) and (80) show the principal force and moment coefficients for the present blade when run on-rotor and in the wind tunnel. Best matches have been selected in both cases between the two data sets and no significance should be placed on the apparent phase shifts between them. In the first figure good agreement exists between

the data sets over the positive or upwind half cycle for both normal and tangential force coefficients. Over the negative or downwind half cycle agreement is poorer because of the effects of the upstream pass in the case of the atmospheric data. Pitching moments are here small and absolute level differences are likely to be caused by errors in instrumentation and pitch trim and are thus not significant. There is however a significantly different shape, the on-rotor blade suffering a stall whilst the blade in tunnel did not.

Vawt function incidence for the bin average blade speed ratio of 3.36 in this example would be 17.3°. This compares with the tunnel run maximum incidence of 12.5° and suggests a windspeed interference factor of about 0.28 here.

Turning to the second figure at a blade speed ratio of 2.19 again shows good agreement in shape between the two data sets for normal force and would perhaps be better with a smaller amplitude of wind tunnel motion. Tangential force coefficient compares reasonably as far as amplitude is concerned but the tunnel data does not adequately duplicate the rapid drop in coefficient in the period after stall. Pitching moment coefficient matches upwind stall fairly well but downstream the pattern and magnitude is missed. Vawt function incidence for the bin stagnation pressure blade speed ratio of 2.19 is 27.2° and comparing this with the 17.5° tunnel maximum amplitude suggests an inflow interference factor of about 0.36 in this example.

The above comparison suggests that wind tunnel simulations of simple incidence patterns can provide approximate correlations with the results of atmospheric tests but that these correlations are poor particularly on the downstream or negative incidence half cycle. It is clear that because of inflow and other effects, incidence as seen by the blade is markedly lower than the two vector model would suggest to the point where the difference between it and the sinisoidal pattern is minimal. In this situation it seems inappropriate to concentrate on the vawt wave form model in preference to the simpler sinusoid. In the Glasgow facility, vawt function incidence at run time is obtained from a 'lookup table' in the micro computer driving incidence and it would seem sensible to suggest that this facility be programmed with a more appropriate incidence function once such a function is developed.

8.6.0 Rotor coefficient data

As descibed elsewhere all revolutions of data gathered in the present work have been subjected to the DATPROC package which has analysed them for about 40 attributes including maxima and minima of forces and pressures and azimuthal angles when these occurred, wind strengths, rotor speeds, blade speed ratios, turbulence levels and average Reynolds numbers. Some of these data are presented below, in particular data relating to the rotor blade tangential and normal force and these have also been transformed into power coefficient and rotor thrust.

8.6.1 Rotor torque coefficient

Shown in figures(60) and (61) for the four blade leanout angles for which data was taken in the present experiment are mean and ±1 standard deviation plots of rotor torque. Rotor torque coefficient C_Q is defined as

$$C_Q = \frac{Q}{\frac{1}{2} \rho W^2 r A}$$

where Q is the developed torque, ρ is the air density, W the free wind speed, r the rotor radius and A the rotor projected area. This latter rotor projected area is the trapezoid formed by the radii to the ends of the 1m length of blade containing the pressure tapped chord when viewed from a distance.

Comparing the figures(60) and (61) shows a marked difference between the curves using the two wind speeds. Stagnation pressure derived wind speed shows a marked improvement in scatter but the trends derived by the two windspeeds are significantly different. Using anemometer windspeed results in an essentially flat response from low to medium windspeed followed by a gentle decline from a windspeed ratio of about 0.3 where separation might be expected to start, whereas with stagnation pressure based windspeed there is a definite maximum at about 0.25 windspeed ratio. The latter performance where performance peaks at a blade speed ratio of about 4 would be in keeping with observation of practical machines.

Blade leanout angle shows a clear trend with a fall in C_q roughly in line with the cosine of the blade leanout angle. This relationship over blade leanout angle is preserved with anemometer wind also.

8.6.2 Rotor power coefficient

Further displayed in figures(60) and (61) are plots of rotor power coefficient for the four blade leanout angles. Power coefficient C_P is defined as

$$C_P = \frac{P}{\frac{1}{2} \rho A W^3}$$

where P is the developed aerodynamic power and other terms are as defined above. Here the two windspeed measuring methods are in agreement in so far as a steep decline in coefficient with wind speed is concerned. However with respect to the effect of blade leanout, anemometer wind shows no significant effect whereas stagnation pressure wind shows a substantial effect particularly at low windspeeds.

8.6.3 Rotor thrust coefficient

Also displayed in figures(60) and (61) are the rotor thrust coefficients of all atmospheric run data for the four blade leanout angles. The coefficients have been determined from the formula

$$C_F = \frac{Nfmax_{up} + Nfmax_{down}}{\frac{1}{2} \rho W^2 A \cos(\text{blade leanout})}$$

where $Nfmax_{up}$ and $Nfmax_{down}$ are the maximum normal forces encountered during the up and the downstream passes respectively as determined from the integrated blade pressures. This formula is not strictly correct since the upstream and downstream maxima will not necessarily occur at the same time, nevertheless the magnitude of the error is not likely to be very significant since the errors are associated with the cosine of the difference between the azimuthal angles at which the maxima occur.

There is a clear trend in the force coefficients, with the upright zero leanout blades generating the highest coefficients and the heavily inclined

blades the least. Further, the coefficients span a wide range, with very high values at low wind speeds reflecting the existence of the rear blade pass and conventional values at high winds. These results go some way to explaining why maximum machine loadings are less severe than was feared in the early days of modern wind turbine design.

8.6.3 Maximum/ average tangential forces and rotor torque

Useful power from a wind turbine rotor will be a function of its average torque over a revolution, whilst gearbox cost for a commercial wind turbine will be a function primarily of peak torque. The ratio of peak/average torque is therefore of consequence since it describes the torque 'efficiency' of the prime mover- the rotor. The more nearly the average torque is to the peak torque the lower the cost of the gearbox for the rated power.

The first graph in figure(81) shows the ratio of average to peak blade tangential forces which is equivalent to the ratio of average to peak torques. It is clear that for zero blade leanout angles the torque efficiency is a function of blade speed ratio. It reaches a maximum of about 0.3 at a wind speed ratio of about 0.35 and rises with rising blade speed ratio; a result that ties in with the results of upwind to downwind tangential effort set out in table(20). Results for non-zero blade leanout angles show nearly identical characteristics though there is a suggestion that inclined results have lower efficiencies.

8.6.4 Average tangential/ maximum normal forces

A second measure of a rotors 'efficiency' is the useful average tangential force compared to the maximum blade normal force, which might be treated as a structural cost. It is likely that this 'efficiency' is the most significant of the three efficiencies discussed in this section since blade stresses are usually the most significant and difficult to deal with of the stresses in a wind turbine. The second graph in figure(81) shows this benefit/cost ratio. As with the torque ratios above, this ratio rises to a plateau at a windspeed ratio of about 0.35 with an efficiency of about 0.06 for upright or zero leanout blades. Non zero leanout results are lower, probably by around 0.01 or so for the wind speeds covered in the data set,

but there is no sign of the curve flattening for the 45° data.

8.6.5 Average tangential forces/ rotor thrust

The third of the measures of efficiency dealt with in figure(81) is the useful average tangential force compared to the rotor thrust load or tower load. This problem of tower thrust is not negligible by virtue of the elevation at which it occurs and the consequent implications for tower foundations particularly if the turbine is to be sited offshore or if the ground substrata are of poor load bearing capacity.

As will be seen from the graphs the zero leanout data suggests that this rotor thrust efficiency plateaus at around the 0.35 windspeed ratio region at about 0.035 for upright blades but, as with the blade maximum normal forces, the available data for the 45° leanout condition does not show a maxima.

These results might offer some tentative encouragement for the vawt rotor designs employing inclined or leant out blades, for here the 'efficiency' of the rotor is better than for upright bladed rotors particularly in higher winds where it counts most. On the other hand in the case of the V vawt blade leanout generates an additional overturning moment which probably outweighs this benefit.

8.7.0 Summary

This chapter has presented some of the data obtained from the test blade whilst mounted on-rotor over a range of windpeeds, rotor speeds and blade leanout angles. Data has been presented in averaged format based on blade speed ratio and in scatter plots of basic statistics of blade and rotor performance.

Good correlation has been found between the present data and that from the 17m Sandia Labs machine both in terms of the normal force coefficient pattern and the incidence pattern with azimuth, at least at moderate incidence. It is found that upstream to downstream blade performance changes markedly over the blade speed ratio range, that blade forces on-rotor are substantially lower than those in tunnel and that rotor thrust coefficients are very high. Rotor forces in general

fall as the cosine of the blade leanout angle.

Simulation of the vawt blade environment in tunnel using the vawt function waveform of incidence with time appears not to justify the effort. Incidence patterns on-rotor are very different from this function having pronounced asymmetry in amplitude rather than ramp rate to maximum incidence.

CHAPTER 9

CONCLUSIONS AND SUGGESTIONS FOR FURTHER WORK

9.0.0 Introduction

Aerodynamic loading of a wind turbine in operation is still poorly understood and modelled and one of the main reasons for this is the poor database of rotor loads available. This project was intended to be primarily one of aerodynamic testing to provide such a data base of aerodynamic structural loading. However, as has been seen in earlier chapters, logistics and instrumentation have played a large and vital part in the project's progress. A significant and important advance in the method of use of pressure transducers to measure very small pressures has been made and this has been crucial to the success of the project. Exhaustive efforts to build a reliable and maintainable rig have enabled aerodynamic testing whenever a good wind has been available and have been an essential adjunct to the technique. This chapter reviews and summarises the main points that have arisen from an analysis of the aerodynamic data won and of the instrumentation technique used.

9.1.0 Aerodynamic conclusions

Some 118 wind tunnel runs and 1760 revolutions of atmospheric data totalling about 50 Mbytes were gathered in the course of the project. Necessarily only a tiny proportion of this data has been presented in this thesis, principally in Chapters 7 and 8. The following section attempts to summarise the main conclusions that have been drawn from the aerodynamic analysis so far conducted. In no way can the data be considered to have been fully analysed but some important conclusions have nevertheless been drawn.

1) Aerodynamic performance of the instrumented blade module when tested in wind tunnel was consistent with published data, but showed a lower than expected Reynolds number sensitivity.

2) Normal force data collected on-rotor compared well with similar data collected from the Sandia Laboratories 17m machine.

3) Blade forces and moments are grossly less on-rotor than in tunnel. This can be partly explained by substantial differences in blade incidence arising from substantial interference factors which apply even in the strongest winds analysed. But there remains a difference in the gradients of maximum Cn against incidence inferred from stagnation point position and this difference probably arises from the two dimensional nature of attached flow in tunnel compared to fully three dimensional flow on-rotor.

4) Dynamic stall appears to be of the mixed type in the examples studied. Separation starts at a point mid chord and moves forward to the leading edge area. This is followed a few units of reduced time later by the passage of a vortex starting near the leading edge and rolling back to the trailing edge.

5) Reduced time delays in tunnel between attainment of static stall incidence and moment and normal force stall are 2.56 and 7.62 with standard deviations of 0.65 and 1.03 respectively. Moment stall delay agrees well with established data, but normal force delay is substantially greater.

6) Front or upwind blade pass does most work. The ratio F/R changes greatly with blade speed ratio being high (of order 7) in low winds and falling to 0.75 around bsr=2.5 and then rising again to 1.2 at bsr=2.2 Traces of normal force agree in gross terms with the more sophisticated of the multiple streamtube rotor models.

7) Upstream blade stall begins at a blade speed ratio of about 3.0, downstream stall at about 2.5

8) Simulation of wind turbine blade incidence in wind tunnel using the vawt function provides little if any benefit. Real on-rotor conditions are so different that the fine difference between vawt and sine at the angles of attack experienced in practice is lost.

9) Use of stagnation point to provide a surrogate incidence works up to and slightly beyond moment stall. Below static stall incidence accuracy and linearity is good and appears

better than any signal available from a single pressure tapping point. Beyond static stall incidence, stagnation point position can be used whilst pitch rate is substantial and normal force stall has not yet occurred, but the relationship between position and incidence is no longer linear and accuracy is less good. Good correlation exists between normal force and stagnation point position in most dynamic situations up to an incidence approaching 20°. Transferability of stagnation point incidence between wind tunnel and rotor has not been yet been established.

10) Flow probes projecting forward of the leading edge by only a fraction of a chord render available little more data than is available from stagnation point position.

11) Stagnation pressure derived wind speed considerably and usefully reduces scatter of aerodynamic coefficient response, but causes distortion of the resulting picture.

12) Blade force harmonic content changes markedly with blade speed ratio. First harmonic of normal force becomes very dominant at high wind speed. Tangential force first harmonic falls with windspeed, the second remains more or less constant and higher harmonics, the third, fourth and sixth, increase with wind. Pitching moment harmonics increase strongly as wind strength rises.

13) Rotor coefficients behave as in the table below

coeff ↓	low wind	high wind
torque	0.05	0.025
power	0.4	0.05
thrust	3	1

Coefficients fall roughly as the cosine of the leanout angle.

14) Rotor goodness (the ratio of average tangential to maximum tangential force, maximum normal force and rotor thrust) plateaus at windspeed ratios above about 0.35. There is no significant difference with leanout for the ratio average to maximum tangential force, but

the ratio average tangential to maximum normal force is worse with leanout. By contrast the ratio average tangential force to rotor thrust is better with leanout. These results would support the use of a slower rotor running speed.

15) No significant correlation with turbulence as measured by the means described in the preceding chapters has been noted.

16) No effect of blade passing on closely sited anemometers was detectable.

9.2.0 Software temperature compensation of transducer output

Thermal compensation of semiconductor piezo resistive pressure transducers must be considered a success. A considerable logistic overhead no doubt exist because of the need for a doubling of data streams (though there need be only a very modest increase in the amount of data), but the convenience and security of knowing the status of each transducer throughout the data gathering period must justify this. The method does not prejudge any transducer performance save that of consistency and thus allows any thermal characteristic to be accommodated. Computational overhead using this method was judged to be minimal.

Chapter 3 shows that present electronics was able to give zero pressure readings to an accuracy of about 40Pa to 95% confidence. With good calibration, to a standard higher than that achieved in the present work, reliable measurements could probably be made to within this figure over the whole pressure range. More optimal settings of amplification and transducer excitation could also have been made and the sample and hold system omitted at the present frequency of data acquisition.

For very stable temperature conditions, for example in an open jet wind tunnel, most of the transducers used in the present project would appear to be sufficiently accurate without any compensation system and indeed one team is using this system. Cost and availability considerations for these transducer schemes would appear very attractive.

Insistence on high quality components, hardwiring

of signal leads and rotating the instrument rack were judged worthwhile as were proper rotor starting methods and improvements to the instrumentation.

9.3.0 General conclusions regarding site suitability

Aerodynamic turbulence at the Rutherford site is high, average windspeeds are low and the orientation is poor, the prevailing southwesterly wind coming over the Ridgeway as shown in photographs at the beginning of this thesis. Consequently good strong winds are available only very infrequently and are usually associated with storms so that rain is threatening if not present. Aerodynamic research using pressure transducers requires dry conditions and consequently use of this instrumentation on this site cannot be recommended.

For work on small machines it is recommended that the experimental rig be trailer mounted, commissioned at the research establishment responsible and then towed to a good wind site. Perhaps a year might have been saved from the present project had this been done.

9.4.0 Further work

The present project has been successful in obtaining a small but significant data set, but there remains much analysis to be carried out on the existing data and there is also a need for much more data to fill in some of the sparse areas in the present data set. Some of the more obvious areas and important areas of further work are set out below.

1) Flow probe separation from leading edge of blade needs to be investigated to arrive at an optimum where blade presence has less effect.

2) An empirical code to obtain incidence from stagnation point position in the manner of dynamic stall models of force coefficients might be an alternative.

3) Analysis of existing statistics of the present data for implied inflow factor, flowfield expansion and swerve, that is difference in heading between anemometer and rotor measured wind direction.

4) Gross blade force differences between tunnel and on-rotor tests need to be investigated to determine if they can be accounted for by present theory. Although pitching rates at static stall incidence in the two environments are comparable, could effective rates up to normal force stall account for differences? Are stall reduced time delays in atmosphere comparable with results in tunnel?

5) Comparison of existing rotor models by many authors with present data.

6) Much more data needed to improve confidence in conclusions and to extend data set into high windspeed ratio area.

It is anticipated that considerable further reduction and interpretation of the data will be undertaken both on its own by the present author and supervisor and in conjunction with other data which will be produced by the same rig under a new contract.

9.5.0 Conclusion

The vertical axis wind turbine as distinct from the horizontal configuration has substantial mechanical economies which can only be realised if the more complicated transient aerodynamics of the rotor flow can be understood and accommodated in the design. This project has attempted to examine aerodynamic blade forces imposed on the structure, as opposed to its response, by using integrated pressures from around the blade. The technique relies on pressure measurement of quickly changing pressures of very small magnitude from transducers subject to high acceleration and significant temperature extremes. A novel technique has been used which has successfully won a significant body of data. Rotor flowfield modelling will be advanced by this data set.

REFERENCES

1 Abbot IH von Doenhoff AE; Theory of Wing Sections; Dover 1959

2 AGARD; Special course on unsteady aerodynamics; Report 679 1980

3 Akins RE Klimas PC Croll RH; Pressure distributions on an operating vertical axis wind turbine blade element; Proceedings of US Wind Workshop VI Minneapolis St Paul June 1983.

4 Anderson JD; Fundamentals of Aerodynamics; McGraw Hill, 1986

5 Anderson MB, Powles SRJ, Harris A, Tan CC; The Analysis of Data from a 25 metre Stall Regulated Vertical Axis Wind Turbine; Proc European Wind Energy Conference Glasgow 1989.

6 Angell RK Musgrove PJ Galbraith RAMcD; Unsteady Wind Tunnel Testing of Thick Section Aerofoils for Use on Large Scale Vertical Axis Wind Turbines; Proc British Wind Energy Association Conference 1988.

7 Baker JR; *; J Wind Engineering *; 1983

8 'Beaufort' Windwatch Wind Directions V1 #2 1986

9 Beddoes TS; A synthesis of unsteady aerodynamic effects including stall hysteresis; Paper 17 Proc First European Rotorcraft & Powered Lift Aircraft Forum, University of Southampton 1975.

10 Beddoes TS; An analytic model for trailing edge stall; RP 637 Westland Helicopters 1981.

11 Beddoes TS; Representation of airfoil behaviour; AGARD Proc 334 Prediction of Aerodynamic Loads on Rotorcraft; 1982.

12 Beddoes TS; Practical computation of unsteady lift; Vertica V8 #1 1984.

13 Bendat JS, Piersol AG; Engineering Applications of Correlations and Spectral Analysis; Wiley 1980.

14 Berg H Tijdeman H; Theoretical and experimental results for the dynamic response of pressure measuring systems;NLR report NLR-TR F.238

15 Betz A; Windmills in the light of modern research; NACA TN-474 1922.

16 British Wind Energy Association; Wind Power For The UK a BWEA Position Paper; BWEA 1987

17 Brigham EO; The Fast Fourier Transform; Prentice Hall.

18 Brochier G, Fraunie' P, Beguier C, Paraschivoiu I; Experimental study of dynamic stall on Darrieus wind turbines; Proceedings 20th Intersociety Energy Conversion Engineering Conference, Miami Florida 1985.

19 Bryer DW, Walshe DE, Gardner HC; Pressure Probes Selected for Three Dimensional Flow Measurements; NPL/HMSO 1958.

20 Butterfield CP; Three Dimensional Airfoil Performance Measurements on a Rotating Wing; Proc European wind Energy Conference 1989.

21 Clayton BR Morsi YSM; Unsteady Aerodynamics Related to Vertical Axis Rotors; Proc British Wind Energy Association Conference Reading 1984.

22 Daley DC, Jumper EJ; Experimental investigation of dynamic stall for a pitching airfoil; J Aircraft V21 #10 1984.

23 Dean RC; Aerodynamic measurements; MIT 1953

24 Eggleston DM, Stoddard FS; Wind Turbine Engineering Design; Van Nostrand Reinhold; 1987

25 Entran Ltd; Pressure transducer instruction and selection manual; Entran Ltd.

26 Epstein AH Kerrebrock JL Thompkins WT Jnr; A miniature high frequency sphere probe; MIT

27 Ericsson LE, Reding JP; Unsteady flow concepts for dynamic stall analysis; J Aircraft V21 #8 1984.

28 Everett KN, Gerner AA, Durston DA; Seven-Hole Cone Probes for High Angle Flow Measurement: Theory and Calibration; AIAA J V21 #7.

29 Favier D, Maresca O, Rabont J; Dynamic Stall due to Fluctuations of Velocity and Incidence; AIAA J Vol 20 July 1982

30 Francis MS, Keesee JE; Airfoil Dynamic Stall Performance with Large-Amplitude Motions; AIAA J V23 #11

31 Galbraith RAMcD, Niven AJ, Seto LY; On the Duration of Low Speed Dynamic Stall; ICAS-86-2.4.3

32 Galbraith RAMcD Barroman J Leishman JG; Description of the Sample and Hold Circuits for the Glasgow University Dynamic Stall Facility; GU AERO Report 8208 1982

33 Galbraith RAMcD; personal communication; 1989

34 Gangwani ST; Synthesised airfoil data method for prediction of dynamic stall and unsteady airloads; Vertica V8 #2 1984.

35 Gault DE; A correlation of low-speed, airfoil-section stalling characteristics with Reynolds number and airfoil geometry; NACA TN3963 1957.

36 Glauert H; The analysis of experimental results in the windmill brake and vortex ring states of an airscrew; Aeronautical Research Committee Reports and Memoranda No.1026 1926.

37 Grubb M; The Integration of Wind Energy on Power Systems; Wind Directions Vol 7&8 #4,1&2

38 Harris A, Clayton BR, Galbraith RAMcD, Garside AJ, Angell RK, Foster JE; Vertical Axis Wind Turbine Aerodynamic Research in the UK; Proc European Wind Energy Conference Glasgow 1989.

39 Houghton EL, Carruthers NB; Aerodynamics for Engineering Students; Arnold, 1982.

40 Inman BR; An engineering evaluation of pressure transducers and the dynamic response of pressure sensing systems; MSc thesis Cranfield Institute of Technology 1972.

41 Jacobs EN, Sherman A; Airfoil section characteristics as affected by variations of the Reynolds number; NACA Rpt 586, 1937.

42 Jaras TF; Wind Energy 1987: Wind Turbine Shipments and Applications; Wind Data Centre, Stadia Inc, USA 1987.

43 Klimas PC; Tailored Airfoils for Vertical Axis Wind Turbines; Sandia National Laboratories Albuquerque NM USA; 1984.

44 Klimas PC; personal communication via RL Hales; 1987.

45 Kerrebrock JL Epstein AH Thompkins WT; A Miniature High Frequency Sphere Probe; Massachusetts Institute of Technology.

46 Kulite Semiconductors; Temperature compensation techniques for semiconductor strain gage sensors; application note AN-06A; Kulite Semiconductor Products Inc.

47 Lee JD Lee TD; Statistics and computer methods in BASIC; Van Nostrand Reinhold 1982

48 Lin JC, Walsh MJ; Turbulent Roughness Drag Due to Surface Waviness at Low Roughness Reynolds Numbers; J Aircraft V21 #12 1984.

49 Ly Ke Hein; Measurements on an Oscillating Aerofoil with Applications to Wind Energy Conversion; report ME R 80/7, PhD Thesis; University of Auckland, New Zealand, 1980

50 Mallon JR Bernstein H; Temperature Compensation and Shunt Calibration of Semiconductor Pressure Transducers; Twelfth Transducer Workshop June 1983 Melbourne Florida USA.

51 Maydew RC, Klimas PC; Aerodynamic Performance of Vertical and Horizontal Axis Wind Turbines; J Energy V5 #3 1981.

52 McCroskey WJ, Carr LW, McAlister KW; Dynamic Stall Experiments on Oscillating Airfoils; AIAA J; V14 #1 1976.

53 McCroskey WJ, Fisher RK; Detailed Aerodynamic Measurements on a Model Rotor in the Blade Stall Regime; J American Helicopter Soc. V17 #1 1972.

54 McCroskey WJ, McAlister KW, Carr LW, Pucci SL, Lambert O, Indegrand RF; Dynamic Stall on Advanced Airfoil Sections; J American Helicopter Soc. V26 #3 1981.

55 Migliore PG; Straight Bladed Darrieus Wind Turbines: A Protagonists View; Deptartment of Mechanical Engineering University of California, Davis.

56 Morgan CA Gardner P Mays ID Anderson MB; The Demonstration of a Stall Regulated 100kW Vertical Axis Wind Turbine; Proc European Wind Energy Conference Glasgow 1989.

57 Moss GF, Murdin PM; Two dimensional low speed tunnel tests on the NACA-0012 section including measurements made during pitching oscillations at the stall; HMSO CP1145 1971.

58 Moulang B; personal communication 1984.

59 Mueller TJ; The influence of laminar separation and transition on low Reynolds number airfoil hysteresis; J Aircraft V22 #9 1985.

60 Newland DE; Random Vibrations and Spectral Analysis; Longmans 1987.

61 Nyland EW England DR Anderson RC; On the dynamics of short pressure probes: some design factors affecting frequency response; NASA TN-6151.

62 Nyland EW and Anderson RC; Some limitations on the use of damping in short pressure probes; NASA TN D-6526; 1971.

63 Nyland EW England DR Gebben VD; System for testing pressure probes using a simple pressure generator; NASA TM X-1981.

64 Oler JW, Strickland JH, Im BJ, Graham GH; Dynamic Stall Regulation of the Darrieus Turbine; Proc Workshop on Unsteady Separated Flow USAF Academy 1983.

65 Oler JW, Strickland JH, Im BJ, Graham GH; Unsteady effects on airfoil angle of attack measurements. Informal Report to Sandia Laboratories; personal communication with Strickland JH 1985.

66 Ostowari C, Wentz WH Jnr; Modified Calibration Technique of a Five-Hole Probe for High Flow Angles; Experiments in Fluids 1 1983

67 Paraschivoiu I, Parrouffe JM; Unsteady Potential Flow for Oscillating Airfoils; Canadian Aeronautics and Space Journal V31 #2 1985.

68 Paraschivoiu I, Fraunie P, Beguier C; Streamtube Expansion Effects on the Darrieus Wind Turbine; J. Propusion V1 #2 1984

69 Parachivoiu I Allet A; Dynamic Stall Models for Darrieus Rotors; Proc Canadian Wind Energy Assoc Conference 1986.

70 Pope A; The Forces and Moments Over an NACA 0015 Airfoil Through 1800 Angle of Attack; Aero Digest V58 #4 April 1949

71 Rae WH, Pope A; Low Speed Wind Tunnel Testing; Wiley, 1984

72 Raghunathan S, Ombaka OO; A thick symmetrical aerofoil oscillating about zero incidence angle; Int. J. Heat and Fluid Flow 1986.

73 Read S, Sharpe DJ; An extended multiple streamtube theory for vertical axis wind turbines; Second BWEA Workshop April 1980.

74 Riegels; Aerofoil Sections; Butterworths 1961.

75 Riley J; personal communication 1985.

76 Roark RJ Young WC; Formulas for stress and strain; McGraw Hill 1976

77 Samet M, Einav S; Directional Pressure Probe; Rev. Sci Instrum 55(4) 1984.

78 Schweikhard WS; Test techniques, instrumentation and data processing; AGARD LS-72 Distortion induced engine instability November 1974

79 Sensym Ltd; Low and mid pressure range monolithic pressure transducers.

80 Sensym Ltd; SPX50 SPX100, SPX200 Integrated cicuit pressure transducers; Sensym Ltd.

81 Seto LY, Galbraith RAMcD; The Effect of Pitch Rate on the Dynamic Stall of a NACA 23012 Aerofoil; Procedings of the Eleventh European Rotorcraft Forum 1985.

82 Seto LY Galbraith RAMcD; The Collected Data For Ramp Function Tests on a NACA 23012 Aerofoil GU AERO Report 8413 1984.

83 Sharpe DJ; Refinements and developments of the multiple streamtube theory for the aerodynamic performance of vertical axis wind turbines; Proc BWEA Conference Reading UK 1984.

84 Sheldahl RE Klimas PC; Aerodynamic characteristics of seven symmetrical airfoil sections through 1800 angle of attack for use in aerodynamic analysis of VAWTs; SAND80-2114, Sandia Laboratories, Albuquerque NM 1981.

85 Shida Y, Kuwahara K, Ono K, Takami H; Computation of Dynamic Stall of a NACA-0012 Airfoil; AIAA J V25 #3 1985.

86 Sitaram N, Treaster AL; A Simplified Method of Using Four-Hole Probes to Measure Three-Dimensional Flow Fields; J of Fluids Engineering V107/31 1985.

87 Seetheram HC, Wentz WH Jnr, Walker JK; Measurement of Post-Separated Flowfields on Airfoils; J Aircraft V14 #1 1977.

88 Stacey G; Experimental and theoretical developments of the variable geometry vertical axis wind turbine; PhD thesis University of Reading 1983.

89 Strickland JH, Graham GM; Dynamic Stall Inception Correlation for Airfoils Undergoing Constant Pitch Rate Motions; AIAA J V24 #4 1985

90 Strickland JH, Graham GM; Force coefficients for a NACA-0015 airfoil undergoing constant pitch rate motions; AIAA J V25 #4 1986

91 Tinsley Strain Measurement Ltd; Miniature pressure transducers, instructions for use; Tinsley Strain Measurement Ltd.

92 Tomlin; Basic Practical Signal Processing: Course Notes; Cranfield Institute of Technology 1987.

93 van Bussel GJW; A comparison of open air performance measurements using different methods; Proc Ninth BWEA Conference, Edinburgh, 1987.

94 Vezza M, Galbraith RA McD; A method for predicting unsteady potential flow about an aerofoil; Int J Numerical Methods in Fluids V5 1985.

95 Vittecoq P, Laneville A; The Aerodynamic Forces for a Darrieus Rotor with Straight Blades: Wind Tunnel Measurements; J of Wind Engineering and Industrial Aerodynamics 15 1983 pp381 388.

96 Walker JH, Helin HE, Strickland JH; An experimental investigation of an airfoil undergoing large amplitude pitching motions; AIAA J V23 #8 1985.

97 Welsh BL Pyne CR; A method to improve the temperature stability of semiconductor strain gauge transducers; J. Phys. E: Sci Instrum., Vol 13 1980.

98 Wickens RH; Wind Tunnel Investigation of Dynamic Stall of an NACA 0018 Airfoil Oscillating in Pitch; National Aeronautical Establishment Aeronautical Note NAE-AN-27/ NRC 24262

99 Wilmer AC; Aerodynamic Investigation into the feasability of a 25 m vertical axis windmill; Aero Report 124 BAe Filton 1979.

100 Wilmer AC; Low Reynolds Number Tests on the NACA 0015 Section; Proceedings of First BWEA Wind Energy Workshop Cranfield 1979.

101 Wilson RE, Klimas PC; Drag Coefficient for the NACA 0015 Darrieus Rotor Blades; Sixth Biennial Wind Energy Conference and Workshop, American Solar Energy Soc 1983.

102 Zervos A, Morfiadakis E, Stefanatos N; Testing of Blade Profiles for Vertical Axis Wind Turbines; Proc European Wind Energy Conference Glasgow 1989.

APPENDIX 1

TEMPERATURE COEFFICIENT OF TEMPERATURE COMPENSATION MODULE

11.1.0 Introduction

Inconsistency in signal from Kulite transducers has been noted in the main text. A short test was carried out to determine if the temperature compensation resistors present in the temperature compensation module could be responsible for the observed errors and a description of the tests and the analysis used is given below. The analysis concludes that temperature effects on the compensation module could indeed be responsible for some of the noted observations.

11.1.1 Method of tests

A compensation module of the type used with the cylindrical transducers originally intended for use in the leading edge stations was selected at random for these tests. A number of transducers had been left over from earlier projects at Cranfield and these had been salvaged and earmarked for the present project. Unfortunately during the salvage operation some temperature compensation modules had become separated from their transducers and it was one of these that was used for the present tests.

DC resistance of one of the resistors contained in the module was measured as the latter was moved from cool to warm environments and back again. Dewar flasks (thermos) of water were used for this purpose. The Thurlby 5½ digit DMM type 1905a was used for these measurements and the results are plotted in figure(8).

A least squares fit to these data gives a resistance gradient of 5.6 ohms/degC corresponding to a temperature coefficient of 230 ppm/degC

11.1.2 Calculation of sensitivity of output to temperature effect

Referring to figure(83) for the circuit used for the transducer and temperature compensation module,

consider the effect of temperature in resistor rsh on the transducer output, point G.

Resistance of resistor pair KG and RSH, at temp 0

req0=kg*rsh0/(kg+rsh0)

voltage at G

g0=req0/(req0+ru)

resistance of KG and RSH, at temperature 1

req1=kg*rsh1/(kg+rsh1)

G is then at

g1=req1/(req1+ru)

the change in output of G with change in temperature is then

g1-g0=req1/(req1+ru)-req0/(req0+ru)

taking typical values for kg and ru at 2000 ohms and ignoring rse (small cf ru etc)

req0=2000*24000/(2000+24000)=1846.15

req1=2000*24000*1.000230/(2000+24000*1.000230)=1846.
g0=1846.15/(1846.15+2000)=0.48

g1=1846.19/(1846.19+2000)=0.48

the thermal change is then 0.000004415

this is the per-volt-excitation figure for one °C change.

For 20 V excitation and 20°C the figure will be 0.001766010

this compares with a typical Kulite sensitivity of about 2mV per 1kPa or in other words about equal to the dynamic pressure under typical operating conditions.

APPENDIX 2

CENTRIFUGAL EFFECT ON BLADE REFERENCE PRESSURE

11.2.0 Introduction and analysis

Pressure transducers used in this project have been of the differential type that is they are sensitive to the difference between two pressures. In the present work one side of the transducer is exposed to the pressure provided by a tapping in the aerodynamic surface of the blade and the other side, a reference pressure provided by a tube connected to a manifold system in turn connected to a tube leading along the rotor crossarm to the rotor hut. Air in the tube in the crossarm and indeed in the manifold system leading to the transducer, is subject to a radial acceleration which will raise the pressure in this system and thus affect the readings taken by the transducer. Analysis of this pressure below shows that it is comparable with the dynamic pressure at the blade.

consider a volume of air in the tube

(force acting radially outward)$=p.A+A.\rho_{local}.r.\Omega^2.dr$

(force acting radially inward)$=A.(p+dp)$

for equilibrium

$A.(p+dp)=p.A+A.\rho_{local}.r.\Omega^2.dr$

where

A is the cross sectional area of the tube
p is the local pressure in the pipe
ρ_{local} is the local air density
r is the local radius
Ω is the angular velocity

cancelling terms leaves

$\rho_{local}.r.\Omega^2.dr=dp$

but ρ_{local} = mass/volume

and from the universal gas law p.v=m.Rg.T

density = p/(Rg.T)
where Rg is the specific gas constant, v volume, m mass,

and T the absolute temperature

substituting

$$\frac{p.r.\Omega^2.dr}{Rg.T} = \frac{1}{p} . dp$$

integrating

$$\frac{\Omega^2}{Rg.T} * \int_0^R r.dr = \int_0^p \frac{1}{p} dp$$

$$\frac{\Omega^2}{Rg.T} \left[\frac{1}{2} . r^2 \right]_0^R = [\ln p]_{p_o}^{p}$$

$$\frac{\Omega^2}{Rg.T} * \frac{1}{2} * R^2 = \ln (p_R / p_o)$$

so

$$p_r - p_o = p_o * \exp \left[\frac{1.\Omega^2.R^2}{2.Rg.T} \right] - p_o$$

for a rotor speed of 2 revolutions per second, a barometric or static pressure of 1 bar, a radius of 3m, and a temperature of 290K this evaluates to a reference pressure of 857 Pa: equal to the dynamic pressure.

APPENDIX 3

DUCT EXPERIMENTS.

11.3.0 Introduction

As explained in the main text it was necessary to site the pressure transducers remote from aerodynamic pressure tapping holes because of restrictions of physical space inside the blade. In fact a duct length of 50mm was required for some transducers and it was considered sensible to adopt this length for them all for convenience, should any kind of correction exercise have been necessary. Tests were carried out to determine the effects of a 50mm duct and in particular a duct with a fairly sharp right angle bend, since such bends would be necessary in the in-blade installation. The computer code of Nyland and Anderson reference(62) based on the work of Berg and Tijman reference(14) and others has been used for reference to compare with this experimental work.

Dean reference(23) suggests that a pressure tapping hole 1mm in diameter gives errors of order 0.6% at the Mach numbers experienced on the present wind turbine blade, a two millimetre hole doubling this error. However wind tunnel models are usually constructed with much smaller holes of perhaps 0.25mm diameter. The literature suggests that larger diameter ducts perform better, but that little advantage would result from a large duct following a small tapping. Since 1mm bore tubing was very readily available and would result in a less easily blocked duct than the smaller sizes, it was decided to use this diameter.

11.3.1 Experiment

Figure(82) shows the experimental set up used to determine the response of various ducts to excitation at a range of frequencies. A power oscillator drove a small loudspeaker to which was fixed a brass plate forming a small chamber with the loudspeaker diaphragm. The plate had essentially two holes through it, one of 1mm diameter over which a Sensym SPX50D pressure transducer was fixed whilst the other was provided with a short stub of

1mm bore tube to facilitate connection of duct tubing. Another transducer of the same type, had a fitting attached which allowed it to be connected to the above stub tube using any duct configuration of interest. Both transducers were attached using double sided sponge tape, as in the in blade situation. The set up was then essentially like that on the blade surface in that a rapidly changing pressure was present at the entrance to a pressure tapping and that this pressure was conveyed to a pressure transducer along a duct just like that used in the real blade.

The transducers were excited at 9V to increase their sensitivity to the very weak sound from the loudspeaker and had their outputs amplified one thousandfold by a pair of instrumentation amplifiers. Amplified signals were measured using Beckman 110, Fluke 77 and Thurlby 1905a multimeters and a Gould digital storage oscilloscope. Attempts to measure phase shift with the oscilloscope, in spite of very great care having been taken, and ac voltage with the Thurlby meter, resulted in low quality data and were abandoned.

Figure(82) also shows the results of the tests with straight and bent ducts. Due to the very variable response of the loudspeaker with frequency, the ratio of the response of the two transducers has been taken as the amplitude ratio or amplification factor of the duct. The small effect of the difference in sensitivity of the two transducers has also been corrected.

It is clear that the introduction of the bend has no effect, but that the filler wire markedly reduces the magnitude of the resonant peak at the same time as reducing the resonant frequency. The speed of sound in the duct from these tests, is only about one third of that in free air and in the case of the duct with filler wire, less than one quarter. The increase in damping as a result of the wire is responsible for this effect. Noteworthy is that the response of the filled and unfilled systems is virtually identical up to about 250Hz because improvements in the Q factor, the ratio of the response at resonance to that at zero frequency, is lost by a reduction in the resonant frequency.

Plainly, if usable response at frequencies higher than about 100Hz were required, attention would be necessary to the geometry of the duct. Nyland and Anderson discuss the technique of the use of

maximum duct diameter together with careful tayloring of damping by the use of porous fillers and multiple tubes, to maintain high resonant frequency and high damping and hence high usable frequency.

APPENDIX 4

DERIVATION OF RATE OF CHANGE OF INCIDENCE WITH AZIMUTH OF VAWT BLADE BASED ON VAWT TWO VECTOR MODEL.

Vawt wave defined as:

$$\alpha = \arctan\left[\frac{\sin(\Psi)}{\beta+\cos(\Psi)}\right]$$

differentiating using standard form:

$$\frac{d(\alpha)}{d(\Psi)} = \frac{d}{d(\Psi)}\left[\frac{\sin(\Psi)}{\beta+\cos(\Psi)}\right] * \frac{1}{1+\left[\frac{\sin(\Psi)}{\beta+\cos(\Psi)}\right]^2}$$

using the quotient rule:

$$= \frac{(\beta+\cos(\Psi))*\cos(\Psi) + \sin^2(\Psi)}{(\beta+\cos(\Psi))^2} * \frac{1}{1+\left[\frac{\sin(\Psi)}{\beta+\cos(\Psi)}\right]^2}$$

$$= \frac{\beta*\cos(\Psi)+1}{(\beta+\cos(\Psi))^2 * \frac{(\beta+\cos(\Psi))^2 + \sin^2(\Psi)}{(\beta+\cos(\Psi))^2}}$$

so that

$$\frac{d(\alpha)}{d(\Psi)} = \frac{\beta*\cos(\Psi)+1}{\beta^2+2*\beta*\cos(\Psi)+1}$$

where

Ψ = 'azimuth' ie $\Psi = \Omega*t$

β = blade speed ratio

For the azimuth at which the static stall incidence is achieved

$$\alpha = \arctan\left[\frac{\sin(\Psi)}{\beta+\cos(\Psi)}\right]$$

substituting $\cos^2(\Psi)=1-\sin^2(\Psi)$

$$\tan(\alpha) = \frac{\sin(\Psi)}{\beta+\mathrm{sqr}(1-\sin^2(\Psi))}$$

expanding and rearranging gives quadratic in $\sin(\Psi)$

$$\sin^2(\Psi)*[\tan^2(\alpha)+1] - \sin(\Psi)*[2*\beta*\tan(\alpha)] + \tan^2(\alpha)*[\beta^2-1] = 0$$

solving this yields:

$$\Psi = \arcsin\left[\frac{\beta\pm\mathrm{sqr}[(1-\beta^2)*\tan^2(\alpha)+1]}{\tan(\alpha)+1/\tan(\alpha)}\right]$$

TABLE 1

TRANSDUCER SELECTION CONSISTENCY TESTS

Transducer: Kulite Flatpack 1066-4-71

xpt #	temp [°C]	baro as read [mmHg]	baro true [Pa]	excite volts [V]	Vi raw [μV]	Vo raw [μV]	Vo corr [μV]	Vi corr [μV]	Vo @ 1 bar [μV]
1	18.2	751.75	99926	20.0272	69820	-11327	-11312	69725	-11129
2	18.2	751.80	99933	20.0289	69775	-11220	-11204	69674	-11037
3	18.4	751.95	99949	20.0282	69718	-11066	-11050	69620	-10925
4	18.5	752.30	99994	20.0298	69764	-11039	-11023	69660	-11009
5	18.6	752.40	100006	20.0303	69768	-10987	-10970	69662	-10985
6	18.7	752.45	100011	20.0294	69775	-10967	-10951	69673	-10978
7	18.7	752.60	100031	20.0291	69764	-10924	-10908	69663	-10985
8	18.8	752.90	100069	20.0291	69825	-10961	-10945	69724	-11117
9	18.8	752.95	100076	20.0284	69815	-10852	-10837	69716	-11025
10	18.8	753.15	100102	20.0305	70187	-11604	-11586	70080	-11840
11	18.9	753.35	100127	20.0313	69744	-10575	-10558	69635	-10874
12	18.9	753.50	100147	20.0313	69796	-10638	-10621	69687	-10987
13	18.9	753.65	100167	20.0314	69900	-10867	-10850	69790	-11265
14	18.9	753.75	100181	20.0318	69776	-10549	-10532	69665	-10980
15	18.5	756.95	100612	20.0245	69766	-9574	-9562	69681	-11081
16	18.6	756.95	100611	20.0259	70114	-10223	-10210	70023	-11725
17	18.7	756.95	100609	20.0271	69779	-9585	-9572	69685	-11083
18	18.8	756.95	100608	20.0247	69889	-9885	-9873	69803	-11379
19	19.0	756.95	100604	20.0242	69707	-9475	-9464	69623	-10962
20	19.1	756.95	100603	20.0249	70187	-10533	-10520	70100	-12014
21	19.3	757.15	100626	20.0284	69695	-9190	-9177	69596	-10729
22	19.3	757.40	100659	20.0283	69701	-9118	-9105	69603	-10740
23	19.4	757.40	100657	20.0294	69722	-9149	-9136	69620	-10766
24	19.5	757.50	100669	20.0292	69736	-9180	-9167	69634	-10826
25	19.5	757.70	100696	20.0289	69728	-9099	-9086	69627	-10811
26	19.5	757.95	100729	20.0289	69846	-9244	-9231	69745	-11038
27	19.5	758.20	100762	20.0297	70184	-9887	-9872	70080	-11762
28	19.6	758.25	100767	20.0310	69879	-9203	-9189	69771	-11091
29	19.7	758.35	100779	20.0297	69796	-8993	-8980	69693	-10911
30	19.7	758.50	100799	20.0311	70335	-10095	-10079	70226	-12060
31	19.7	758.55	100805	20.0302	69779	-8866	-8853	69674	-10850
32	19.2	752.25	99976	20.0240	69650	-11647	-11633	69567	-11574
33	19.4	752.25	99973	20.0252	70223	-12980	-12964	70135	-12897
34	19.6	751.90	99923	20.0252	70207	-13004	-12988	70119	-12797
35	19.6	751.80	99910	20.0239	69771	-12072	-12058	69688	-11834
36	19.7	750.55	99742	20.0287	69831	-12620	-12602	69731	-11963
37	20.4	749.20	99551	20.0279	69737	-13069	-13051	69640	-11938
38	20.5	749.05	99530	20.0300	70150	-14008	-13987	70045	-12821
39	20.5	749.05	99530	20.0299	69867	-13337	-13317	69763	-12151
40	20.5	749.05	99530	20.0299	69680	-12942	-12923	69576	-11757
41	18.5	742.50	98692	20.0241	69934	-15124	-15106	69850	-11861

TABLE 2

Transducer offset and sensitivity drift between two calibrations carried out on the 30.07.87/06.08.87 and 11.09.87/15.09.87

transducer number ↓	min of sig	max of sig	min for zero appld	max for zero appld	mean for 0Pa appld	20411 zero ord	20411 temp grad	mean offset or sensit	21832 zero ord	21832 temp grad	mean offset or sensit	diff betw cal means	absolu offset change * old sensit [Pa]	absolu sensit change [1/1]
averages>													94	0.016
std devs>													68	0.013
0 vic	-0.299	0.073	-0.299	0.073	-0.113	0.854	-0.088	0.864	0.886	-0.083	0.896	0.032	124	
0 voc	-1.855	0.914	0.846	0.914	0.880	-3490	-453	-3888	-3513	-405	-3870	19		0.005
1 vic	0.305	0.652	0.305	0.651	0.478	-0.759	-0.088	-0.801	-0.774	-0.112	-0.827	-0.026	88	
1 voc	-0.835	1.493	-0.835	-0.781	-0.808	3822	580	3354	3893	499	3490	136		0.041
2 vic	0.088	0.437	0.088	0.437	0.263	-0.692	-0.349	-0.784	-0.738	-0.364	-0.833	-0.050	172	
2 voc	-0.854	1.558	-0.854	-0.720	-0.787	3909	561	3468	3972	447	3620	153		0.044
3 vic	-0.233	0.117	-0.233	0.116	-0.059	-0.467	-0.036	-0.465	-0.477	-0.060	-0.474	-0.009	33	
3 voc	-0.481	1.902	-0.481	-0.453	-0.467	3969	544	3715	3992	450	3782	68		0.018
4 vic	-0.123	0.225	-0.122	0.225	0.051	1.002	-0.091	0.998	0.958	-0.090	0.953	-0.045	227	
4 voc	0.948	3.089	0.948	1.013	0.981	4468	622	5078	4504	504	4997	-80		0.016
5 vic	-0.375	0.015	-0.375	0.015	-0.180	-0.338	0.131	-0.362	-0.354	0.128	-0.377	-0.016	53	
5 voc	-0.402	2.334	-0.402	-0.333	-0.367	3540	447	3376	3549	354	3419	43		0.013
6 vic	-0.158	0.228	-0.158	0.227	0.035	-0.384	0.074	-0.381	-0.403	0.059	-0.401	-0.020	79	
6 voc	-0.413	1.808	-0.413	-0.366	-0.390	4237	550	4022	4269	434	4099	77		0.019
7 vic	-0.462	0.223	-0.462	0.223	-0.119	-0.078	-0.075	-0.069	-0.075	-0.100	-0.063	0.006	22	
7 voc	-0.100	2.557	-0.100	-0.039	-0.070	3762	511	3727	3567	390	3540	-187		0.050
8 vic	0.081	0.505	0.081	0.504	0.292	-0.057	-0.392	-0.171	-0.069	-0.442	-0.198	-0.027	110	
8 voc	-0.248	2.041	-0.248	-0.082	-0.165	4183	583	4087	4236	500	4153	66		0.016
9 vic	-0.462	-0.039	-0.462	-0.039	-0.251	-0.274	0.085	-0.295	-0.315	0.064	-0.331	-0.036	157	
9 voc	-0.346	1.860	-0.346	-0.272	-0.309	4494	584	4314	4500	497	4346	32		0.007
10 vic	-0.520	-0.040	-0.519	-0.041	-0.280	-0.038	0.115	-0.070	-0.052	0.064	-0.070	-0.000	1	
10 voc	-0.092	2.307	-0.092	-0.038	-0.065	4060	506	4027	4064	422	4037	10		0.003
11 vic	0.169	0.640	0.171	0.640	0.406	-0.152	-0.108	-0.195	-0.148	-0.140	-0.205	-0.010	34	
11 voc	-0.215	2.350	-0.215	-0.161	-0.188	3529	507	3434	3584	435	3502	69		0.020
12 vic	0.033	0.480	0.034	0.480	0.257	0.016	-0.128	-0.017	-0.007	-0.189	-0.055	-0.038	164	
12 voc	-0.052	2.121	-0.052	0.022	-0.015	4291	618	4282	4348	504	4340	58		0.014
13 vic	-0.375	0.122	-0.374	0.121	-0.127	0.056	0.414	0.003	0.050	0.409	-0.002	-0.005	19	
13 voc	-0.104	2.359	-0.104	0.108	0.002	3959	475	3959	3978	410	3978	19		0.005
14 vic	-0.230	0.232	-0.230	0.232	0.001	0.304	-0.022	0.304	0.285	-0.062	0.285	-0.019	77	
14 voc	0.283	2.671	0.283	0.314	0.298	3986	525	4143	4014	445	4147	4		0.001
15 vic	-0.002	0.446	-0.002	0.445	0.222	-0.193	-0.304	-0.260	-0.228	-0.354	-0.306	-0.046	185	
15 voc	-0.322	1.969	-0.322	-0.186	-0.254	4190	583	4042	4241	480	4119	77		0.019

TABLE 2 CONTINUED

Item	min of sig	max of sig	min for zero appld	max for zero appld	mean for 0Pa appld	20411 zero ord	20411 temp grad	mean offset or sensit	21832 zero ord	21832 temp grad	mean offset or sensit	diff betw cals means	absolu offset change * old sensit [Pa]	absolu sensit change [1/1]
16 vic	-0.195	0.236	-0.195	0.236	0.021	-0.953	0.062	-0.952	-0.958	-0.019	-0.959	-0.007	24	
16 voc	-0.966	1.432	-0.966	-0.934	-0.950	3904	509	3420	3935	457	3500	80		0.023
17 vic	-0.495	-0.074	-0.495	-0.074	-0.284	-0.972	0.330	-1.066	-1.001	0.300	-1.086	-0.020	74	
17 voc	-1.150	1.107	-1.150	-0.995	-1.073	4411	581	3788	4419	498	3885	97		0.026
18 vic	0.009	0.410	0.010	0.410	0.210	-0.764	-0.295	-0.825	-0.785	-0.335	-0.856	-0.030	106	
18 voc	-0.879	1.491	-0.879	-0.766	-0.823	4002	596	3512	4047	521	3618	106		0.030
19 vic	-0.418	0.015	-0.417	0.014	-0.202	-0.462	0.402	-0.543	-0.493	0.334	-0.560	-0.017	67	
19 voc	-0.632	1.749	-0.632	-0.452	-0.542	4123	546	3827	4128	441	3889	62		0.016
20 vic	-0.296	0.132	-0.294	0.131	-0.082	-0.267	0.318	-0.292	-0.280	0.274	-0.303	-0.010	36	
20 voc	-0.362	2.209	-0.362	-0.221	-0.291	3731	516	3581	3752	442	3623	42		0.012
21 vic	-0.820	-0.373	-0.819	-0.374	-0.597	-1.200	-0.409	-0.956	-1.314	-0.478	-1.029	-0.073	285	
21 voc	-1.039	1.384	-1.039	-0.859	-0.949	4435	542	3920	4409	447	3985	65		0.016
22 vic	-0.838	-0.439	-0.837	-0.439	-0.638	-0.429	-0.109	-0.360	-0.486	-0.163	-0.382	-0.022	69	
22 voc	-0.384	2.825	-0.384	-0.327	-0.355	3208	408	3063	3196	354	3070	7		0.002
23 vic	-0.085	0.305	-0.085	0.304	0.110	-0.617	-0.054	-0.623	-0.641	-0.112	-0.653	-0.030	93	
23 voc	-0.656	2.053	-0.656	-0.598	-0.627	3457	510	3137	3493	427	3225	88		0.028
24 vic	-0.211	0.165	-0.211	0.164	-0.024	-0.243	0.020	-0.243	-0.270	-0.029	-0.269	-0.026	115	
24 voc	-0.272	1.803	-0.272	-0.233	-0.253	4594	691	4419	4627	573	4482	63		0.014
25 vic	-0.497	-0.128	-0.497	-0.129	-0.313	-0.302	0.034	-0.312	-0.329	-0.003	-0.328	-0.016	68	
25 voc	-0.338	1.836	-0.338	-0.300	-0.319	4544	614	4348	4550	538	4379	31		0.007
26 vic	-0.274	0.086	-0.273	0.085	-0.094	0.246	-0.195	0.264	0.226	-0.241	0.248	-0.016	66	
26 voc	0.237	2.693	0.237	0.311	0.274	3935	552	4086	3954	470	4083	-3		0.001
27 vic	-0.668	-0.285	-0.667	-0.286	-0.476	-0.679	-0.431	-0.474	-0.744	-0.452	-0.528	-0.055	226	
27 voc	-0.549	1.842	-0.549	-0.393	-0.471	4383	562	4119	4372	472	4149	31		0.007
28 vic	-0.336	0.022	-0.336	0.021	-0.158	-0.026	0.263	-0.067	-0.034	0.249	-0.073	-0.006	24	
28 voc	-0.117	2.194	-0.117	-0.015	-0.066	4183	580	4145	4193	460	4163	18		0.004
29 vic	-0.714	-0.362	-0.714	-0.364	-0.539	0.056	-0.053	0.085	0.032	-0.076	0.072	-0.013	49	
29 voc	0.069	2.698	0.069	0.107	0.088	3838	496	3882	3828	423	3865	-17		0.004
30 vic	0.059	0.407	0.060	0.406	0.233	0.011	-0.118	-0.017	-0.005	-0.131	-0.036	-0.019	81	
30 voc	-0.042	2.144	-0.042	0.013	-0.015	4209	645	4200	4267	534	4259	59		0.014
31 vic	-0.616	-0.255	-0.615	-0.256	-0.435	-0.017	0.047	-0.037	-0.043	0.040	-0.060	-0.023	86	
31 voc	-0.072	2.589	-0.072	-0.020	-0.046	3772	508	3749	3770	431	3750	1		0.000

TABLE 3

CALIBRATION 20411B11

Table of applied calibration pressures and predicted pressures from fitted calibration coefficients and transducer/ amplifier outputs

std dev zero appl spots›					20.4	4.3	12.6	10.1	12.8	5.4	5.9	8.9	37.2	22.2	22.0	15.6	19.3	26.8
averages›		0.36	1.34		13.9													
item›						0	1	2	3	4	5	6	7	8	9	10	11	12
spot no	appl [Pa]	av resid	% error	av pred	pred std	pred [Pa]	pred [Pa]	pred [Pa]	pred [Pa]	pred [Pa]	pred [Pa]	pred [Pa]	pred [Pa]	pred [Pa]	pred [Pa]	pred [Pa]	pred [Pa]	pred [Pa]
204P01	0	-12	1.21	-12	16	10	-10	-5	-11	0	1	13	45	-18	-27	-7	-16	-15
204P02	951	-6	0.60	946	17	955	943	947	960	963	957	979	998	930	935	960	935	931
204P03	0	-21	2.14	-21	17	-9	-20	-16	-16	-3	-7	3	36	-33	-33	-13	-28	-27
204P04	1942	45	2.34	1987	17	1997	1987	1989	2005	2004	1998	2018	2037	1973	1970	2009	1979	1972
204P05	0	-18	1.84	-18	16	-5	-20	-15	-11	3	-7	7	35	-28	-33	-8	-26	-29
204P06	3932	27	0.69	3960	19	3968	3956	3966	3983	3978	3970	3996	4012	3945	3942	3986	3953	3945
204P07	0	-19	1.94	-19	16	-9	-19	-17	-10	3	-4	6	32	-29	-33	-10	-25	-31
204P08	4903	2	0.05	4906	17	4916	4907	4913	4924	4925	4919	4941	4957	4895	4895	4927	4899	4892
204P09	0	-17	1.75	-17	15	-5	-19	-12	-10	3	-4	6	32	-26	-25	-10	-25	-35
204P10	6865	-66	0.97	6798	17	6812	6801	6806	6800	6823	6815	6825	6855	6792	6792	6804	6795	6787
204P11	0	-18	1.80	-18	15	-2	-14	-14	-11	1	-4	8	26	-29	-26	-11	-25	-34
204P12	9307	-121	1.30	9186	23	9209	9198	9199	9152	9220	9220	9201	9246	9191	9195	9156	9194	9184
204P13	0	-18	1.85	-18	14	-10	-21	-18	-9	2	-5	11	24	-26	-24	-12	-24	-34
204P14	0	-14	1.37	-14	9	1	-9	-7	-15	-3	-6	-1	15	-14	-14	-20	-10	-23
204P15	990	26	2.65	1017	11	1036	1021	1027	1026	1026	1024	1038	1047	1016	1016	1017	1017	1001
204P16	0	-13	1.27	-13	11	4	-5	-2	-15	2	-3	3	19	-10	-10	-20	-10	-23
204P17	1991	13	0.67	2004	11	2021	2007	2009	2017	2014	2010	2023	2033	2003	1999	2010	2004	1989
204P18	0	-15	1.48	-15	11	1	-9	-6	-15	2	-6	-2	19	-14	-15	-20	-10	-28
204P19	4972	-26	0.52	4946	12	4963	4948	4955	4956	4957	4958	4967	4975	4950	4941	4954	4953	4934
204P20	0	-14	1.39	-14	11	4	-5	-3	-14	-7	-3	3	19	-14	-14	-24	-10	-23
204P21	6963	-46	0.66	6917	14	6939	6925	6929	6909	6930	6933	6933	6953	6921	6916	6915	6926	6907
204P22	0	-10	0.95	-10	12	2	-1	4	-14	-2	-0	11	26	-2	-10	-24	-6	-22
204P23	9346	-120	1.29	9225	25	9259	9245	9255	9177	9240	9249	9227	9270	9255	9237	9177	9243	9230
204P24	0	-8	0.80	-8	11	-1	-4	1	-10	-6	-1	11	30	-6	-11	-17	-6	-17
204P25	0	-5	0.46	-5	10	4	-6	-0	-10	3	-4	0	33	-12	-9	-6	-9	-6
204P26	9297	-68	0.74	9228	21	9250	9239	9237	9187	9246	9247	9220	9282	9236	9243	9196	9238	9240
204P27	0	2	0.19	2	8	0	-2	1	-2	8	3	9	36	-3	-4	3	-3	-2
204P28	6943	-28	0.41	6915	10	6920	6914	6916	6908	6924	6920	6920	6956	6910	6910	6914	6914	6915
204P29	0	0	0.01	0	9	0	-3	-0	-2	7	1	9	36	-5	-4	-1	-7	-2
204P30	4943	15	0.30	4957	12	4967	4954	4959	4968	4966	4957	4973	4997	4951	4948	4975	4954	4953
204P31	0	0	0.03	0	9	1	-3	-2	-2	7	1	10	36	-8	-8	-0	-7	-3
204P32	1961	30	1.54	1992	10	1988	1982	1985	1999	1996	1987	2003	2023	1976	1975	2000	1984	1988
204P33	0	1	0.11	1	8	2	-4	-2	-3	10	2	6	35	-7	-7	1	-4	-5
204P34	981	40	4.12	1021	8	1015	1015	1018	1023	1022	1015	1029	1046	1006	1008	1025	1011	1014
204P35	0	1	0.09	1	8	5	-4	-2	-3	10	2	6	35	-7	-6	1	-4	-5

TABLE 3 CONTINUED

		8.1	13.5	19.9	13.2	11.1	21.7	17.0	12.9	34.2	20.1	28.9	20.4	31.9	31.1	23.7	15.5	26.8	25.0	23.5
		13	14	15	16	17	18	19	20	21	22	23	24	25	26	27	28	29	30	31
spot	appl	pred	pred	pred	pred	pred	pred	pred	pred	pred	pred	pred	pred	pred	pred	pred	pred	pred	pred	pred
no	[Pa]	[Pa]	[Pa]	[Pa]	[Pa]	[Pa]	[Pa]	[Pa]	[Pa]	[Pa]	[Pa]	[Pa]	[Pa]	[Pa]	[Pa]	[Pa]	[Pa]	[Pa]	[Pa]	[Pa]
204P01	0	-2	-9	-21	-1	-11	-24	-1	-12	-36	-17	-27	-4	-30	-34	-24	-17	-31	-28	-18
204P02	951	956	946	941	949	963	928	950	961	923	947	927	946	920	925	938	938	941	925	942
204P03	0	-9	-19	-27	-23	-3	-37	-16	-10	-43	-25	-40	-23	-50	-44	-26	-27	-32	-37	-28
204P04	1942	1992	1984	1978	1995	1997	1972	1989	2003	1968	1990	1964	1989	1960	1964	1981	1982	1987	1969	1987
204P05	0	-6	-18	-22	-19	-4	-31	-14	-9	-40	-22	-37	-19	-43	-38	-26	-22	-29	-31	-23
204P06	3932	3968	3956	3950	3967	3970	3941	3957	3978	3934	3964	3933	3957	3933	3937	3951	3952	3963	3939	3959
204P07	0	-7	-22	-24	-20	-5	-30	-17	-10	-42	-26	-37	-20	-43	-40	-23	-20	-28	-34	-26
204P08	4903	4910	4903	4902	4912	4911	4887	4897	4918	4880	4905	4881	4903	4876	4881	4900	4905	4903	4893	4902
204P09	0	-7	-18	-22	-21	-1	-28	-18	-11	-40	-21	-36	-15	-44	-36	-22	-17	-24	-24	-23
204P10	6865	6809	6798	6801	6793	6807	6784	6798	6801	6776	6791	6777	6797	6774	6773	6797	6801	6786	6784	6789
204P11	0	-8	-15	-19	-21	-1	-24	-18	-13	-39	-24	-36	-20	-44	-37	-24	-18	-25	-28	-28
204P12	9307	9209	9195	9197	9160	9195	9179	9194	9165	9158	9155	9174	9188	9178	9155	9183	9200	9154	9182	9158
204P13	0	-8	-15	-24	-21	-7	-22	-25	-12	-38	-22	-36	-15	-39	-40	-25	-22	-22	-26	-30
204P14	0	-9	-10	-17	-11	-12	-10	-20	-15	-28	-17	-20	-19	-12	-24	-18	-10	-28	-24	-28
204P15	990	1019	1021	1016	1032	1012	1017	1006	1017	1001	1015	1006	1015	1015	1008	1005	1011	1004	1002	1004
204P16	0	-9	-10	-11	-7	-15	-11	-20	-18	-28	-17	-24	-19	-12	-23	-24	-10	-31	-19	-28
204P17	1991	2006	2009	2006	2021	2006	2004	1994	2008	1990	2004	1990	1995	1995	1995	1990	2002	1994	1989	1994
204P18	0	-11	-10	-13	-11	-15	-11	-24	-15	-28	-20	-27	-23	-16	-28	-24	-14	-31	-24	-28
204P19	4972	4947	4953	4944	4963	4935	4947	4934	4946	4931	4943	4931	4938	4938	4931	4933	4943	4935	4932	4936
204P20	0	-13	-6	-17	-3	-19	-7	-24	-19	-32	-18	-24	-19	-16	-23	-24	-10	-31	-24	-25
204P21	6963	6931	6925	6920	6925	6914	6918	6912	6911	6898	6904	6901	6905	6910	6899	6907	6919	6896	6902	6899
204P22	0	-11	-6	-10	5	-27	-5	-18	-21	-27	-15	-17	-10	-8	-18	-16	-3	-31	-13	-18
204P23	9346	9242	9238	9241	9221	9207	9235	9230	9188	9211	9191	9225	9231	9235	9206	9221	9232	9173	9221	9197
204P24	0	-9	-2	-14	5	-19	0	-14	-13	-27	-12	-13	-5	-8	-18	-16	-4	-24	-13	-15
204P25	0	-1	-0	4	-5	12	5	-6	-2	-3	-8	-13	-12	-22	-13	-8	-8	-14	-14	-17
204P26	9297	9244	9237	9255	9205	9242	9239	9241	9210	9224	9201	9224	9218	9224	9210	9226	9229	9191	9223	9202
204P27	0	2	4	11	-0	12	10	-1	6	-1	0	0	-3	-14	-6	-1	1	0	-1	-3
204P28	6943	6917	6919	6924	6913	6927	6923	6915	6918	6915	6909	6909	6904	6901	6904	6909	6912	6906	6905	6907
204P29	0	0	3	6	0	14	8	-1	3	-2	-3	-3	-7	-18	-7	-1	-2	-4	-7	-6
204P30	4943	4954	4961	4961	4963	4968	4957	4947	4967	4954	4961	4946	4942	4936	4948	4950	4951	4957	4940	4952
204P31	0	-2	3	3	0	16	7	-1	5	-4	-1	-4	-7	-13	-9	-1	4	-0	-3	-5
204P32	1961	1986	1992	1993	1997	2003	1998	1990	2003	1996	1998	1990	1986	1971	1989	1990	1988	1998	1985	1991
204P33	0	-1	3	5	1	17	9	0	7	2	-1	-0	-3	-13	-5	2	1	-4	-4	-5
204P34	981	1015	1023	1021	1024	1036	1029	1019	1035	1024	1025	1021	1023	1011	1021	1020	1024	1024	1016	1019
204P35	0	0	3	5	-3	14	7	-1	3	1	-1	-1	-3	-9	-6	-0	3	-4	-5	-5

TABLE 3 CONTINUED

item>						0	1	2	3	4	5	6	7	8	9	10	11	12
spot no	appl [Pa]	av resid	% error	av pred	pred std	pred [Pa]	pred [Pa]	pred [Pa]	pred [Pa]	pred [Pa]	pred [Pa]	pred [Pa]	pred [Pa]	pred [Pa]	pred [Pa]	pred [Pa]	pred [Pa]	pred [Pa]
211P03	0	-9	0.88	-9	8	-7	3	-5	-4	-5	-8	-12	-35	-7	-4	-4	-5	-10
211P04	1059	-18	1.74	1041	9	1043	1050	1041	1053	1038	1040	1038	1012	1037	1042	1050	1037	1032
211P05	0	-8	0.77	-8	8	-2	-2	-5	-4	-9	-5	-13	-39	-14	-4	-4	-9	-13
211P06	2050	30	1.45	2079	9	2083	2085	2079	2093	2075	2074	2080	2049	2073	2081	2093	2078	2075
211P07	0	-6	0.59	-6	8	-1	1	-3	-0	-10	-8	-13	-35	-7	0	-3	-6	-10
211P08	3962	3	0.07	3965	11	3967	3970	3964	3981	3961	3959	3964	3932	3957	3962	3980	3964	3959
211P09	0	-7	0.70	-7	8	3	-2	-4	-1	-7	-6	-11	-37	-11	2	-7	-9	-9
211P10	5962	7	0.12	5969	8	5977	5972	5970	5976	5970	5969	5968	5941	5965	5978	5973	5966	5965
211P11	7914	-48	0.61	7866	11	7879	7882	7870	7849	7874	7875	7854	7842	7872	7880	7845	7867	7869
211P12	0	-9	0.91	-9	8	0	-2	-11	-2	-10	-7	-9	-43	-9	-3	-5	-10	-11
211P13	0	18	1.82	18	10	-1	18	14	16	-0	9	0	4	24	16	16	20	33
211P14	1049	44	4.19	1093	9	1077	1089	1088	1097	1079	1079	1081	1075	1102	1092	1097	1092	1104
211P15	0	18	1.80	18	9	2	18	14	12	1	8	-1	5	27	14	18	21	31
211P16	2079	64	3.09	2143	11	2123	2140	2141	2149	2120	2128	2128	2127	2147	2134	2151	2145	2155
211P17	0	21	2.10	21	9	6	18	18	20	6	11	4	5	27	24	18	25	35
211P18	3893	22	0.57	3915	11	3896	3903	3907	3920	3898	3901	3903	3893	3916	3913	3916	3916	3922
211P19	0	18	1.76	18	10	5	13	12	15	4	8	4	-5	28	22	13	20	25
211P20	5864	3	0.06	5868	10	5850	5861	5864	5865	5857	5858	5852	5850	5873	5868	5858	5866	5875
211P21	0	15	1.50	15	9	4	11	11	14	3	9	1	-6	21	19	8	17	21
211P22	7973	-21	0.27	7951	16	7936	7948	7951	7919	7943	7951	7925	7939	7965	7958	7917	7953	7965
211P23	0	15	1.45	15	10	3	8	10	13	2	8	2	-12	17	22	9	13	21
211P24	0	16	1.56	16	21	5	9	4	11	-7	1	-19	-70	27	33	19	23	31
211P25	990	42	4.24	1032	25	996	1020	1014	1037	998	1012	1000	942	1035	1043	1038	1035	1052
211P26	0	26	2.61	26	24	-1	16	14	22	-4	9	-10	-60	38	37	27	34	43
211P27	2059	79	3.85	2139	29	2094	2124	2118	2143	2101	2107	2102	2042	2139	2142	2147	2137	2155
211P28	0	27	2.66	27	24	-0	20	12	22	0	5	-9	-60	34	37	27	34	47
211P29	3982	50	1.26	4032	24	4003	4020	4013	4042	4000	4005	4005	3944	4040	4043	4046	4037	4050
211P30	0	27	2.68	27	23	-4	20	16	22	1	9	-9	-56	38	37	27	33	47
211P31	5992	45	0.76	6037	25	6009	6022	6020	6036	6007	6010	6003	5952	6048	6050	6035	6039	6050
211P32	0	20	2.03	20	21	0	15	7	18	-0	6	-13	-60	34	33	24	29	42
211P33	7983	3	0.04	7986	28	7958	7981	7970	7960	7959	7962	7934	7906	8003	8006	7963	7987	8004
211P34	0	19	1.86	19	21	1	15	8	17	-5	3	-13	-64	31	34	24	29	37

TABLE 3 CONTINUED

trans ›		13	14	15	16	17	18	19	20	21	22	23	24	25	26	27	28	29	30	31
spot no	appl [Pa]	pred [Pa]	pred [Pa]	pred [Pa]	pred [Pa]	pred [Pa]	pred [Pa]	pred [Pa]	pred [Pa]	pred [Pa]	pred [Pa]	pred [Pa]	pred [Pa]	pred [Pa]	pred [Pa]	pred [Pa]	pred [Pa]	pred [Pa]	pred [Pa]	pred [Pa]	pred [Pa]
211P03	0	-3	-12	-19	-9	-8	-24	-3	-3	-15	-8	-13	-18	-11	-2	-14	-9	-3	-9	3
211P04	1059	1048	1037	1030	1048	1041	1027	1045	1047	1035	1046	1040	1032	1041	1047	1037	1038	1053	1042	1053
211P05	0	-2	-8	-18	-9	-6	-20	2	-4	-12	-8	-6	-13	-2	-2	-12	-5	-3	-2	4
211P06	2050	2083	2074	2066	2089	2081	2064	2080	2090	2078	2084	2078	2068	2075	2084	2077	2076	2094	2082	2094
211P07	0	-3	-8	-14	-5	-5	-22	2	-3	-10	-5	-6	-13	-2	1	-9	-3	4	1	5
211P08	3962	3967	3962	3949	3972	3966	3947	3967	3974	3959	3972	3963	3954	3965	3970	3956	3966	3982	3971	3984
211P09	0	-3	-9	-15	-4	-6	-20	3	-3	-12	-6	-6	-18	-6	-1	-13	-7	-1	2	-0
211P10	5962	5972	5967	5957	5972	5968	5960	5978	5973	5961	5969	5973	5958	5973	5976	5965	5973	5979	5978	5978
211P11	7914	7875	7867	7858	7856	7869	7857	7878	7855	7853	7854	7873	7859	7881	7868	7861	7876	7857	7878	7865
211P12	0	-2	-10	-22	-7	-5	-20	-6	-3	-15	-5	-7	-17	-5	-5	-17	-5	-2	-9	-5
211P13	0	8	17	29	16	10	22	16	12	37	20	28	21	27	27	29	19	23	26	28
211P14	1049	1081	1089	1104	1097	1082	1099	1091	1087	1111	1099	1101	1098	1098	1104	1101	1090	1105	1095	1103
211P15	0	9	18	27	15	5	22	14	11	34	18	25	25	27	29	26	18	27	27	28
211P16	2079	2128	2141	2148	2147	2131	2150	2132	2141	2160	2151	2149	2148	2148	2157	2158	2140	2156	2148	2159
211P17	0	9	18	28	19	8	27	18	15	38	22	28	30	27	30	28	23	27	31	32
211P18	3893	3900	3912	3919	3918	3906	3924	3907	3915	3935	3925	3926	3922	3924	3930	3923	3917	3928	3929	3924
211P19	0	6	17	25	11	8	28	10	11	33	20	28	21	27	28	29	19	26	32	21
211P20	5864	5854	5865	5870	5863	5861	5881	5864	5861	5884	5872	5881	5878	5882	5880	5879	5872	5875	5880	5870
211P21	0	4	16	26	8	4	28	9	9	29	17	24	21	28	25	23	18	22	24	15
211P22	7973	7944	7953	7958	7931	7953	7974	7956	7930	7968	7941	7970	7967	7979	7962	7963	7964	7942	7974	7942
211P23	0	7	12	21	9	7	26	5	10	30	18	27	22	28	26	20	20	24	25	13
211P24	0	9	13	16	8	5	12	20	13	46	24	31	24	50	42	24	14	30	26	23
211P25	990	1015	1026	1029	1031	1021	1032	1037	1037	1066	1044	1061	1050	1062	1062	1047	1035	1060	1050	1051
211P26	0	13	20	23	20	9	29	30	24	58	38	55	38	58	58	40	26	48	43	40
211P27	2059	2118	2128	2128	2139	2124	2145	2143	2146	2175	2159	2170	2160	2172	2176	2151	2143	2174	2168	2165
211P28	0	14	20	23	20	9	32	32	25	57	38	54	38	58	58	42	27	48	43	44
211P29	3982	4017	4024	4030	4030	4019	4031	4029	4036	4062	4051	4057	4038	4059	4061	4046	4022	4059	4046	4051
211P30	0	14	20	31	20	9	33	32	22	61	35	55	38	54	55	44	23	48	43	40
211P31	5992	6024	6026	6034	6031	6021	6050	6041	6031	6072	6058	6070	6045	6072	6073	6058	6029	6063	6058	6056
211P32	0	12	16	21	17	7	19	25	15	50	29	41	25	46	45	31	13	40	33	30
211P33	7983	7974	7977	7984	7963	7980	8009	7997	7972	8025	7993	8022	8001	8033	8023	8001	7988	7997	8017	8000
211P34	0	11	12	21	13	1	20	25	13	48	26	37	20	46	42	33	13	37	28	30

TABLE 4

CALIBRATION 21832B11

Table of applied calibration pressures and predicted pressures from fitted calibration coefficients and transducer and amplifier outputs

std dev zero appl spots>					14.8	7.0	13.5	19.8	14.0	11.7	8.4	29.8	27.1	8.0	7.3	11.1	8.0	23.3
averages>		0.36	0.94		10.5													
item >						0	1	2	3	4	5	6	7	8	9	10	11	12
spot no.	appl'd [Pa]	av resid	% error	av pred	std pred	pred [Pa]	pred [Pa]	pred [Pa]	pred [Pa]	pred [Pa]	pred [Pa]	pred [Pa]	pred [Pa]	pred [Pa]	pred [Pa]	pred [Pa]	pred [Pa]	pred [Pa]
218P01	0	14	1.40	14	23	13	23	42	22	11	7	60	62	4	6	17	-9	50
218P02	990	109	11.04	1100	22	1098	1103	1123	1116	1099	1093	1152	1142	1083	1092	1105	1074	1126
218P03	2010	66	3.26	2076	21	2069	2081	2097	2096	2068	2062	2123	2111	2057	2068	2086	2050	2100
218P04	0	15	1.49	15	22	11	23	42	22	15	12	59	57	3	11	13	-6	47
218P05	4864	94	1.94	4958	20	4952	4961	4974	4974	4950	4944	5007	4986	4939	4945	4973	4933	4981
218P06	0	21	2.10	21	22	18	29	48	33	23	20	72	64	12	16	21	1	50
218P07	6688	125	1.86	6813	19	6808	6821	6825	6811	6806	6801	6855	6842	6795	6805	6813	6793	6838
218P08	0	12	1.22	12	22	12	25	38	28	18	14	64	53	3	7	13	-9	40
218P09	8855	9	0.10	8865	21	8864	8880	8881	8834	8863	8861	8888	8898	8854	8866	8832	8851	8896
218P10	0	21	2.15	21	21	16	28	43	36	21	25	73	64	10	16	24	2	46
232P01	0	-5	0.55	-5	9	-3	-4	-14	-4	-4	-4	-18	-16	-1	-3	-7	-3	-25
232P02	990	-3	0.32	987	9	996	989	981	1003	995	991	983	971	994	984	989	989	969
232P03	0	-6	0.57	-6	9	2	6	-8	-0	0	-1	-9	-22	-0	-6	-6	-0	-22
232P04	1971	-4	0.19	1967	11	1971	1972	1960	1984	1964	1965	1962	1947	1966	1957	1977	1971	1943
232P05	0	-3	0.33	-3	11	1	-0	-14	-4	-3	-2	-18	-25	-0	-6	-7	-3	-27
232P06	4864	-19	0.38	4846	12	4842	4845	4834	4859	4840	4845	4840	4826	4848	4833	4855	4849	4819
232P07	0	-0	0.05	-0	9	-8	-2	-15	-3	-3	0	-10	-17	5	1	4	14	-10
232P08	6835	-54	0.79	6781	11	6774	6781	6765	6776	6780	6785	6770	6772	6796	6776	6782	6799	6768
232P09	0	-3	0.27	-3	12	-9	0	-14	-2	-1	-2	-11	-26	-2	-12	-9	-3	-31
232P10	8846	-97	1.10	8748	19	8750	8755	8732	8714	8752	8761	8722	8742	8763	8744	8712	8758	8721
232P11	0	1	0.12	1	12	-10	1	-11	2	-1	5	1	-12	11	10	15	27	1
232P12	0	-3	0.27	-3	11	-9	-19	-13	-18	-9	-12	-43	-8	4	-4	-2	3	-3
232P13	961	1	0.07	962	9	964	951	955	962	958	958	930	954	967	960	967	964	954
232P14	0	-5	0.45	-5	10	-3	-11	-9	-18	-6	-11	-42	-15	-2	-8	-11	-3	-7
232P15	1932	-3	0.17	1929	10	1933	1923	1925	1933	1924	1921	1896	1916	1928	1920	1937	1932	1916
232P16	0	-5	0.49	-5	10	-2	-8	-11	-12	-4	-9	-41	-17	-3	-6	-10	2	-11
232P17	3913	-19	0.48	3894	11	3897	3884	3880	3898	3884	3883	3863	3881	3888	3886	3907	3896	3886
232P18	0	-4	0.44	-4	10	-5	-10	-13	-13	-6	-7	-40	-18	-2	-5	-9	4	-13
232P19	6865	-44	0.64	6821	11	6822	6821	6814	6806	6817	6819	6784	6811	6825	6816	6818	6834	6810
232P20	0	-9	0.86	-9	11	-2	-16	-20	-15	-6	-6	-38	-27	-10	-8	-12	-0	-22
232P21	8855	-45	0.50	8811	19	8823	8815	8801	8769	8814	8822	8763	8802	8821	8814	8778	8830	8805
232P22	0	-9	0.89	-9	12	-17	-23	-28	-21	-19	-16	-36	-30	-6	-6	-10	4	-23
232P23	0	-14	1.43	-14	8	2	-12	-19	-13	-13	-8	-23	-27	-11	-6	-15	-5	-24
232P24	981	-11	1.11	970	8	990	972	967	984	973	976	965	952	965	973	973	973	957
232P25	0	-17	1.69	-17	8	3	-17	-22	-18	-19	-7	-27	-32	-12	-10	-13	-11	-27
232P26	1971	-12	0.61	1959	8	1974	1959	1954	1972	1957	1960	1953	1944	1959	1961	1972	1965	1947
232P27	0	-14	1.43	-14	8	0	-14	-18	-14	-16	-6	-26	-29	-11	-9	-13	-5	-24
232P28	6884	-66	0.96	6818	8	6832	6819	6814	6817	6818	6829	6814	6809	6824	6825	6818	6830	6810

TABLE 4 CONTINUED

std all spots›		8.2	12.0	16.0	14.2	8.6	11.3	20.2	10.2	14.2	10.3	16.0	17.2	16.8	11.6	14.5	9.6	11.0	17.1	17.9
		13	14	15	16	17	18	19	20	21	22	23	24	25	26	27	28	29	30	31
spot no.	appl [Pa]	pred [Pa]	pred [Pa]	pred [Pa]	pred [Pa]	pred [Pa]	pred [Pa]	pred [Pa]	pred [Pa]	pred [Pa]	pred [Pa]	pred [Pa]	pred [Pa]	pred [Pa]	pred [Pa]	pred [Pa]	pred [Pa]	pred [Pa]	pred [Pa]	pred [Pa]
218P01	0	-3	16	31	-27	8	-10	36	10	22	5	23	17	-40	-6	16	-19	4	27	33
218P02	990	1084	1104	1113	1064	1092	1073	1120	1103	1111	1100	1109	1102	1046	1081	1099	1066	1095	1110	1118
218P03	2010	2058	2077	2086	2045	2071	2055	2097	2079	2085	2077	2084	2081	2017	2062	2082	2046	2076	2084	2100
218P04	0	2	20	31	-28	8	-8	40	11	24	8	24	16	-40	-3	16	-16	7	27	29
218P05	4864	4942	4960	4965	4928	4949	4935	4977	4966	4966	4964	4967	4962	4908	4945	4957	4931	4965	4969	4991
218P06	0	11	24	32	-24	15	-2	42	16	29	13	30	20	-35	-1	25	-8	10	29	40
218P07	6688	6803	6817	6818	6775	6808	6796	6838	6813	6815	6812	6824	6823	6765	6797	6812	6787	6815	6827	6847
218P08	0	-1	16	24	-32	4	-12	32	6	18	7	19	11	-44	-10	13	-15	2	20	29
218P09	8855	8863	8868	8880	8810	8867	8855	8899	8851	8871	8848	8886	8881	8833	8848	8864	8852	8850	8883	8890
218P10	0	9	24	30	-24	13	-1	40	18	27	18	32	25	-31	3	19	-3	12	31	40
232P01	0	-13	-19	-21	9	-7	2	-4	4	-1	0	-7	2	17	3	-4	-4	-3	-14	-15
232P02	990	982	981	980	1016	989	990	981	995	987	990	977	983	998	990	989	989	990	976	975
232P03	0	-7	-12	-13	21	-2	-1	-11	-7	-12	-9	-17	-6	9	0	-8	-2	-7	-15	-15
232P04	1971	1964	1958	1952	2002	1970	1977	1965	1975	1966	1977	1960	1970	1976	1975	1970	1968	1975	1956	1961
232P05	0	-10	-15	-17	22	1	12	4	7	-2	2	-5	4	17	5	-1	5	1	-13	-12
232P06	4864	4846	4838	4829	4884	4842	4851	4841	4857	4847	4859	4839	4848	4860	4853	4850	4853	4858	4836	4835
232P07	0	13	-3	-9	14	-8	1	-3	2	-1	2	-6	9	18	8	4	5	3	-9	-14
232P08	6835	6794	6776	6756	6797	6768	6782	6781	6783	6782	6788	6778	6789	6805	6792	6787	6795	6787	6778	6765
232P09	0	-13	-22	-24	19	-2	13	6	5	7	8	-0	10	18	6	10	7	5	-6	-11
232P10	8846	8747	8723	8724	8755	8758	8776	8770	8745	8762	8747	8763	8762	8788	8757	8763	8772	8734	8750	8718
232P11	0	26	14	-2	15	-22	-6	-15	-7	-10	-3	-7	1	18	9	2	4	6	-9	-14
232P12	0	0	-1	7	12	3	6	-10	-0	-4	-2	-1	-4	17	9	1	9	0	6	-2
232P13	961	959	965	962	981	970	969	948	964	966	970	959	956	974	971	965	967	966	962	957
232P14	0	-1	-1	-6	8	6	6	-14	0	-6	-2	-4	-4	17	5	-7	9	0	1	-6
232P15	1932	1923	1926	1925	1953	1938	1939	1916	1934	1929	1940	1926	1927	1942	1938	1928	1937	1938	1927	1927
232P16	0	-1	-6	-2	7	4	3	-15	-2	-5	-2	-1	-9	17	2	-9	5	-0	-1	-9
232P17	3913	3899	3895	3888	3919	3905	3900	3882	3905	3900	3908	3889	3886	3911	3901	3892	3904	3908	3893	3891
232P18	0	-4	-7	-5	7	7	10	-14	-4	-5	0	-2	-5	17	6	-10	9	2	-3	-5
232P19	6865	6828	6820	6818	6842	6829	6830	6814	6823	6820	6823	6819	6816	6845	6829	6824	6839	6823	6825	6811
232P20	0	-2	-8	-16	6	-2	4	-23	-8	-13	-4	-10	-10	17	-4	-12	6	-2	-5	-9
232P21	8855	8829	8817	8812	8811	8825	8825	8813	8795	8807	8798	8817	8816	8852	8809	8810	8845	8796	8821	8793
232P22	0	-1	-6	-13	6	1	4	-22	-7	-10	-1	-8	-7	17	-0	-13	14	3	-6	-4
232P23	0	-6	-10	-17	-10	-1	-8	-23	-14	-19	-15	-21	-27	-2	-17	-19	-7	-20	-23	-24
232P24	981	975	969	967	980	977	972	958	975	965	971	963	959	980	974	967	974	969	957	960
232P25	0	-5	-15	-16	-11	-7	-14	-28	-16	-21	-20	-22	-28	-6	-19	-24	-12	-20	-25	-24
232P26	1971	1965	1960	1953	1974	1969	1959	1947	1966	1956	1962	1954	1946	1965	1960	1957	1958	1961	1949	1953
232P27	0	-8	-7	-16	-11	-3	-11	-27	-14	-19	-14	-19	-28	-2	-12	-20	-6	-17	-22	-20
232P28	6884	6833	6823	6816	6824	6823	6815	6808	6815	6816	6815	6811	6803	6833	6818	6812	6830	6812	6812	6804

TABLE 4 CONTINUED

item >						0	1	2	3	4	5	6	7	8	9	10	11	12
spot no↓	applied [Pa]	av resid	% error	av pred	std pred	pred [Pa]	pred [Pa]	pred [Pa]	pred [Pa]	pred [Pa]	pred [Pa]	pred [Pa]	pred [Pa]	pred [Pa]	pred [Pa]	pred [Pa]	pred [Pa]	pred [Pa]
232P29	0	-15	1.46	-15	9	5	-15	-22	-15	-17	-5	-26	-30	-7	-8	-12	-7	-31
232P30	7865	-89	1.13	7776	11	7796	7779	7776	7760	7773	7787	7762	7767	7792	7783	7768	7795	7770
232P31	0	-15	1.53	-15	8	-2	-20	-27	-15	-22	-11	-25	-31	-12	-7	-11	-4	-30
232P32	8816	-96	1.09	8720	16	8742	8718	8708	8686	8719	8734	8697	8713	8736	8733	8698	8742	8720
232P33	0	-14	1.41	-14	9	-8	-21	-30	-20	-23	-10	-24	-35	-16	-6	-11	-2	-22
232P43	0	-3	0.31	-3	5	2	0	-2	-2	-6	-4	-8	-8	-2	-4	-10	-6	-12
232P44	981	12	1.20	992	10	991	989	990	1002	985	992	993	978	984	984	992	984	980
232P45	0	-9	0.86	-9	5	2	-8	-4	-6	-7	-4	-8	-11	-6	-8	-10	-9	-12
232P46	1952	5	0.25	1956	6	1960	1954	1963	1973	1956	1954	1965	1952	1952	1951	1970	1955	1951
232P47	0	-11	1.08	-11	6	6	-9	-5	-3	-7	-3	-8	-9	-3	-3	-10	-6	-12
232P48	3913	-3	0.09	3909	8	3902	3907	3906	3932	3908	3911	3921	3903	3903	3910	3928	3908	3906
232P49	0	-3	0.30	-3	4	-1	4	-2	1	-2	3	1	-1	3	1	-2	1	1
232P50	5855	-4	0.07	5851	7	5847	5849	5851	5868	5851	5855	5865	5850	5855	5856	5866	5857	5855
232P51	0	-7	0.65	-7	8	2	-4	-4	1	-2	3	1	-1	1	1	2	5	1
232P52	7796	-31	0.40	7765	12	7782	7769	7776	7761	7774	7778	7771	7773	7782	7785	7765	7781	7779
232P53	0	-9	0.91	-9	7	2	-8	-4	-2	-2	-3	1	-5	-3	1	-2	1	-8
232P54	8836	-52	0.58	8784	18	8797	8793	8798	8768	8799	8804	8788	8798	8805	8810	8774	8809	8805
232P55	0	1	0.11	1	7	-5	4	4	5	2	6	9	2	9	5	6	12	9
232P56	0	1	0.09	1	5	6	-1	0	-5	-2	-1	-0	2	-7	-5	-3	-9	-0
232P57	971	0	0.00	971	5	973	967	972	980	972	969	974	967	966	969	974	961	970
232P58	0	3	0.30	3	5	-2	-0	6	-0	-1	-2	-1	2	-3	-1	-3	-5	5
232P59	1932	12	0.60	1943	6	1948	1942	1945	1956	1945	1940	1953	1943	1940	1943	1959	1938	1943
232P60	0	0	0.02	0	4	-2	-0	0	-1	3	-1	-1	2	-7	-1	-3	-8	0
232P61	3903	17	0.44	3920	9	3920	3913	3918	3936	3916	3912	3932	3917	3909	3913	3933	3906	3911
232P62	0	3	0.31	3	5	2	-0	4	3	2	-1	4	2	-7	-1	-3	-5	-0
232P63	5884	-12	0.20	5872	7	5871	5866	5872	5888	5877	5873	5885	5872	5865	5877	5883	5865	5870
232P64	0	3	0.33	3	7	-1	-1	4	-1	-2	-1	4	2	-7	-5	-3	-9	-0
232P65	7796	-5	0.07	7791	6	7787	7791	7803	7780	7790	7797	7794	7798	7791	7800	7781	7786	7798
232P66	0	5	0.53	5	5	-1	3	7	3	2	3	8	5	2	3	5	-2	4
232P67	8924	-27	0.30	8897	13	8899	8899	8909	8871	8909	8907	8892	8911	8904	8915	8872	8897	8909
232P68	0	-2	0.15	-2	4	2	-1	1	3	-3	-1	4	1	-7	-1	1	-6	-1
232P69	0	7	0.71	7	5	2	7	9	3	11	3	8	15	4	3	8	6	17
232P70	990	21	2.11	1011	6	1004	1006	1011	1018	1010	1008	1021	1015	1003	1007	1021	1003	1015
232P71	0	5	0.52	5	5	5	8	12	3	12	-1	8	18	6	2	8	2	13
232P72	1922	44	2.31	1967	8	1951	1963	1965	1979	1966	1954	1974	1970	1959	1960	1979	1960	1973
232P73	0	13	1.27	13	7	-2	13	19	12	13	5	11	20	14	6	12	7	23
232P74	3923	78	1.98	4001	16	3948	3988	3992	4011	3993	3980	4008	3998	3988	3986	4010	3986	4007
232P75	0	29	2.86	29	13	-12	25	26	23	25	16	29	30	21	15	24	21	40
232P76	5894	63	1.07	5957	15	5922	5950	5957	5956	5953	5939	5959	5955	5956	5950	5958	5947	5964
232P77	0	5	0.47	5	5	3	7	5	3	11	-0	8	15	4	3	9	2	13
232P78	7855	39	0.49	7894	8	7884	7895	7900	7883	7901	7895	7897	7904	7896	7903	7888	7896	7909
232P79	0	14	1.36	14	6	-4	10	12	14	11	10	17	18	11	12	13	9	20
232P80	8875	31	0.35	8906	13	8896	8911	8913	8880	8918	8910	8897	8915	8917	8925	8884	8909	8927
232P81	0	10	1.04	10	6	-4	10	7	10	10	7	21	18	11	8	13	9	16

TABLE 4 CONTINUED

item→		13	14	15	16	17	18	19	20	21	22	23	24	25	26	27	28	29	30	31
spot no↓	appld [Pa]	pred [Pa]	pred [Pa]	pred [Pa]	pred [Pa]	pred [Pa]	pred [Pa]	pred [Pa]	pred [Pa]	pred [Pa]	pred [Pa]	pred [Pa]	pred [Pa]	pred [Pa]	pred [Pa]	pred [Pa]	pred [Pa]	pred [Pa]	pred [Pa]	pred [Pa]
232P29	0	-5	-8	-17	-11	-2	-12	-24	-15	-20	-16	-24	-24	3	-17	-21	-6	-15	-24	-19
232P30	7865	7793	7781	7776	7778	7784	7775	7772	7769	7768	7770	7770	7764	7793	7771	7770	7792	7766	7769	7762
232P31	0	-6	-9	-15	-11	-5	-12	-21	-14	-18	-15	-20	-28	-2	-17	-19	-6	-15	-20	-19
232P32	8816	8748	8729	8729	8715	8735	8724	8724	8704	8719	8704	8717	8708	8742	8714	8719	8741	8702	8720	8701
232P33	0	-7	-10	-21	-3	2	-12	-23	-11	-18	-11	-18	-20	3	-13	-16	-2	-9	-18	-15
232P43	0	-3	-6	5	4	8	5	-3	2	1	-1	-3	-8	-2	-8	-3	-3	-8	-8	-9
232P44	981	978	977	986	1005	1008	1013	997	1011	1006	1004	998	994	993	993	993	988	995	982	989
232P45	0	-10	-14	-8	-8	-0	-2	-9	-3	-5	-8	-11	-17	-7	-12	-11	-10	-16	-17	-15
232P46	1952	1951	1954	1954	1962	1956	1961	1944	1961	1960	1964	1952	1952	1951	1953	1957	1950	1961	1948	1955
232P47	0	-7	-14	-12	-20	-10	-15	-16	-10	-11	-11	-15	-22	-11	-18	-16	-12	-16	-18	-19
232P48	3913	3905	3904	3897	3906	3905	3910	3895	3918	3911	3918	3907	3906	3906	3910	3911	3907	3921	3906	3915
232P49	0	1	-2	-4	-8	-7	-7	-13	-9	-5	-8	-4	-8	-3	-5	-5	-2	-5	-4	-5
232P50	5855	5852	5851	5850	5845	5841	5843	5835	5848	5849	5853	5848	5843	5847	5849	5846	5845	5853	5844	5852
232P51	0	7	2	-4	-16	-17	-18	-21	-15	-15	-14	-11	-17	-11	-12	-11	-10	-8	-13	-9
232P52	7796	7784	7776	7776	7753	7753	7752	7748	7750	7758	7750	7755	7747	7760	7756	7761	7763	7751	7756	7755
232P53	0	1	-6	-14	-16	-17	-18	-21	-15	-11	-13	-14	-21	-15	-15	-7	-14	-12	-17	-12
232P54	8836	8811	8802	8805	8756	8773	8767	8772	8755	8768	8757	8779	8771	8782	8768	8780	8787	8762	8780	8772
232P55	0	10	5	-1	-8	-13	-1	-15	-9	1	-4	3	-8	-2	-3	5	-4	6	0	2
232P56	0	-2	-1	3	2	7	-6	8	3	-5	-1	-0	8	6	3	-3	11	8	5	7
232P57	971	964	973	970	980	973	968	973	980	973	975	963	973	970	971	966	965	976	967	972
232P58	0	-5	-1	3	10	11	13	12	7	9	7	6	9	6	3	2	2	3	3	3
232P59	1932	1941	1939	1937	1949	1943	1938	1945	1954	1942	1950	1935	1943	1934	1942	1938	1935	1950	1934	1947
232P60	0	-6	-5	-1	3	6	6	11	5	1	3	2	4	2	2	-2	-0	-1	-1	-0
232P61	3903	3907	3914	3918	3938	3927	3915	3922	3936	3921	3929	3915	3920	3917	3922	3914	3920	3931	3915	3930
232P62	0	-4	3	8	10	9	6	14	8	5	6	2	9	2	5	2	4	2	3	7
232P63	5884	5867	5873	5873	5875	5871	5860	5875	5875	5861	5873	5862	5871	5869	5870	5861	5871	5879	5868	5883
232P64	0	-6	-1	8	14	15	13	20	13	7	9	5	9	2	4	1	5	6	2	3
232P65	7796	7789	7794	7798	7780	7790	7790	7795	7783	7785	7780	7790	7793	7792	7791	7786	7793	7788	7799	7797
232P66	0	-6	-2	-2	6	9	10	16	9	9	9	8	13	6	8	5	5	9	7	10
232P67	8924	8903	8901	8913	8878	8909	8897	8916	8884	8891	8879	8899	8903	8902	8891	8890	8904	8874	8899	8889
232P68	0	-4	-2	0	2	-4	-10	1	-4	-7	-3	-7	-1	-3	-5	-7	2	5	1	4
232P69	0	6	6	12	3	-4	1	11	3	4	9	11	14	-3	12	16	3	4	14	9
232P70	990	1011	1015	1010	1014	1002	1003	1011	1017	1006	1014	1009	1023	1005	1016	1011	1008	1015	1014	1017
232P71	0	6	6	13	3	-4	1	5	3	6	3	1	5	-3	9	9	-2	0	5	2
232P72	1922	1960	1967	1963	1969	1953	1964	1963	1972	1969	1974	1970	1976	1954	1974	1969	1958	1973	1972	1976
232P73	0	6	15	21	10	-3	17	9	7	20	13	16	19	6	19	27	2	12	19	16
232P74	3923	3984	3993	3994	3999	3988	4011	3993	4012	4009	4013	4017	4021	3998	4016	4012	3999	4022	4018	4024
232P75	0	16	27	32	22	11	41	32	25	38	30	50	50	23	38	46	27	36	50	41
232P76	5894	5935	5956	5960	5952	5933	5982	5943	5950	5972	5967	5969	5965	5957	5980	5986	5936	5970	5971	5970
232P77	0	6	6	8	3	-7	1	7	0	4	3	4	9	-3	8	12	-5	4	5	6
232P78	7855	7901	7900	7900	7877	7884	7893	7896	7881	7888	7883	7895	7901	7891	7898	7889	7890	7886	7904	7899
232P79	0	9	14	12	10	5	9	20	16	11	13	20	27	10	18	14	17	17	21	20
232P80	8875	8914	8913	8924	8878	8899	8906	8914	8885	8898	8885	8911	8912	8913	8909	8903	8908	8887	8916	8907
232P81	0	11	10	10	6	4	-1	14	7	3	9	15	18	6	10	9	17	16	16	17

TABLE 5

BLADE AMPLIFIER DATA LOGGER CONNECTION SCHEDULE

INSIDE SURFACE

surface/ function	tap #	x/c [1/1]	cable #	in col	amp board	out col	pin #	bank #	MUX #
pressure	0	0.9500	9	g\u	4	s	8	5	47
temp	0		9	r	5	u	16	5	95
pressure	1	0.8209	9	k\w	4	v	7	5	41
temp	1		9	y	5	g	15	5	89
pressure	2	0.7021	9	s\t	4	u	6	5	35
temp	2		9	p	5	y	14	5	83
pressure	3	0.5934	9	o\v	4	g	5	5	29
temp	3		9	n	5	o	13	5	77
pressure	4	0.4947	9	ry\rg	4	y	4	5	23
temp	4		9	ru	5	r	12	5	71
pressure	5	0.4057	8	g\u	4	o	3	5	17
temp	5		8	r	5	n	11	5	65
pressure	6	0.3264	8	k\w	4	r	2	5	11
temp	6		8	y	5	k	10	5	59
pressure	7	0.2564	8	o\v	4	n	1	5	5
temp	7		8	n	5	w	9	5	53
pressure	8	0.1956	8	s\t	4	s	8	4	46
temp	8		8	p	5	u	16	4	94
pressure	9	0.1437	8	ry\rg	4	v	7	4	40
temp	9		8	ru	5	g	15	4	88
pressure	10	0.1004	7	o\v	4	u	6	4	34
temp	10		7	n	5	y	14	4	82
pressure	11	0.0655	7	s\t	4	g	5	4	28
temp	11		7	p	5	o	13	4	76
pressure	12	0.0386	7	ry\rg	4	y	4	4	22
temp	12		7	ru	5	r	12	4	70
pressure	13	0.0192	6	k\w	4	o	3	4	16
temp	13		6	y	5	n	11	4	64
pressure	14	0.0069	6	o\v	4	r	2	4	10
temp	14		6	n	5	k	10	4	58
pressure	15	0.0010	6	s\t	4	n	1	4	4
temp	15		6	p	5	w	9	4	52
t bridge	na	na	6	na	na	na	na	na	na
excite V	na	na	7	r\y	3	s	8	3	45
anem r	na	na	anem	r	3	n	1	3	3
anem u	na	na	anem	u	3	r	2	3	9
anem g	na	na	anem	g	3	o	3	3	15
anem y	na	na	anem	y	3	y	4	3	21

colour code:
g=green, k=black, n=brown, o=orange, p=pink, r=red,
s=slate(grey), t=turquoise, u=blue, v=violet, w=white,
y=yellow.

TABLE 5 CONTINUED

OUTSIDE SURFACE

function	tap #	x/c	cable #	in col	amp board	out col	pin	bank	MUX #
pressure	16	0.0010	4	o\v	1	s	8	1	43
temp	16		4	n	2	u	16	1	91
pressure	17	0.0069	4	k\w	1	v	7	1	37
temp	17		4	y	2	g	15	1	85
pressure	18	0.0192	4	g\u	1	u	6	1	31
temp	18		4	r	2	y	14	1	79
pressure	19	0.0386	3	ry\rg	1	g	5	1	25
temp	19		3	ru	2	o	13	1	73
pressure	20	0.0655	3	s\t	1	y	4	1	19
temp	20		3	p	2	r	12	1	67
pressure	21	0.1004	3	o\v	1	o	3	1	13
temp	21		3	n	2	n	11	1	61
pressure	22	0.1437	2	ry\rg	1	r	2	1	7
temp	22		2	ru	2	k	10	1	55
pressure	23	0.1956	2	s\t	1	n	1	1	1
temp	23		2	p	2	w	9	1	49
pressure	24	0.2564	2	o\v	1	s	8	0	42
temp	24		2	n	2	u	16	0	90
pressure	25	0.3264	2	k\w	1	v	7	0	36
temp	25		2	y	2	g	15	0	84
pressure	26	0.4057	2	g\u	1	u	6	0	30
temp	26		2	r	2	y	14	0	78
pressure	27	0.4947	1	ry\rg	1	g	5	0	24
temp	27		1	ru	2	o	13	0	72
pressure	28	0.5934	1	s\t	1	y	4	0	18
temp	28		1	p	2	r	12	0	66
pressure	29	0.7021	1	o\v	1	o	3	0	12
temp	29		1	n	2	n	11	0	60
pressure	30	0.8209	1	k\w	1	r	2	0	6
temp	30		1	y	2	k	10	0	54
pressure	31	0.9500	1	g\u	1	n	1	0	0
temp	31		1	r	2	w	9	0	48
t bridge	na	na	4	p&t	na	na	na	na	na
t bridge	na	na	5	u	na	na	na	na	na
excite V	na	na	3	g\k	3	v	7	3	39
prb pitot	32	na	5	k\w	3	n	1	2	2
temp	na	na	5	y	3	g	5	2	26
prb incid	33	na	5	o\v	3	r	2	2	8
temp	na	na	5	n	3	u	6	2	32
probe yaw	34	na	5	s\t	3	o	3	2	14
temp	na	na	5	p	3	v	7	2	38
rotor torq	na	na	torque	y\w	3	y	4	2	20

colour code:
g=green, k=black, n=brown, o=orange, p=pink, r=red,
s=slate(grey), t=turquoise, u=blue, v=violet, w=white,
y=yellow.

TABLE 6

WIND TUNNEL DATA AQUISITION CONNECTIONS

surface/ function	tap #	x/c	used	MUX #	bank	pin	col	tunnel syst#	tun col
dyn press	na	na	na	na	na	na	na	0	ext
inside	0	0.9500	yes	47	5	8	s	1	k
inside	1	0.8209	yes	41	5	7	v	2	u
inside	2	0.7021	yes	35	5	6	u	3	g
inside	3	0.5934	yes	29	5	5	g	4	y
inside	4	0.4947	yes	23	5	4	y	5	w
inside	5	0.4057	yes	17	5	3	o	6	k
inside	6	0.3264	yes	11	5	2	r	7	n
inside	7	0.2564	yes	5	5	1	n	8	v
inside	8	0.1956	yes	46	4	8	s	9	o
inside	9	0.1437	yes	40	4	7	v	10	p
inside	10	0.1004	yes	34	4	6	u	11	t
inside	11	0.0655	yes	28	4	5	g	12	s
inside	12	0.0386	yes	22	4	4	y	13	ru
inside	13	0.0192	yes	16	4	3	o	14	rg
inside	14	0.0069	yes	10	4	2	r	15	ry
inside	15	0.0010	yes	4	4	1	n	16	rw
outside	16	0.0010	yes	43	1	8	s	17	rk
outside	17	0.0069	yes	37	1	7	v	18	rn
outside	18	0.0192	yes	31	1	6	u	19	uy
outside	19	0.0386	yes	25	1	5	g	20	uw
outside	20	0.0655	yes	19	1	4	y	21	uk
outside	21	0.1004	yes	13	1	3	o	22	uo
outside	22	0.1437	yes	7	1	2	r	23	gy
outside	23	0.1956	no	1	1	1	n	na	na
outside	24	0.2564	yes	42	0	8	s	25	gw
outside	25	0.3264	no	36	0	7	v	na	na
outside	26	0.4057	yes	30	0	6	u	27	go
outside	27	0.4947	no	24	0	5	g	na	na
outside	28	0.5934	yes	18	0	4	y	29	gu
outside	29	0.7021	no	12	0	3	o	na	na
outside	30	0.8209	yes	6	0	2	r	31	su
outside	31	0.9500	yes	0	0	1	n	32	gk
probe inci	33	na	yes	8	2	2	r	29	sg
probe pito	32	na	yes	2	2	1	n	30	ny
incidence	na	na	na	na	na	na	na	31	coax
ground	na	na	na	na	na	na	na	35	nw

colour code:
g=green, k=black, n=brown, o=orange, p=pink, r=red,
s=slate(grey), t=turquoise, u=blue, v=violet, w=white,
y=yellow.

TABLE 7

BLADE SURFACE TAPPING POSITIONS FOR
WIND TUNNEL AND ON ROTOR TESTS

surface	tapping number	colour code used in pressure coeff plots	x/c	y/c	used in wind tunnel
inside	0	green	0.9500	-0.0101	yes
inside	1	blue	0.8209	-0.0299	yes
inside	2	red	0.7021	-0.0455	yes
inside	3	black	0.5934	-0.0577	yes
inside	4	green	0.4947	-0.0666	yes
inside	5	blue	0.4057	-0.0723	yes
inside	6	red	0.3264	-0.0748	yes
inside	7	black	0.2564	-0.0745	yes
inside	8	green	0.1956	-0.0714	yes
inside	9	blue	0.1437	-0.0660	yes
inside	10	red	0.1004	-0.0586	yes
inside	11	black	0.0655	-0.0497	yes
inside	12	green	0.0386	-0.0397	yes
inside	13	blue	0.0192	-0.0289	yes
inside	14	red	0.0069	-0.0178	yes
inside	15	black	0.0010	-0.0069	yes
outside	16	black	0.0010	0.0069	yes
outside	17	red	0.0069	0.0178	yes
outside	18	blue	0.0192	0.0289	yes
outside	19	green	0.0386	0.0397	yes
outside	20	black	0.0655	0.0497	yes
outside	21	red	0.1004	0.0586	yes
outside	22	blue	0.1437	0.0660	yes
outside	23	green	0.1956	0.0714	no
outside	24	black	0.2564	0.0745	yes
outside	25	red	0.3264	0.0748	no
outside	26	blue	0.4057	0.0723	yes
outside	27	green	0.4947	0.0666	no
outside	28	black	0.5934	0.0577	yes
outside	29	red	0.7021	0.0455	no
outside	30	blue	0.8209	0.0299	yes
outside	31	green	0.9500	0.0101	yes

TABLE 8

STATIC WIND TUNNEL RUNS

run number	tunnel instr vel [m/s]	stagn press vel [m/s]	Reyn number stagn press	oscil freq [Hz]	alpha min [°]	alpha max [°]
54	44.15	40.25	766021	0.00	-1.2	25.6
73	44.18	40.06	766787	0.00	-5.1	24.7
90	41.87	40.40	773116	0.00	-4.1	25.5
93	57.94	54.52	1037463	0.00	-4.7	25.2
94	41.92	39.20	745994	0.00	-5.5	24.8
124	42.18	38.66	752942	0.00	-7.2	29.7
125	18.12	16.84	322245	0.00	-8.4	28.9
126	30.95	29.35	565060	0.00	-7.3	29.6
127	42.42	39.72	762327	0.00	-7.3	29.6
128	55.46	51.98	986382	0.00	-7.2	29.6
170	54.40	51.17	960107	0.00	-8.5	28.7

TABLE 9

RAMP WIND TUNNEL RUNS

run number	tunnel instr vel [m/s]	stagn press vel [m/s]	Reyn number/ stagn press	ramp rate [rad/s]	alpha min [°]	alpha max [°]	red ramp rate
171	41.55	40.76	762645	0.27	-1.0	31.8	0.01
172	41.80	41.10	766814	1.47	-0.9	31.8	0.03
173	41.73	41.23	769203	2.88	-1.0	31.9	0.07
174	41.69	41.17	768065	5.23	-1.0	32.5	0.12
175	41.77	40.63	768792	6.48	-1.4	32.5	0.15
176	53.82	49.08	923364	5.33	-0.2	28.1	0.10

TABLE 10

SINE WIND TUNNEL RUNS

run number	tunnel instr vel [m/s]	stagn press vel [m/s]	Reyn number/ stagn press	oscil freq [Hz]	alpha min [°]	alpha max [°]	red freq
55	39.91	39.69	748824	2.19	7.4	22.4	0.052
56	39.53	39.12	738191	3.81	7.7	22.3	0.092
57	22.45	20.64	389360	1.10	-10.0	10.1	0.050
58	21.17	20.71	393038	1.10	-12.2	12.7	0.050
59	20.96	20.47	389572	1.10	-14.7	15.1	0.051
60	21.05	20.54	392026	1.10	-16.7	17.6	0.050
61	21.08	20.71	395202	1.10	-18.9	19.9	0.050
62	20.99	20.68	395700	1.10	-20.3	22.2	0.050
63	21.87	20.32	388846	1.10	-20.3	24.3	0.051
64	20.94	20.69	397096	1.10	-20.3	25.7	0.050
65	31.39	30.55	581281	1.65	-10.2	10.5	0.051
66	32.76	30.67	585281	1.65	-12.3	13.5	0.051
67	31.30	30.40	580205	1.65	-14.7	16.0	0.051
68	31.30	30.35	579273	1.65	-17.2	18.6	0.051
69	32.60	30.08	573956	1.65	-19.3	20.5	0.052
70	31.36	30.49	581807	1.65	-20.3	22.9	0.051
71	31.40	30.56	583191	1.65	-20.3	25.5	0.051
72	31.46	30.85	588647	1.65	-20.3	25.7	0.050
74	42.18	40.93	774366	2.19	-9.7	9.4	0.050
75	41.67	41.21	781944	2.19	4.7	24.5	0.050
76	41.90	40.62	766439	2.19	-13.2	12.8	0.051
77	41.92	40.38	770524	2.19	-15.3	15.6	0.051
78	41.19	41.36	784826	2.19	-0.8	25.7	0.050
79	42.21	40.77	771343	2.19	-17.9	17.6	0.051
80	41.43	39.99	756711	2.19	-33.5	31.1	0.052
81	41.55	40.33	763080	2.19	-20.3	22.6	0.051
82	41.36	40.28	762194	2.19	-20.3	24.6	0.051
83	41.35	40.28	762070	2.19	-20.3	25.7	0.051
84	41.52	40.52	773223	1.54	-20.3	25.7	0.036
85	41.43	40.19	766914	1.01	-20.3	25.7	0.024
86	41.50	40.19	764836	1.01	-12.9	12.0	0.024
87	41.36	39.72	760209	1.54	-13.4	12.2	0.037

TABLE 10 CONTINUED

SINE WIND TUNNEL RUNS

run number	tunnel instr vel [m/s]	stagn press vel [m/s]	Reyn number/ stagn press	oscil freq [Hz]	alpha min [°]	alpha max [°]	red freq
88	41.34	40.04	764078	1.54	-20.3	21.9	0.036
91	41.50	40.18	768961	3.11	-14.9	13.8	0.073
92	41.57	39.52	756287	3.46	-20.3	23.4	0.083
120	57.29	55.35	1059352	1.39	-11.8	12.6	0.024
121	55.72	53.57	1010782	2.11	-12.8	13.6	0.037
122	56.02	54.32	1022024	3.02	-8.1	8.2	0.052
123	54.15	53.28	999589	3.02	4.3	24.9	0.053
129	55.56	54.67	1037312	3.02	7.6	21.8	0.052
130	55.30	54.32	1013420	3.02	0.0	28.3	0.052
131	55.55	53.84	1001637	3.02	-12.5	12.5	0.053
132	20.81	20.11	382716	1.10	-21.5	21.9	0.052
133	20.82	20.07	382951	1.10	-23.7	23.9	0.052
134	20.88	19.95	381743	1.10	-27.8	27.7	0.052
135	31.60	30.29	577987	1.65	-23.3	23.7	0.051
136	31.54	29.98	572205	1.65	-25.9	26.0	0.052
137	31.27	29.51	564843	1.65	-28.3	28.2	0.053
138	54.91	51.86	995333	1.39	-23.6	22.9	0.025
139	54.57	51.22	966416	1.39	-28.4	28.2	0.026
140	54.49	51.60	968136	2.11	-24.3	23.0	0.039
141	54.41	51.31	957272	2.11	-28.1	27.7	0.039
142	42.09	40.22	754572	1.01	-23.2	22.8	0.024
143	42.07	39.79	746497	1.01	-28.5	28.8	0.024
144	41.99	40.05	751422	1.54	-23.6	23.0	0.036
145	42.05	40.00	752575	1.54	-28.5	28.1	0.036
146	42.00	40.06	753723	2.20	-24.2	23.2	0.052
147	42.09	40.00	752533	2.20	-26.2	25.5	0.052
148	42.16	39.97	749912	2.20	-28.3	27.9	0.052
149	53.75	50.91	960641	3.02	-23.9	22.6	0.056
150	54.64	53.74	1002678	5.23	7.1	21.5	0.092
153	54.53	53.20	1015350	3.02	4.4	23.9	0.053
154	54.28	53.40	1007600	3.02	4.0	24.2	0.053

TABLE 11

VAWT WAVE WIND TUNNEL RUNS

run number	tunnel instr vel [m/s]	stagn press vel [m/s]	Reyn number/ stagn press	oscil freq [Hz]	alpha min [°]	alpha max [°]	red freq/
95	20.43	20.06	378546	1.09	-11.6	11.0	0.051
96	20.42	19.88	377283	1.09	-10.6	10.9	0.052
97	20.18	19.04	365514	1.09	-11.3	11.4	0.054
98	21.20	18.30	352354	1.09	-12.7	12.9	0.056
99	19.59	18.83	359281	1.09	-14.0	14.7	0.055
100	20.00	19.62	372250	1.09	-9.9	10.3	0.052
101	19.96	19.58	373750	1.09	-12.6	12.8	0.052
102	19.75	19.57	374485	1.09	-14.7	15.1	0.053
103	20.08	19.58	374654	1.09	-17.0	17.7	0.052
104	20.18	19.37	371770	1.09	-18.8	20.1	0.053
105	30.33	29.13	557470	1.65	-19.8	15.9	0.053
106	30.62	29.62	565274	1.65	-12.6	13.1	0.053
107	30.34	29.34	559872	1.65	-15.0	16.1	0.053
108	30.32	29.24	558105	1.65	-17.4	17.9	0.053
109	31.69	29.11	555441	1.65	-19.5	20.3	0.053
110	42.00	40.70	774580	2.19	-10.4	11.0	0.051
111	42.17	40.96	779435	2.19	-12.9	13.2	0.050
112	42.12	40.76	775561	2.19	-15.2	15.8	0.051
113	42.11	40.55	771649	2.19	-17.6	18.2	0.051
114	42.21	40.47	770161	2.19	-19.7	20.7	0.051
115	41.31	40.11	765479	1.01	-11.8	12.2	0.024
116	41.23	39.91	759538	1.53	-12.6	13.1	0.036
117	53.74	47.76	914011	1.39	-12.3	12.4	0.027
118	55.81	53.90	1016968	2.11	-12.8	13.4	0.037
119	55.56	53.60	1005699	3.02	-13.2	13.6	0.053
155	55.26	53.87	1007781	2.11	-23.9	23.1	0.037
156	54.45	52.31	973148	2.11	-13.9	12.9	0.038
157	20.50	18.80	352746	1.09	-23.5	22.7	0.055
158	19.60	18.93	357226	1.09	-25.5	25.0	0.054
159	19.59	18.68	353370	1.09	-28.6	28.3	0.055
161	31.33	29.90	567446	1.65	-25.8	25.5	0.052
162	31.30	29.76	564651	1.65	-28.2	28.2	0.052
163	31.07	29.62	563602	1.65	-23.7	23.0	0.053
164	41.83	39.81	753348	1.53	-23.2	23.4	0.036
165	41.83	39.73	749619	2.20	-23.4	23.5	0.052
166	41.84	40.99	773430	2.20	-25.8	25.8	0.051
167	41.67	25.60	482958	2.20	-4.7	28.9	0.081
168	41.89	39.81	753289	1.01	-28.8	28.3	0.024
169	51.15	48.27	915957	1.22	-28.6	28.3	0.024

TABLE 12

MAIN AERODYNAMIC COEFFICIENTS OVER A RANGE OF REYNOLD'S NUMBERS FOR A SERIES OF STATIC RUNS.

Reynold's number based on stagnation pressure. All runs at nominal reduced frequency of 0.05 and maximum incidence of 22.5° nominal.

Linear regression fit to all ten static runs for stall incidence gives gradient of 0.18°/million and stall incidence at 0.75 million of 12.5°. Similarly fit to C_N gives gradient of 0.125 C_N/million and a value of 1.19 at 0.75 million.

run number Reynolds number	Cn max	@ α [°]	Ct max	@ α [°]	Cm min	@ α [°]	Cm break α [°]
125 322000	1.14	11.9	0.22	11.9	-0.15	28.9	11.9
126 565000	1.18	12.9	0.24	12.9	-0.15	29.6	12.0
127 762000	1.18	12.0	0.23	12.3	-0.16	28.7	11.7
128 986000	1.23	12.9	0.25	12.9	-0.13	29.1	11.7

TABLE 13

MAIN AERODYNAMIC COEFFICIENTS OVER A RANGE OF REDUCED FREQUENCIES FOR RAMP WAVEFORM RUNS.

Blade Reynold's number 0.96 million for run 176 and 128, 0.75 million nominal based on chord for all others. Maximum incidence of 31.8°. α^ is reduced pitch rate at static stall angle [pitch rate*chord/tunnel velocity] with pitch rate expressed in radians/sec.

run number red freq	α^ [rad/s *c/ vel]	Cn max	@ α [°]	Ct max	@ α [°]	Cm min	@ α [°]	moment break α [°]
127 0.000	static	1.18	12.0	0.24	12.3	-0.16	28.7	11.7
128 0.000	static	1.23	12.9	0.25	12.9	-0.13	29.1	11.7
171 0.0010	0.0010	1.27	12.4	0.26	12.4	-0.20	31.8	11.8
172 0.0053	0.0053	1.65	18.1	0.34	15.0	-0.19	21.1	11.8
173 0.0103	0.0103	1.87	20.9	0.40	17.4	-0.25	21.2	15.8
174 0.0188	0.0188	2.33	27.0	0.49	21.2	-0.46	29.1	16.5
175 0.0233	0.0233	2.32	30.9	0.52	22.1	-0.48	31.6	16.7
NB interpolatd from 174/5 0.0148	0.0148	2.34	23.4	0.46	%	-0.44	%	16.32
176 0.0148	0.0148	2.09	22.3	0.47	18.1	-0.38	27.7	17.5

TABLE 14

MAIN AERODYNAMIC COEFFICIENTS OVER A RANGE OF REDUCED FREQUENCIES FOR A SERIES OF SINE WAVE RUNS.

Blade at Reynold's number of 0.75 million nominal based on chord. Maximum incidence of 22.5° nominal. $\alpha\hat{}$ is the reduced pitch rate at the static stall angle on the upstroke. Pitch rate expressed in radians/sec

run # red freq k	$\alpha\hat{}$ [rad*c /vel]	Cn max	@ α [°]	Ct max	@ α [°]	Cm min	@ alpha [°]	Cm break alpha [°]
127 0.000	0	1.18	12.0	0.24	12.3	-0.16	28.7	11.7
142 0.023	0.008	1.67	19.0	0.36	16.9	-0.16	20.4	13.0
144 0.034	0.011	1.78	20.3	0.40	17.8	-0.23	21.0	14.1
146 0.049	0.016	1.93	22.3	0.44	19.7	-0.27	22.7	16.7
92 0.079	0.026	1.87	23.1	0.49	21.6	-0.31	23.4	18.6

TABLE 15

MAIN AERODYNAMIC COEFFICIENTS OVER A RANGE OF REYNOLD'S NUMBERS FOR A SERIES OF SINISOIDAL INCIDENCE WAVEFORMS.

Reynolds number based on stagnation pressure. All runs at nominal reduced frequency of 0.05 and maximum incidence of 22.5° nominal. α^ is reduced pitch rate at static stall angle [pitch rate/*chord/tunnel velocity]: pitch rate expressed in radians/sec.

run # Reynolds #	α^ [rad/s *c/ vel]	Cn max	@ α [°]	Ct max	@ α [°]	Cm min	@ α [°]	Cm break α [°]
62 396000	0.016	1.77	20.6	0.37	18.4	-0.22	21.5	16.8
70 582000	0.016	1.99	21.8	0.42	19.1	-0.26	22.1	16.7
81 763000	0.016	1.86	21.7	0.44	19.6	-0.25	22.2	17.6
149 961000	0.017	1.85	22.1	0.39	19.4	-0.28	22.4	15.4

TABLE 16

MAIN AERODYNAMIC COEFFICIENTS OVER A RANGE OF MAXIMUM INCIDENCE SINE WAVEFORM RUNS.

Blade Reynold's number 0.75 million nominal based on chord and stagnation pressure. Reduced frequency of 0.05 nominal for all runs. α^ is reduced pitch rate at static stall angle [pitch rate*chord/tunnel velocity]. Pitch rate expressed in radians/sec.

run # nom max α	α^ [rad/s *c/v]	Cn max	@ α [°]	Ct max	@ α [°]	Cm min	@ α [°]	Cm break α [°]
st run 127 28.0	0	1.18	12.0	0.24	12.3	-0.16	28.7	11.7
74 10.0	na	1.06	9.4	0.16	9.4	na	na	na
76 12.5	0.003	1.28	12.7	0.26	12.8	na	na	na
77 15.0	0.008	1.45	15.5	0.32	15.2	-0.05	15.2	14.2
79 17.5	0.011	1.59	17.4	0.37	16.9	-0.13	17.6	15.5
81 22.5	0.017	1.86	21.7	0.44	19.6	-0.25	22.1	16.4
147 25.0	0.019	2.06	23.9	0.46	20.2	-0.32	24.2	16.5
148 30.0	0.023	2.22	25.5	0.48	21.0	-0.39	26.0	17.3

TABLE 17

MAIN AERODYNAMIC COEFFICIENTS OVER A RANGE OF MAXIMUM INCIDENCE VAWT WAVEFORM RUNS.

Blade Reynold's number 0.75 million nominal based on chord and stagnation pressure. Reduced frequency of 0.05 nominal for all runs. α^ is reduced pitch rate [pitch_rate*chord/tunnel velocity] at static stall taken to be 12.5°. Pitch rate expressed in radians/sec.

run # nom max α / nom min α	bsr α^	Cn max	@ α [°]	Ct max	@ α [°]	Cm min	@ α [°]	Cm break α [°]
stat run 127								
28.0	na	1.18	12.0	0.24	12.3	-0.16	28.7	11.7
110	5.76							
+ve 10.0	na	1.13	10.6	0.19	10.4	na	na	na
-ve 10.0	na	1.02	10.3	0.16	10.0	na	na	na
111	4.62							
+ve 12.5	0.0041	1.30	13.2	0.27	13.2	na	na	na
-ve 12.5	0.0000	1.21	12.9	0.23	12.8	na	na	na
112	3.86							
+ve 15.0	0.0064	1.46	15.8	0.33	15.5	-0.06	15.7	14.9
-ve 15.0	0.0086	1.36	15.2	0.30	15.2	-0.05	7.2	na

TABLE 17 CONTINUED

nom max α and diffs	run #	bsr α^	Cn max	@ α [°]	Ct max	@ α [°]	Cm min [°]	@ α [°]	Cm break α [°]
	113	3.33							
+ve	17.5	0.0090	1.62	18.2	0.37	17.3	-0.16	18.2	14.9
-ve	17.5	0.0138	1.52	17.6	0.36	17.5	-0.06	5.2	17.1
	114	2.92							
+ve	20.0	0.0109	1.74	20.0	0.40	18.2	-0.20	20.4	15.9
-ve	20.0	0.0190	1.69	19.7	0.42	19.3	-0.11	19.6	18.1
	165	2.61							
+ve	22.5	0.0127	1.95	21.9	0.43	18.9	-0.25	22.1	16.2
-ve	22.5	0.0248	1.91	23.2	0.47	22.0	-0.24	23.4	19.6
	166	2.37							
+ve	25.0	0.0136	2.04	23.1	0.46	19.4	-0.31	24.0	16.2
-ve	25.0	0.0298	2.07	25.5	0.50	23.3	-0.32	25.7	22.0
	162	2.00							
+ve	30.0	0.0165	2.04	23.4	0.45	19.8	-0.32	24.8	16.0
-ve	30.0	0.0448	2.27	27.5	0.54	24.9	0.39	27.9	21.9

TABLE 18

STATISTICAL ANALYSIS OF DYNAMIC STALL TIME DELAYS

From static to moment and normal force stall

run no.	motn type	tunnl instr vel [m/s]	stagn press vel [m/s]	Reyn number /stagn	sample freq [Hz] press	oscil freq/ ramp rate [Hz]/ [rad /s]	alpha min [°]	alpha max [°]	red freq /red ramp rate	fram @ stat stal	fram @ mom stal	delt mom stal red time dely tunn vel	red time dely on stgn vel	fram @ Nf stal	delt Nf stal red time dely tunn vel	red time dely on stgn vel
avg>												2.56	2.47		7.55	7.28
std>												0.65	0.63		1.10	1.07
54	stat	44.15	40.25	766021	100.00	0.000	-1.2	25.6	0.000							
73	stat	44.18	40.06	766787	100.00	0.000	-5.1	24.7	0.000							
90	stat	41.87	40.40	773116	100.00	0.000	-4.1	25.5	0.000							
93	stat	57.94	54.52	1037463	100.00	0.000	-4.7	25.2	0.000							
94	stat	41.92	39.20	745994	100.00	0.000	-5.5	24.8	0.000							
124	stat	42.18	38.66	752942	100.00	0.000	-7.2	29.7	0.000							
125	stat	18.12	16.84	322245	100.00	0.000	-8.4	28.9	0.000							
126	stat	30.95	29.35	565060	100.00	0.000	-7.3	29.6	0.000							
127	stat	42.42	39.72	762327	100.00	0.000	-7.3	29.6	0.000							
128	stat	55.46	51.98	986382	100.00	0.000	-7.2	29.6	0.000							
170	stat	54.40	51.17	960107	100.00	0.000	-8.5	28.7	0.000							
55	sine	39.91	39.69	748824	280.82	2.194	7.4	22.4	0.052	26	39	13 3.08	3.06	66	40 9.47	9.42
56	sine	39.53	39.12	738191	488.04	3.813	7.7	22.3	0.092	34	55	21 2.83	2.81	89	55 7.42	7.35
57	sine	22.45	20.64	389360	140.29	1.096	-10.0	10.1	0.050							
58	sine	21.17	20.71	393038	140.29	1.096	-12.2	12.7	0.050							
59	sine	20.96	20.47	389572	140.29	1.096	-14.7	15.1	0.050	75	86	11 2.74	2.68	104	29 7.22	7.05
60	sine	21.05	20.54	392026	140.29	1.096	-16.7	17.6	0.050	67	79	12 3.00	2.93	97	30 7.50	7.32
61	sine	21.08	20.71	395202	140.55	1.098	-18.9	19.9	0.050	63	72	9 2.25	2.21	91	28 7.00	6.88
62	sine	20.99	20.68	395700	140.55	1.098	-20.3	22.2	0.050	59	70	11 2.74	2.70	85	26 6.47	6.37
63	sine	21.87	20.32	388846	140.55	1.098	-20.3	24.3	0.051	57	67	10 2.59	2.41	84	27 7.00	6.51
64	sine	20.94	20.69	397096	140.55	1.098	-20.3	25.7	0.050	54	61	7 1.74	1.72	78	24 5.96	5.89
65	sine	31.39	30.55	581281	210.57	1.645	-10.2	10.5	0.051							
66	sine	32.76	30.67	585281	210.57	1.650	-12.3	13.5	0.051							
67	sine	31.30	30.40	580205	210.57	1.645	-14.7	16.0	0.051	74	87	13 3.22	3.13			
68	sine	31.30	30.35	579273	210.57	1.645	-17.2	18.6	0.051	68	82	14 3.47	3.36	102	34 8.42	8.17
69	sine	32.60	30.08	573956	210.57	1.650	-19.3	20.5	0.052	64	75	11 2.83	2.61	95	31 7.97	7.36
70	sine	31.36	30.49	581807	210.57	1.645	-20.3	22.9	0.051	60	70	10 2.48	2.41	91	31 7.69	7.48
71	sine	31.40	30.56	583191	210.57	1.645	-20.3	25.5	0.051	57	68	11 2.73	2.66	86	29 7.21	7.01
72	sine	31.46	30.85	588647	210.57	1.645	-20.3	25.7	0.050	55	64	9 2.24	2.20	82	27 6.72	6.59
74	sine	42.18	40.93	774366	280.82	2.194	-9.7	9.4	0.051							
75	sine	41.67	41.21	781944	280.82	2.194	4.7	24.5	0.050	30	38	8 1.98	1.96	65	35 8.66	8.56
76	sine	41.90	40.62	766439	280.82	2.194	-13.2	12.8	0.051							
77	sine	41.92	40.38	770524	280.82	2.194	-15.3	15.6	0.051	78	89	11 2.74	2.64	105	27 6.72	6.47
78	sine	41.19	41.36	784826	280.82	2.194	-0.8	25.7	0.050	35	45	10 2.44	2.45	66	31 7.58	7.61
79	sine	42.21	40.77	771343	280.82	2.194	-17.9	17.6	0.051	72	84	12 3.01	2.90			
80	sine	41.43	39.99	756711	280.82	2.194	-33.5	31.1	0.052	58	79	21 5.16	4.98	97	39 9.59	9.26
81	sine	41.55	40.33	763080	280.82	2.194	-20.3	22.6	0.051	64	74	10 2.47	2.39	93	29 7.15	6.94
82	sine	41.36	40.28	762194	280.82	2.190	-20.3	24.6	0.051	62	73	11 2.71	2.63	92	30 7.38	7.18

TABLE 18 CONTINUED

run no.	motn type	tunnl instr vel [m/s]	stagn press vel	Reyn number /stagn	sample freq [Hz] press [m/s]	oscil freq/ ramp rate [Hz]/ [rad /s]	alpha min [°]	alpha max [°]	red freq /red ramp rate	fram @ stat stal	fram @ mom stal	delt mom stal	red time dely tunn vel	red time dely on stgn vel	fram @ Nf stal	delt Nf stal	red time dely tunn vel	red time dely on stgn vel
83	sine	41.35	40.28	762070	280.82	2.194	-20.3	25.7	0.051	57	67	10	2.45	2.39	82	25	6.13	5.98
84	sine	41.52	40.52	773223	196.73	1.537	-20.3	25.7	0.036	55	62	7	2.46	2.40	76	21	7.39	7.21
85	sine	41.43	40.19	766914	129.28	1.010	-20.3	25.7	0.024	54	60	6	3.20	3.11	71	17	9.08	8.81
86	sine	41.50	40.19	764836	129.28	1.010	-12.9	12.0	0.024									
87	sine	41.36	39.72	760209	197.12	1.540	-13.4	12.2	0.037									
88	sine	41.34	40.04	764078	196.73	1.537	-20.3	21.9	0.036	62	69	7	2.45	2.37	84	22	7.71	7.46
91	sine	41.50	40.18	768961	398.09	3.110	-14.9	13.8	0.073									
92	sine	41.57	39.52	756287	443.26	3.463	-20.3	23.4	0.083	69	85	16	2.50	2.38	109	40	6.25	5.94
120	sine	57.29	55.35	1059352	177.78	1.389	-11.8	12.6	0.024									
121	sine	55.72	53.57	1010782	270.20	2.111	-12.8	13.6	0.037	86	95	9	3.09	2.97				
122	sine	56.02	54.32	1022024	385.95	3.015	-8.1	8.2	0.052									
123	sine	54.15	53.28	999589	385.95	3.015	4.3	24.9	0.053	35	46	11	2.57	2.53	69	34	7.95	7.82
129	sine	55.56	54.67	1037312	385.95	3.015	7.6	21.8	0.052	41	51	10	2.40	2.36	77	36	8.64	8.50
130	sine	55.30	54.32	1013420	385.95	3.015	0.0	28.3	0.052	48	55	7	1.67	1.64	79	31	7.40	7.27
131	sine	55.55	53.84	1001637	385.95	3.015	-12.5	12.5	0.053									
132	sine	20.81	20.11	382716	140.55	1.098	-21.5	21.9	0.051	64	75	11	2.71	2.62	91	27	6.66	6.44
133	sine	20.82	20.07	382951	140.55	1.098	-23.7	23.9	0.052	62	69	7	1.73	1.67	87	25	6.17	5.95
134	sine	20.88	19.95	381743	140.55	1.098	-27.8	27.7	0.052	58	67	9	2.23	2.13	83	25	6.19	5.91
135	sine	31.60	30.29	577987	210.75	1.646	-23.3	23.7	0.051	66	74	8	2.00	1.92	95	29	7.25	6.95
136	sine	31.54	29.98	572205	210.75	1.646	-25.9	26.0	0.052	64	72	8	2.00	1.90	92	28	6.99	6.64
137	sine	31.27	29.51	564843	210.75	1.646	-28.3	28.2	0.053	62	70	8	1.98	1.87	89	27	6.68	6.30
138	sine	54.91	51.86	995333	177.78	1.389	-23.6	22.9	0.025	65	68	3	1.54	1.46	82	17	8.75	8.26
139	sine	54.57	51.22	966416	177.78	1.389	-28.4	28.2	0.026	60	64	4	2.05	1.92	75	15	7.67	7.20
140	sine	54.49	51.60	968136	270.49	2.113	-24.3	23.0	0.039	72	79	7	2.35	2.23	96	24	8.06	7.63
141	sine	54.41	51.31	957272	270.49	2.113	-28.1	27.7	0.039	67	73	6	2.01	1.90	87	20	6.71	6.32
142	sine	42.09	40.22	754572	129.42	1.010	-23.2	22.8	0.024	63	67	4	2.17	2.07	81	18	9.77	9.33
143	sine	42.07	39.79	746497	129.42	1.011	-28.5	28.8	0.024	57	61	4	2.17	2.05	73	16	8.67	8.20
144	sine	41.99	40.05	751422	196.73	1.537	-23.6	23.0	0.036	67	72	5	1.78	1.70	89	22	7.83	7.46
145	sine	42.05	40.00	752575	196.73	1.537	-28.5	28.1	0.036	62	69	7	2.49	2.37	81	19	6.77	6.44
146	sine	42.00	40.06	753723	280.98	2.194	-24.2	23.2	0.052	71	81	10	2.49	2.38	101	30	7.48	7.13
147	sine	42.09	40.00	752533	280.98	2.195	-26.2	25.5	0.052	69	79	10	2.50	2.37	99	30	7.49	7.12
148	sine	42.16	39.97	749912	280.98	2.195	-28.3	27.9	0.052	67	78	11	2.75	2.61	95	28	7.00	6.64
149	sine	53.75	50.91	960641	385.95	3.015	-23.9	22.6	0.056	79	87	8	1.86	1.76	110	31	7.20	6.82
150	sine	54.64	53.74	1002678	544.37	5.234	7.1	21.5	0.092	49	58	9	1.22	1.20	94	45	6.12	6.02
153	sine	54.53	53.20	1015350	385.95	3.015	4.4	23.9	0.053	44	48	4	0.94	0.92	71	27	6.36	6.20
154	sine	54.28	53.40	1007600	385.95	3.015	4.0	24.2	0.053	47	60	13	3.05	3.00	71	24	5.63	5.54
171	ramp	41.55	40.76	762645	42.70	0.270	-1.0	31.8	0.0010									
172	ramp	41.80	41.10	766814	213.31	1.474	-0.9	31.8	0.0054	73	75	2	1.31	1.28	90	17	11.1	10.9
173	ramp	41.73	41.23	769203	426.62	2.876	-1.0	31.9	0.0105	80	88	8	2.61	2.58	103	23	7.50	7.41
174	ramp	41.69	41.17	768065	550.05	5.231	-1.0	32.5	0.0191	71	80	9	2.27	2.25	97	26	6.57	6.49
175	ramp	41.77	40.63	768792	550.05	6.480	-1.4	32.5	0.0239	67	77	10	2.53	2.46	92	25	6.33	6.16
176	ramp	53.82	49.08	923364	550.05	5.325	-0.2	28.1	0.0163	70	78	8	2.61	2.38	85	15	4.89	4.46

TABLE 18 CONTINUED

run no.	motn type	tunnl instr vel [m/s]	stagn press vel	Reyn number /stagn	sample freq [Hz] press [m/s]	oscil freq/ ramp rate [Hz]/ [rad /s]	alpha min [°]	alpha max [°]	red freq /red ramp rate	fram @ stat stal	fram @ mom stal	delt mom stal	red time dely tunn vel	red time dely on stgn vel	fram @ Nf stal	delt Nf stal	red time dely tunn vel	red time dely on stgn vel
95	vawt	20.43	20.06	378546	140.15	1.095	-11.6	11.0	0.051									
96	vawt	20.42	19.88	377283	140.15	1.095	-10.6	10.9	0.052									
97	vawt	20.18	19.04	365514	140.15	1.095	-11.3	11.4	0.054									
98	vawt	21.20	18.30	352354	140.15	1.090	-12.7	12.9	0.056									
99	vawt	19.59	18.83	359281	140.15	1.095	-14.0	14.7	0.055	87	106	19	4.42	4.25	116	29	6.75	6.49
100	vawt	20.00	19.62	372250	140.15	1.095	-9.9	10.3	0.053									
101	vawt	19.96	19.58	373750	140.15	1.095	-12.6	12.8	0.053									
102	vawt	19.75	19.57	374485	140.15	1.095	-14.7	15.1	0.053	85	98	13	3.05	3.02	113	28	6.58	6.51
103	vawt	20.08	19.58	374654	140.15	1.095	-17.0	17.7	0.053	78	85	7	1.67	1.63	113	35	8.36	8.15
104	vawt	20.18	19.37	371770	140.15	1.095	-18.8	20.1	0.053	71	82	11	2.64	2.53	104	33	7.92	7.60
105	vawt	30.33	29.13	557470	210.57	1.645	-19.8	15.9	0.053									
106	vawt	30.62	29.62	565274	210.57	1.645	-12.6	13.1	0.052									
107	vawt	30.34	29.34	559872	210.57	1.645	-15.0	16.1	0.053	86	99	13	3.12	3.02				
108	vawt	30.32	29.24	558105	210.57	1.645	-17.4	17.9	0.053	80	92	12	2.88	2.78	114	34	8.16	7.87
109	vawt	31.69	29.11	555441	210.57	1.645	-19.5	20.3	0.053	75	86	11	2.76	2.53	111	36	9.03	8.29
110	vawt	42.00	40.70	774580	280.74	2.193	-10.4	11.0	0.051									
111	vawt	42.17	40.96	779435	280.74	2.193	-12.9	13.2	0.050									
112	vawt	42.12	40.76	775561	280.74	2.193	-15.2	15.8	0.051	87	102	15	3.75	3.63				
113	vawt	42.11	40.55	771649	280.74	2.193	-17.6	18.2	0.051	81	95	14	3.50	3.37	118	37	9.25	8.91
114	vawt	42.21	40.47	770161	280.74	2.193	-19.7	20.7	0.051	76	89	13	3.26	3.12	109	33	8.27	7.93
115	vawt	41.31	40.11	765479	129.15	1.009	-11.8	12.2	0.024									
116	vawt	41.23	39.91	759538	196.46	1.535	-12.6	13.1	0.036									
117	vawt	53.74	47.76	914011	177.65	1.388	-12.3	12.4	0.027									
118	vawt	55.81	53.90	1016968	270.20	2.113	-12.8	13.4	0.037									
119	vawt	55.56	53.60	1005699	385.95	3.015	-13.2	13.6	0.053									
155	vawt	55.26	53.87	1007781	270.49	2.113	-23.9	23.1	0.037	81	90	9	3.06	2.99	106	25	8.51	8.30
156	vawt	54.45	52.31	973148	270.49	2.110	-13.9	12.9	0.038									
157	vawt	20.50	18.80	352746	140.15	1.095	-23.5	22.7	0.055	74	86	12	2.93	2.68	103	29	7.07	6.48
158	vawt	19.60	18.93	357226	140.15	1.095	-25.5	25.0	0.055	71	82	11	2.56	2.48	101	30	6.99	6.75
159	vawt	19.59	18.68	353370	140.15	1.095	-28.6	28.3	0.055	69	80	11	2.56	2.44	94	25	5.83	5.55
161	vawt	31.33	29.90	567446	210.57	1.645	-25.8	25.5	0.052	75	85	10	2.48	2.37	108	33	8.18	7.81
162	vawt	31.30	29.76	564651	210.57	1.645	-28.2	28.2	0.052	73	82	9	2.23	2.12	104	31	7.68	7.30
163	vawt	31.07	29.62	563602	210.57	1.645	-23.7	23.0	0.052	78	90	12	2.95	2.81	113	35	8.61	8.21
164	vawt	41.83	39.81	753348	196.46	1.535	-23.2	23.4	0.036	75	83	8	2.84	2.70	100	25	8.87	8.44
165	vawt	41.83	39.73	749619	281.06	2.196	-23.4	23.5	0.052	81	92	11	2.73	2.59	112	31	7.69	7.30
166	vawt	41.84	40.99	773430	281.06	2.196	-25.8	25.8	0.050	78	89	11	2.73	2.67	109	31	7.69	7.53
167	vawt	41.67	25.60	482958	281.06	2.196	-4.7	28.9	0.081									
168	vawt	41.89	39.81	753289	129.15	1.009	-28.8	28.3	0.024	68	74	6	3.24	3.08	86	18	9.73	9.25
169	vawt	51.15	48.27	915957	156.30	1.221	-28.6	28.3	0.024	70	73	3	1.64	1.54	86	16	8.73	8.24

TABLE 19

SUMMARY DETAILS OF ATMOSPHERIC RUNS

run number	date	time	ave wind [m/s]	anem config	blade lean [°]	rotor revs [rpm]
200	01.05.87	13.31	8.8	0/12	0	120
201	06.06.87	13.40	12.6	1/18	0	120
202	27.07.87	16.36	6.2	6/6	0	120
203	27.07.87	18.05	6.6	6/6	0	60-80
205	31.07.87	11.59	7.6	7/6	45	120
206	31.07.87	13.29	7.2	7/6	45	60
207	31.07.87	15.32	7.5	0/12	30	120
208	31.07.87	16.40	7.2	0/12	30	75
209	31.07.87	18.02	8.2	0/12	0	120
210	31.07.87	19.35	8.2	0/12	0	80-90
219	11.09.87	14.01	8.3	1/18	0	120
220	11.09.87	15.23	10.6	2/18	0	120
221	11.09.87	20.39	10.0	8/12	0	90
222	12.09.87	13.41	13.3	0/12	0	120
223	12.09.87	14.49	11.2	0/12	0	85-100
224	12.09.87	16.16	9.1	0/12	30	90-105
225	12.09.87	17.30	9.5	0/12	30	120
226	14.09.87	13.06	10.0	0/12	45	120
227	14.09.87	14.20	8.6	0/12	45	120
229	14.09.87	16.02	12.7	0/12	45	120
230	14.09.87	17.39	8.8	0/12	15	120
231	14.09.87	19.38	5.6	0/12	15	80-100

TABLE 20

MAIN AERODYNAMIC COEFFICIENTS OVER A RANGE OF BLADE SPEED RATIO AVERAGED RUNS.

α^ is reduced pitch rate [pitch_rate*chord/tunnel_velocity] at static stall incidence; taken to be 12.5°

bsr range and diffs	bsr α^ α^	Cn max	@ α [°]	Ct max	@ α [°]	Up/ down Tan F	Cm min	@ α [°]	Cm brk α [°]
run 127:									
tunn stat	na	1.18	12.0	0.24	12.3	na	-0.16	28.7	11.7
7.1 - 8.3	7.83								
upstream>	na	0.83	7.46	0.07	7.46	7.39	na	na	na
dnstream>	na	0.11	3.21	0.01	3.34		na	na	na
5.7 - 5.8	5.74								
upstream>	na	0.99	9.7	0.12	9.7	3.54	na	na	na
dnstream>	na	0.29	5.2	0.03	5.2		na	na	na
4.6 - 4.7	4.65								
upstream>	0.0022	1.17	12.2	0.19	12.2	2.35	-0.01	11.5	na
dnstream>	na	0.50	7.5	0.07	7.5		-0.05	2.7	na
3.8 - 3.9	3.85								
upstream>	0.0067	1.25	12.6	0.23	12.7	1.78	0.01	9.1	na
dnstream>	na	0.71	9.4	0.12	9.4		-0.05	6.5	na
3.3 - 3.4	3.36								
upstream>	0.0104	1.40	15.0	0.29	15.0	1.21	-0.08	13.8	12.5
dnstream>	na	0.88	11.6	0.19	11.6		-0.00	5.0	na

TABLE 20 CONTINUED

bsr range and diffs	bsr α^ α^	Cn max	@ α [°]	Ct max	@ α [°]	Up/ down Tan F	Cm min	@ α [°]	Cm break α [°]
2.9 - 3.0	2.94								
upstream>	0.0128	1.39	15.2	0.30	15.2	1.02	-0.10	14.2	13.7
dnstream>	0.0098	0.97	12.7	0.22	12.8		-0.37	2.5	na
2.6 - 2.7	2.66								
upstream>	0.0147	1.45	15.5	0.31	15.5	0.77	-0.13	15.3	12.8
dnstream>	0.0219	1.04	13.7	0.25	13.8		-0.01	3.5	na
2.3 - 2.4	2.34								
upstream>	0.0142	1.43	15.4	0.32	15.3	0.80	-0.17	14.1	13.5
dnstream>	0.0286	1.08	14.0	0.25	13.8		-0.06	1.3	13.8
2.0 - 2.3	2.19								
upstream>	0.0170	1.44	15.3	0.33	15.3	1.21	-0.17	14.0	13.7
dnstream>	0.0843	1.32	14.2	0.32	14.8		-0.12	13.9	14.5
Dn stall	2.50								
upstream>	0.0157	1.42	15.4	0.31	15.4	1.24	-0.16	14.1	13.3
dnstream>	0.0358	1.35	15.5	0.32	15.6		-0.13	15.1	14.8

CIT

UNSTEADY
AERODYNAMICS
OF A VAWT
FIGURE 1
RUTHERFORD
APPLETON
WIND TURBINE
TEST SITE

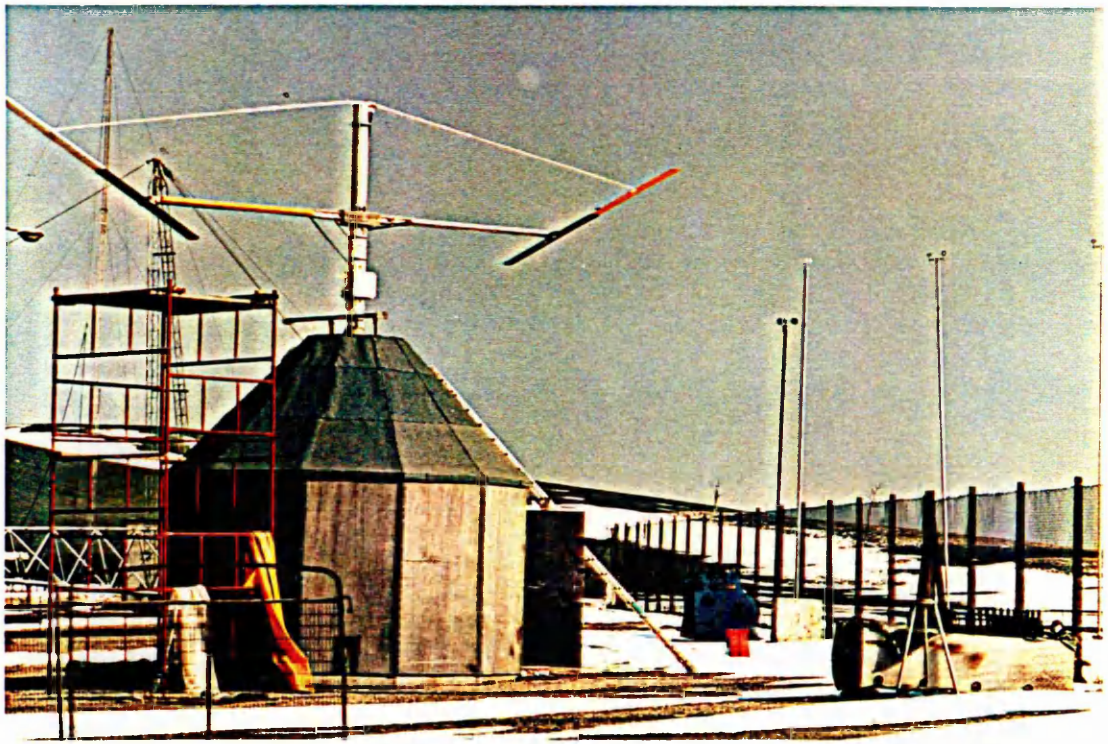

CIT

UNSTEADY AERODYNAMICS OF A VAWT

FIGURE 2

WIND TURBINE RUNNING WITH INSTRUMENTED BLADE MODULE MOUNTED. INSTRUMENTED MODULE IS COLOURED YELLOW AND IS TEAMED WITH DARK BLUE PLAIN MODULE. MODULE FITTED WITH RESTRICTED NUMBER OF KULITE TRANSDUCERS IS MOUNTED ON OTHER CROSS ARM AND ALSO TEAMED WITH A PLAIN MODULE. BLADES HERE SET WITH 60 DEGREE LEANOUT.

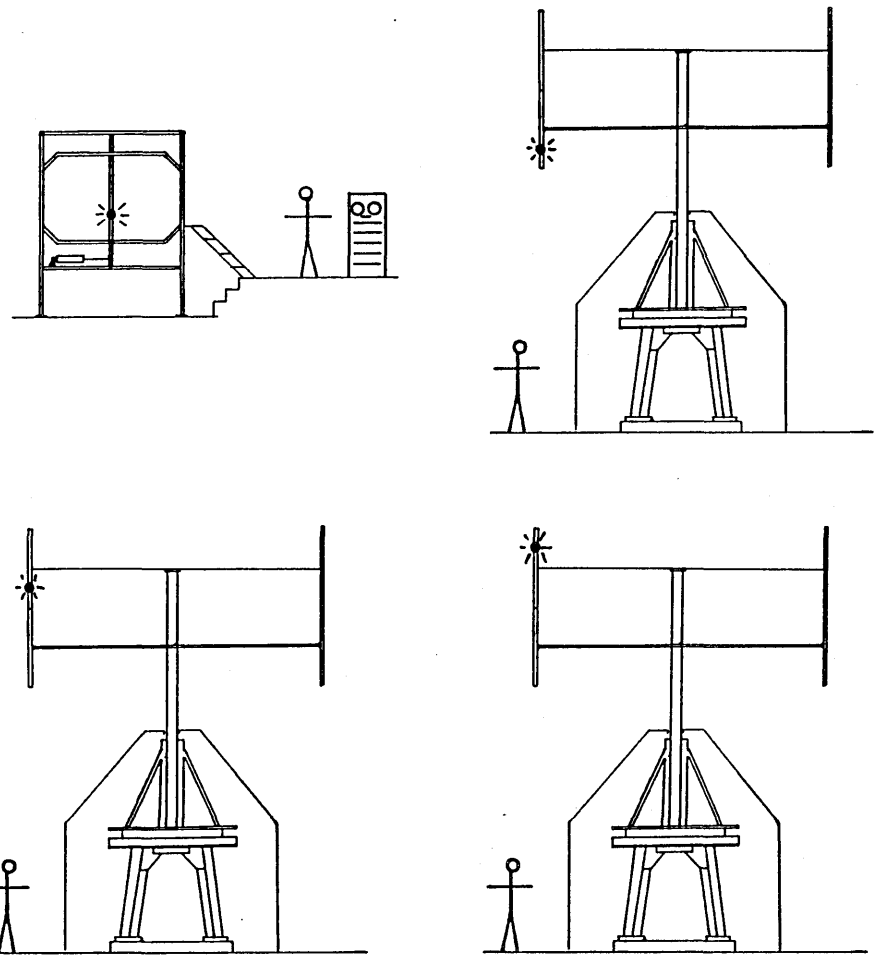

☼ DENOTES MAIN INSTRUMENTATION

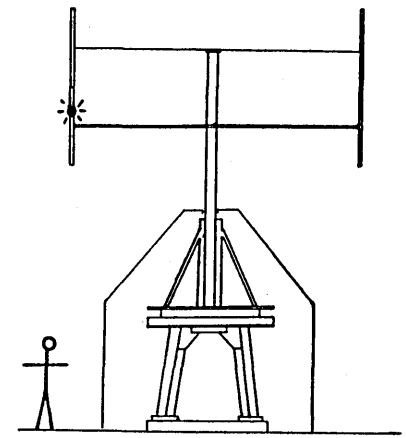

CIT

UNSTEADY AERODYNAMICS OF A VAWT

FIGURE 3

FIVE POSSIBLE CONFIGURATIONS FOR INSTRUMENTED BLADE HALF SPAN MODULE IN WIND TUNNEL AT GLASGOW AND ON ROTOR AT RAL

OR160333/3

PROJECTION

INTERNAL CFRP "DOUBLER" TO SKIN IN HIGHER STRESS AREAS

REAR FACE OF SHEAR WEB TO BE FLAT TO ACCEPT TERMINAL BOARD BONDED BY CIT

SHEAR WEB OF CFRP "TOP HAT" SECTION, TUBE OR SOLID TIMBER, AS PREFERRED BY MANUFACTURER IN CONSULTATION WITH CIT/RAL

PROBE MOUNTING HOLE (REF)

SECTION AA

SECTION BB

SECTION CC

CFRP FILLET

DOUBLER (REF)

"TOP HAT" SECTIONS MUST BE LAID UP IN SITU TO ACCOMMODATE INCLUSIONS

LEADING EDGE TRANSDUCER POCKET

ALIGNMENT OF SOCKET WITH BLADE MODULE CENTRE LINE TO BE WITHIN 0,05°

TRANSDUCER POCKET

TIMBER SHEAR WEB ALTERNATIVE (8)

15,0 15,9

"BRIM" OF TOP HAT SECTION

10,0 20,0

CHANNEL FOR TRANSDUCER WIRES (REF)

SECTION DD

FOAM FILL TO CFRP TOP HAT SHEAR WEB ALTERNATIVE

END OF BLADE MODULE DATUM

LEADING EDGE TRANSDUCER POCKET (REF)

VIEW ON ARROW Y

PROBE MOUNTING HOLE ⌀15,0

MODULE MIDSPAN

LEADING EDGE TRANSDUCER TEMPERATURE COMPENSATOR POCKET

CUT AWAY SECTION TO CENTRE LINE, SHOWS ALTERNATIVE METHODS OF JOINING SHEAR WEBS & LEADING EDGE SPARS TO FISH PLATE SOCKET, PROBE MOUNTING HOLE & MODULE CENTRE SPAN FEATURES

24 OFF HOLES ⌀ 9,0 WITH 90° CSK TO ACCEPT ⌀ 8,0 CSK HD BOLTS (HD MAX ⌀ 17,0)

DISTANCES BACK FROM LEADING EDGE (DATUM) ALONG CHORD

BOLT HOLE PATTERN & OFFSETS FROM LEADING EDGE IDENTICAL TO THAT AT MODULE ENDS.

OUTLINE OF MOUNTING FITTING (REF)

EXTENT OF OPTIONAL LEADING EDGE SPAR

LINE OF SHEAR WEB

0,0 7,5 15,0 22,5 30,0 33,0 +0,0 −0,1 45,0 44,0 60,0 80,0 90,0 100,0 108,0 120,0 139,0 165,0 193,0 204,0 +0,1 −0,0 210,0 213,0 255,0 253,0 265,0 285,0 300,0

FISH PLATE SOCKET

VIEW ON ARROW Z

OR160333/3

TRAILING EDGE CABLE DUCT

ACCESS HATCHWAY

ACCESS HATCHWAY

• INDICATES POCKET ℄

860,0 795,0 771,0 750,0 729,0 705,0 640,0 625,0 375,0 305,0 250,0 195,0 125,0 110,0 100,0 71,0 29,0 0,0

WIRE CHANNELS 1,0 BELOW LEVEL OF ACCESS HATCH SEATING

ACCESS HATCH DETAILS AS DRAWING OR 160333/1

PLAN VIEW ON BLADE MODULE SURFACE

TYPICAL WIRE CHANNEL

COMPONENTS

1 CARBON FIBRE/EPOXY RESIN COMPOSITE - ELEVEN LAYERS EACH OF 0,25mm THICKNESS - EIGHT ARRANGED UNIDIRECTIONALLY SPANWISE & THREE AT ±45°

2 INTERNAL DOUBLER TO SKIN LAYUP AS 1 BUT FEATHERED TO ZERO THICKNESS AS SHOWN

3 DOUGH MOULDING COMPOUND OR COMPOSITE LAYUP CENTRE SPAN PLUG

4 TIMBER SHEAR WEB

5 CARBON COMPOSITE TOP HAT ALTERNATIVE TO 4

6 INTERNAL DOUBLER TO SKIN

7 DOUGH MOULDING COMPOUND PROBE MOUNTING HOLE PLUG

CONTINUED ON OR 160333/4

FIGURE 4

DRN CEO	MATERIAL & SPEC CARBON FIBRE /EPOXY RESIN COMPOSITE	TOLERANCES UNLESS STATED DIMENSIONS BELOW 299,0 ±0,5 ABOVE 299,0 ±1,0 ON LENGTHS & POSN	FINISH SEE SPECIFIC'N	SURFACE TEXTURE µm ✓ UNLESS STATED	JOB No.	PROJ No. EG 53320	2ND MASTER USED ON INSTRUMENTED MODULE 1 9-5-84
CHKD	REMOVE ALL BURRS	ORIGINAL SCALE F/S	0 10 20 30 40 50 mm INCHES		SCIENCE AND ENGINEERING RESEARCH COUNCIL RUTHERFORD APPLETON LABORATORY CHILTON DIDCOT		NB DRG SET INCL OR160335
APPD					Title BLADE MODULE GENERAL ARRANGEMENT UNSTEADY AERODYNAMIC RESPONSE OF A VAWT		OR 160333/3 (OF 4)

OR160341

PROJECTION | THIS DRAWING CONFORMS TO BS 308

ITEM No.	DESCRIPTION	No. OFF	MATERIAL
1	PROBE HEAD	1	ALUMIN. ALLOY
2	MAIN TRANSDUCER BLOCK	1	ALUMIN. ALLOY
3	SUBSIDIARY TRANS BLOCK	1	ALUMIN ALLOY
4	ADAPTER BLOCK	1	ALUMIN ALLOY
5	HOLDING BOLT	4	STAINLESS S
6	COMPENSATOR HOLDER	1	ALUMIN ALLOY
7	SUPPORT TUBE	1	ALUMIN ALLOY

SCALE: FULL SIZE

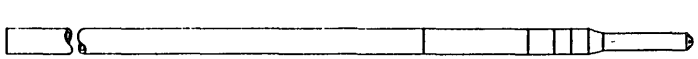

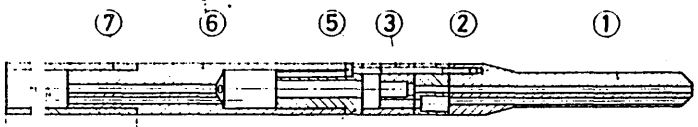

④ SCALE: TWICE FULL SIZE

SUPPORT TUBE 15,0 OD × 2,0 WALL
LENGTHS: 35,0 ± 1/64,0 ± 243,0

⑤

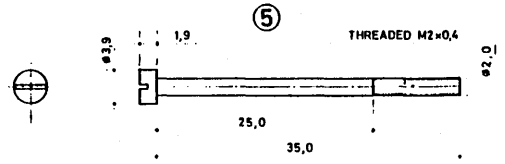

UNDERCUT TO ø11,5×5,0 LONG
PERMISSABLE TO FACILITATE BORING

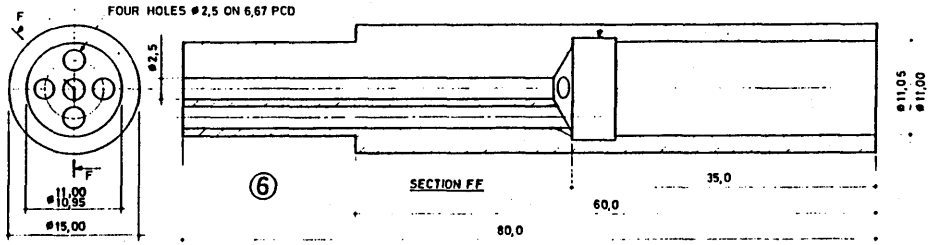

⑥ SECTION FF

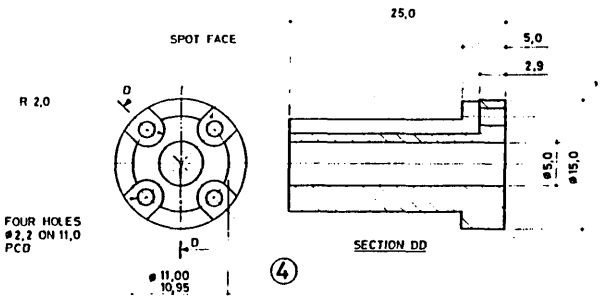

④ SECTION DD

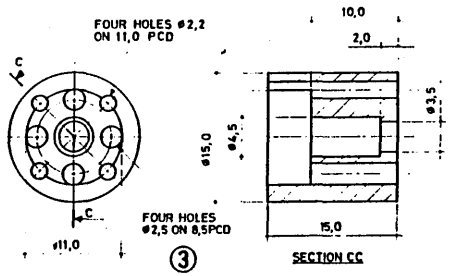

③ SECTION CC

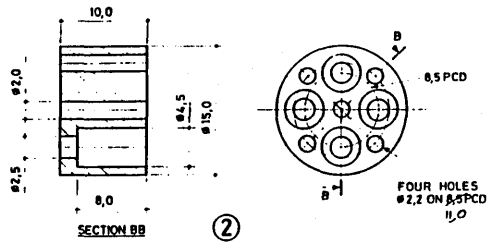

② SECTION BB

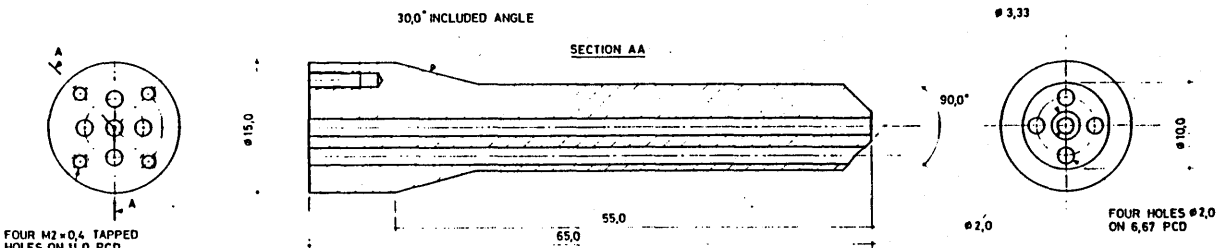

① OR160341

FIGURE 5

DRN. CEO	MATERIAL & SPEC. ALUMIN. ALLOY STAINLESS ST.	TOLERANCES UNLESS STATED ± 0,1	FINISH AS MACHINED	SURFACE TEXTURE µm ✓ UNLESS STATED	JOB No.	PROJ. No.	USED ON
CHKD.	REMOVE ALL BURRS		ORIGINAL SCALE 5×FS	0 2 4 6 8 10 mm / INCHES	SCIENCE AND ENGINEERING RESEARCH COUNCIL RUTHERFORD APPLETON LABORATORY CHILTON OXON.		1 20-7-84 ISSUE DATE MOD No.
APPD.					TITLE INCIDENT FLOW PROBE UNSTEADY AERODYNAMICS OF A VAWT		OR160341

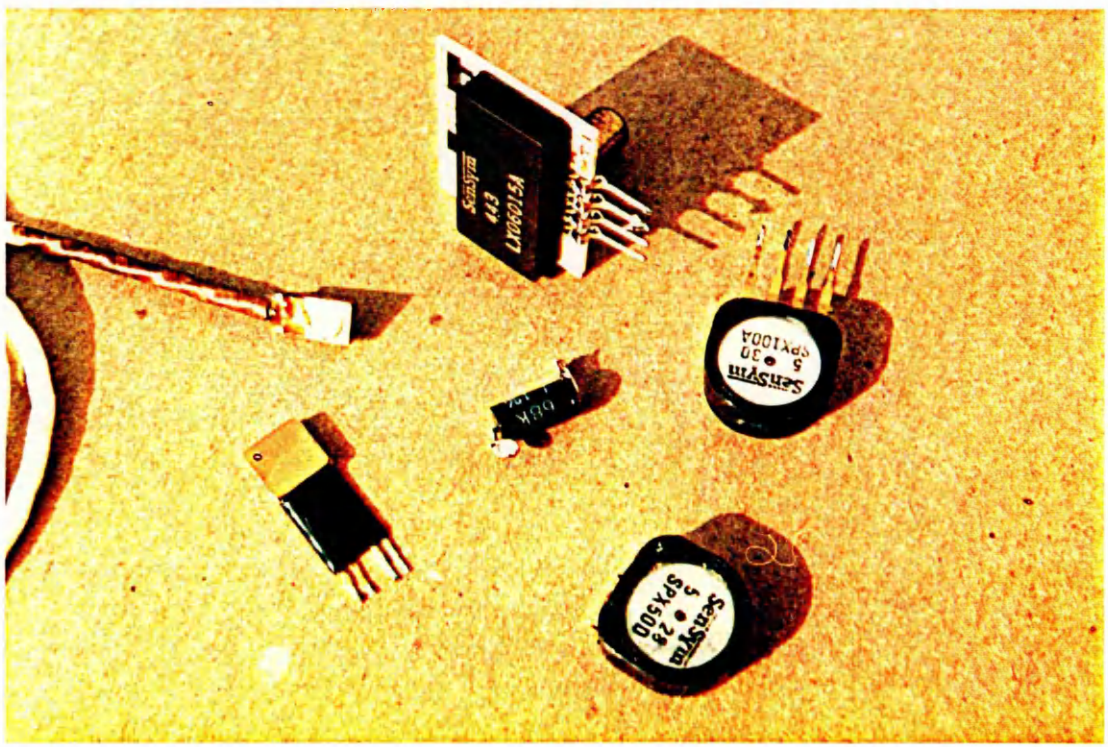

CIT

UNSTEADY AERODYNAMICS OF A VAWT

FIGURE 6

SOME OF THE PRESSURE TRANSDUCERS INVESTIGATED IN THE COURSE OF THE SELECTION PROCEDURE AND TESTS.

XCQ-093-5VG

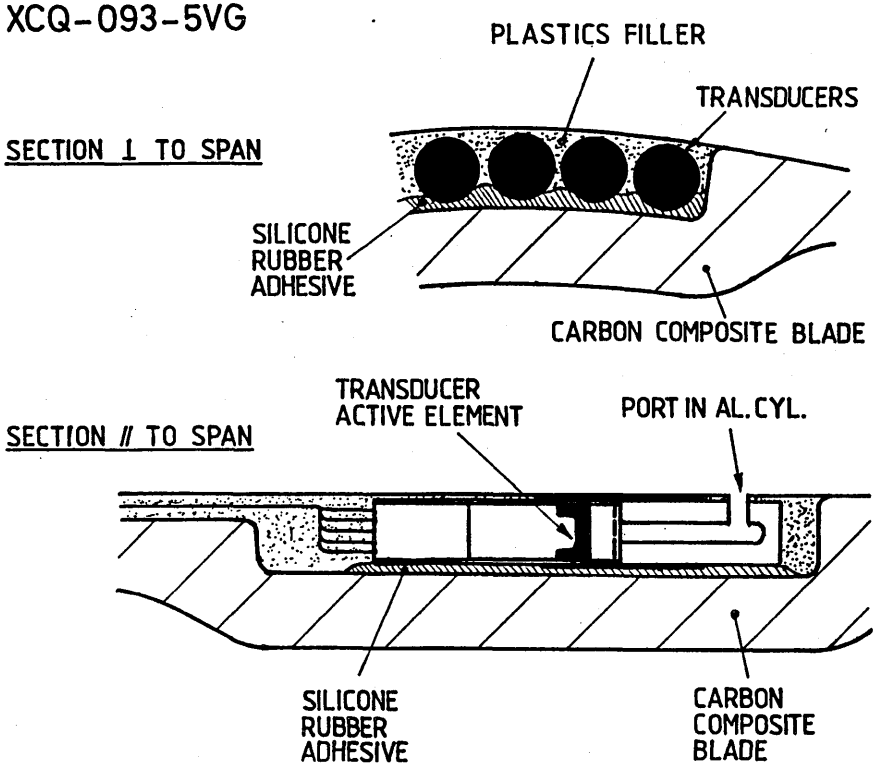

LQ-98-125-5SG

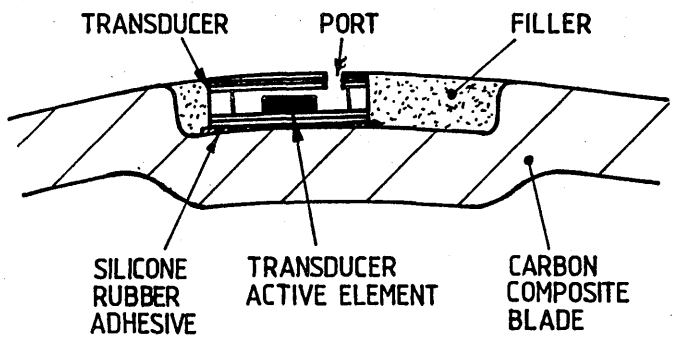

CIT

UNSTEADY AERODYNAMICS OF A VAWT

FIGURE 7

KULITE PRESSURE TRANSDUCER MOUNTING SCHEME. DIAGRAMS SHOW METHOD PROPOSED FOR CYLINDRICAL AND FLATPACK TRANSDUCERS

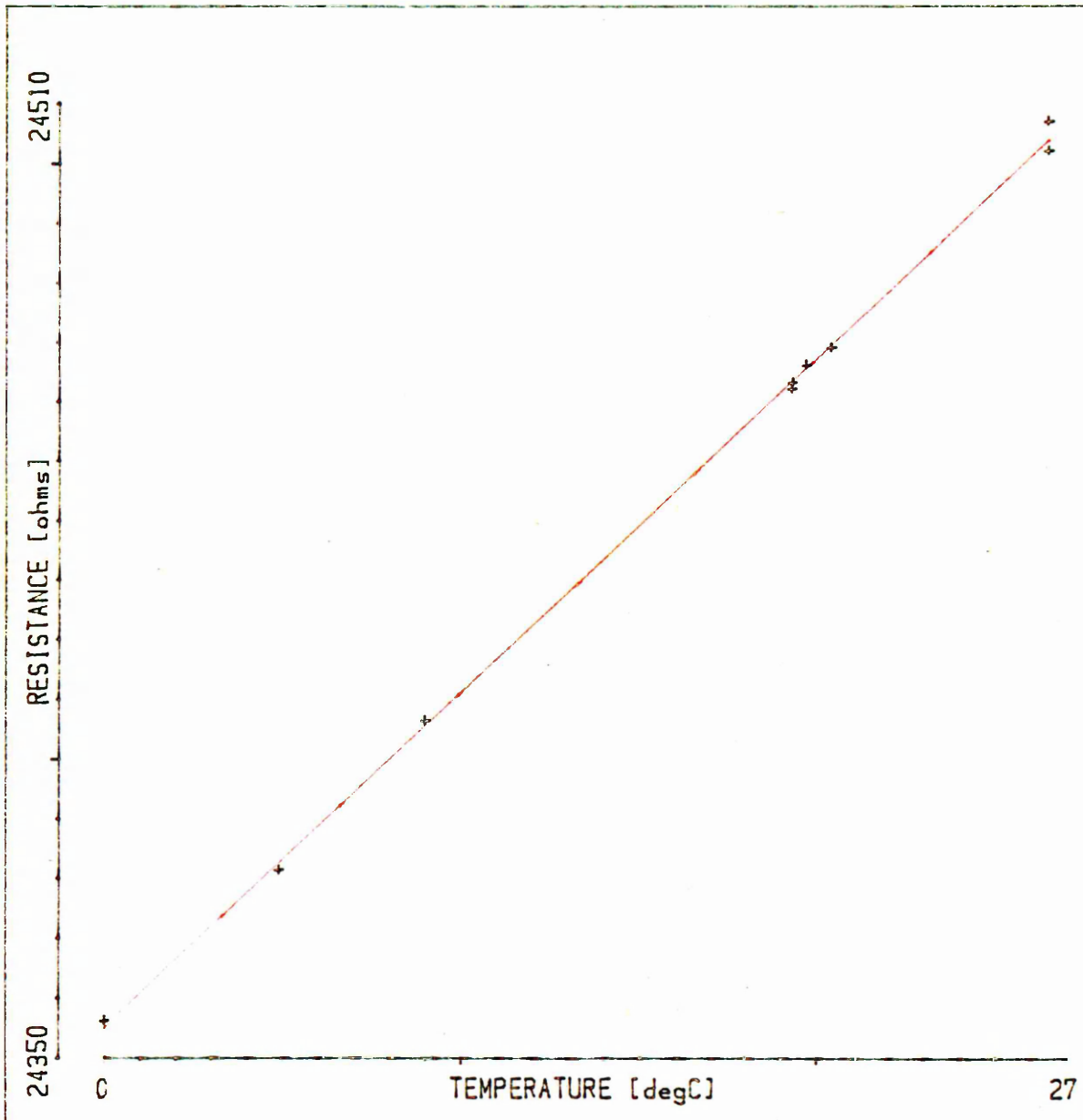

CIT

UNSTEADY AERODYNAMICS OF A VAWT

FIGURE 8

TRANSDUCER CONSISTENCY TESTS

KULITE CYLINDRICAL TEMPERATURE

COMPENSATION MODULE TEMPERATURE

COEFFICIENT

FITTED VALUE: 230 ppm/degC

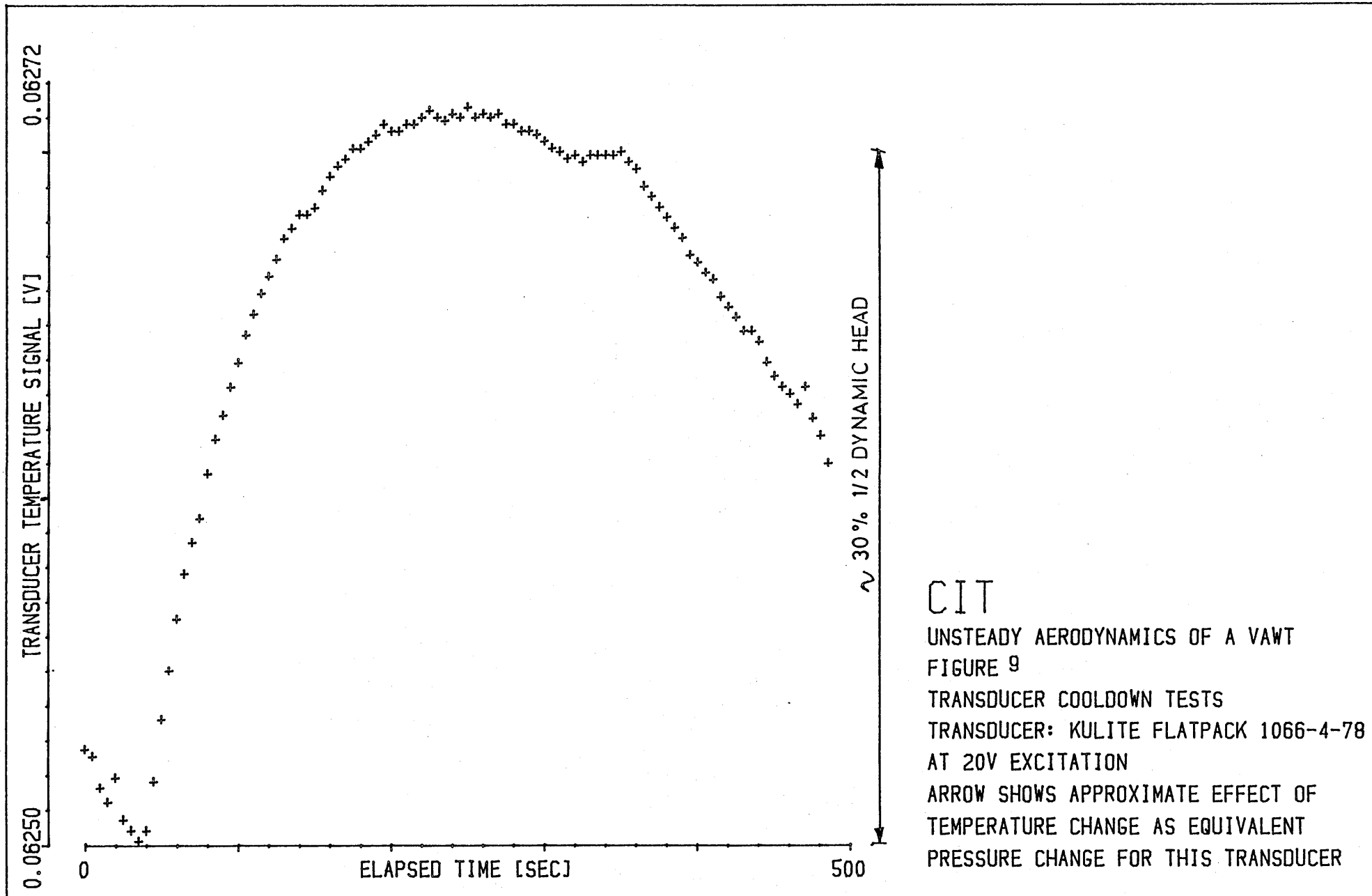

CIT

UNSTEADY AERODYNAMICS OF A VAWT

FIGURE 9

TRANSDUCER COOLDOWN TESTS

TRANSDUCER: KULITE FLATPACK 1066-4-78

AT 20V EXCITATION

ARROW SHOWS APPROXIMATE EFFECT OF TEMPERATURE CHANGE AS EQUIVALENT PRESSURE CHANGE FOR THIS TRANSDUCER

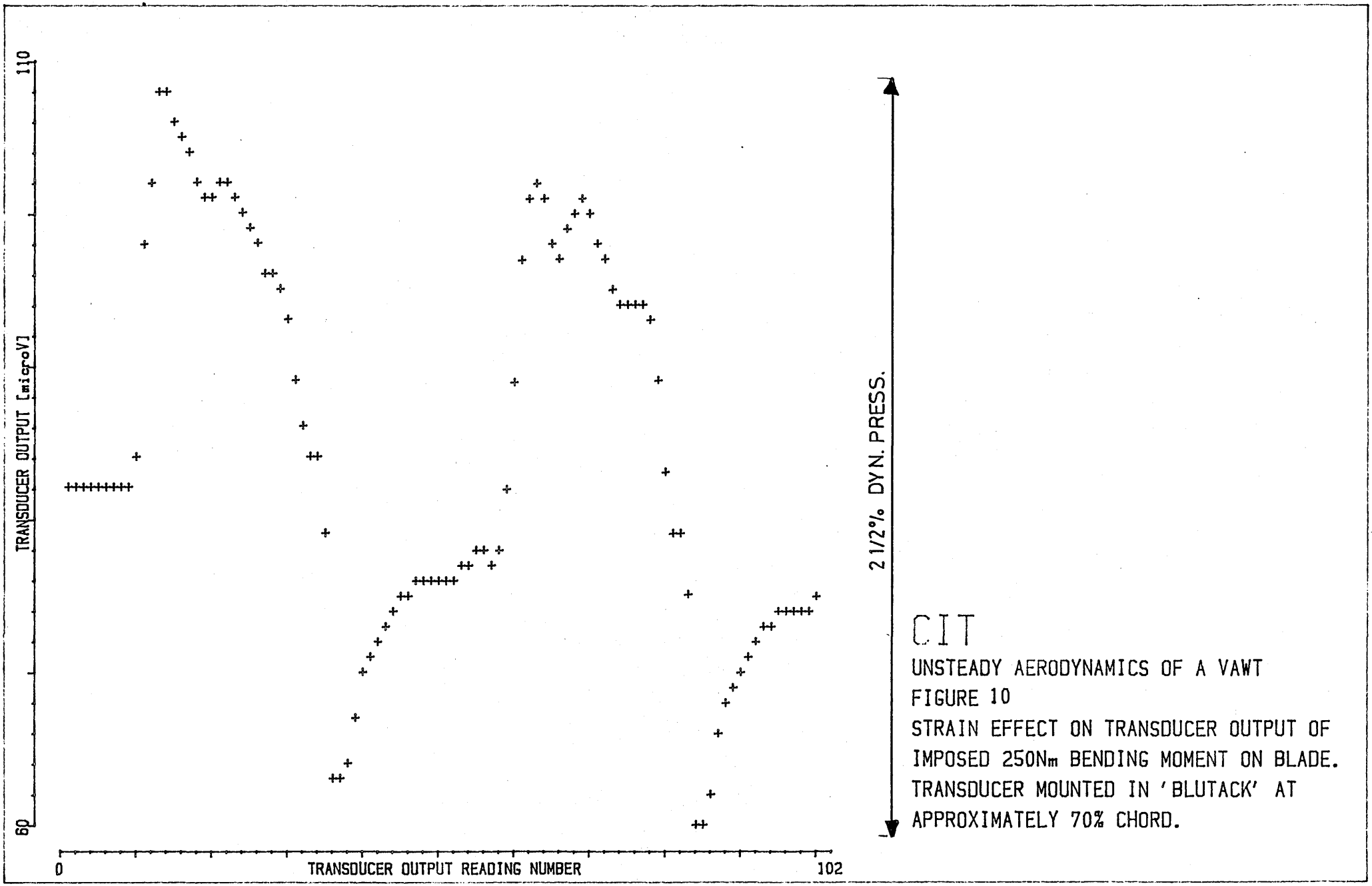

CIT

UNSTEADY AERODYNAMICS OF A VAWT

FIGURE 10

STRAIN EFFECT ON TRANSDUCER OUTPUT OF IMPOSED 250Nm BENDING MOMENT ON BLADE. TRANSDUCER MOUNTED IN 'BLUTACK' AT APPROXIMATELY 70% CHORD.

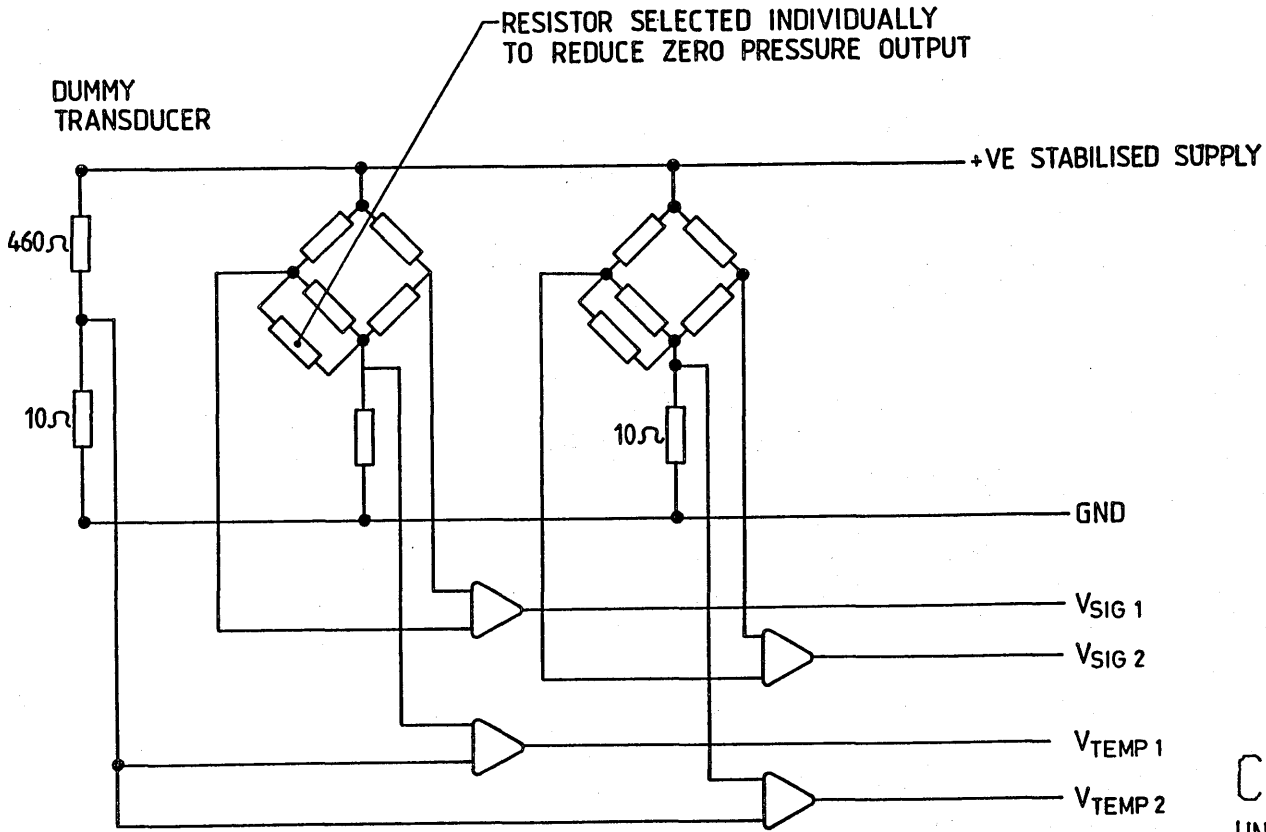

CIT

UNSTEADY AERODYNAMICS OF A VAWT

FIGURE 11

SCHEMATIC CIRCUIT DIAGRAM FOR CONNECTION OF PRESSURE TRANSDUCERS DRAWN CURRENT SIGNAL AND PRESSURE SIGNAL GENERATED AND AMPLIFIED.

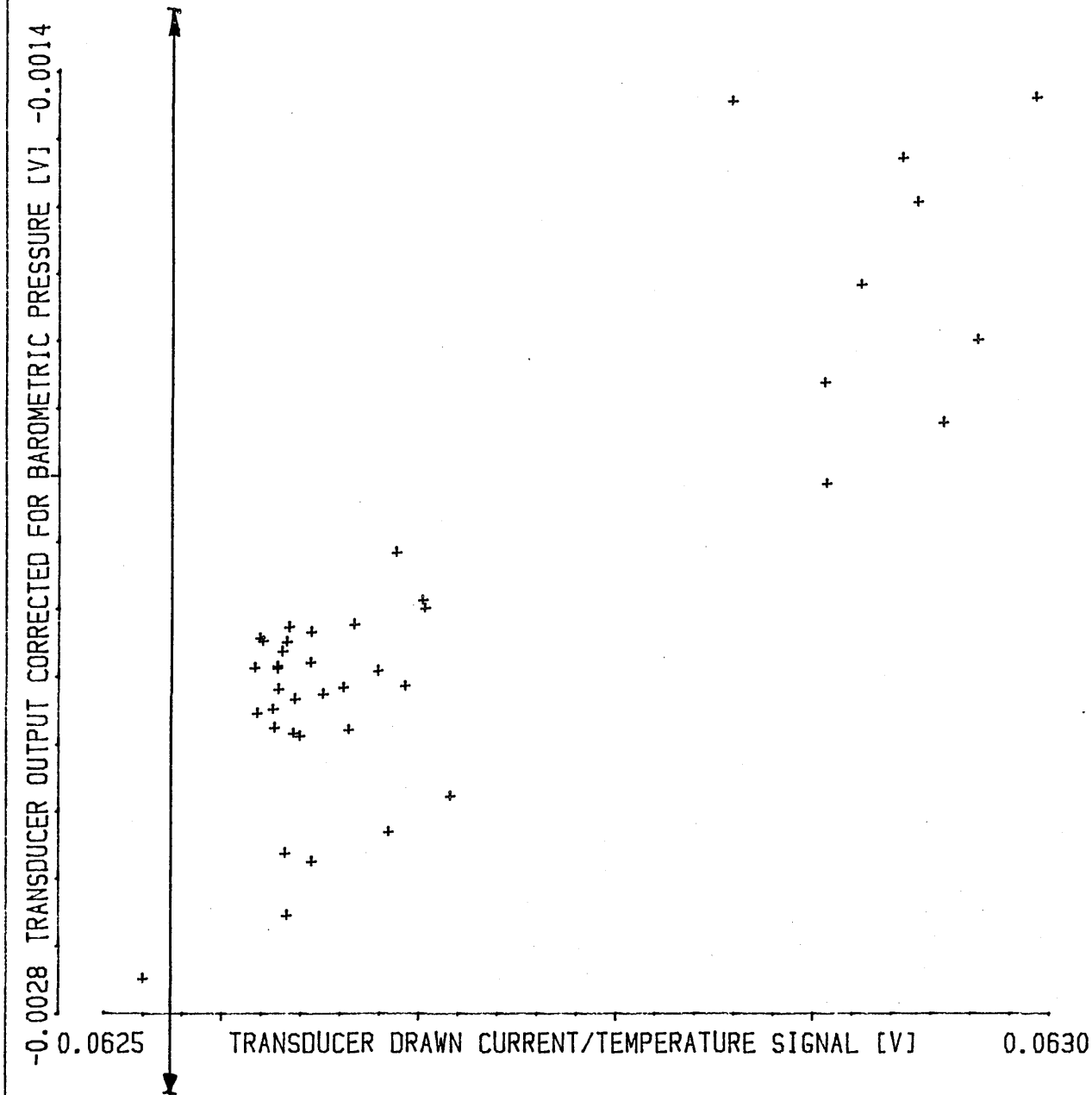

CIT

UNSTEADY AERODYNAMICS OF A VAWT

FIGURE 12

TRANSDUCER CONSISTENCY TESTS

TRANSDUCER: KULITE FLATPACK 1066-4-78

TRANSDUCER ZERO PRESSURE OUTPUT

AGAINST TEMPERATURE SIGNAL.

ARROW SHOWS OUTPUT CHANGE FOR 1kPa -

APPROXIMATE DYNAMIC PRESSURE AT BLADE.

BAROMETRIC CORRECTION BASED ON MANUFACTURER'S

SENSITIVITY FIGURES AT RATED VOLTAGE.

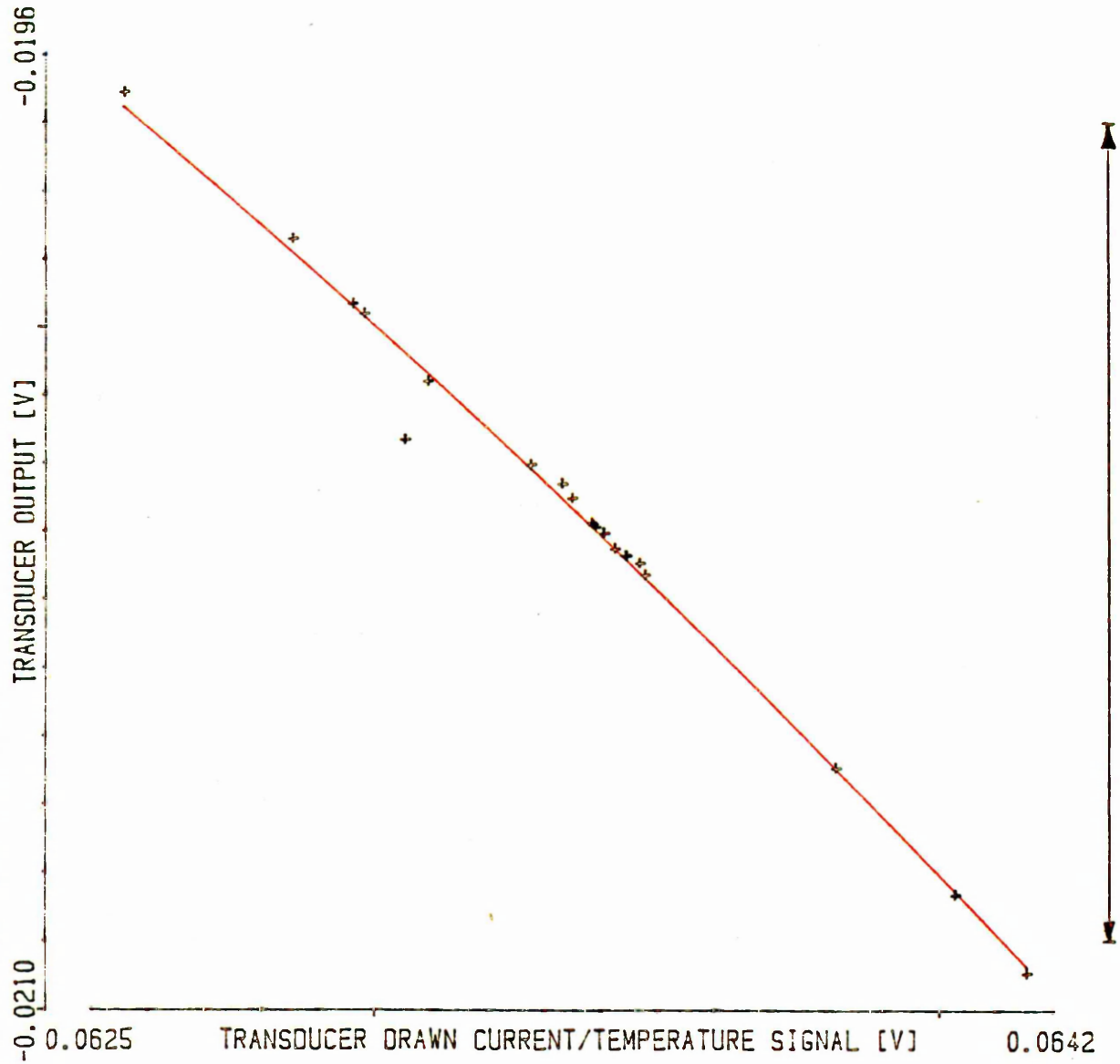

CIT

UNSTEADY AERODYNAMICS OF A VAWT

FIGURE 13

TRANSDUCER CONSISTENCY TESTS

TRANSDUCER: SENSYM SPX50D #2

TRANSDUCER ZERO PRESSURE OUTPUT AGAINST TEMPERATURE SIGNAL.

ARROW SHOWS OUTPUT CHANGE FOR 1kPa - APPROXIMATE DYNAMIC PRESSURE AT BLADE.

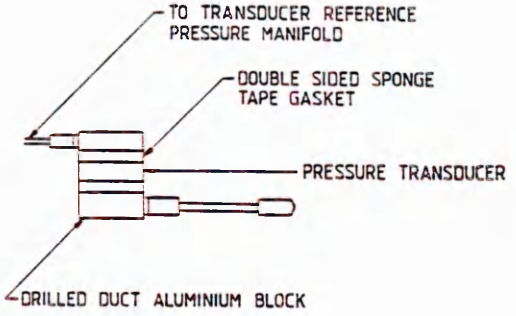

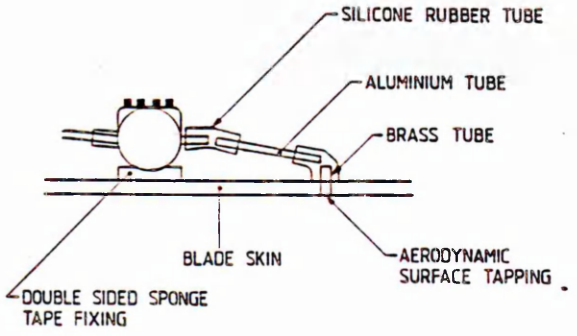

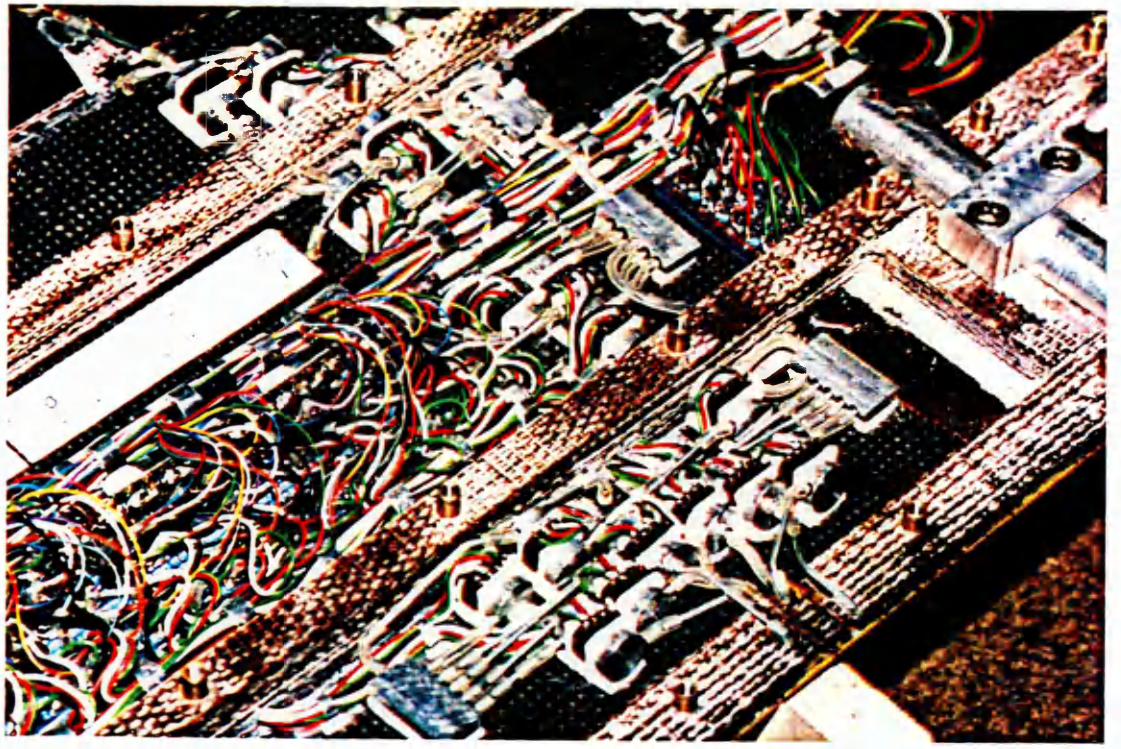

CIT

UNSTEADY AERODYNAMICS OF A VAWT

FIGURE 14

MECHANICAL AND PNEUMATIC CONNECTION OF PRESSURE TRANSDUCERS INSIDE BLADE AERODYNAMIC SURFACE AND REFERENCE PRESSURE MANIFOLD SYSTEM SHOWN.

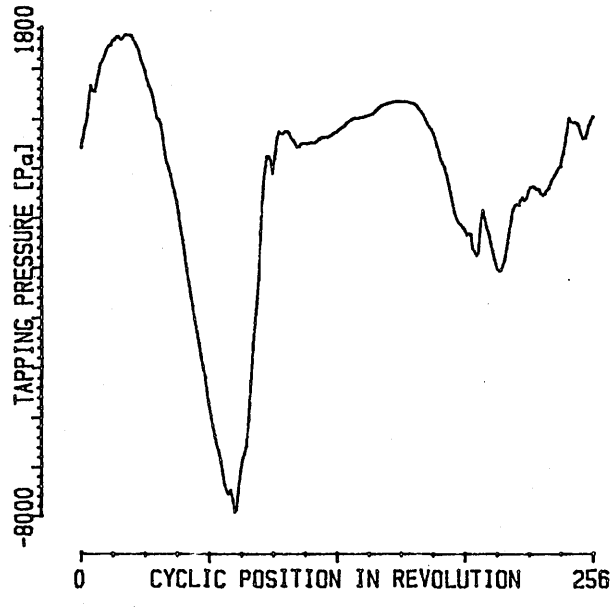

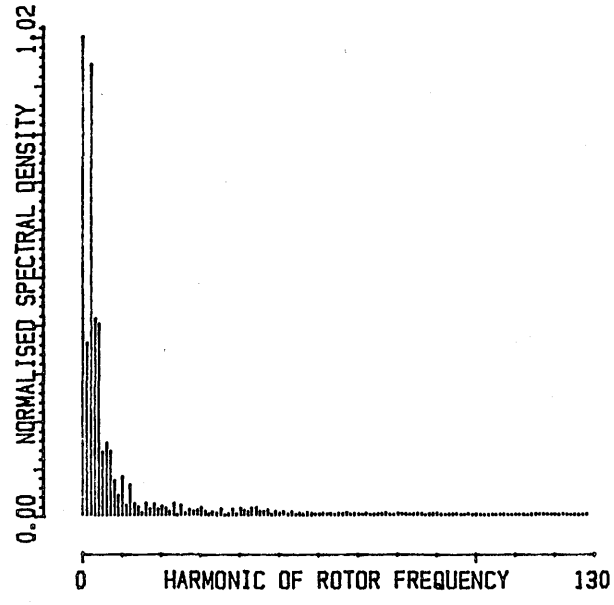

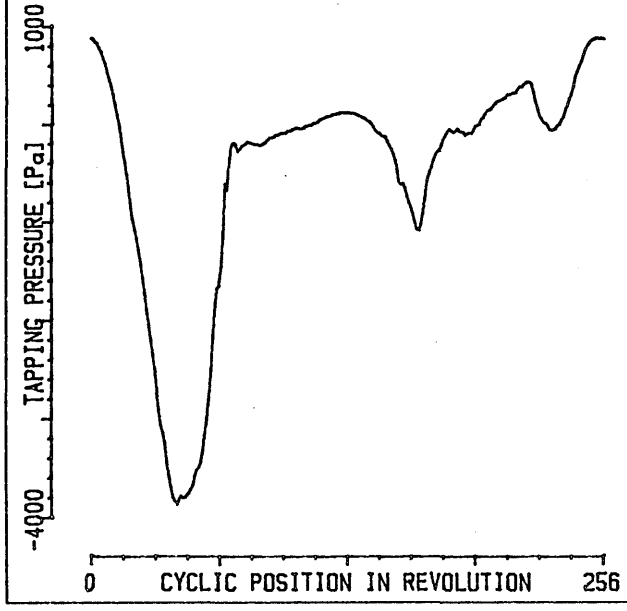

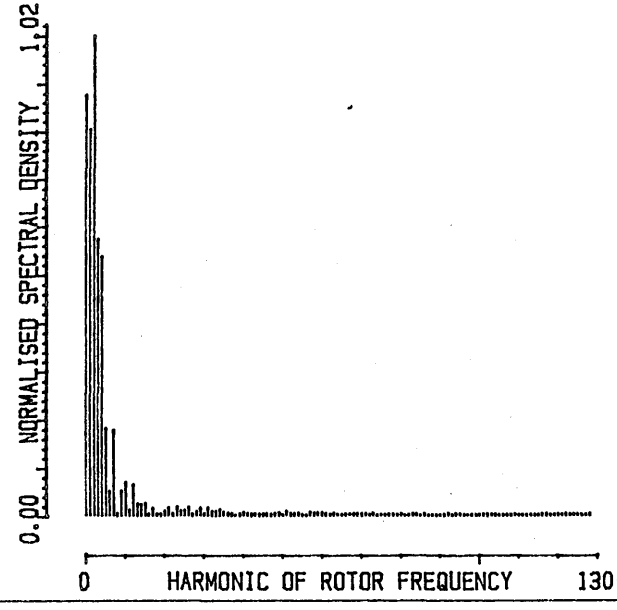

CIT

UNSTEADY AERODYNAMICS OF A VAWT

FIGURE 15

NEAR LEADING EDGE PRESSURE TAPPING TRACES FROM REVS 201.10 AND 221.51 AND THEIR FOURIER TRANSFORMS. ROTOR FREQUENCIES: 1.99Hz AND 1.37Hz RESPECTIVELY. NO PRE-CONDITIONING APPLIED TO SIGNALS.

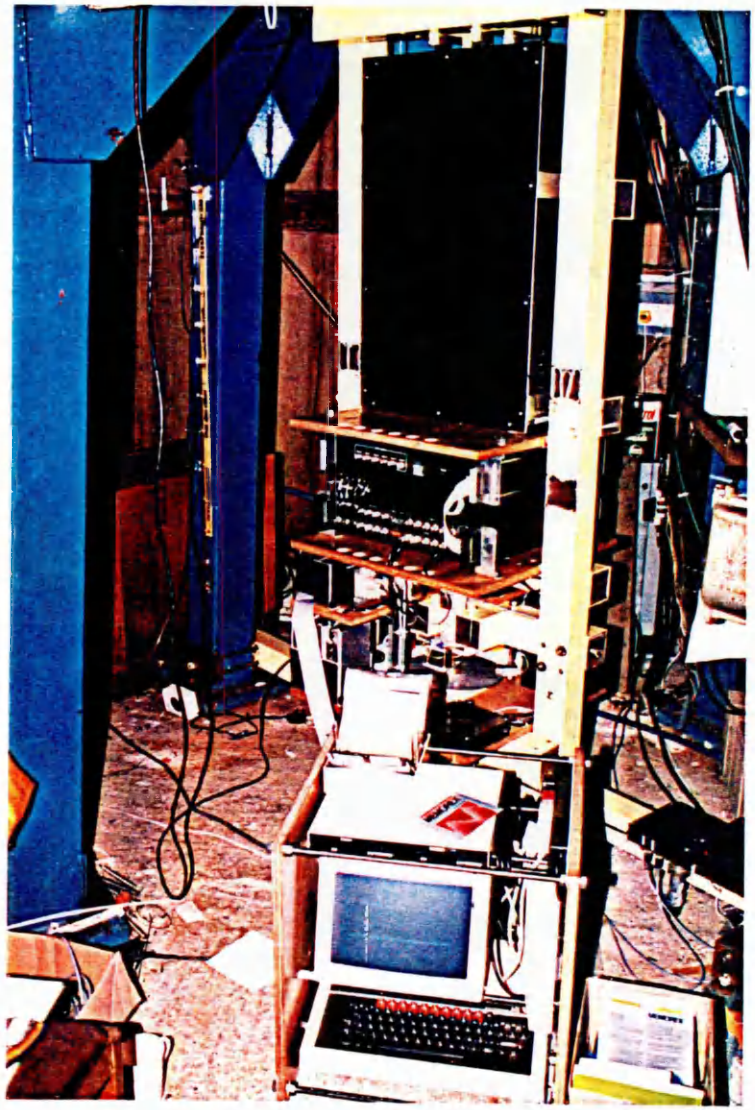

CIT

UNSTEADY AERODYNAMICS OF A VAWT

FIGURE 16

ROTATING INSTRUMENT RACK. PHOTOGRAPH TAKEN DURING DOWNLOADING OF DATA TO BBC MICRO COMPUTER. UPRIGHT BOX CONTAINS AMPLIFIERS. BELOW THESE ARE MULTIPLEXERS AND DATA LOGGER AND BELOW AGAIN ANEMOMETER SIGNAL CONDITIONING. POWER SUPPLIES. OPTICAL DISC. RS423 INTERFACE AND SLIPRINGS. U TUBE MANOMETER FOR TRANSDUCER CALIBRATION MOUNTED ON BLUE PAINTED CHASSIS IN BACKGROUND.

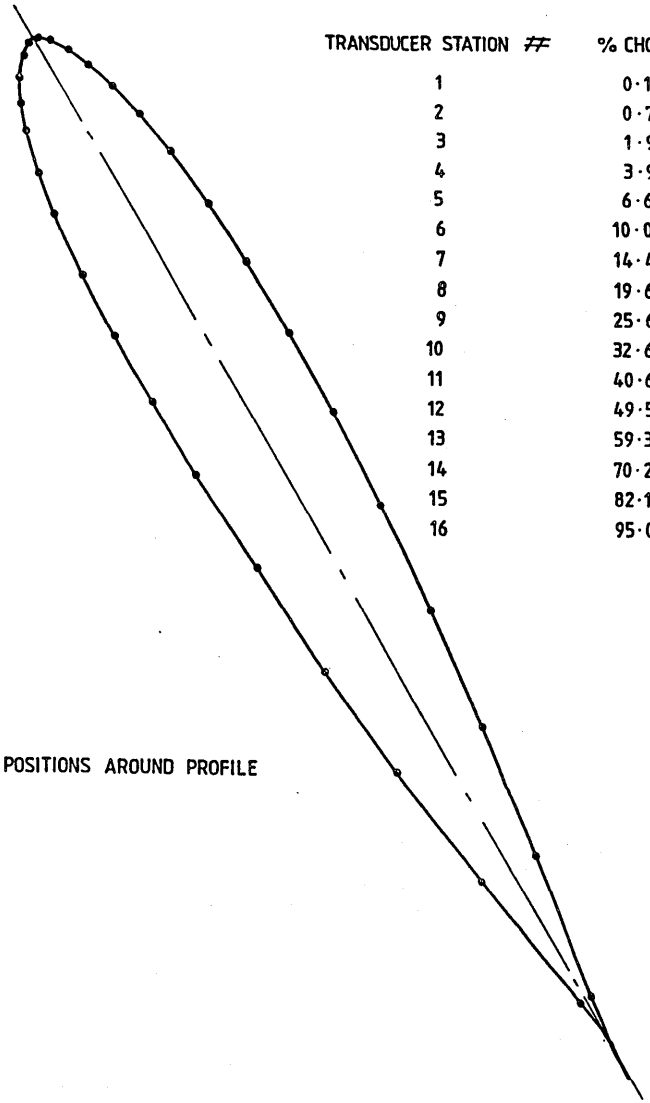

TRANSDUCER STATION #	% CHORD
1	0·1
2	0·7
3	1·9
4	3·9
5	6·6
6	10·0
7	14·4
8	19·6
9	25·6
10	32·6
11	40·6
12	49·5
13	59·3
14	70·2
15	82·1
16	95·0

32 POSITIONS AROUND PROFILE

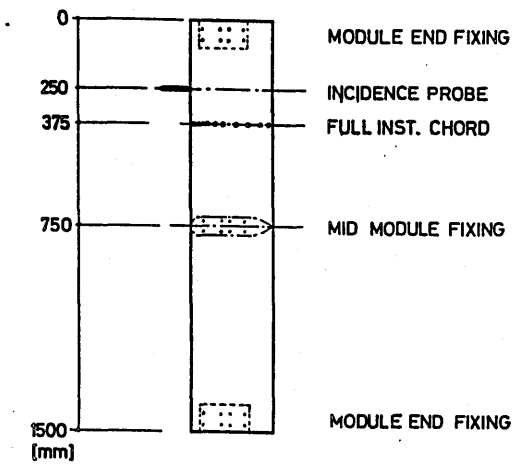

CIT

UNSTEADY AERODYNAMICS OF A VAWT

FIGURE 17

BLADE TAPPING POSITIONS SPANWISE AND CHORDWISE. FLOW PROBE POSITION ALSO SHOWN. NB INSTRUMENTED MODULE FORMS HALF ONLY OF TOTAL ON ROTOR BLADE.

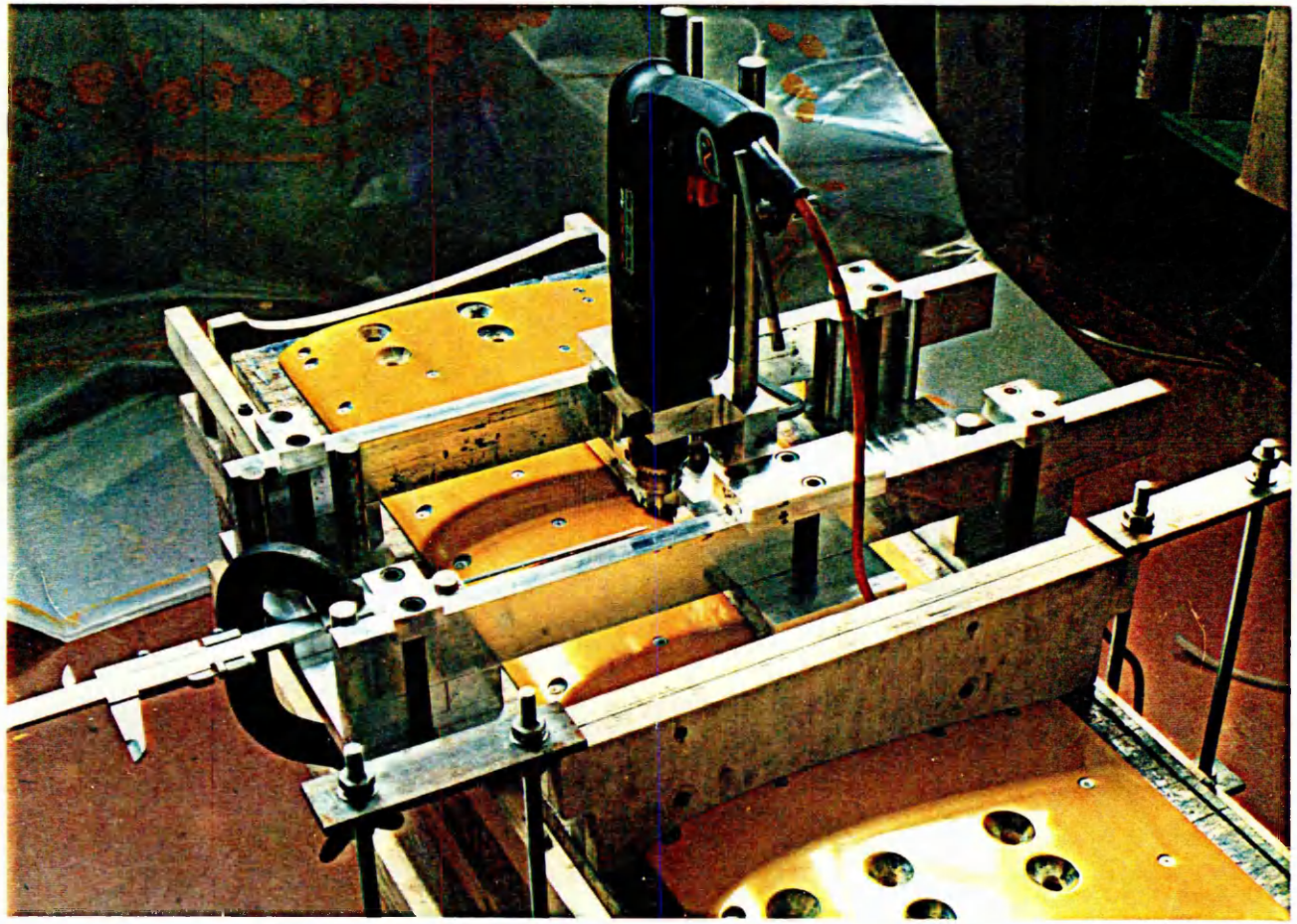

CIT

UNSTEADY AERODYNAMICS OF A VAWT

FIGURE 18

BLADE PRESSURE TAPPING HOLES BEING DRILLED. POSITION SETTING DETERMINED USING VERNIER CALIPER GAUGE. PHOTOGRAPH ALSO SHOWS BLADE FIXING HOLES LATER FILLED WITH BEESWAX.

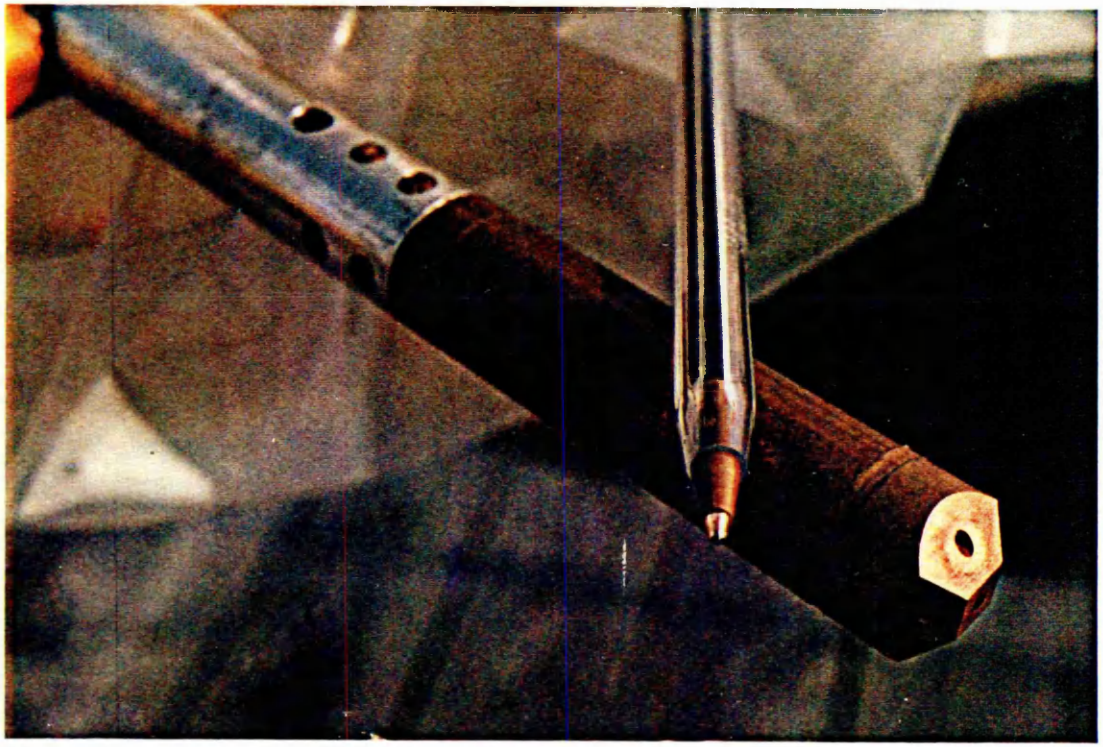

CIT

UNSTEADY AERODYNAMICS OF A VAWT

FIGURE 19

SECOND FLOW PROBE USING THREE SENSYM PRESSURE TRANSDUCERS FOR PITOT PRESSURE. SWEEP FLOW AND INCIDENCE SIGNAL.

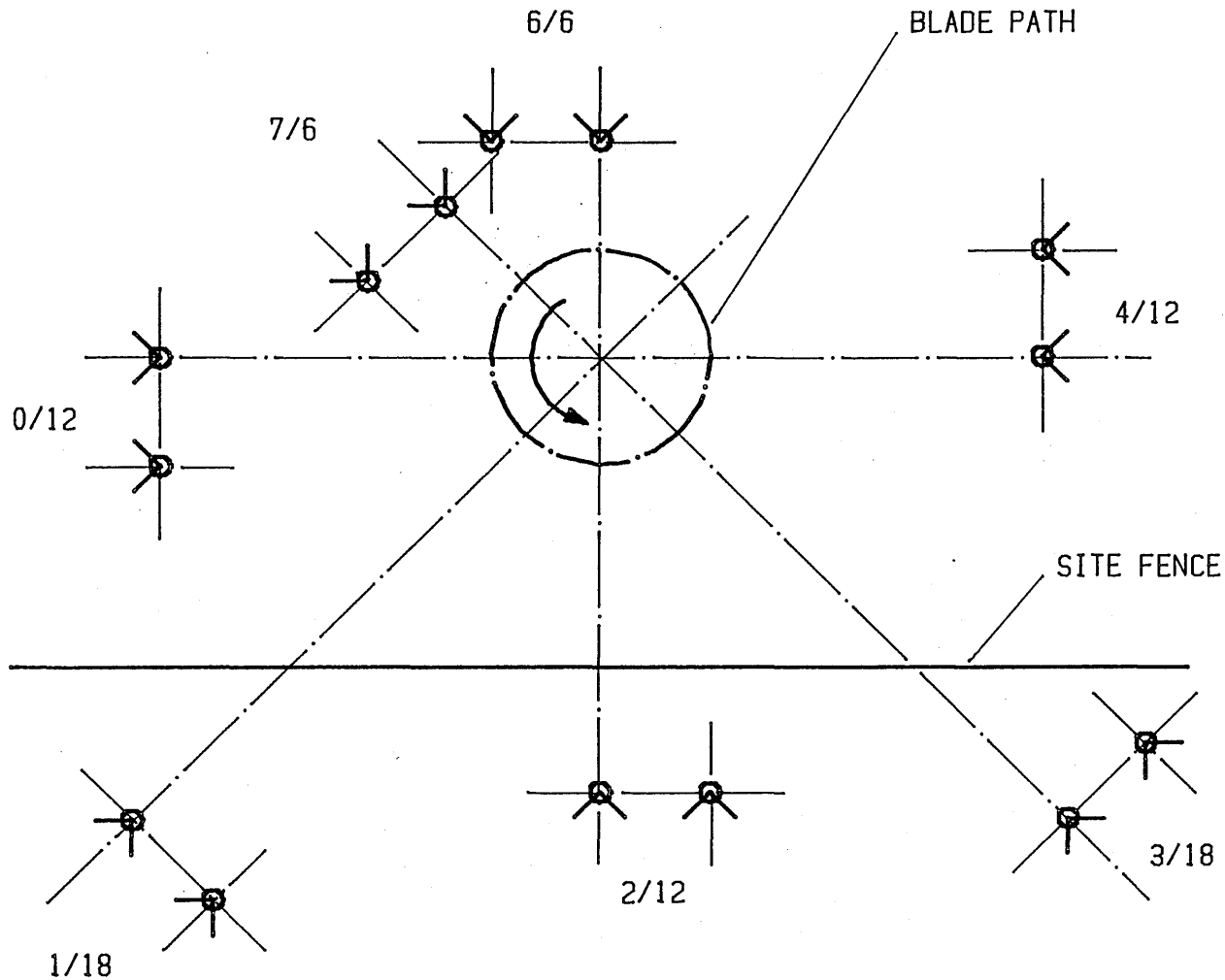

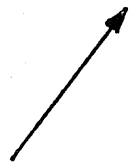

CIT

UNSTEADY AERODYNAMICS OF A VAWT

FIGURE 20

ANEMOMETER TOWER POSITIONS RELATIVE TO ROTOR AND SITE BOUNDARY. ROTOR CENTRE IS 8.7m FROM SITE FENCE AND ANEMOMETER SEPARATION FROM ROTOR CENTRE IS FIGURE AFTER / EG 1/18 IS 18m FROM ROTOR CENTRE.

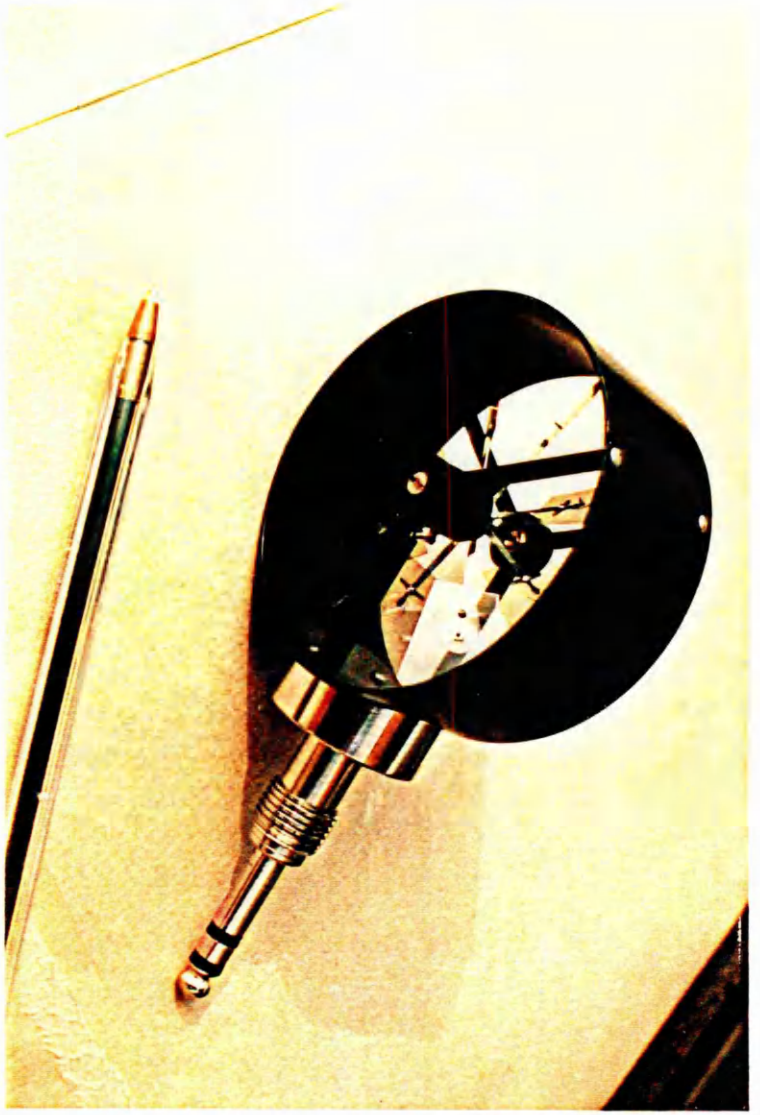

CIT

UNSTEADY AERODYNAMICS OF A VAWT

FIGURE 21

LOWNE FAST RESPONSE ANEMOMETER HEADS SHOWING MICA VANED ROTOR AND SETTING OF HEADS IN TOWER HEAD CROSS TREE USING TEMPLATE.

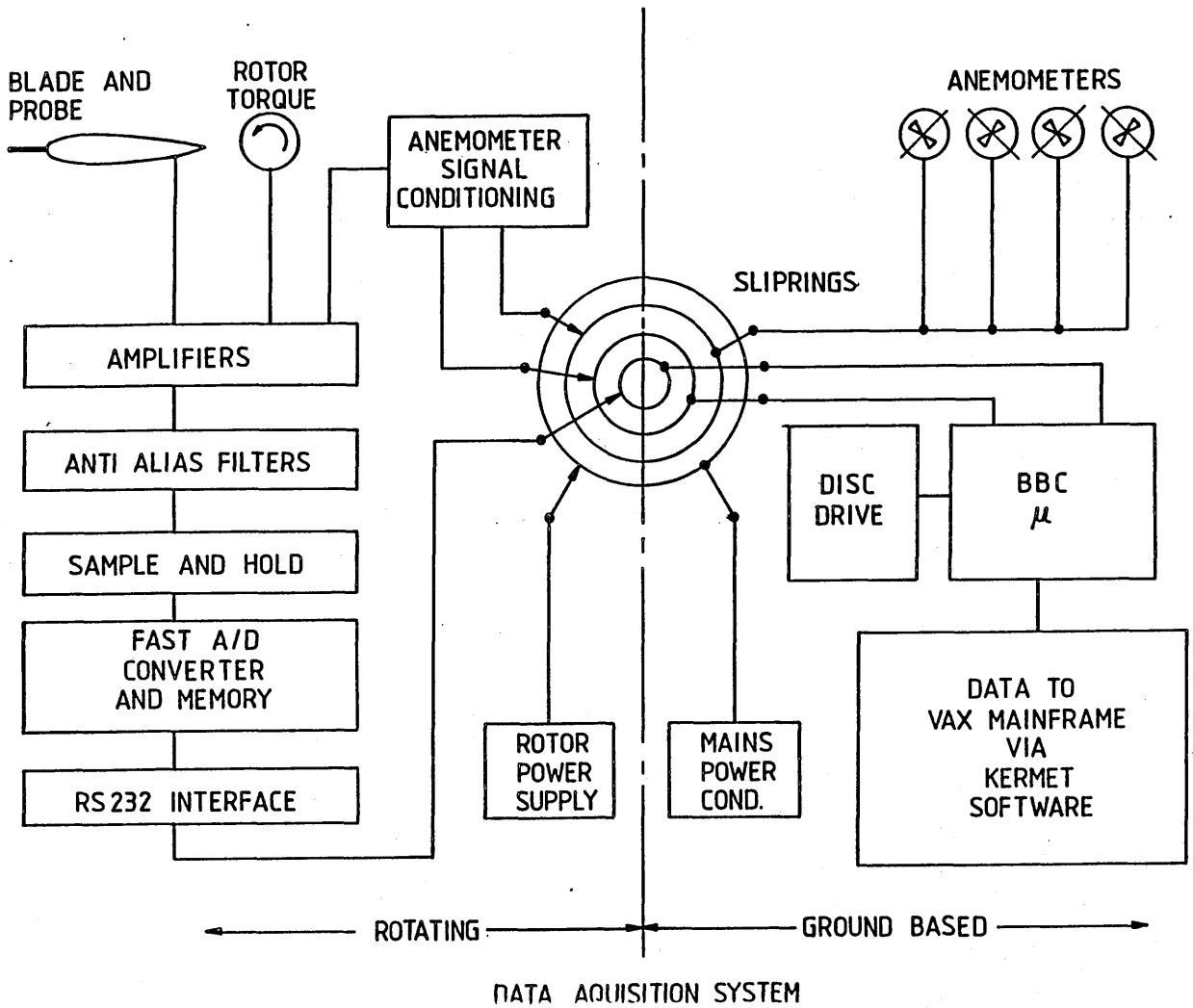

CIT

UNSTEADY AERODYNAMICS OF A VAWT

FIGURE 22

SCHEMATIC OF DIGITAL DATA AQUISITION SYSTEM USED IN ATMOSPHERIC EXPERIMENTS AT RUTHERFORD APPLETON LAB

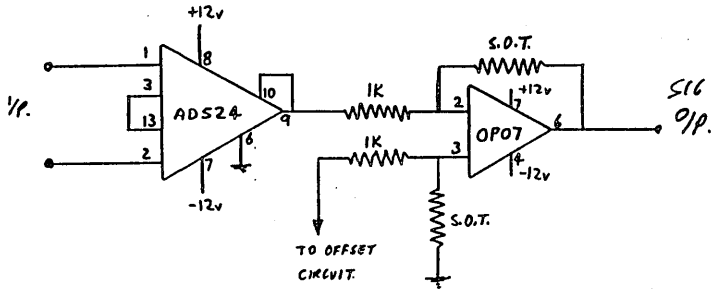

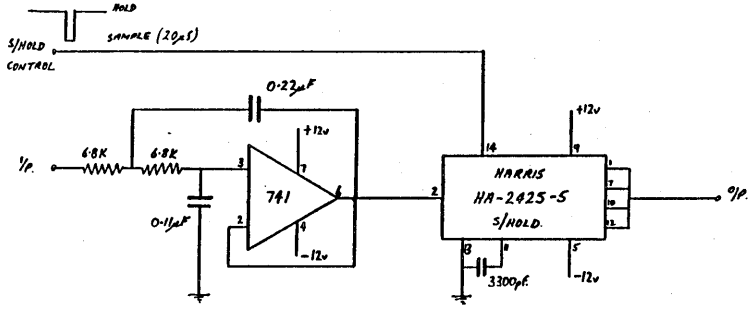

CIT

UNSTEADY AERODYNAMICS OF A VAWT

FIGURE 23

AMPLIFIER. ANTI ALIAS LOW PASS FILTER AND SAMPLE AND HOLD CIRCUITS. SAMPLE AND HOLD CIRCUITS USED ONLY FOR PRESSURE SIGNALS AD524 INSTRUMENTATION AMPLIFIER SET TO GAIN OF 10.0 OP07 OP AMP SET TO 50 ANTI ALIAS CORNER FREQUENCY SET TO 250Hz SAMPLE AND HOLD SET TO UNITY GAIN. OFFSET CIRCUIT NOT USED.

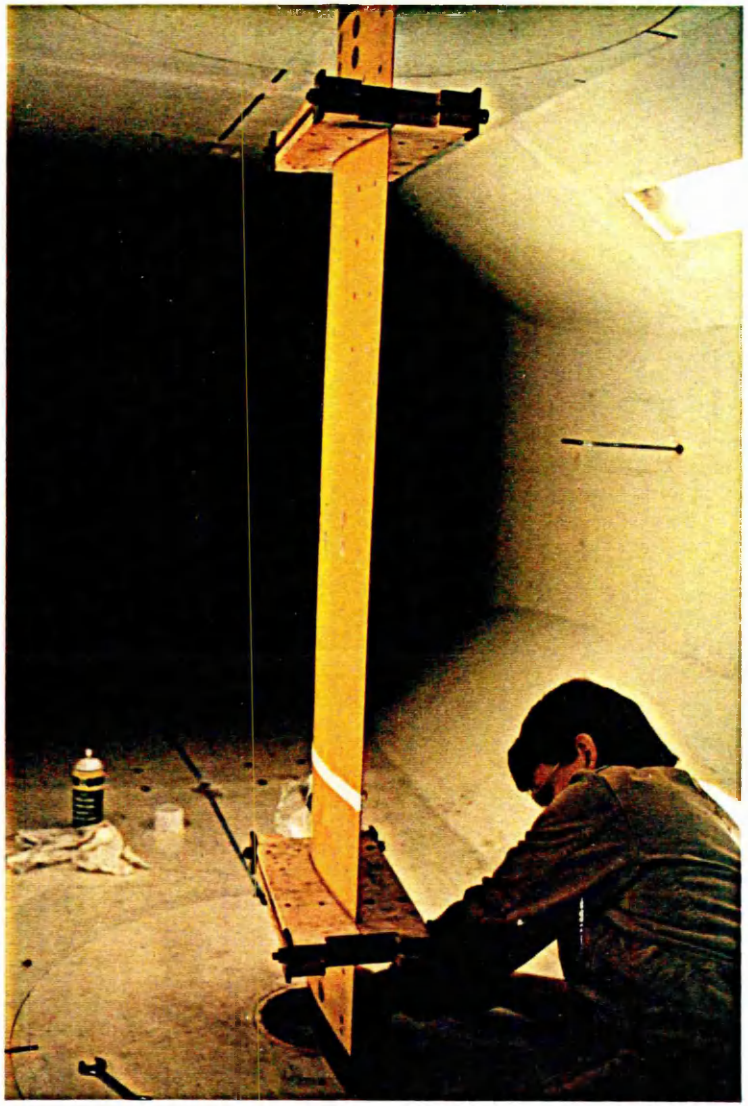

CIT

UNSTEADY AERODYNAMICS OF A VAWT

FIGURE 24

INSTALLATION OF INSTRUMENTED BLADE MODULE INTO UNIVERSITY OF GLASGOW WIND TUNNEL. PHOTOGRAPH SHOWS BLADE END CUFFS AT TOP AND BOTTOM AND POSITION OF TRANSDUCERS IS INDICATED BY WHITE TAPE PROTECTIVE COVERING. ALSO JUST VISIBLE IS FLOW PROBE INSIDE POLYTHENE BAG. AT RIGHT PROJECTING FROM TUNNEL WALL IS TUNNEL SPEED PITOT PROBE.

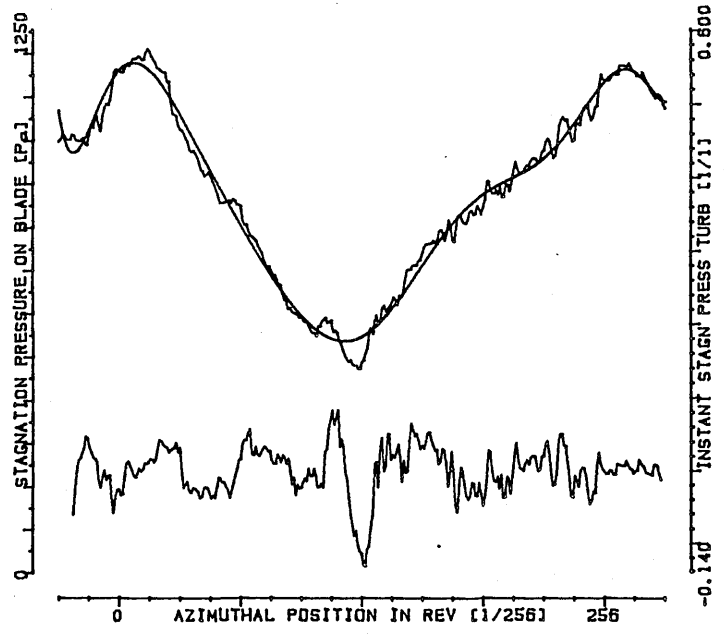

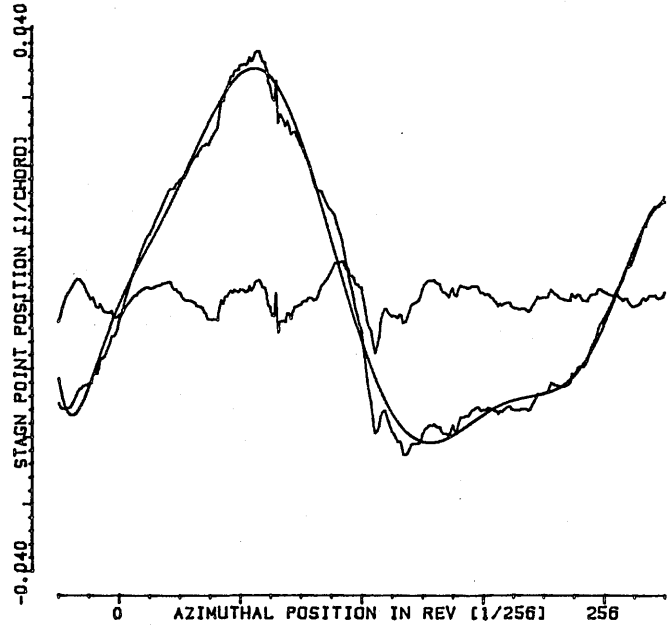

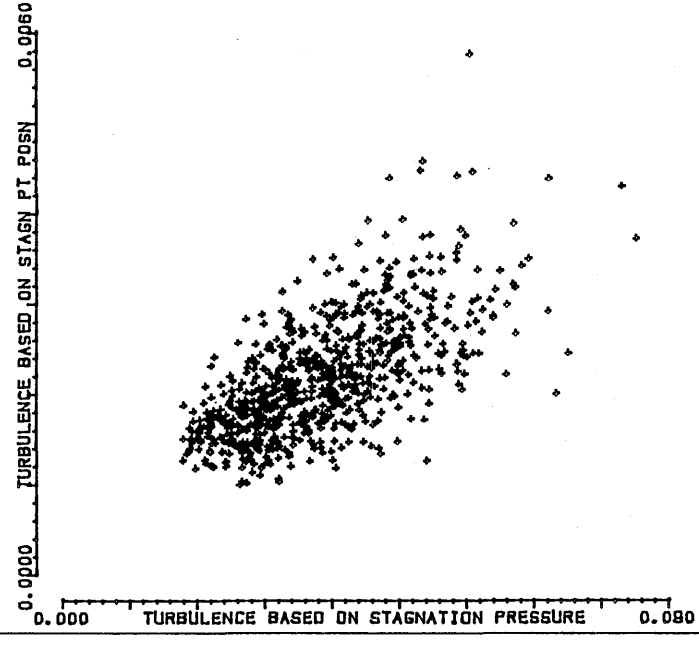

CIT

UNSTEADY AERODYNAMICS OF A VAWT

FIGURE 25

IN ROTOR TURBULENCE MEASURES BASED ON STAGNATION PRESSURE AND STAGNATION POINT POSITION FOR REV 200.2 AND FOR ALL 0 DEG BLADE LEANOUT DATA. RMS PRESSURE TURBULENCE FOR THIS REVOLUTION 0.039 AND RMS POSITION TURBULENCE 2.00E-3

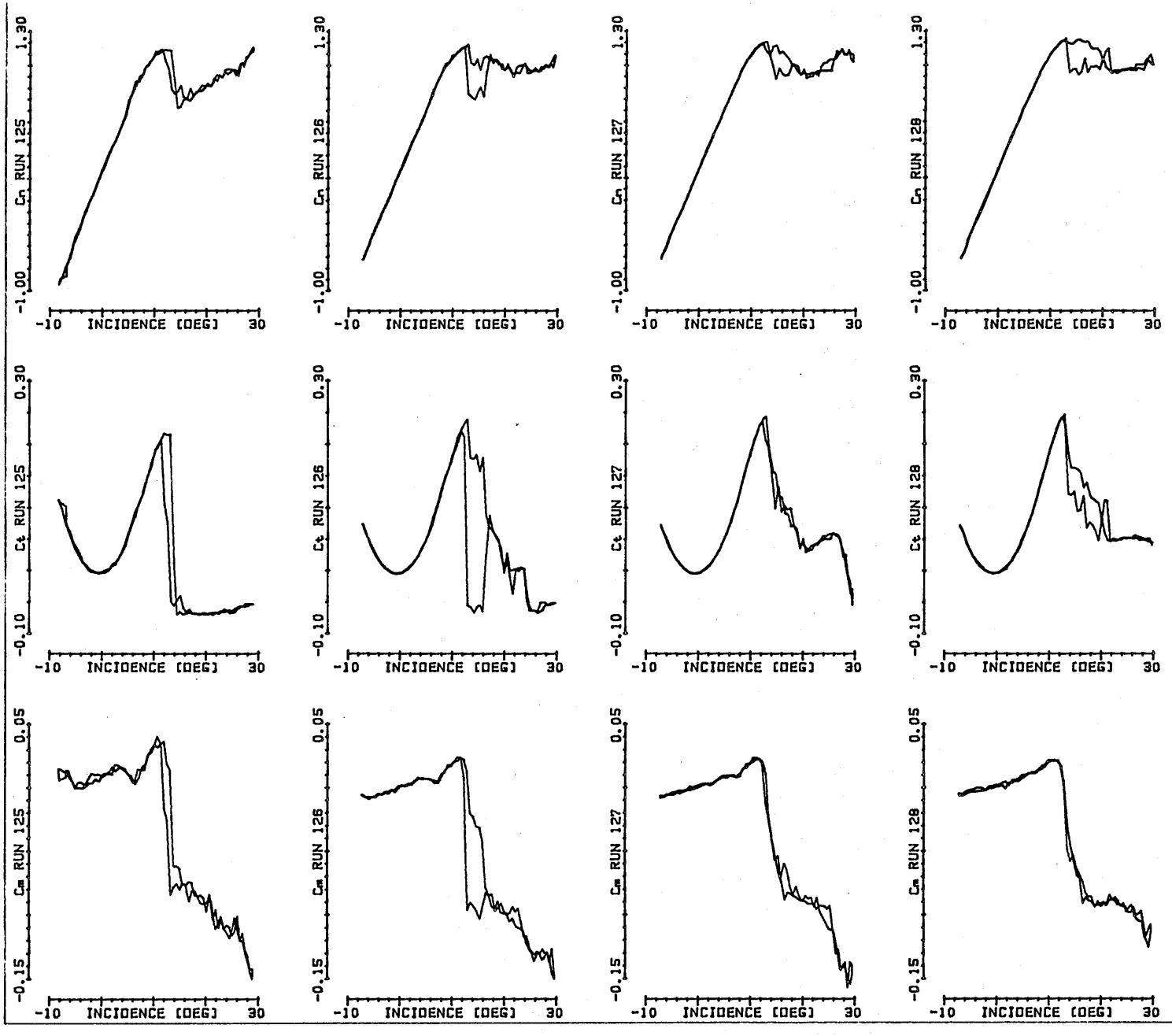

CIT

UNSTEADY AERODYNAMICS OF A VAWT

FIGURE 26

NORMAL AND TANGENTIAL FORCE AND PITCHING MOMENT COEFFS BASED ON STAGNATION PRESSURE FOR FOUR STATIC RUNS OVER A RANGE OF REYNOLDS NUMBER:

RUN:	125	126	127	128
Re:	0.32	0.57	0.76	0.99

MILLION

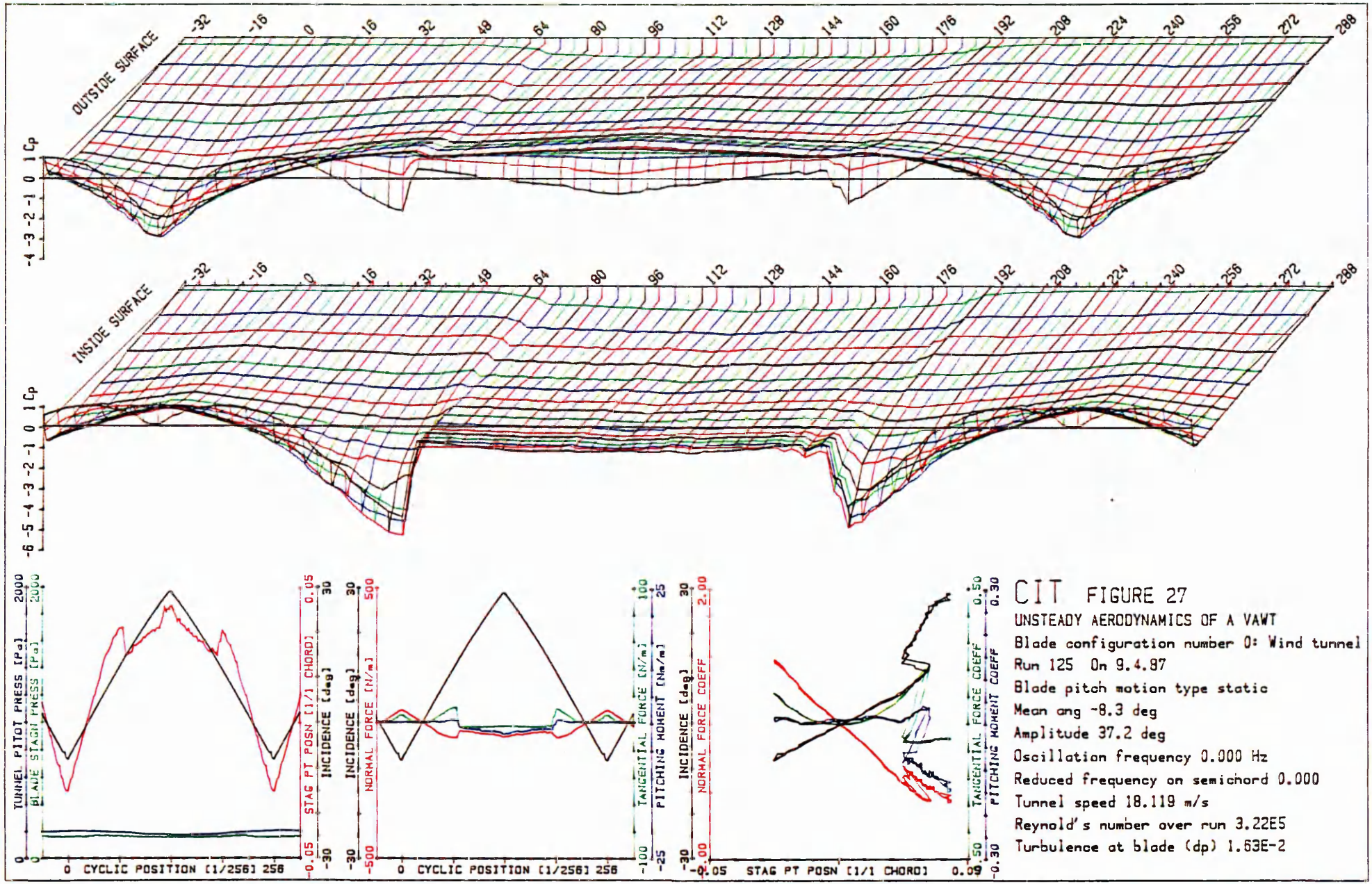

CIT FIGURE 27

UNSTEADY AERODYNAMICS OF A VAWT

Blade configuration number 0: Wind tunnel

Run 125 On 9.4.87

Blade pitch motion type static

Mean ang -8.3 deg

Amplitude 37.2 deg

Oscillation frequency 0.000 Hz

Reduced frequency on semichord 0.000

Tunnel speed 18.119 m/s

Reynold's number over run 3.22E5

Turbulence at blade (dp) 1.63E-2

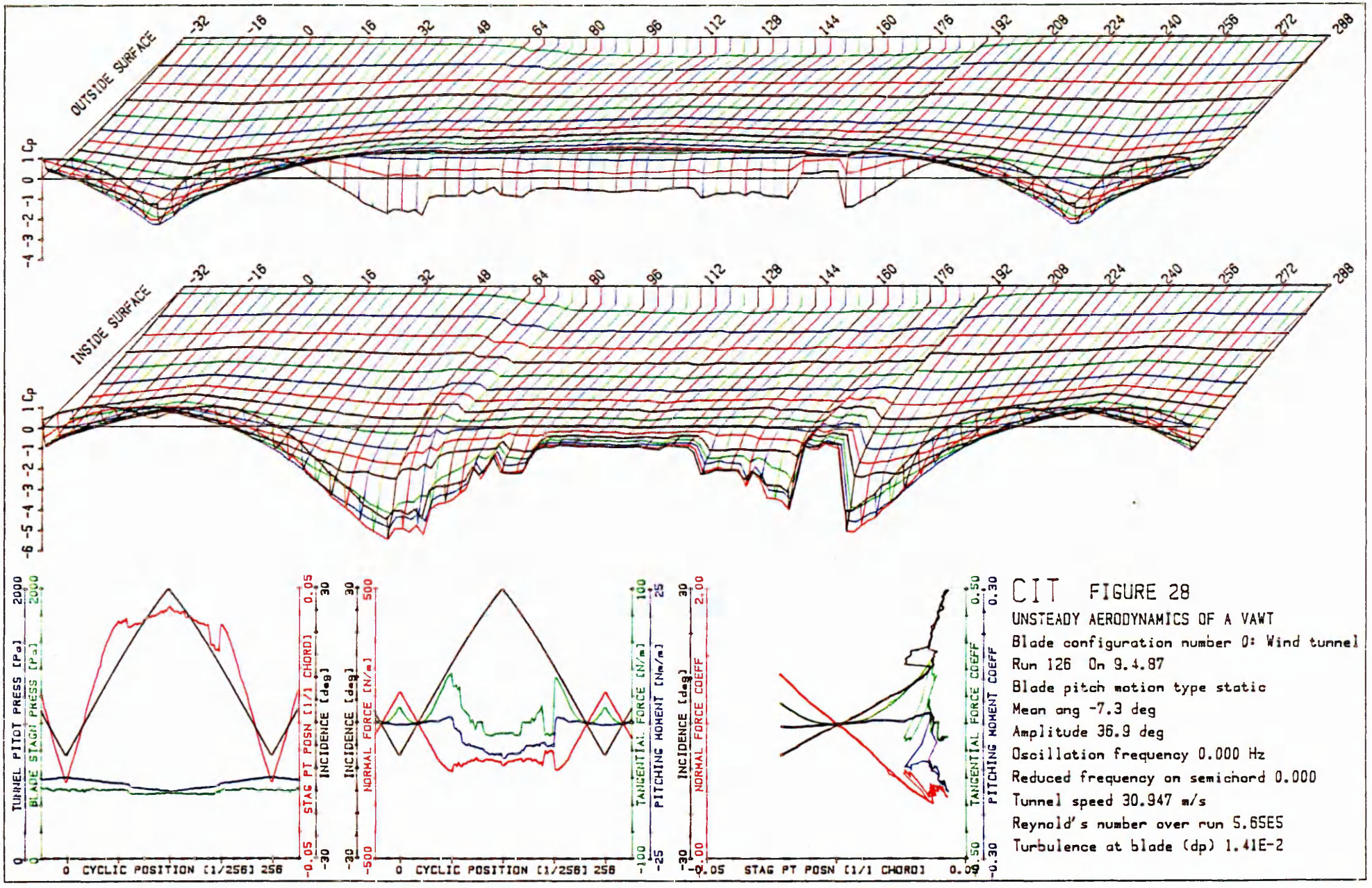

CIT FIGURE 28

UNSTEADY AERODYNAMICS OF A VAWT

Blade configuration number 0: Wind tunnel

Run 126 On 9.4.87

Blade pitch motion type static

Mean ang -7.3 deg

Amplitude 36.9 deg

Oscillation frequency 0.000 Hz

Reduced frequency on semichord 0.000

Tunnel speed 30.947 m/s

Reynold's number over run 5.65E5

Turbulence at blade (dp) 1.41E-2

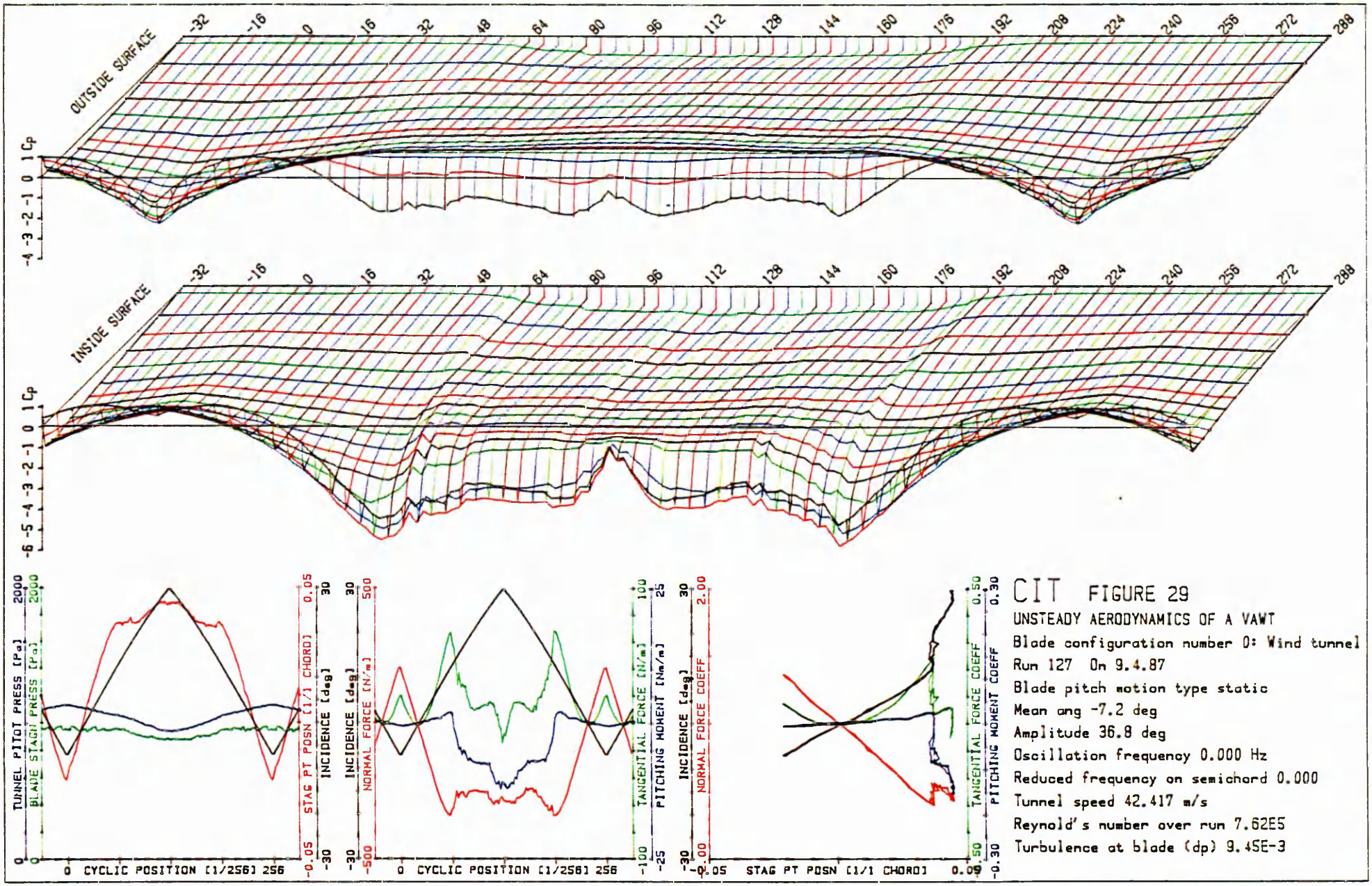

CIT FIGURE 29

UNSTEADY AERODYNAMICS OF A VAWT

Blade configuration number 0: Wind tunnel

Run 127 On 9.4.87

Blade pitch motion type static

Mean ang -7.2 deg

Amplitude 36.8 deg

Oscillation frequency 0.000 Hz

Reduced frequency on semichord 0.000

Tunnel speed 42.417 m/s

Reynold's number over run 7.62E5

Turbulence at blade (dp) 9.45E-3

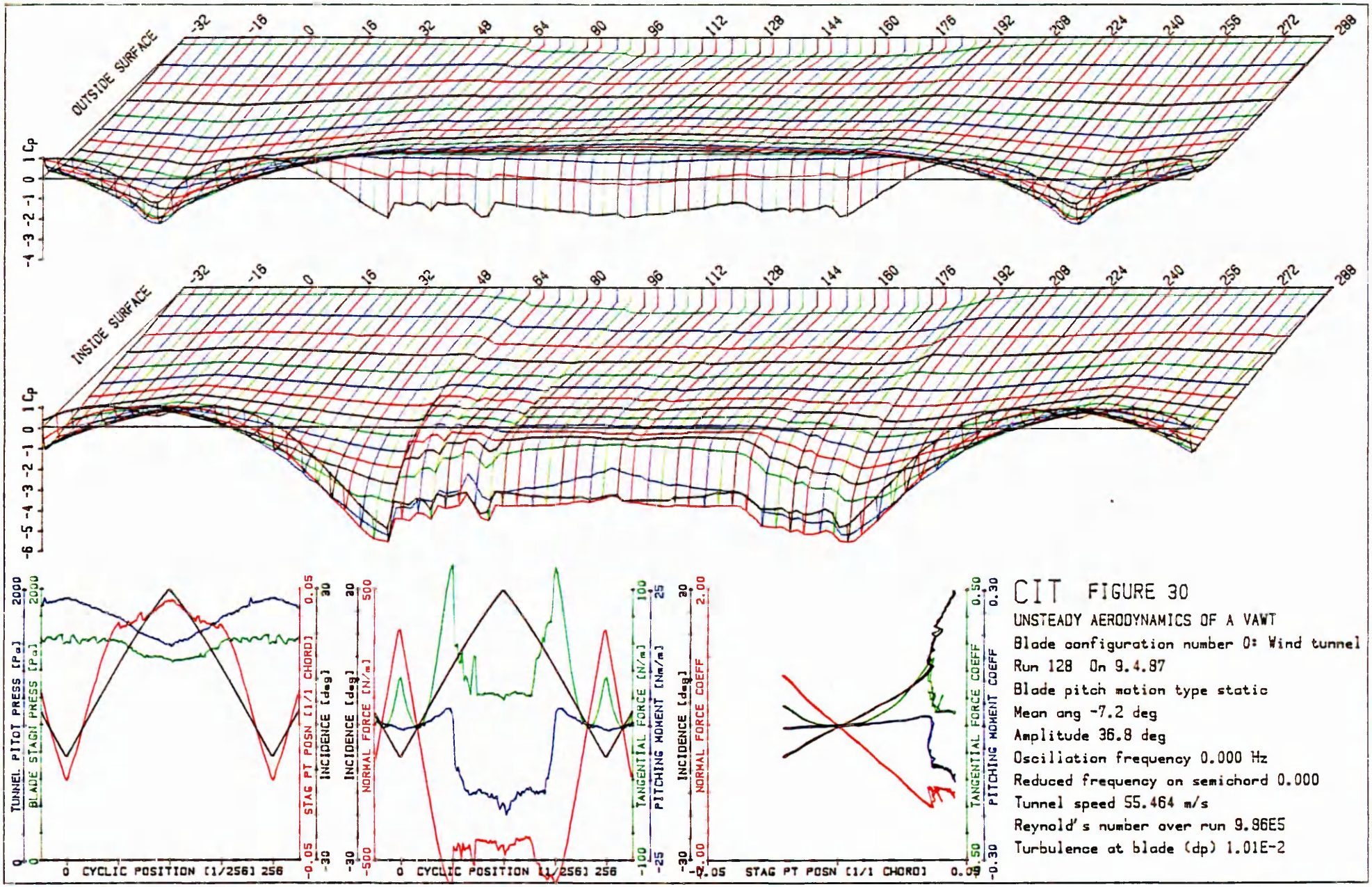

CIT FIGURE 30

UNSTEADY AERODYNAMICS OF A VAWT

Blade configuration number 0: Wind tunnel

Run 128 On 9.4.87

Blade pitch motion type static

Mean ang -7.2 deg

Amplitude 36.8 deg

Oscillation frequency 0.000 Hz

Reduced frequency on semichord 0.000

Tunnel speed 55.464 m/s

Reynold's number over run 9.86E5

Turbulence at blade (dp) 1.01E-2

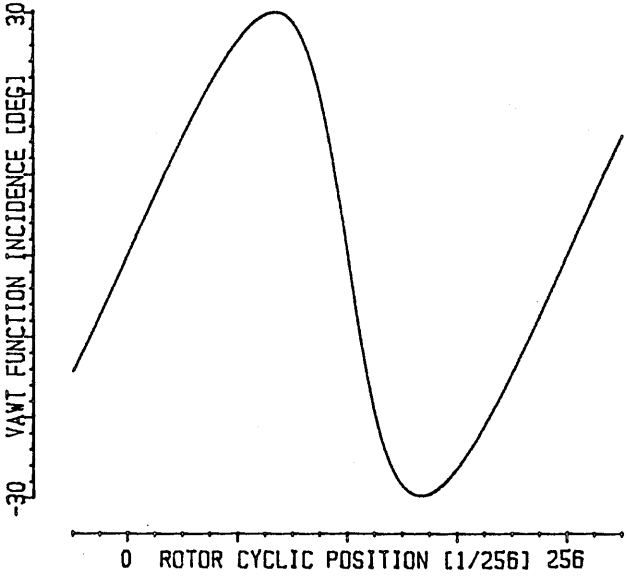

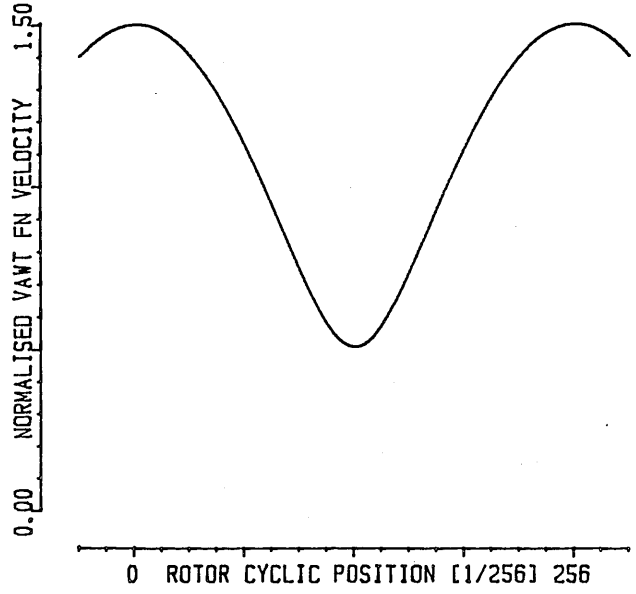

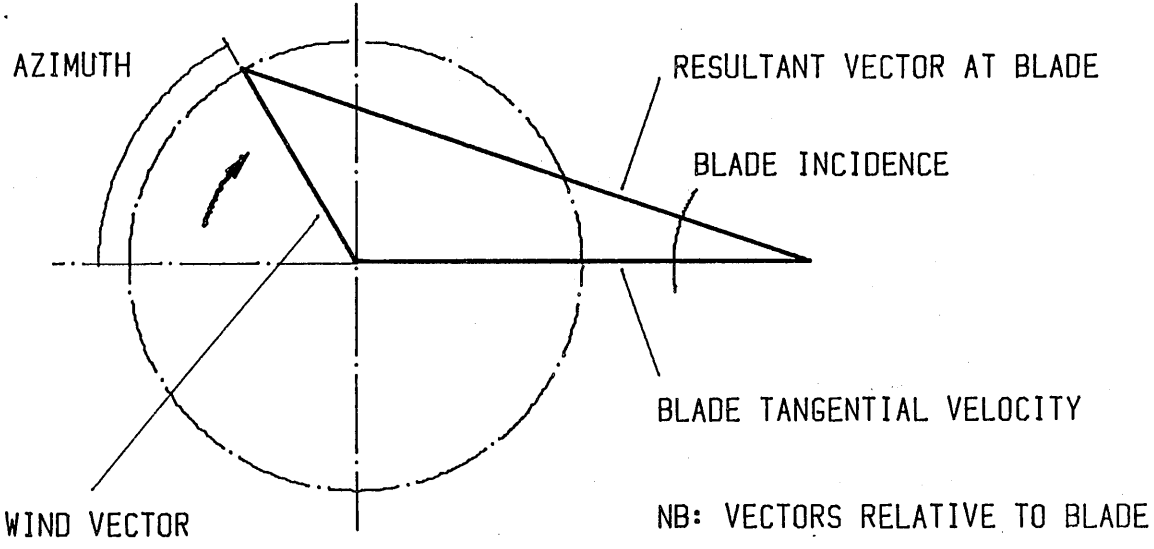

CIT

UNSTEADY AERODYNAMICS OF A VAWT

FIGURE 31

GRAPHS OF VAWT FUNCTION INCIDENCE AND BLADE AIR SPEED NORMALISED ON BLADE TANGENTIAL SPEED FOR A BLADE SPEED RATIO OF 2.0

BOTTOM FIGURE SHOWS TWO VECTORS USED TO GENERATE VAWT FUNCTION.

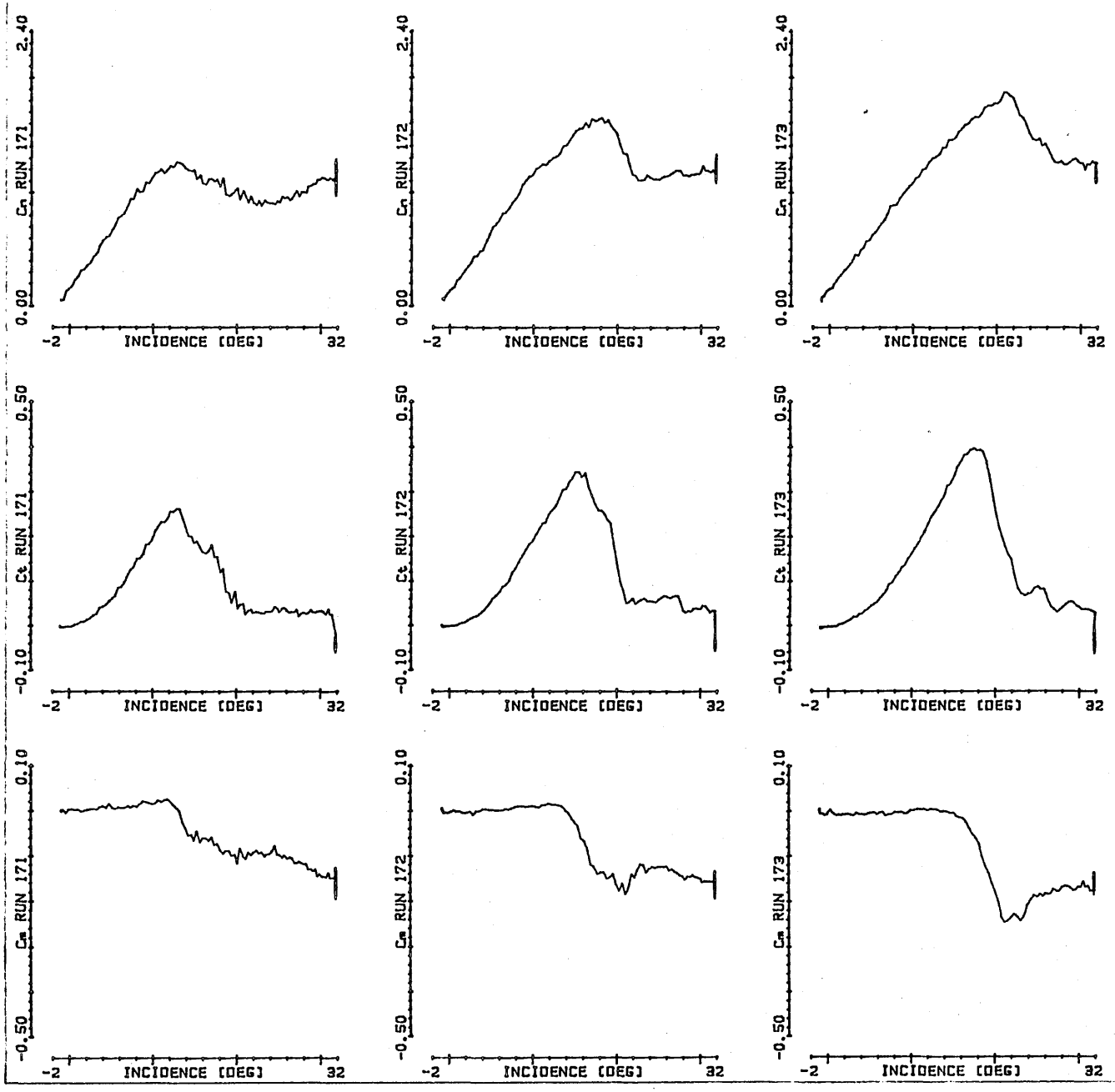

CIT

UNSTEADY AERODYNAMICS OF A VAWT

FIGURE 32

NORMAL AND TANGENTIAL FORCE AND PITCHING MOMENT COEFFS BASED ON STAGNATION PRESSURE FOR THREE RAMP RUNS OVER A RANGE OF REDUCED PITCH RATE

RUN:	171	172	173
alpha^:	0.002	0.011	0.021

NOMINAL REYNOLDS NUMBER 0.75E6

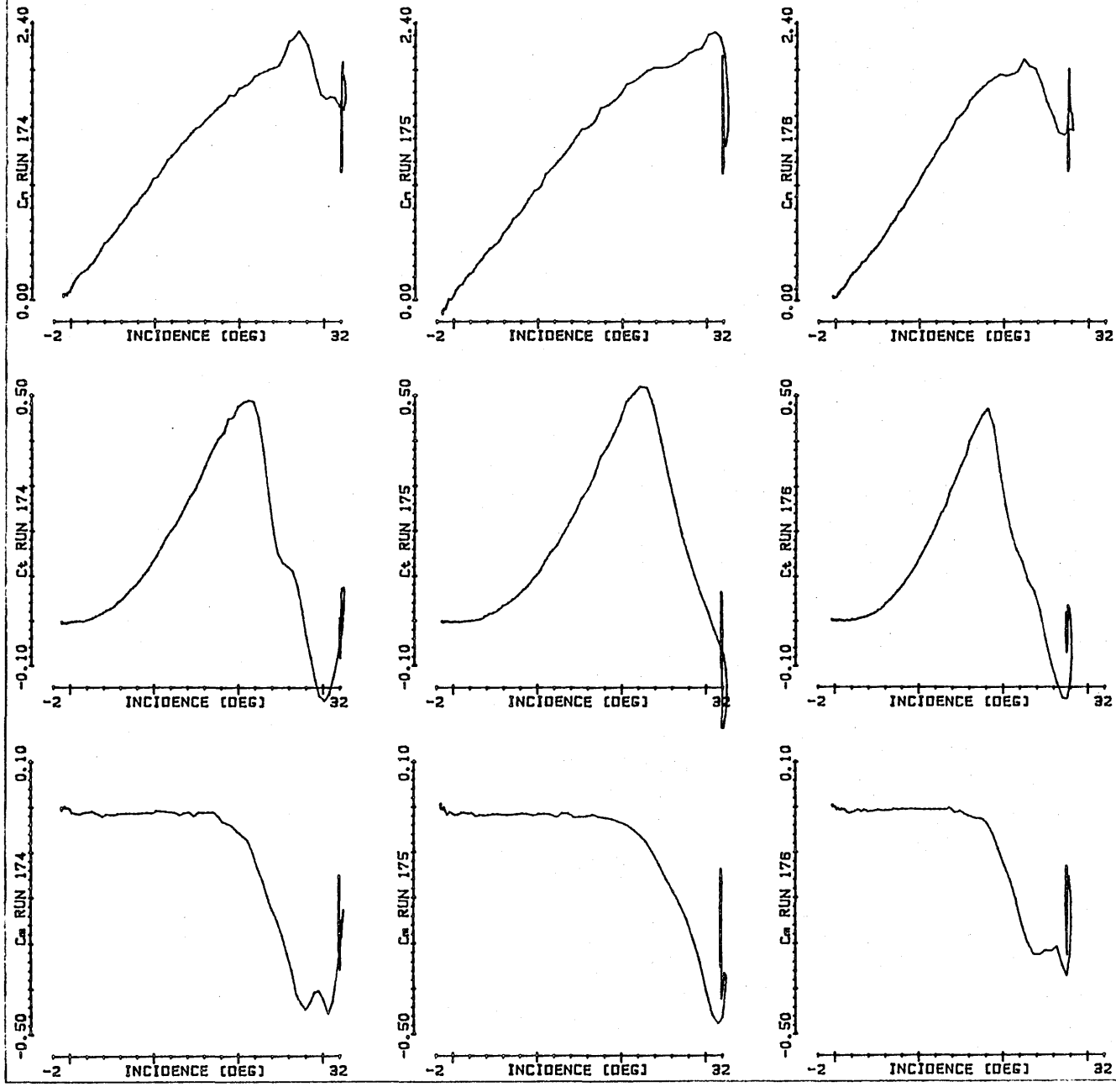

CIT

UNSTEADY AERODYNAMICS OF A VAWT

FIGURE 33

NORMAL AND TANGENTIAL FORCE AND PITCHING MOMENT COEFFS BASED ON STAGNATION PRESSURE FOR THREE RAMP RUNS OVER A RANGE OF REDUCED PITCH RATE

RUN:	174	175	176
alpha^:	0.038	0.048	0.039

[rads/s*c/vel]

NOMINAL REYNOLDS NUMBER 0.75E6

EXCEPT RUN 176 @ Re=0.92E6

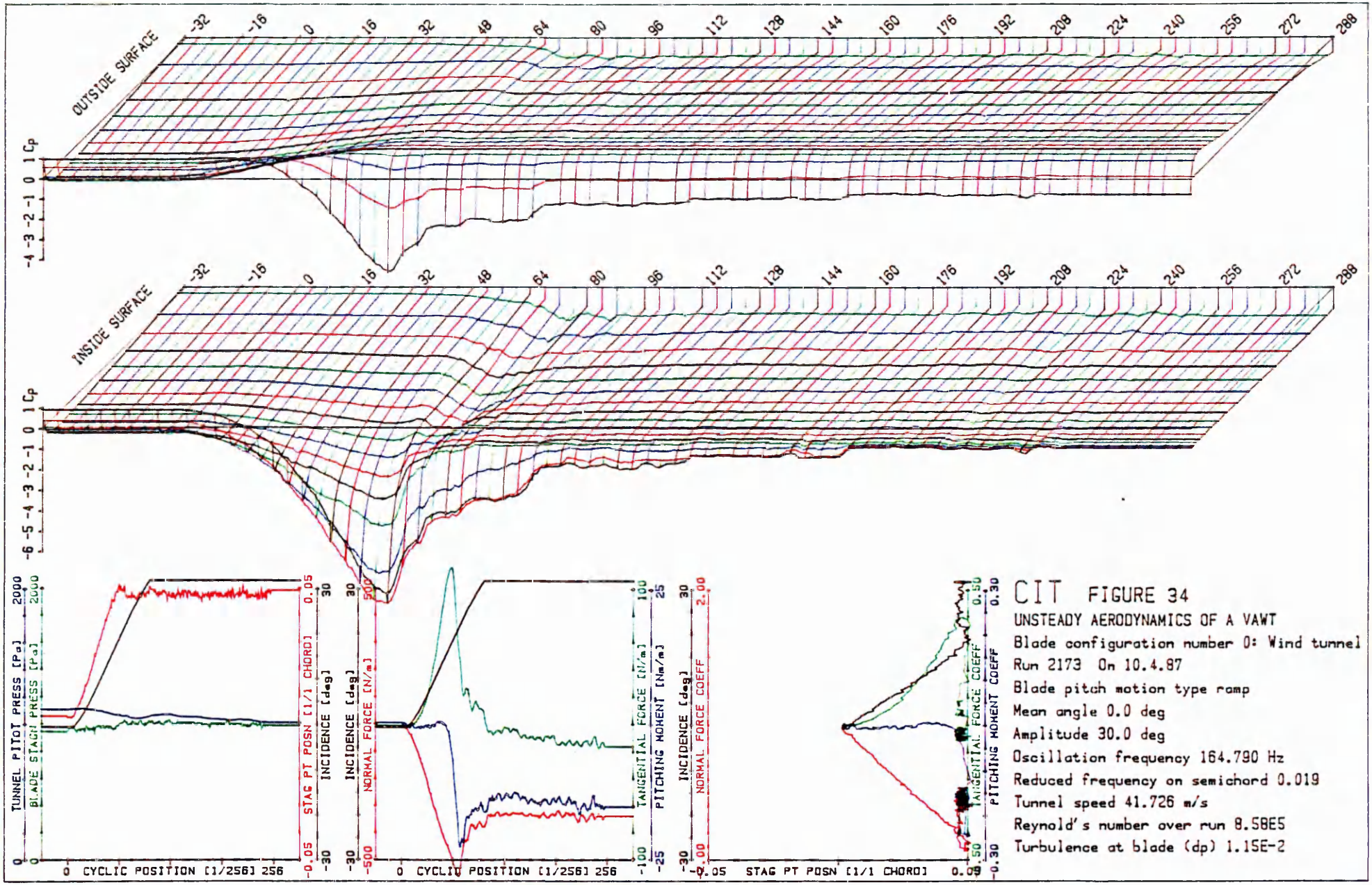

CIT FIGURE 34

UNSTEADY AERODYNAMICS OF A VAWT

Blade configuration number 0: Wind tunnel

Run 2173 On 10.4.87

Blade pitch motion type ramp

Mean angle 0.0 deg

Amplitude 30.0 deg

Oscillation frequency 164.790 Hz

Reduced frequency on semichord 0.019

Tunnel speed 41.726 m/s

Reynold's number over run 8.58E5

Turbulence at blade (dp) 1.15E-2

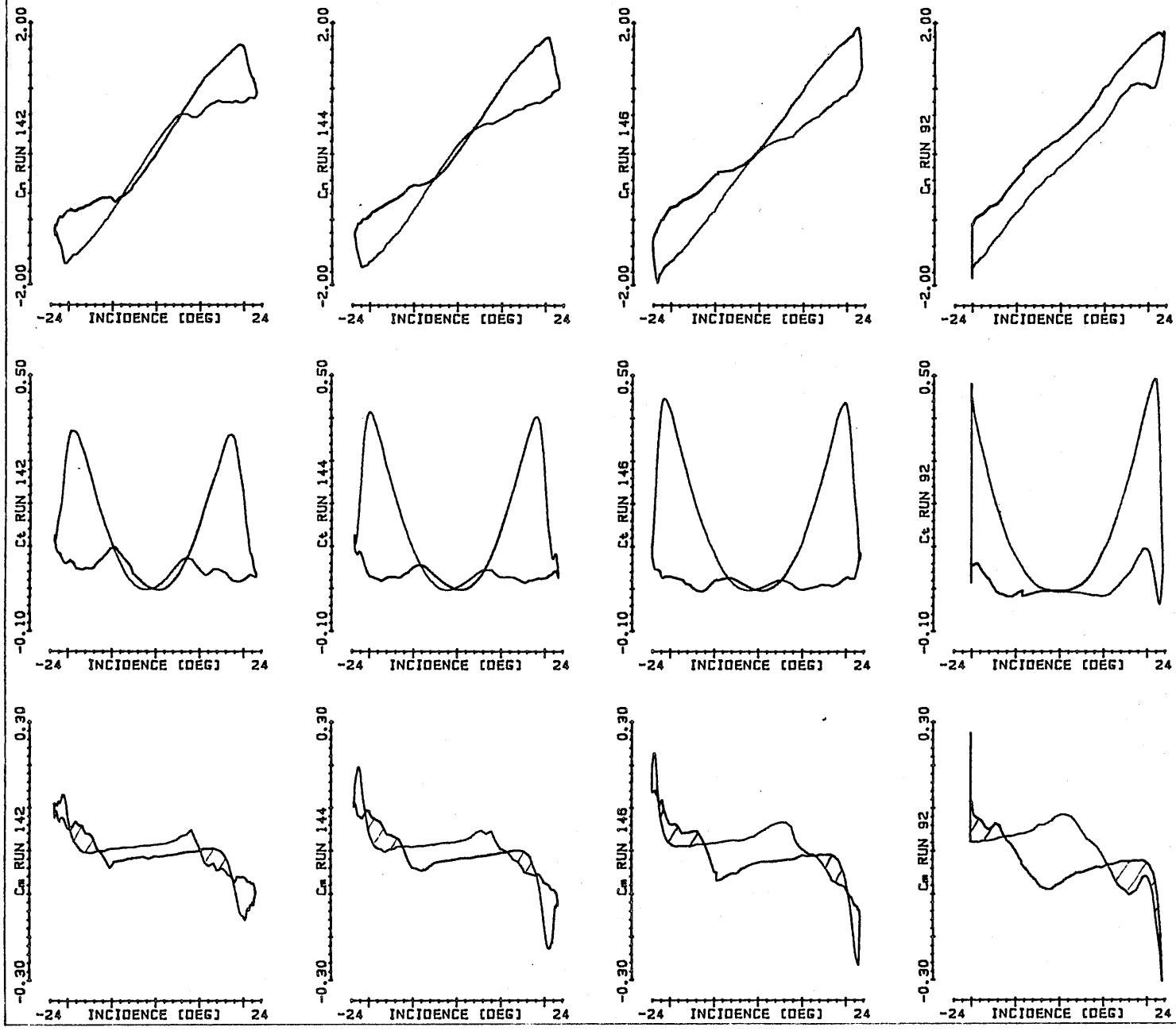

CIT

UNSTEADY AERODYNAMICS OF A VAWT

FIGURE 35

NORMAL AND TANGENTIAL FORCE AND PITCHING MOMENT COEFFS BASED ON STAGNATION PRESSURE FOR FOUR SINE RUNS OVER A RANGE OF REDUCED FREQUENCY:

RUN:	142	144	146	92
k:	0.023	0.034	0.049	0.079

NOMINAL REYNOLDS NUMBER 0.75E6

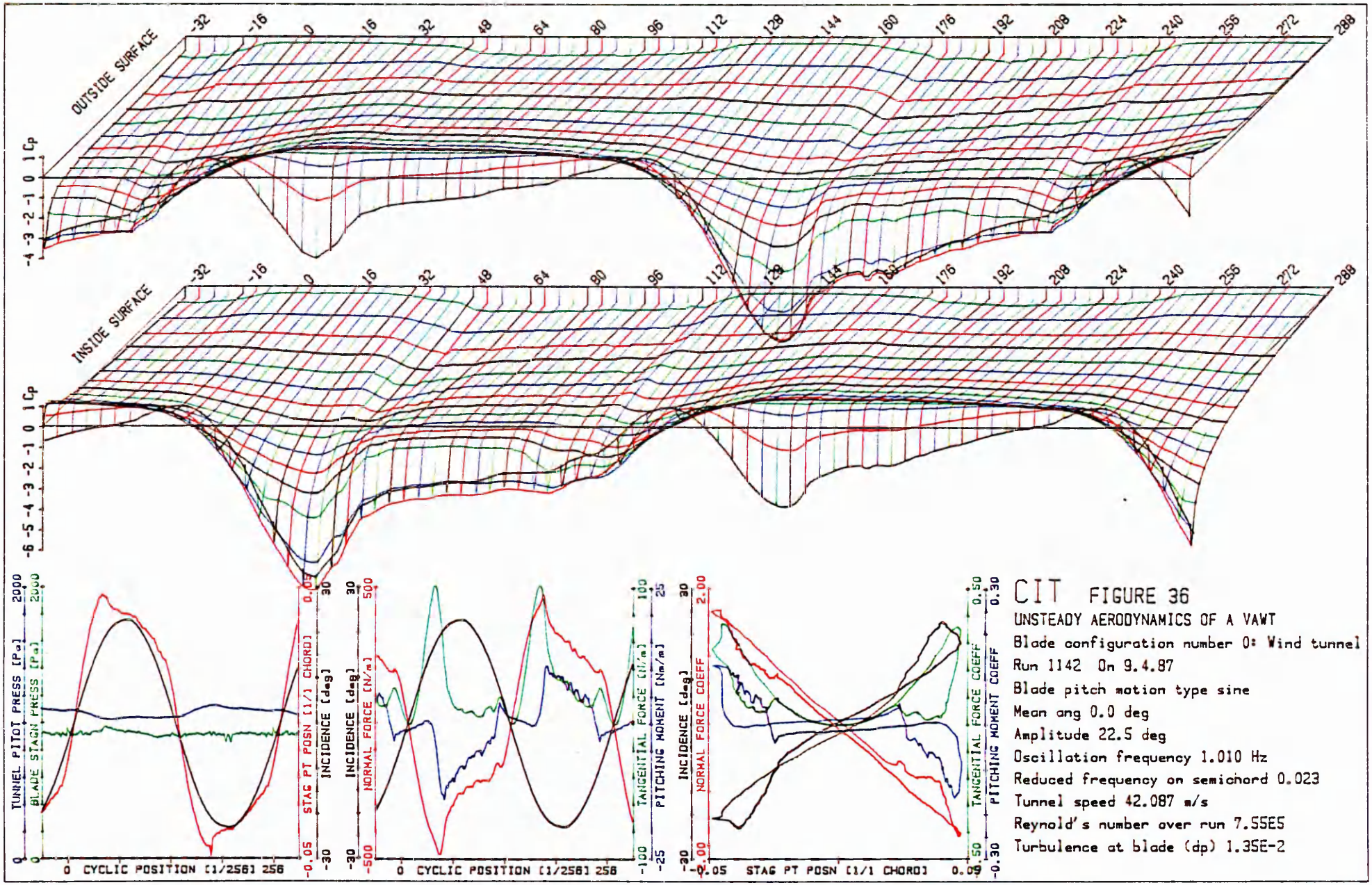

CIT FIGURE 36

UNSTEADY AERODYNAMICS OF A VAWT

Blade configuration number 0: Wind tunnel

Run 1142 On 9.4.87

Blade pitch motion type sine

Mean ang 0.0 deg

Amplitude 22.5 deg

Oscillation frequency 1.010 Hz

Reduced frequency on semichord 0.023

Tunnel speed 42.087 m/s

Reynold's number over run 7.55E5

Turbulence at blade (dp) 1.35E-2

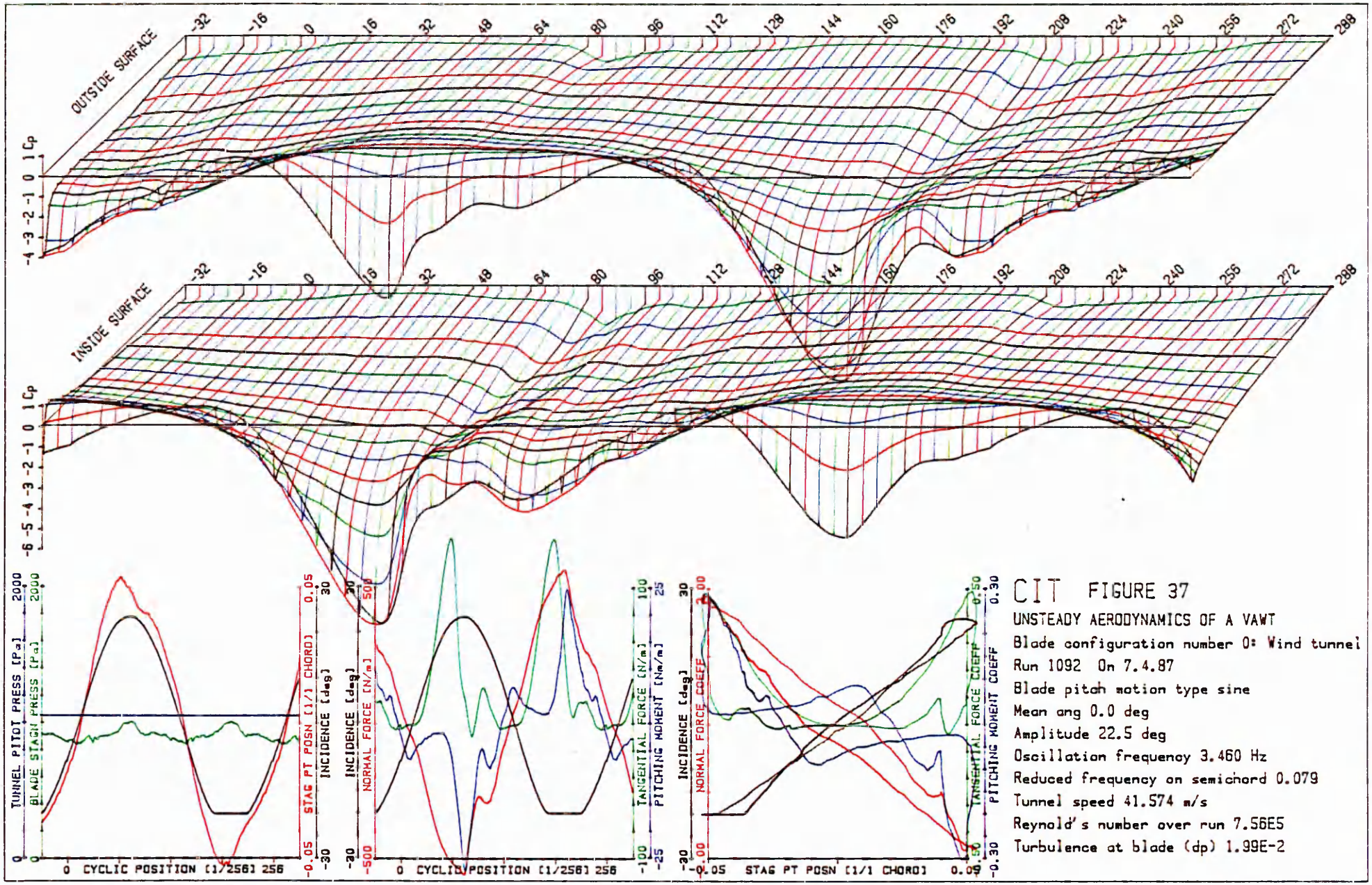

CIT FIGURE 37

UNSTEADY AERODYNAMICS OF A VAWT

Blade configuration number 0: Wind tunnel

Run 1092 On 7.4.87

Blade pitch motion type sine

Mean ang 0.0 deg

Amplitude 22.5 deg

Oscillation frequency 3.460 Hz

Reduced frequency on semichord 0.079

Tunnel speed 41.574 m/s

Reynold's number over run 7.56E5

Turbulence at blade (dp) 1.99E-2

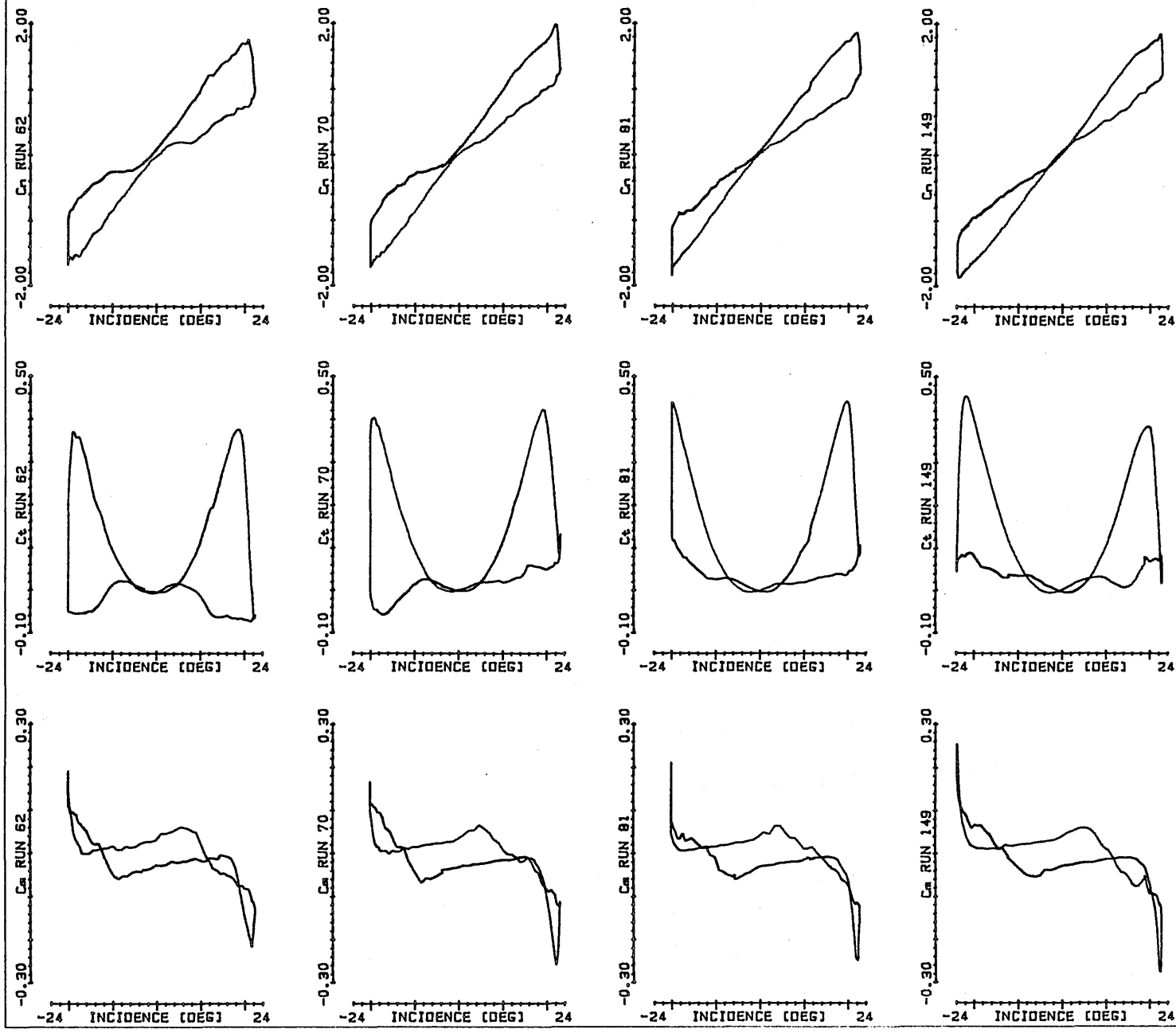

CIT

UNSTEADY AERODYNAMICS OF A VAWT

FIGURE 38

NORMAL AND TANGENTIAL FORCE AND PITCHING MOMENT COEFFS BASED ON STAGNATION PRESSURE FOR FOUR SINE RUNS OVER A RANGE OF REYNOLDS NUMBER:

RUN:	62	70	81	149
Re:	0.40	0.58	0.76	0.96 MILLION

NOMINAL REDUCED FREQUENCY 0.05

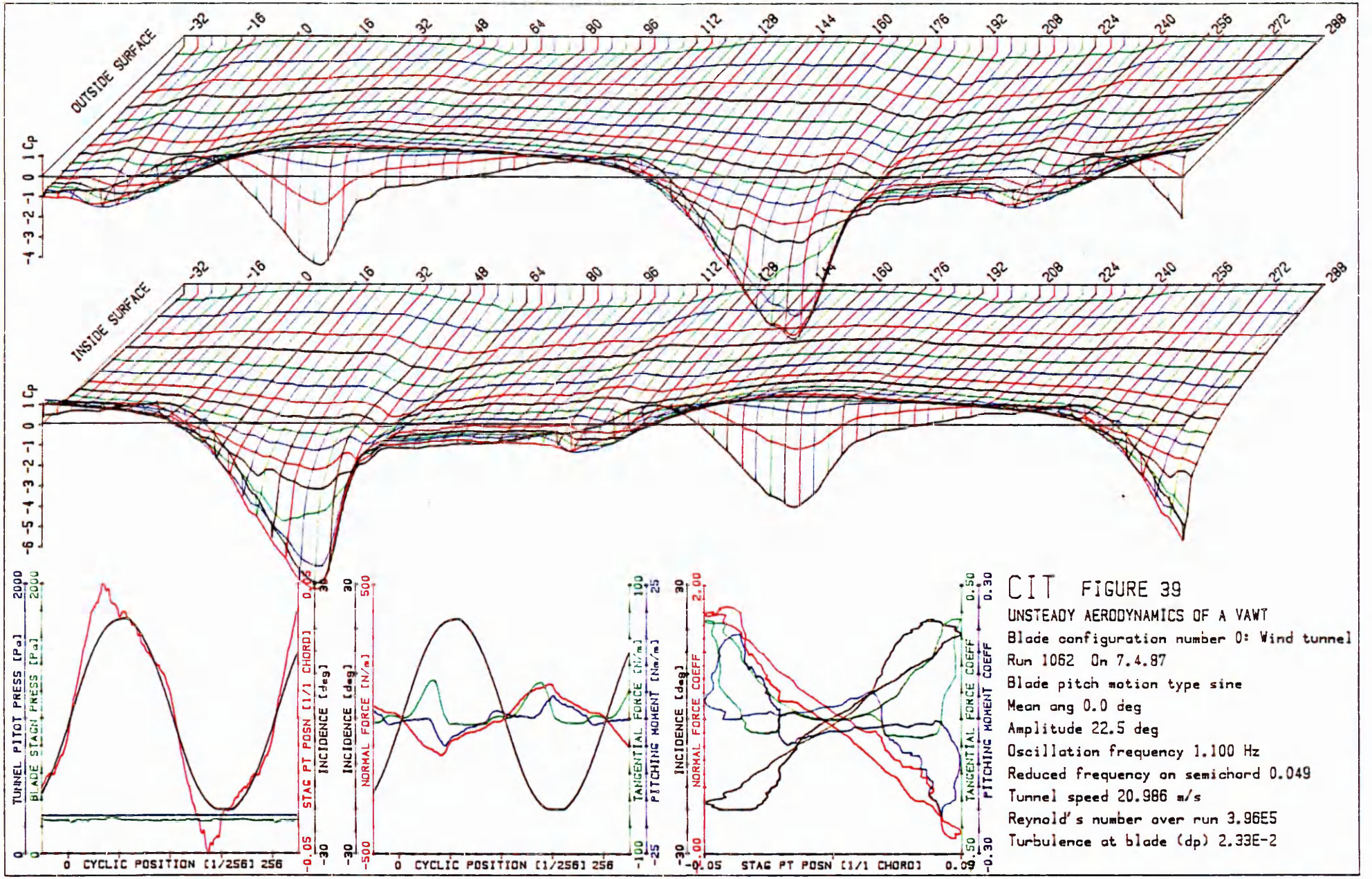

CIT FIGURE 39

UNSTEADY AERODYNAMICS OF A VAWT

Blade configuration number 0: Wind tunnel

Run 1062 On 7.4.87

Blade pitch motion type sine

Mean ang 0.0 deg

Amplitude 22.5 deg

Oscillation frequency 1.100 Hz

Reduced frequency on semichord 0.049

Tunnel speed 20.986 m/s

Reynold's number over run 3.96E5

Turbulence at blade (dp) 2.33E-2

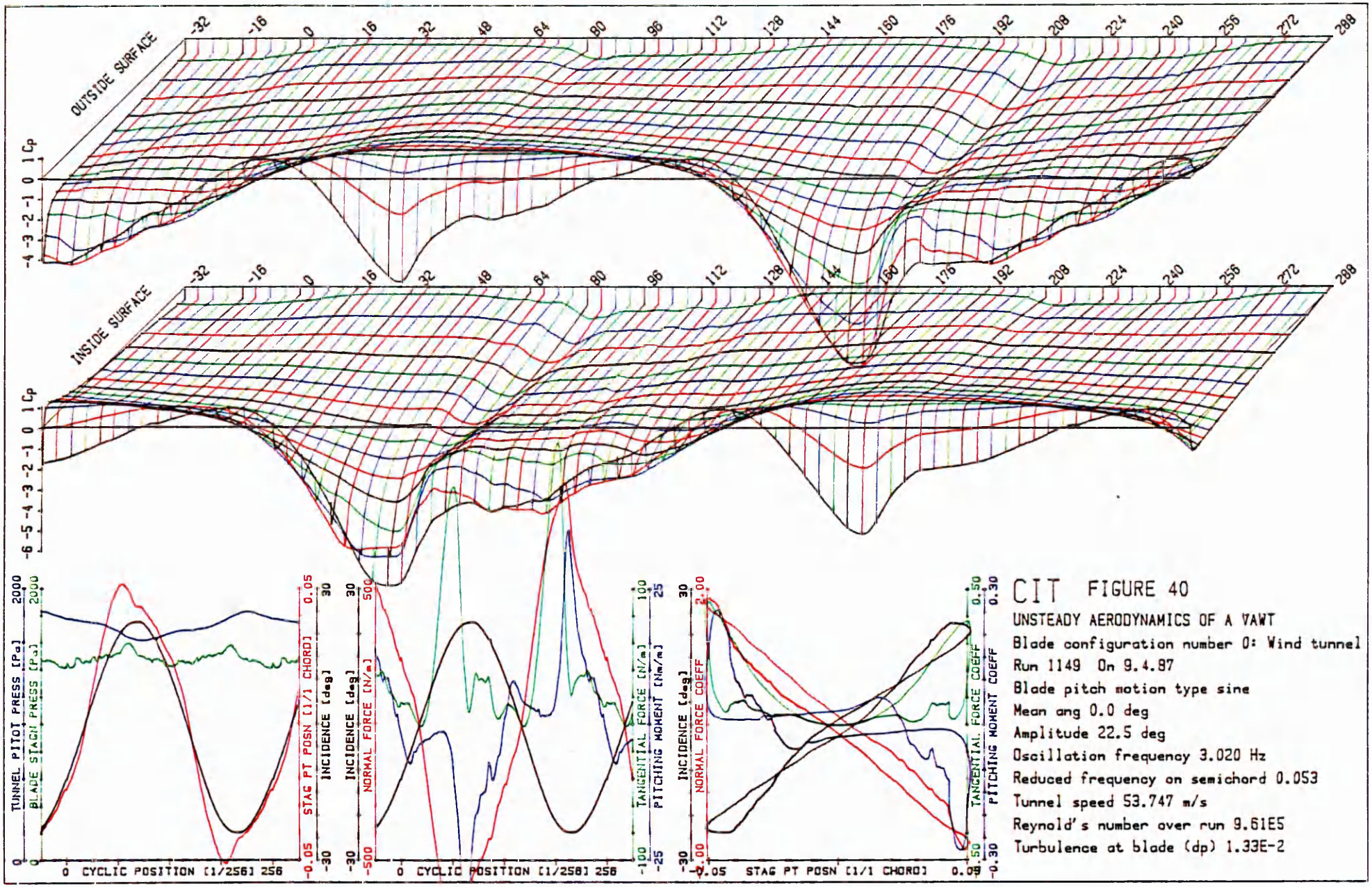

CIT FIGURE 40

UNSTEADY AERODYNAMICS OF A VAWT

Blade configuration number 0: Wind tunnel

Run 1149 On 9.4.87

Blade pitch motion type sine

Mean ang 0.0 deg

Amplitude 22.5 deg

Oscillation frequency 3.020 Hz

Reduced frequency on semichord 0.053

Tunnel speed 53.747 m/s

Reynold's number over run 9.61E5

Turbulence at blade (dp) 1.33E-2

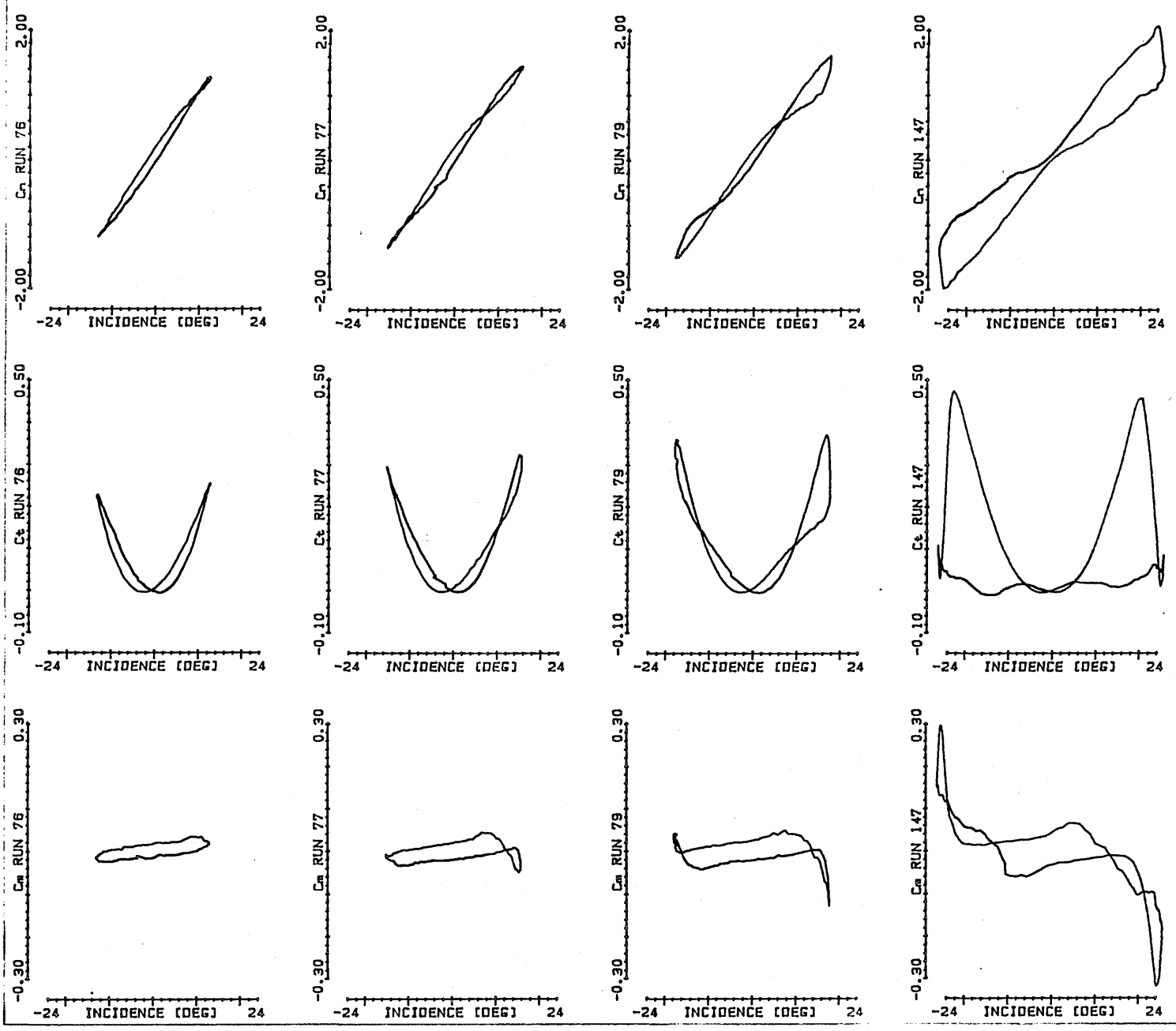

CIT

UNSTEADY AERODYNAMICS OF A VAWT

FIGURE 41

NORMAL AND TANGENTIAL FORCE AND PITCHING MOMENT COEFFS BASED ON STAGNATION PRESSURE FOR FOUR SINE RUNS OVER A RANGE OF MAXIMUM INCIDENCE. NOMINAL REDUCED FREQUENCY FOR ALL RUNS 0.05

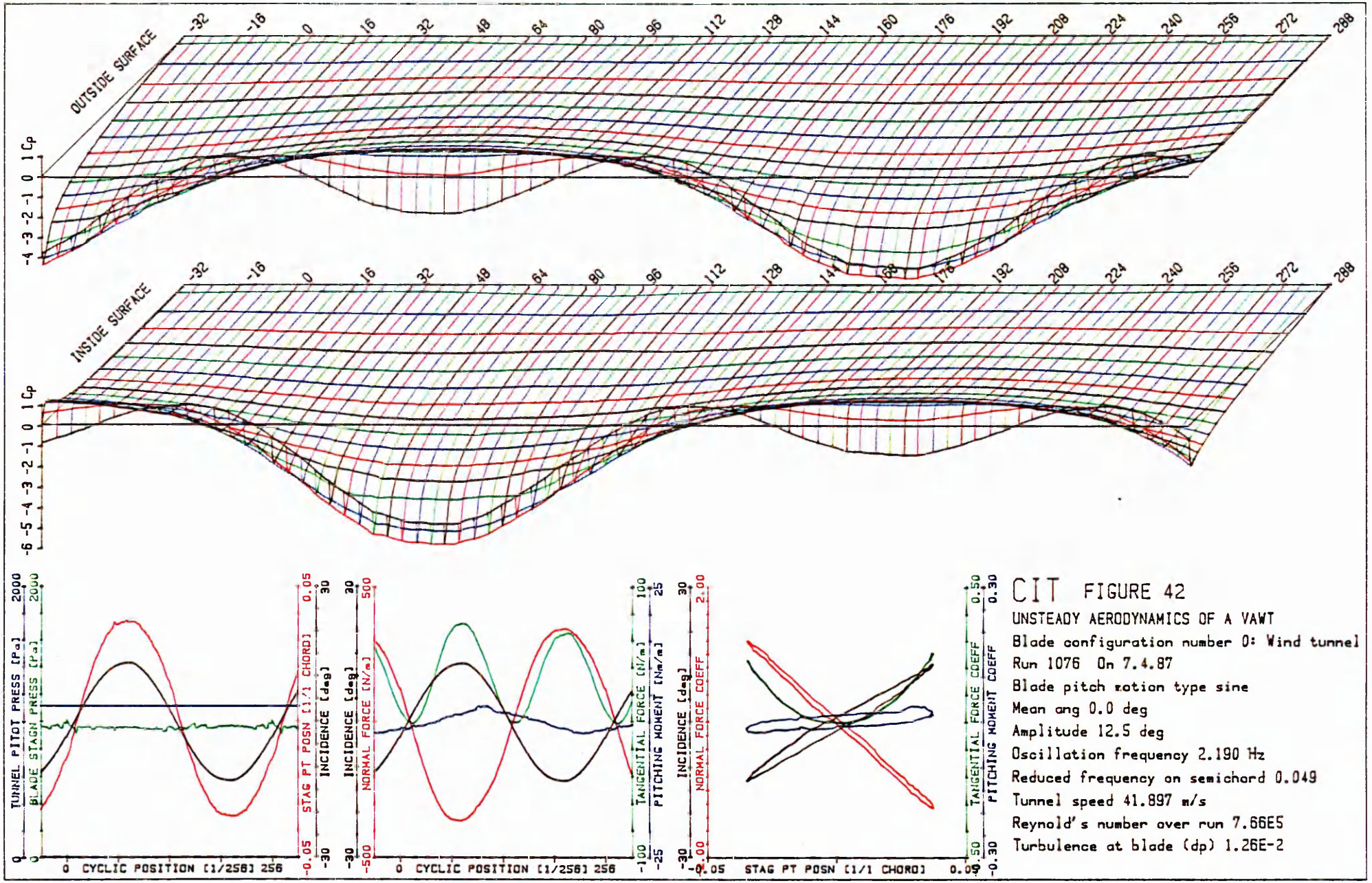

CIT FIGURE 42

UNSTEADY AERODYNAMICS OF A VAWT

Blade configuration number 0: Wind tunnel

Run 1076 On 7.4.87

Blade pitch motion type sine

Mean ang 0.0 deg

Amplitude 12.5 deg

Oscillation frequency 2.190 Hz

Reduced frequency on semichord 0.049

Tunnel speed 41.897 m/s

Reynold's number over run 7.66E5

Turbulence at blade (dp) 1.26E-2

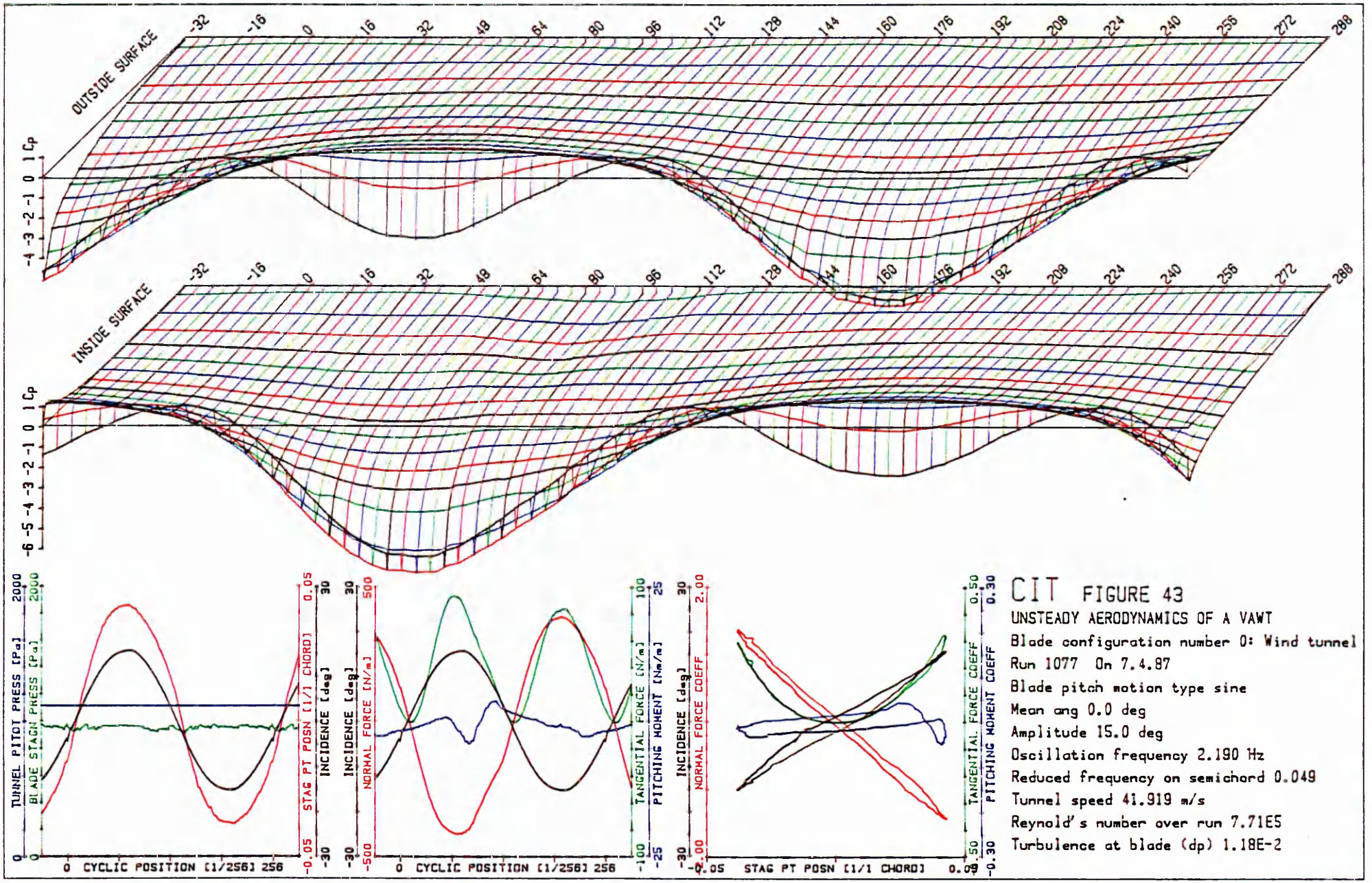

CIT FIGURE 43

UNSTEADY AERODYNAMICS OF A VAWT

Blade configuration number 0: Wind tunnel

Run 1077 On 7.4.87

Blade pitch motion type sine

Mean ang 0.0 deg

Amplitude 15.0 deg

Oscillation frequency 2.190 Hz

Reduced frequency on semichord 0.049

Tunnel speed 41.919 m/s

Reynold's number over run 7.71E5

Turbulence at blade (dp) 1.18E-2

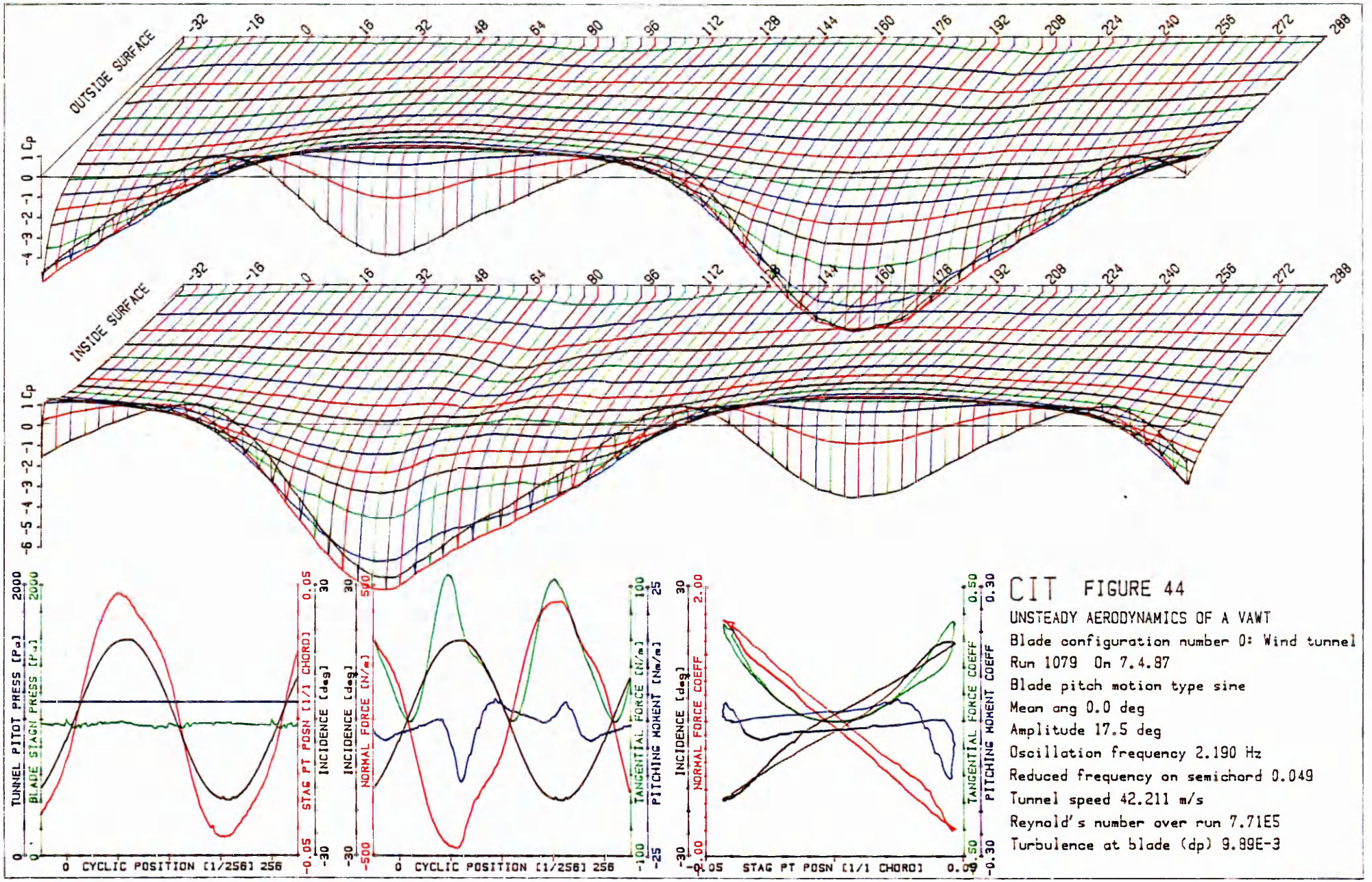

CIT FIGURE 44

UNSTEADY AERODYNAMICS OF A VAWT

Blade configuration number 0: Wind tunnel

Run 1079 On 7.4.87

Blade pitch motion type sine

Mean ang 0.0 deg

Amplitude 17.5 deg

Oscillation frequency 2.190 Hz

Reduced frequency on semichord 0.049

Tunnel speed 42.211 m/s

Reynold's number over run 7.71E5

Turbulence at blade (dp) 9.89E-3

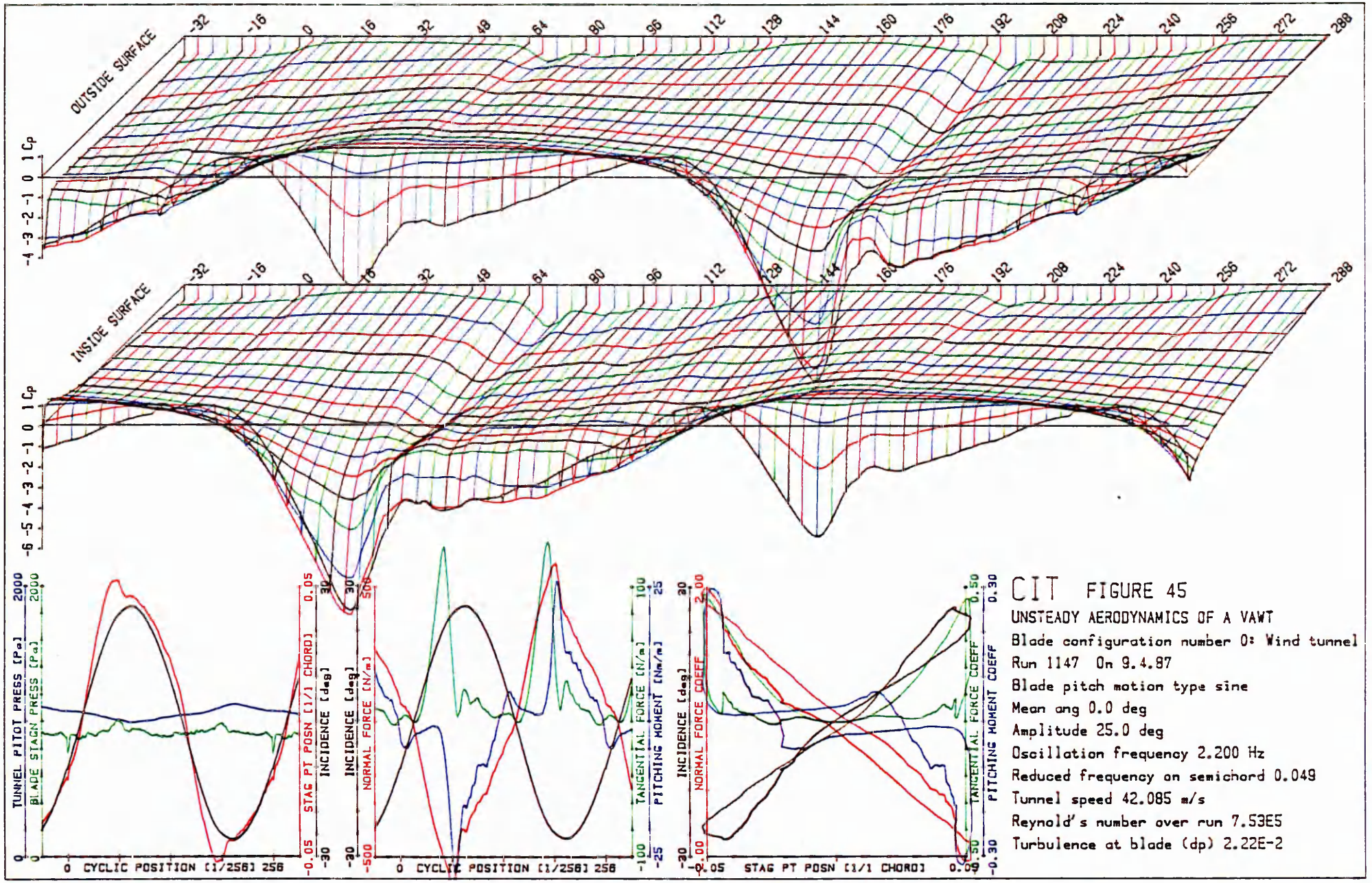

CIT FIGURE 45

UNSTEADY AERODYNAMICS OF A VAWT

Blade configuration number 0: Wind tunnel

Run 1147 On 9.4.87

Blade pitch motion type sine

Mean ang 0.0 deg

Amplitude 25.0 deg

Oscillation frequency 2.200 Hz

Reduced frequency on semichord 0.049

Tunnel speed 42.085 m/s

Reynold's number over run 7.53E5

Turbulence at blade (dp) 2.22E-2

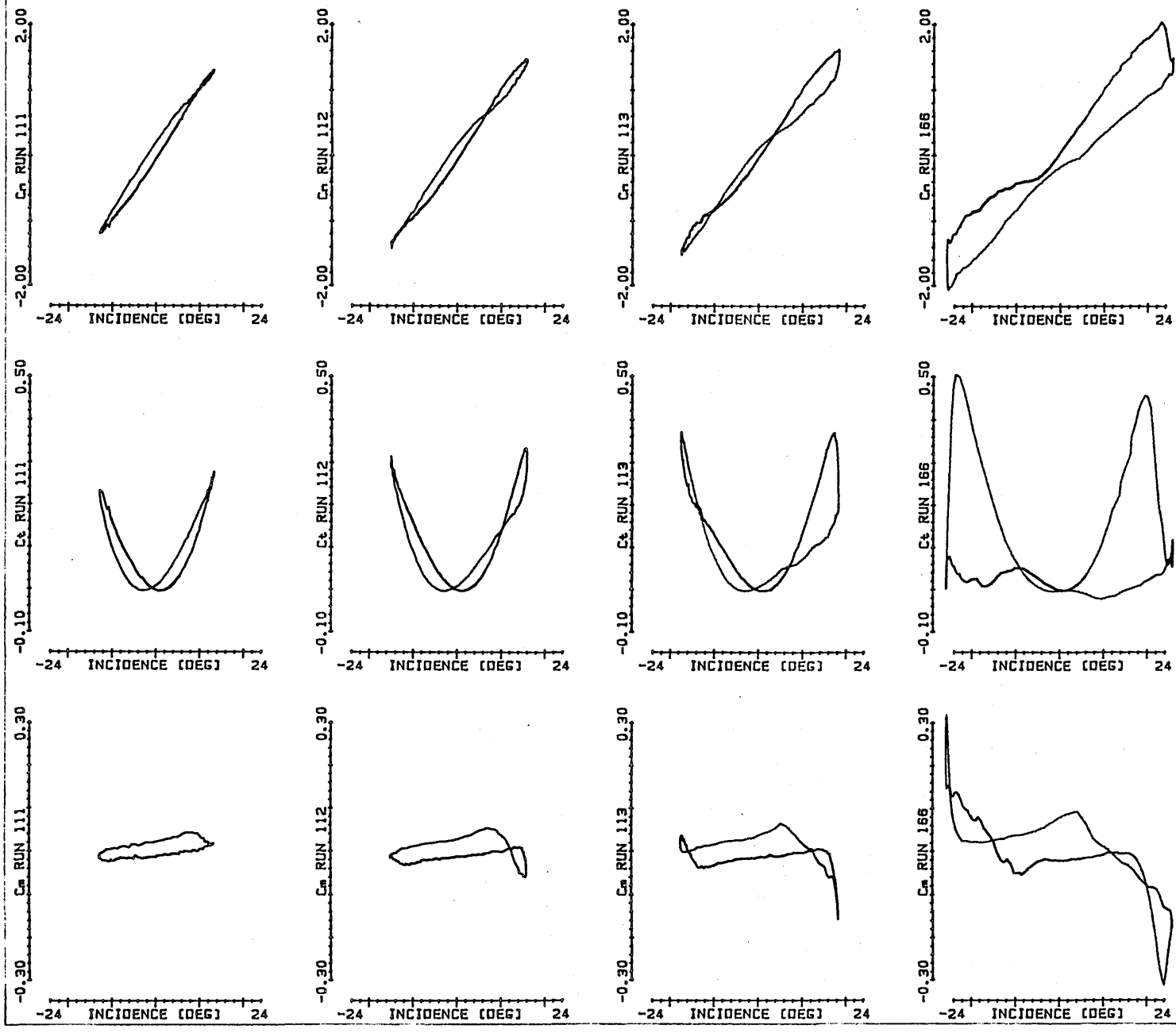

CIT

UNSTEADY AERODYNAMICS OF A VAWT

FIGURE 46

NORMAL AND TANGENTIAL FORCE AND PITCHING MOMENT COEFFS BASED ON STAGNATION PRESSURE FOR FOUR VAWT RUNS OVER A RANGE OF MAXIMUM INCIDENCE. NOMINAL REDUCED FREQUENCY FOR ALL RUNS 0.05 AND NOMINAL REYNOLDS NUMBER 0.75E6

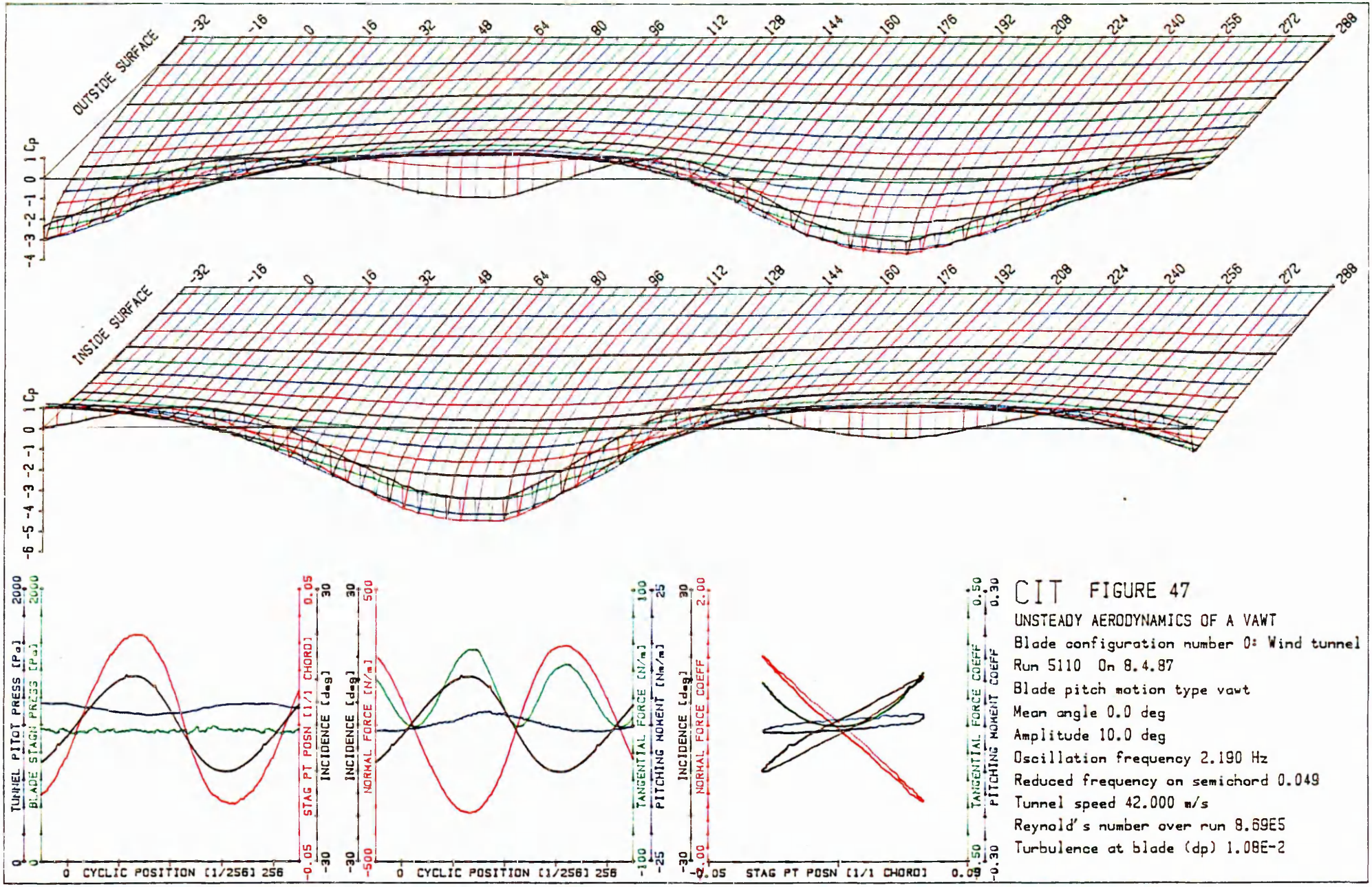

CIT FIGURE 47

UNSTEADY AERODYNAMICS OF A VAWT

Blade configuration number 0: Wind tunnel

Run 5110 On 8.4.87

Blade pitch motion type vawt

Mean angle 0.0 deg

Amplitude 10.0 deg

Oscillation frequency 2.190 Hz

Reduced frequency on semichord 0.049

Tunnel speed 42.000 m/s

Reynold's number over run 8.69E5

Turbulence at blade (dp) 1.08E-2

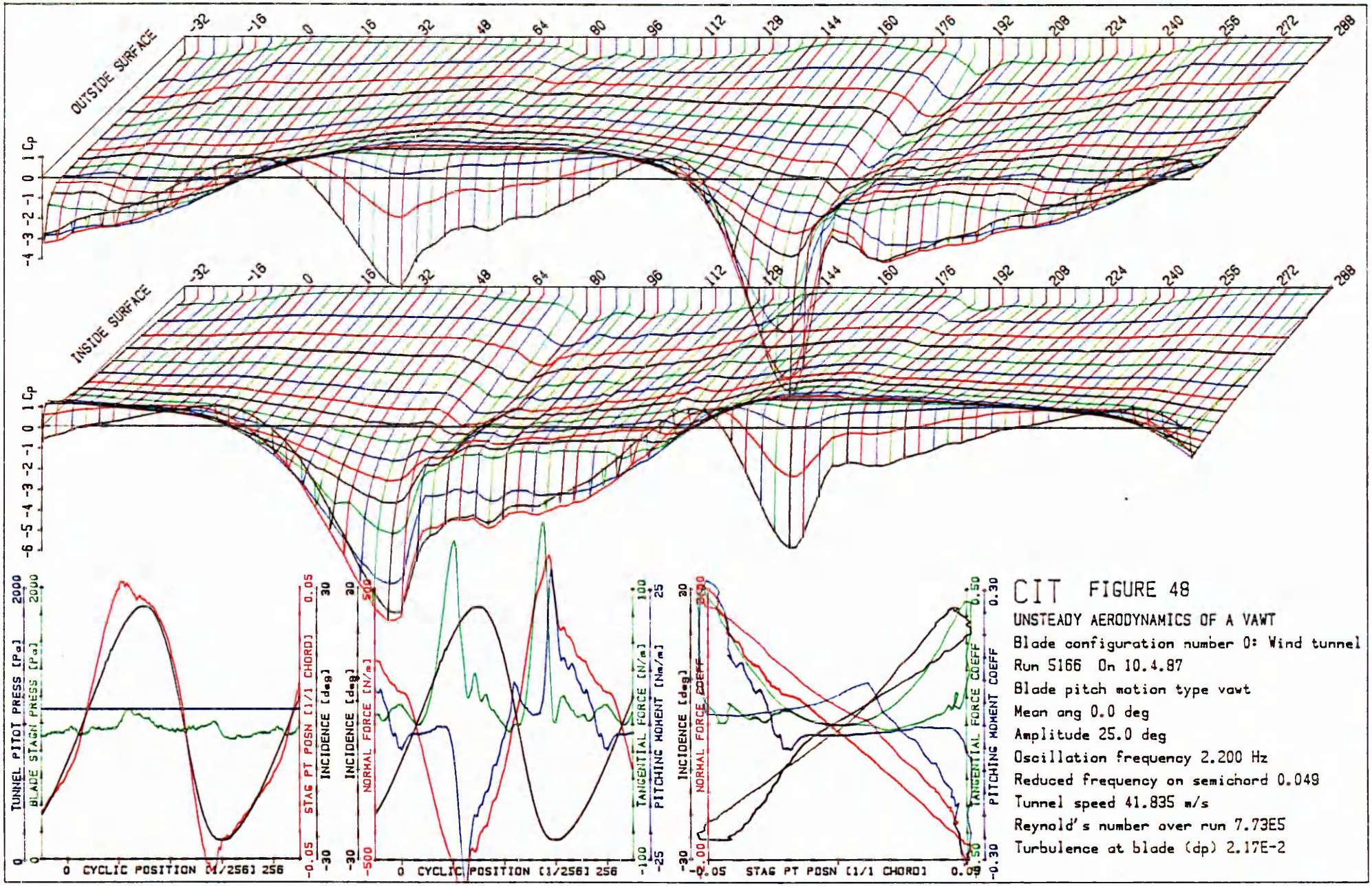

CIT FIGURE 48

UNSTEADY AERODYNAMICS OF A VAWT

Blade configuration number 0: Wind tunnel

Run 5166 On 10.4.87

Blade pitch motion type vawt

Mean ang 0.0 deg

Amplitude 25.0 deg

Oscillation frequency 2.200 Hz

Reduced frequency on semichord 0.049

Tunnel speed 41.835 m/s

Reynold's number over run 7.73E5

Turbulence at blade (dp) 2.17E-2

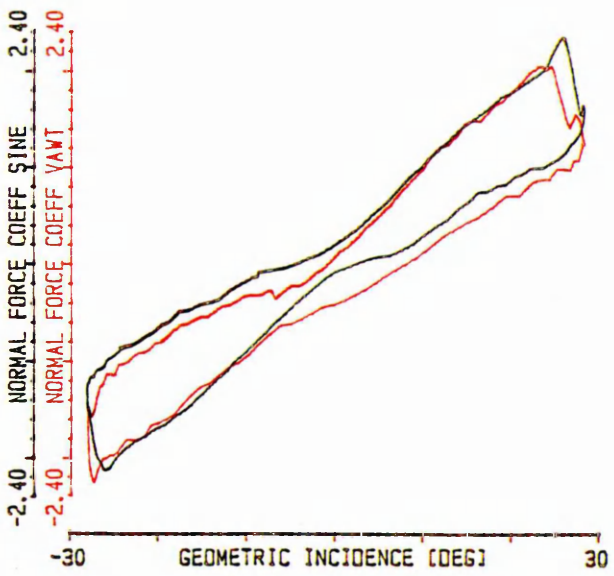

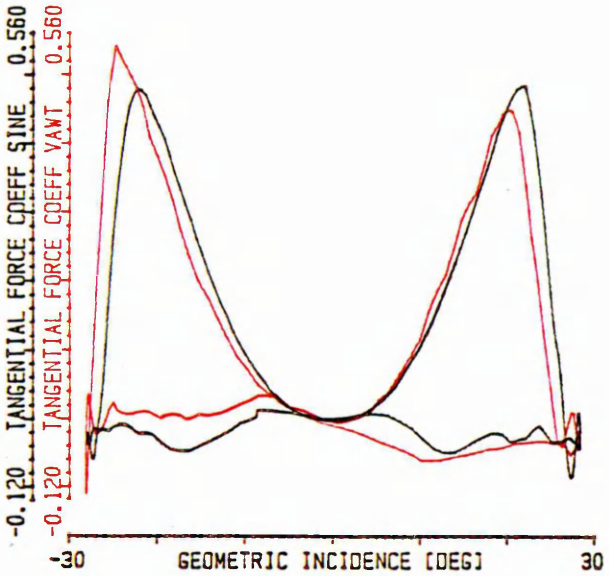

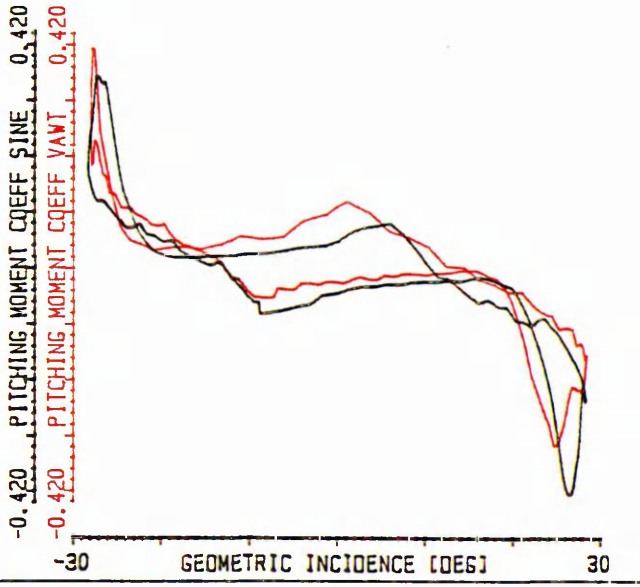

CIT

UNSTEADY AERODYNAMICS OF A VAWT

FIGURE 49

COMPARISON OF PRINCIPAL FORCE AND MOMENT COEFFICIENTS FOR LARGE AMPLITUDE (+/-30DEG) SINE AND VAWT FUNCTION INPUT WAVEFORMS: RUNS 137 AND 162 RESPECTIVELY.

REYNOLDS NUMBER FOR BOTH TESTS: 0.56E6

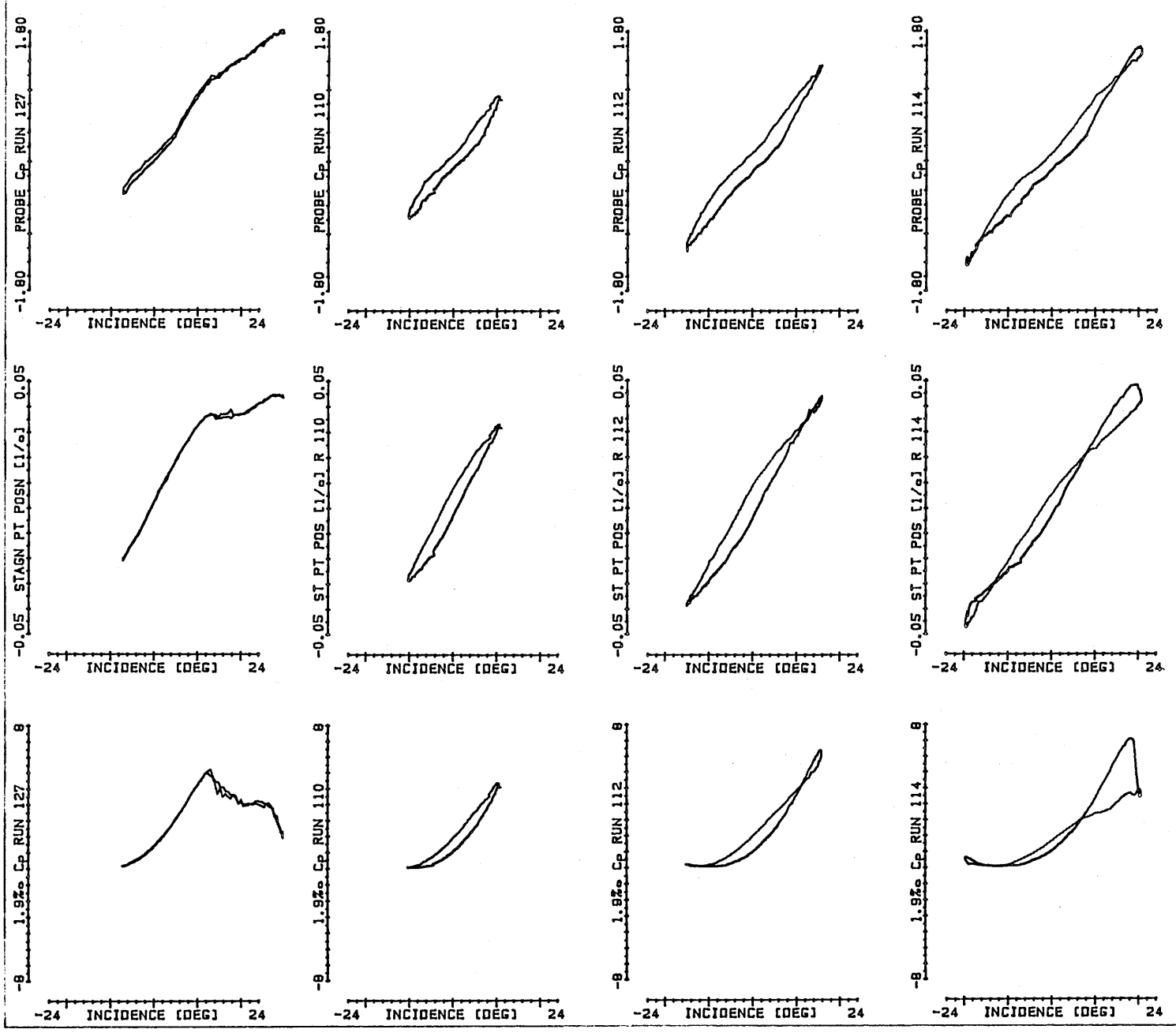

CIT

UNSTEADY AERODYNAMICS OF A VAWT

FIGURE 50

THREE SURROGATE MEASURES OF BLADE INCIDENCE: PROBE NEGATIVE C_p, STAGNATION POINT POSITION [1/CHORD] AND A NEAR LEADING EDGE (1.9%CHORD) NEGATIVE PRESSURE COEFFICIENT FOR ONE STATIC AND THREE VAWT RUNS. NOMINAL REYNOLDS NUMBER 0.75E6 FOR ALL RUNS.

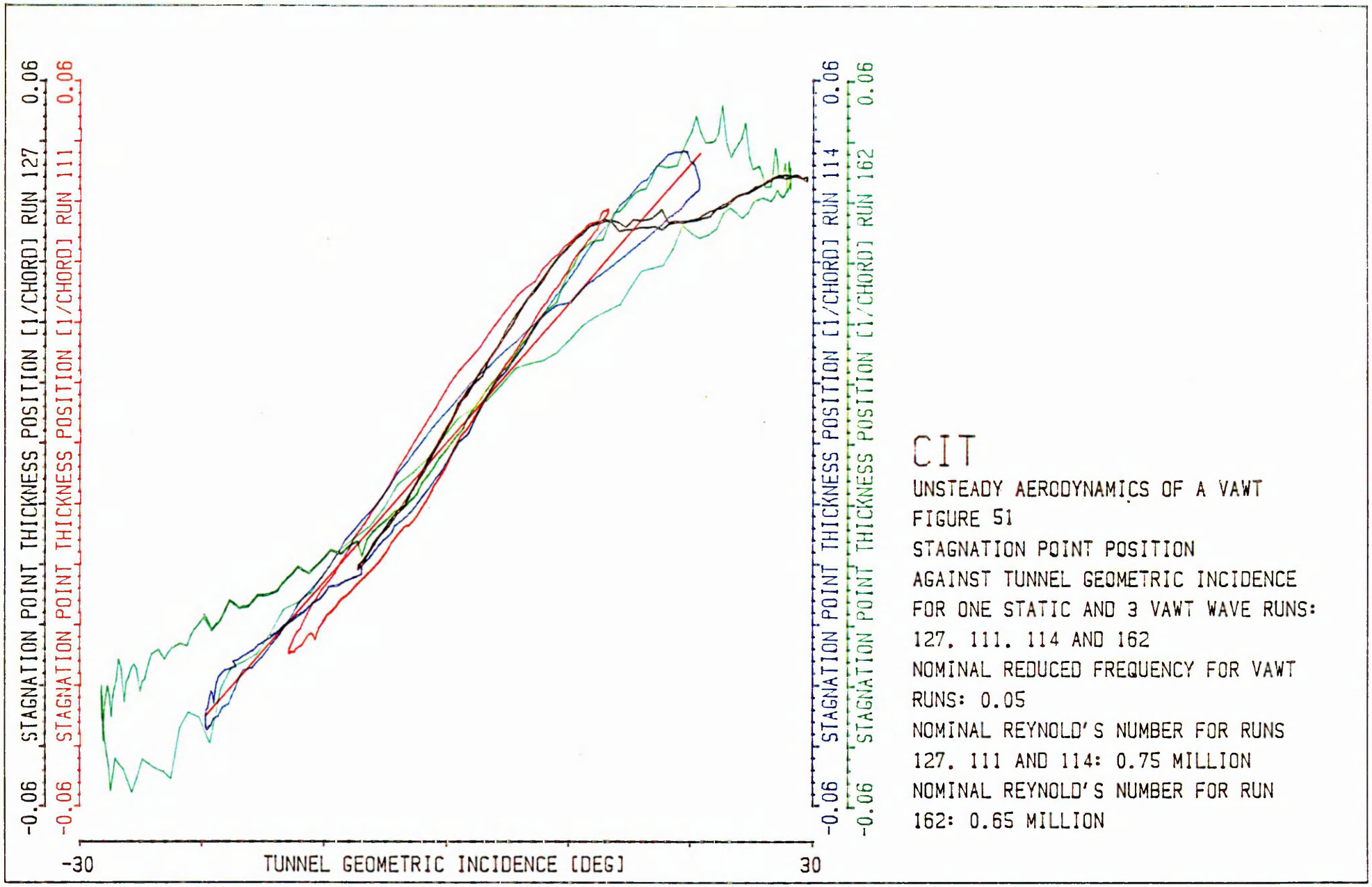

CIT

UNSTEADY AERODYNAMICS OF A VAWT

FIGURE 51

STAGNATION POINT POSITION AGAINST TUNNEL GEOMETRIC INCIDENCE FOR ONE STATIC AND 3 VAWT WAVE RUNS: 127, 111, 114 AND 162

NOMINAL REDUCED FREQUENCY FOR VAWT RUNS: 0.05

NOMINAL REYNOLD'S NUMBER FOR RUNS 127, 111 AND 114: 0.75 MILLION

NOMINAL REYNOLD'S NUMBER FOR RUN 162: 0.65 MILLION

FIGURE 52

UNSTEADY AERODYNAMICS OF A VAWT

EFFECT ON MAXIMUM ACHIEVED STAGNATION POINT OFFSET OF OSCILLATION MOTION TYPE REYNOLDS NUMBER AND REDUCED FREQUENCY FOR ALL WIND TUNNEL RUNS. MAXIMUM ACHIEVED NORMAL FORCE COEFFICIENTS ALSO SHOWN AGAINST MAXIMUM ACHIEVED STAGNATION POINT OFFSETS.

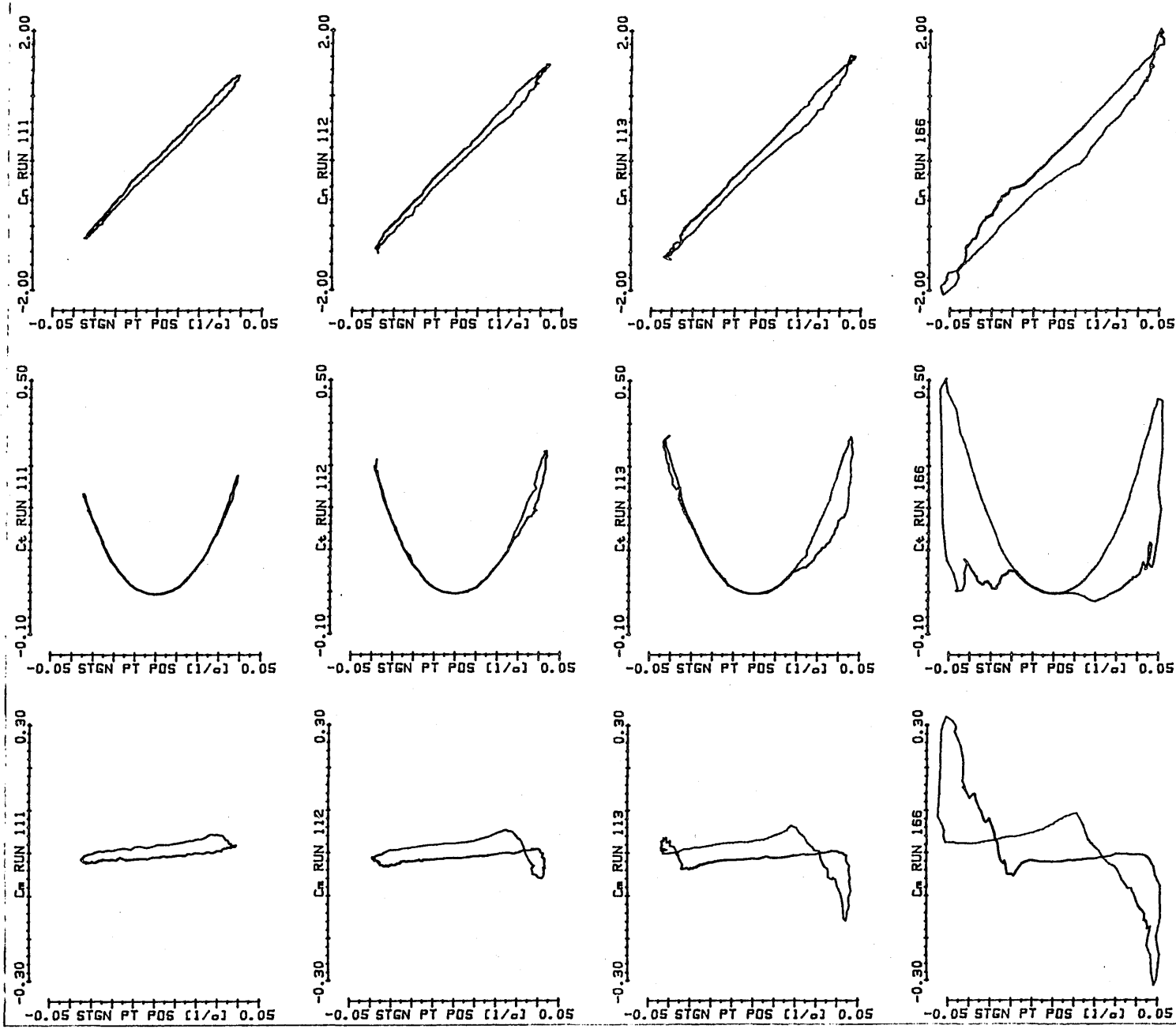

CIT

UNSTEADY AERODYNAMICS OF A VAWT

FIGURE 53

NORMAL AND TANGENTIAL FORCE AND PITCHING MOMENT COEFFS BASED ON STAGNATION PRESSURE FOR FOUR VAWT RUNS OVER A RANGE OF MAXIMUM INCIDENCE. NOMINAL REDUCED FREQUENCY FOR ALL RUNS 0.05 AND NOMINAL REYNOLDS NUMBER 0.75E6

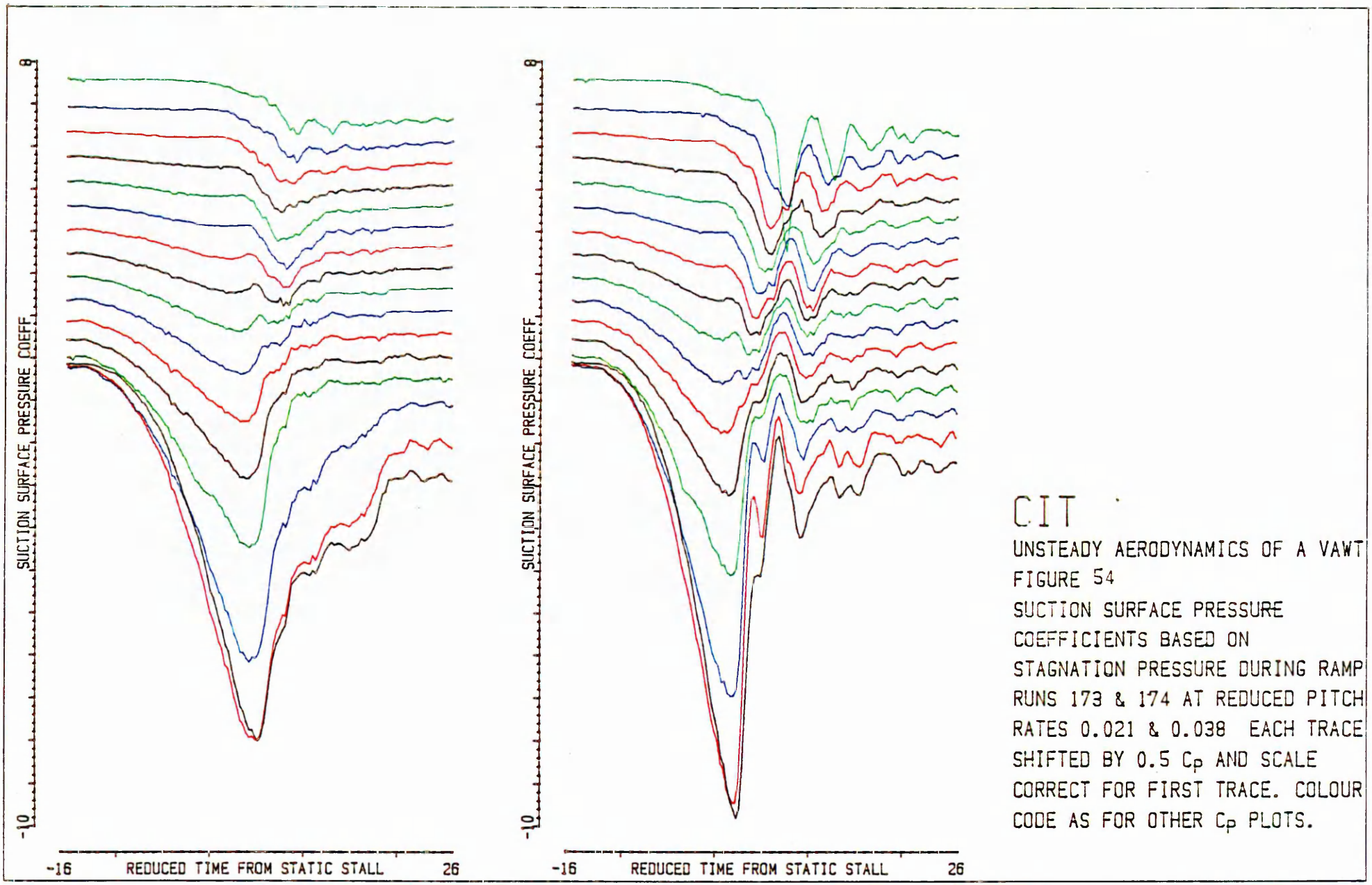

CIT

UNSTEADY AERODYNAMICS OF A VAWT

FIGURE 54

SUCTION SURFACE PRESSURE COEFFICIENTS BASED ON STAGNATION PRESSURE DURING RAMP RUNS 173 & 174 AT REDUCED PITCH RATES 0.021 & 0.038 EACH TRACE SHIFTED BY 0.5 C_p AND SCALE CORRECT FOR FIRST TRACE. COLOUR CODE AS FOR OTHER C_p PLOTS.

CIT
UNSTEADY AERODYNAMICS OF A VAWT
FIGURE 55
COMPARISON OF TRACES USED FOR
TIMING OF DYNAMIC STALL EVENTS
PLOTTED AGAINST REDUCED TIME
FROM ACHIEVEMENT OF STATIC
STALL INCIDENCE. DATA FROM FIVE
RAMP RUNS SHOWN.
NORMAL FORCE COEFFICIENT RUN 174
PITCHING MOMENT COEFFICIENT RUN 174
STAGNATION POINT OFFSET RUN 174
32.8% PRESSURE COEFFICIENT RUN 174
NORMAL FORCE COEFFICIENT RUN 175
PITCHING MOMENT COEFFICIENT RUN 175
STAGNATION POINT OFFSET RUN 175
32.8% PRESSURE COEFFICIENT RUN 175
NORMAL FORCE COEFFICIENT RUN 172
PITCHING MOMENT COEFFICIENT RUN 172
STAGNATION POINT OFFSET RUN 172
32.8% PRESSURE COEFFICIENT RUN 172
NORMAL FORCE COEFFICIENT RUN 171
PITCHING MOMENT COEFFICIENT RUN 171
STAGNATION POINT OFFSET RUN 171
32.8% PRESSURE COEFFICIENT RUN 171
NORMAL FORCE COEFFICIENT RUN 173
PITCHING MOMENT COEFFICIENT RUN 173
STAGNATION POINT OFFSET RUN 173
32.8% PRESSURE COEFFICIENT RUN 173
REDUCED TIME FROM STATIC STALL

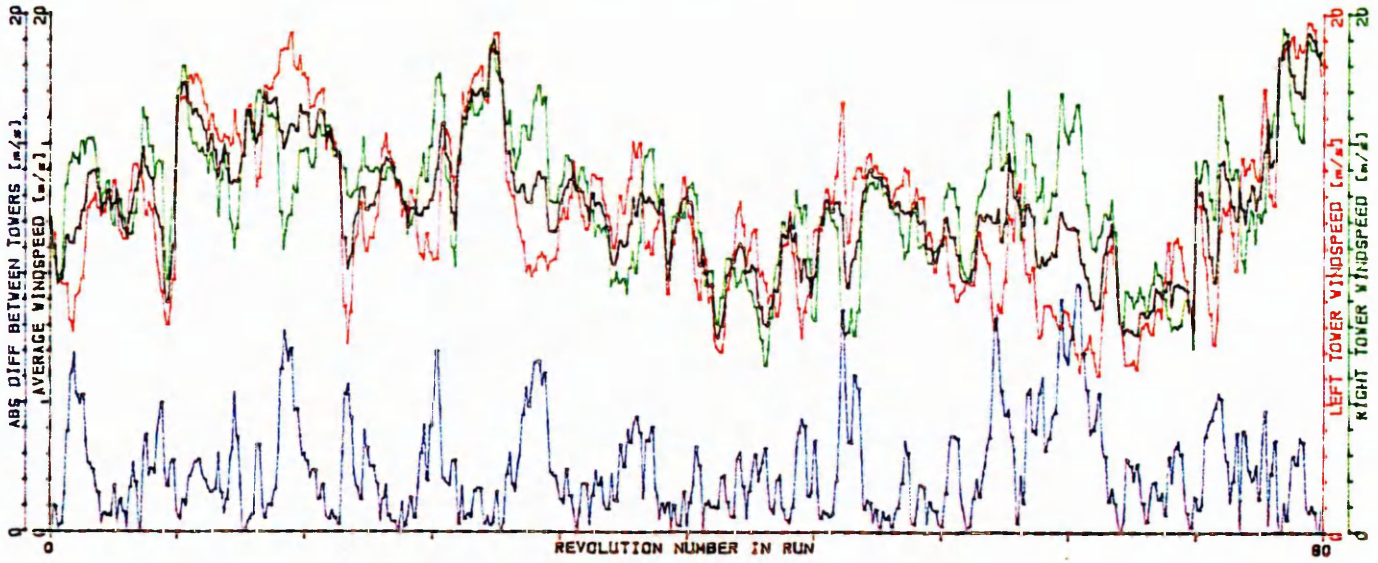

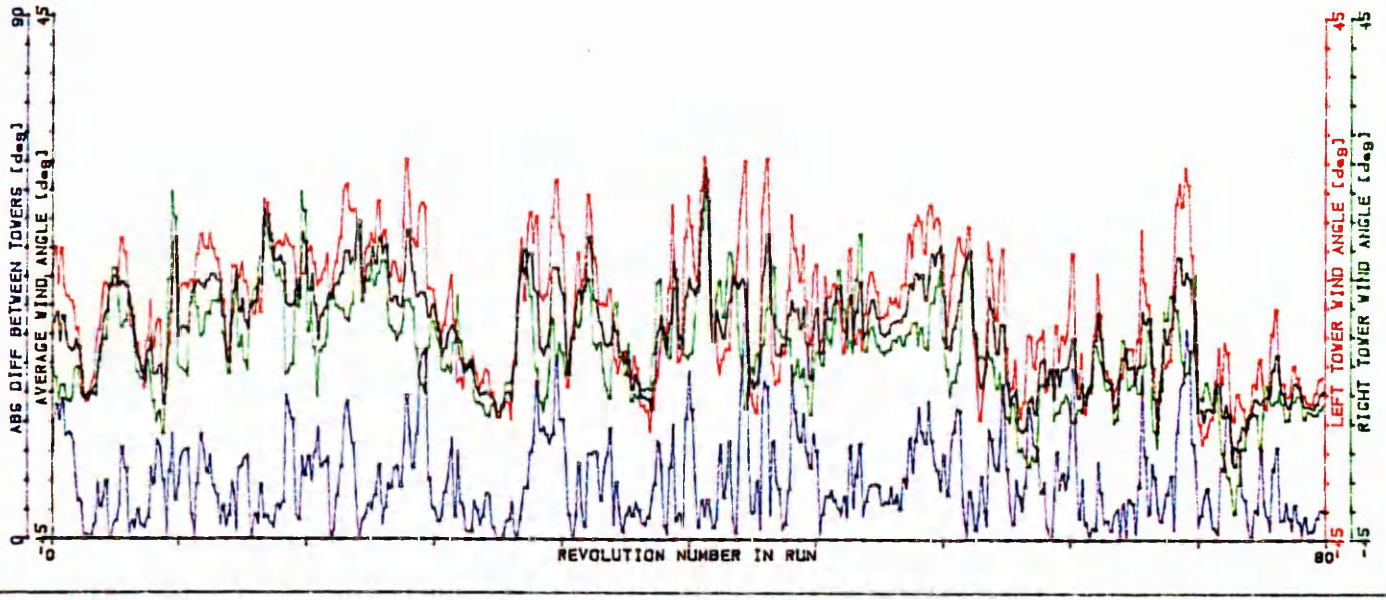

CIT FIGURE 56

UNSTEADY AERODYNAMICS OF A VAWT

WIND STATISTICS.

Run 201 On 06.06.87 At 13.40.31

Anemometer configuration 1/18

Blade configuration number 3

Blade leanout 0 deg

Nominal rotor speed: 120rpm

Datalogger windspeed window 10-15m/s

Average wind over run: 12.56m/s

Min and max speed over run: 7.44-19.29m/s

Std dev of speed over run: 2.39m/s

Avg diff in speed between towers: -0.66m/s

Std dev of windspeed diff: 3.04m/s

Avg dirn of wind rel tower orient: -9.19deg

Standard deviation of wind dirn: 8.97deg

Avg diff in dirn between towers: 7.49deg

Std dev of angular diff: 10.14deg

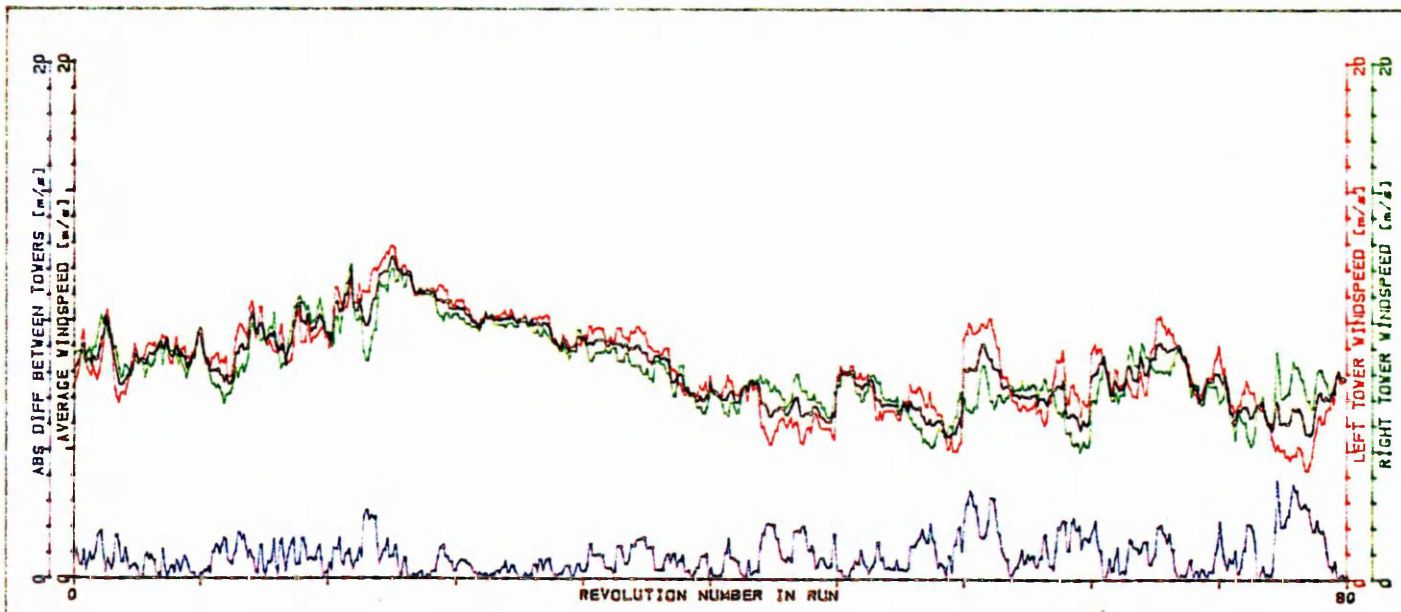

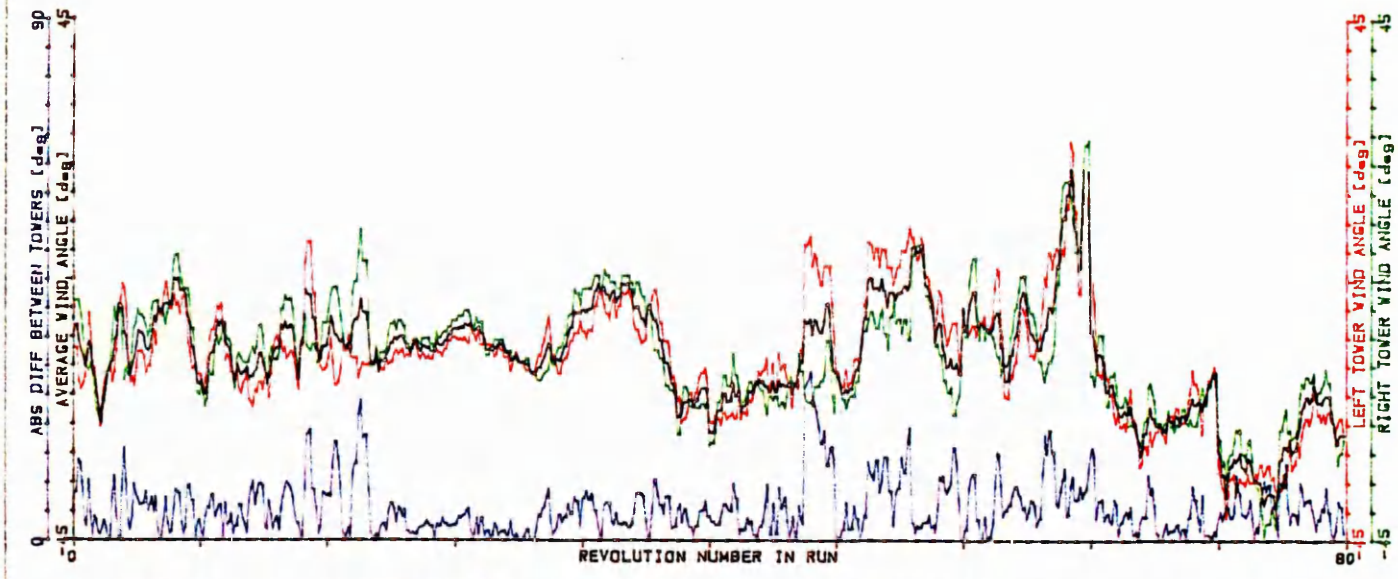

CIT FIGURE 57

UNSTEADY AERODYNAMICS OF A VAWT

WIND STATISTICS.

Run 210 On 31.07.87 At 19.35.14

Anemometer configuration 0/12

Blade configuration number 3

Blade leanout 0 deg

Nominal rotor speed: 80-90rpm

Datalogger windspeed window 8-11m/s

Average wind over run: 8.24m/s

Min and max speed over run: 5.47-12.43m/s

Std dev of speed over run: 1.52m/s

Avg diff in speed between towers: 0.19m/s

Std dev of windspeed diff: 1.18m/s

Avg dirn of wind rel tower orient: -13.23deg

Standard deviation of wind dirn: 9.37deg

Avg diff in dirn between towers: -0.23deg

Std dev of angular diff: 7.59deg

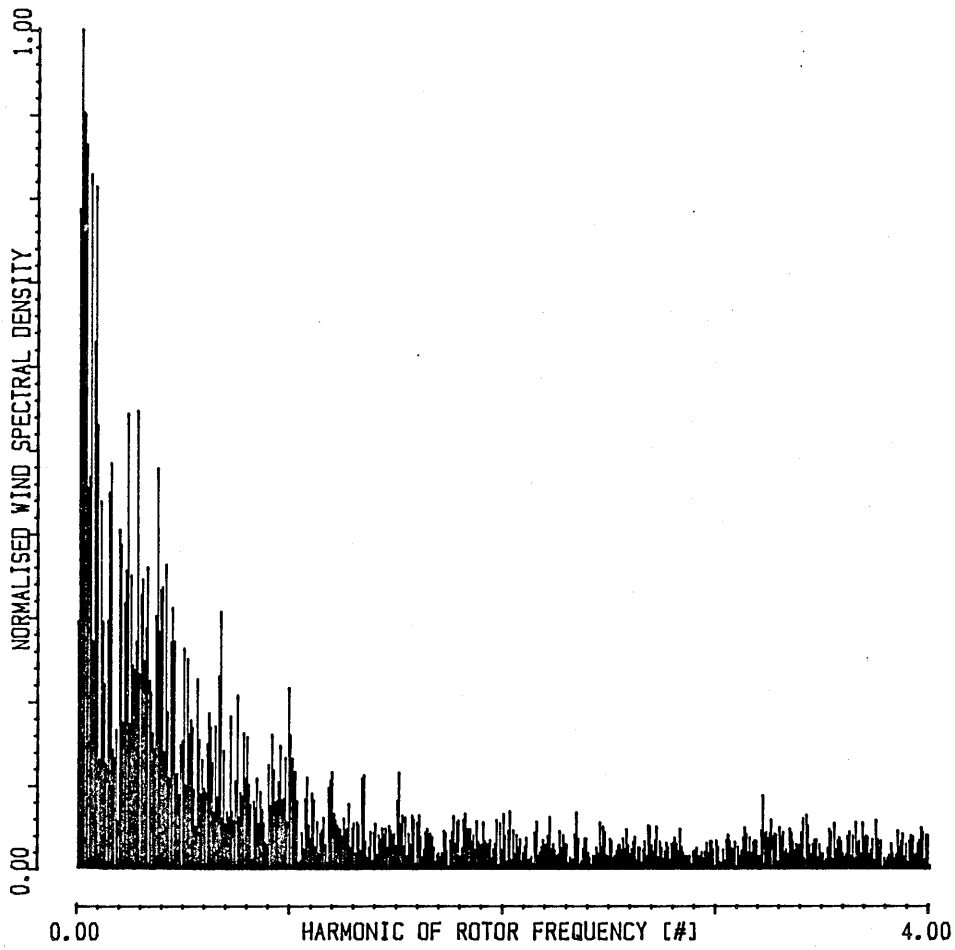

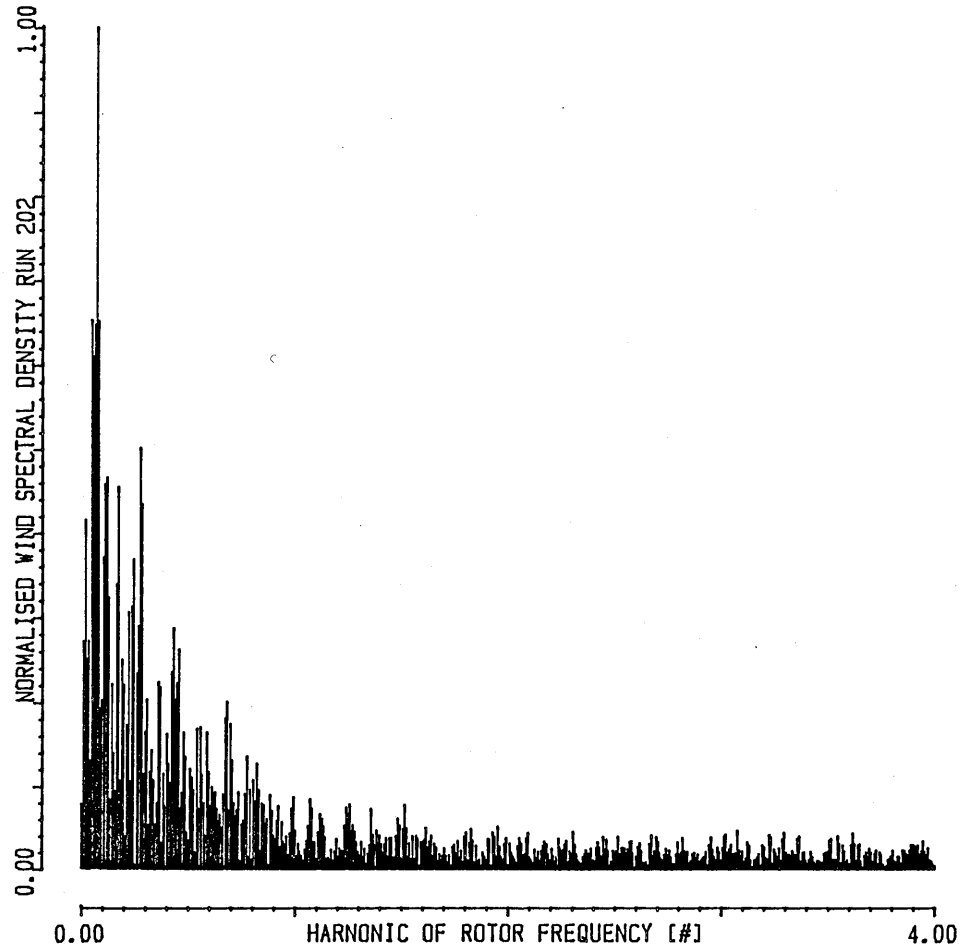

CIT

UNSTEADY AERODYNAMICS OF A VAWT

FIGURE 58

COMPARISON OF DISTANT AND CLOSE ANEMOMETER RESPONSE TO ROTOR. LEFT TRANSFORM SHOWS RUN 201 WITH TOWER 18m DISTANT FROM ROTOR CENTRE, RIGHT RUN 202 6m SEPARATION. RAW SIGNAL CONDITIONED BY SUBTRACTION OF MEAN AND TREND AND COSINE WINDOW

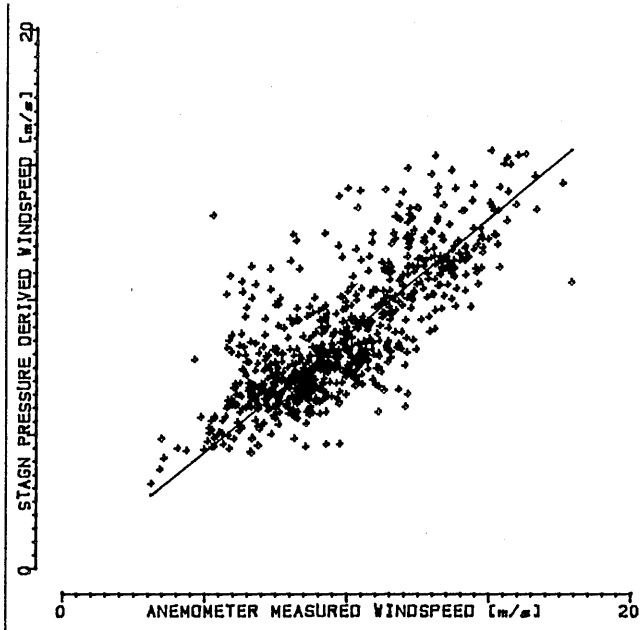

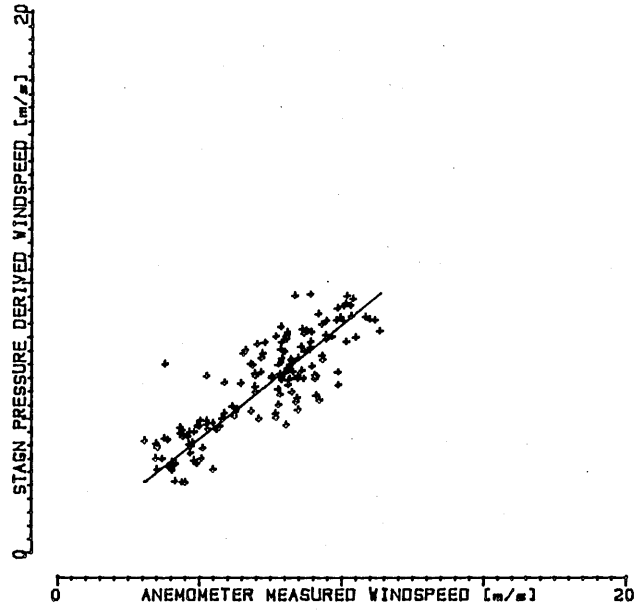

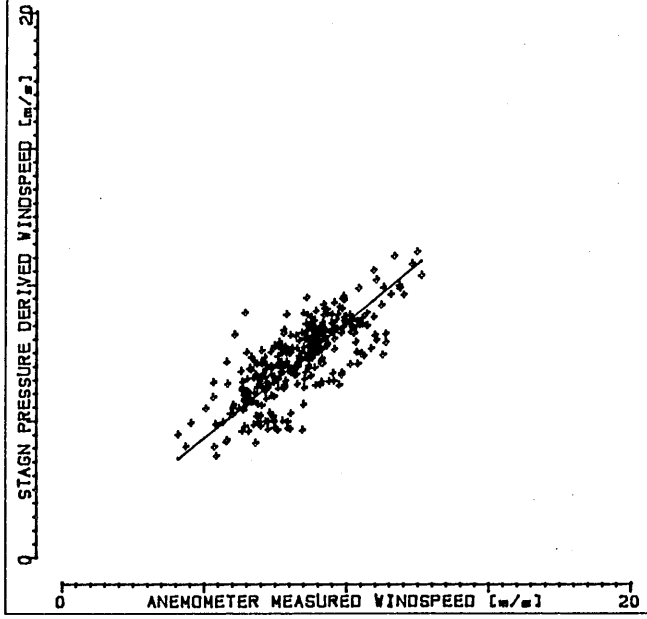

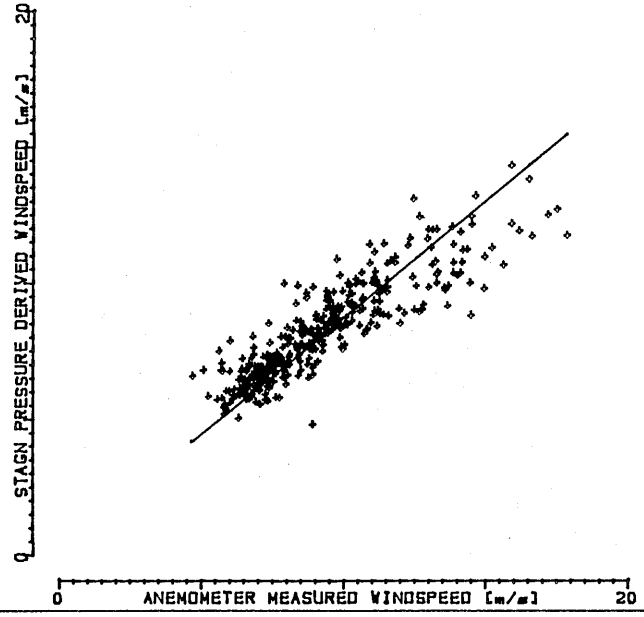

CIT

UNSTEADY AERODYNAMICS OF A VAWT

FIGURE 59

COMPARISON OF ANEMOMETER MEASURED AND STAGNATION PRESSURE BASED WINDSPEED FOR FOUR BLADE LEANOUT ANGLES LEFT TO RIGHT 0 DEG. 15 DEG. 30 DEG AND 45 DEG. FITTED LINE GRADIENTS ARE 0.869, 0.848, 0.862 AND 0.867 RESPECTIVELY.

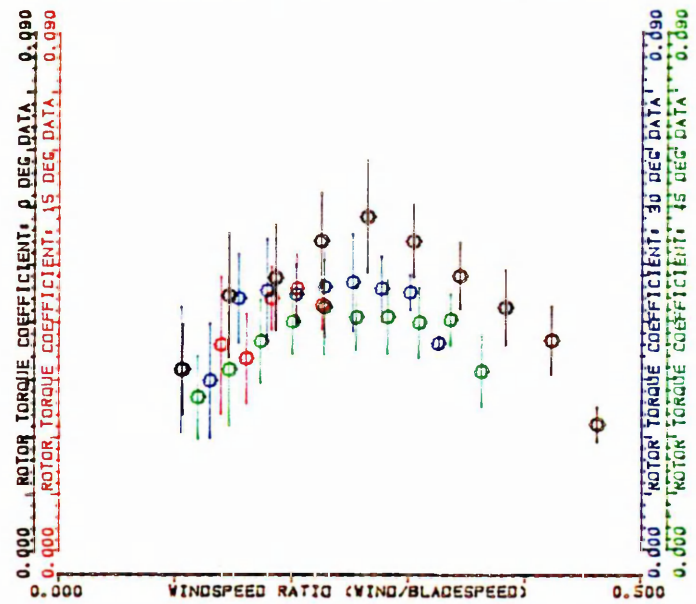

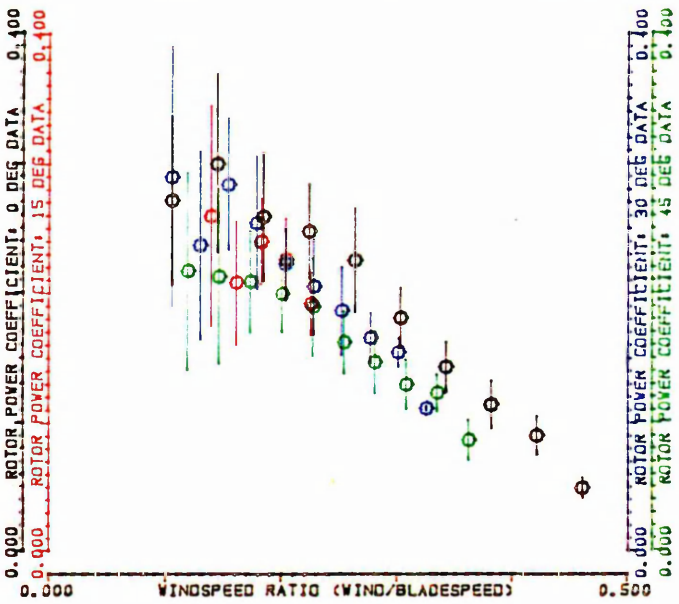

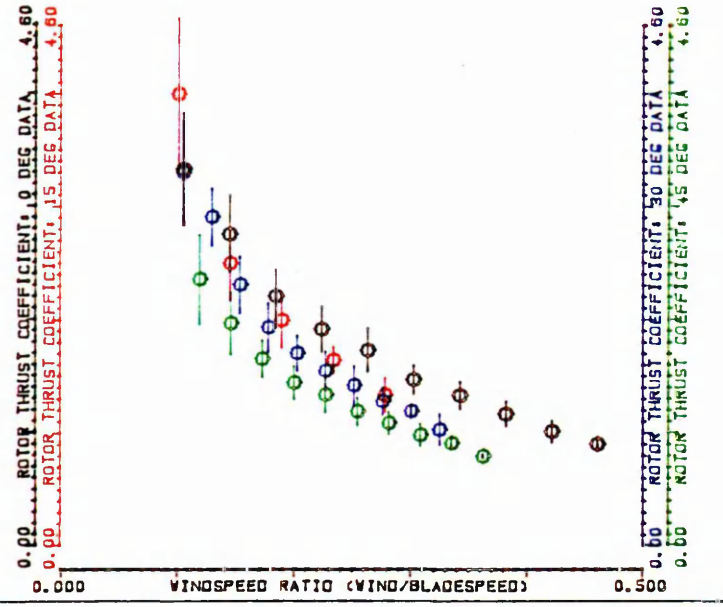

CIT

UNSTEADY AERODYNAMICS OF A VAWT

FIGURE 60

COMPARISON OF ROTOR TORQUE, ROTOR POWER AND ROTOR THRUST COEFFICIENTS FOR FOUR BLADE LEANOUT ANGLES. ALL ATMOSPHERIC DATA SHOWN. MEAN AND +/- ONE STANDARD DEVIATION SHOWN.

WINDSPEED BASED ON BLADE STAGNATION PRESSURE AND BLADE SPEED.

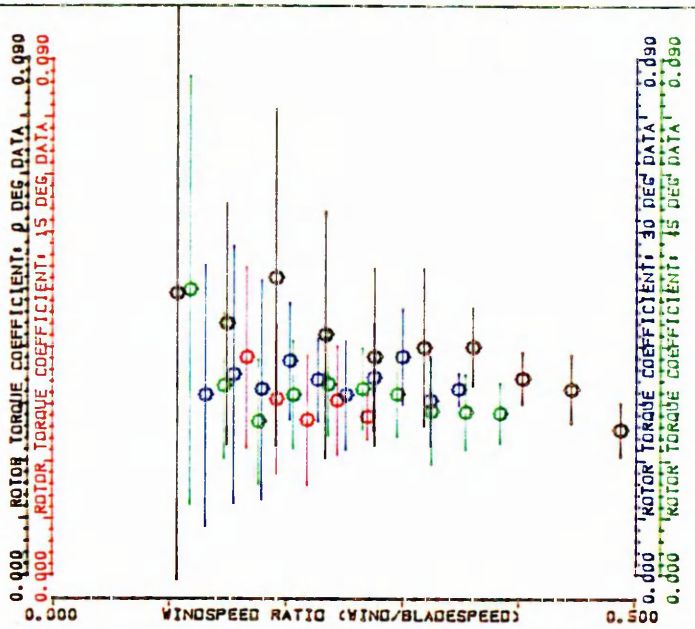

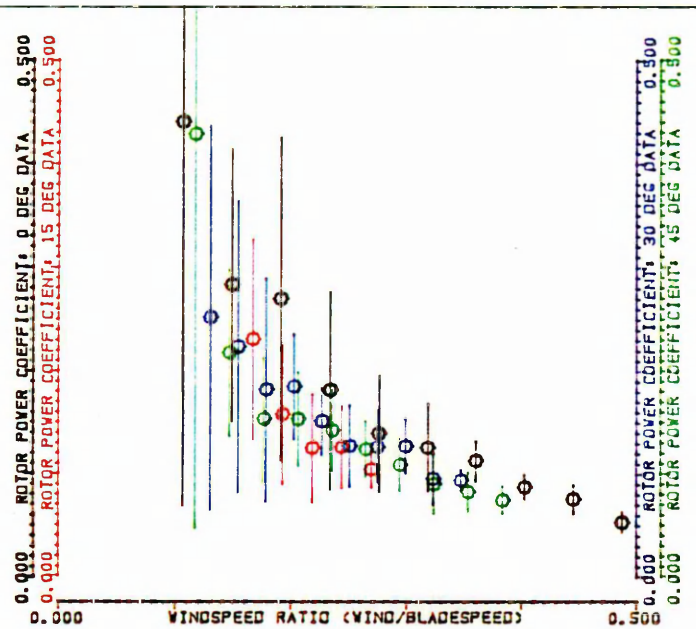

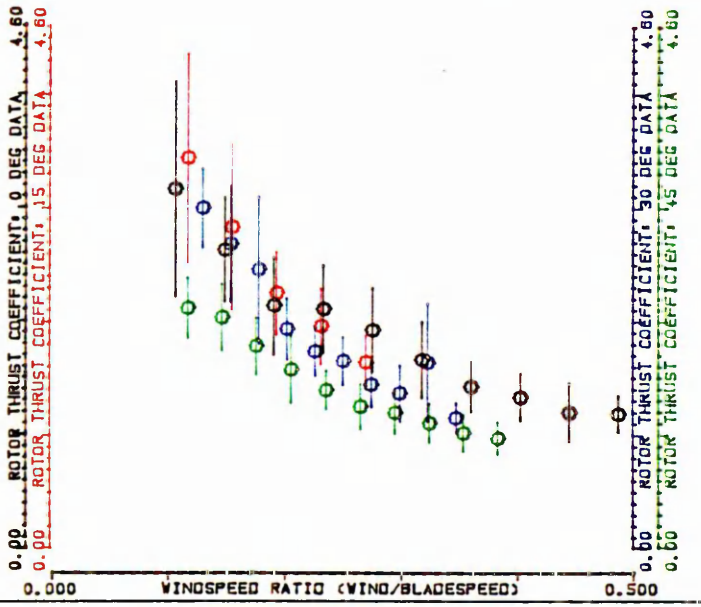

CIT

UNSTEADY AERODYNAMICS OF A VAWT

FIGURE 61

COMPARISON OF ROTOR TORQUE, ROTOR POWER AND ROTOR MAXIMUM THRUST COEFFICIENTS FOR FOUR BLADE LEANOUT ANGLES. MEAN AND +/- ONE STANDARD DEVIATION SHOWN.
ALL ATMOSPHERIC DATA SHOWN.
WINDSPEED BASED ON ANEMOMETER READINGS.

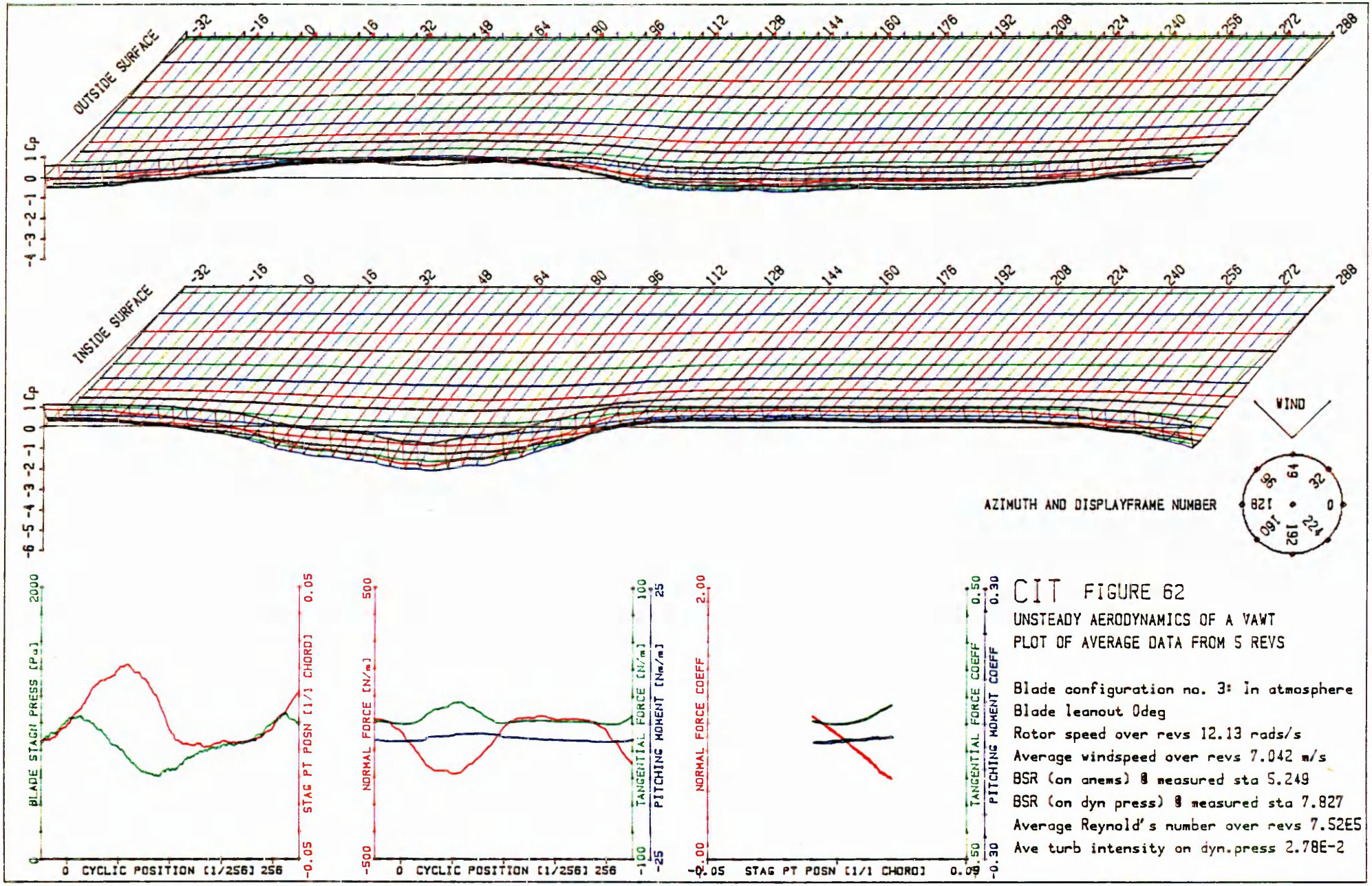

CIT FIGURE 62

UNSTEADY AERODYNAMICS OF A VAWT

PLOT OF AVERAGE DATA FROM 5 REVS

Blade configuration no. 3: In atmosphere
Blade leanout 0deg
Rotor speed over revs 12.13 rads/s
Average windspeed over revs 7.042 m/s
BSR (on anems) @ measured sta 5.249
BSR (on dyn press) @ measured sta 7.827
Average Reynold's number over revs 7.52E5
Ave turb intensity on dyn.press 2.78E-2

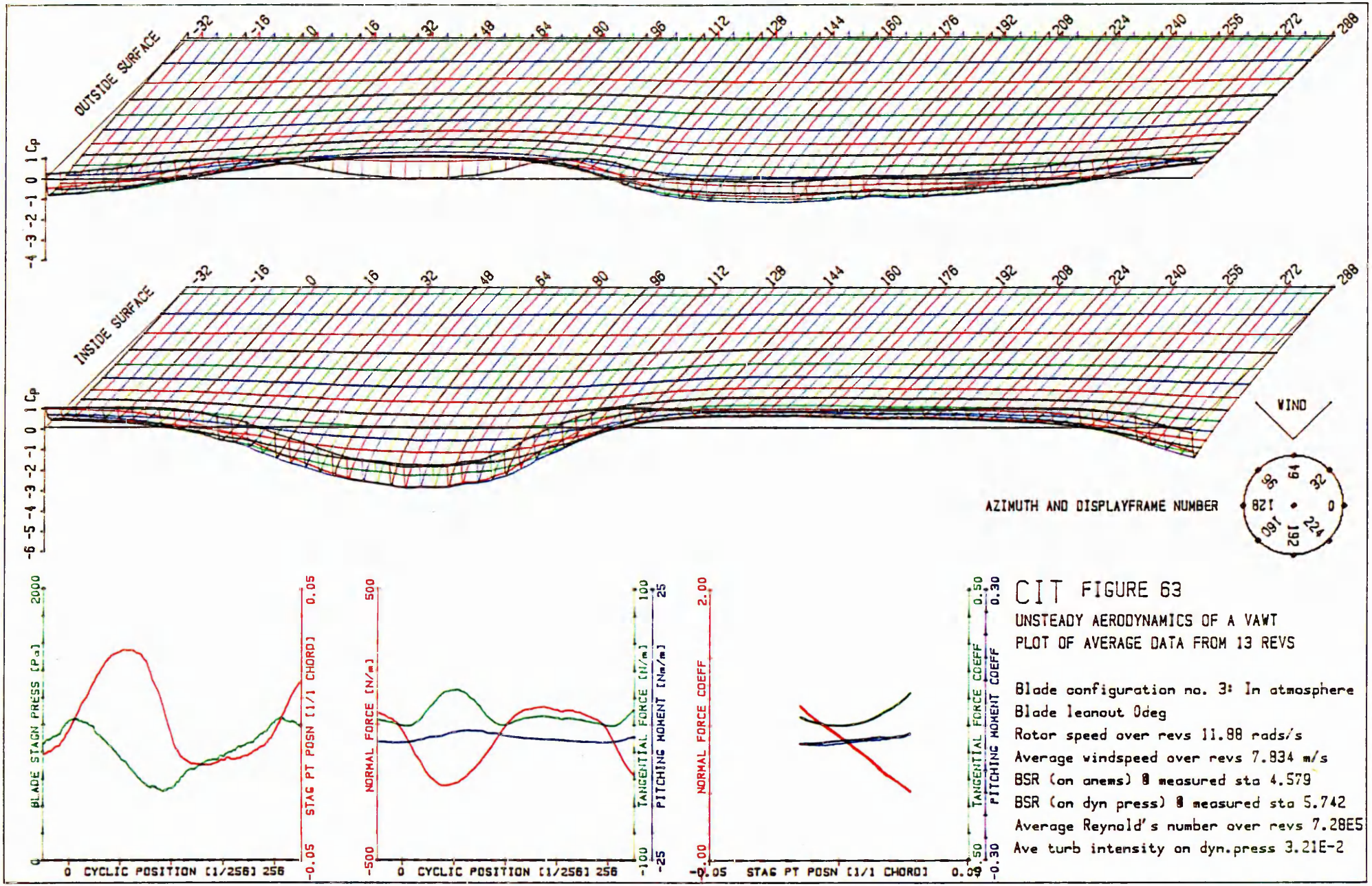

CIT FIGURE 63

UNSTEADY AERODYNAMICS OF A VAWT
PLOT OF AVERAGE DATA FROM 13 REVS

Blade configuration no. 3: In atmosphere
Blade leanout 0deg
Rotor speed over revs 11.88 rads/s
Average windspeed over revs 7.834 m/s
BSR (on anems) @ measured sta 4.579
BSR (on dyn press) @ measured sta 5.742
Average Reynold's number over revs 7.28E5
Ave turb intensity on dyn.press 3.21E-2

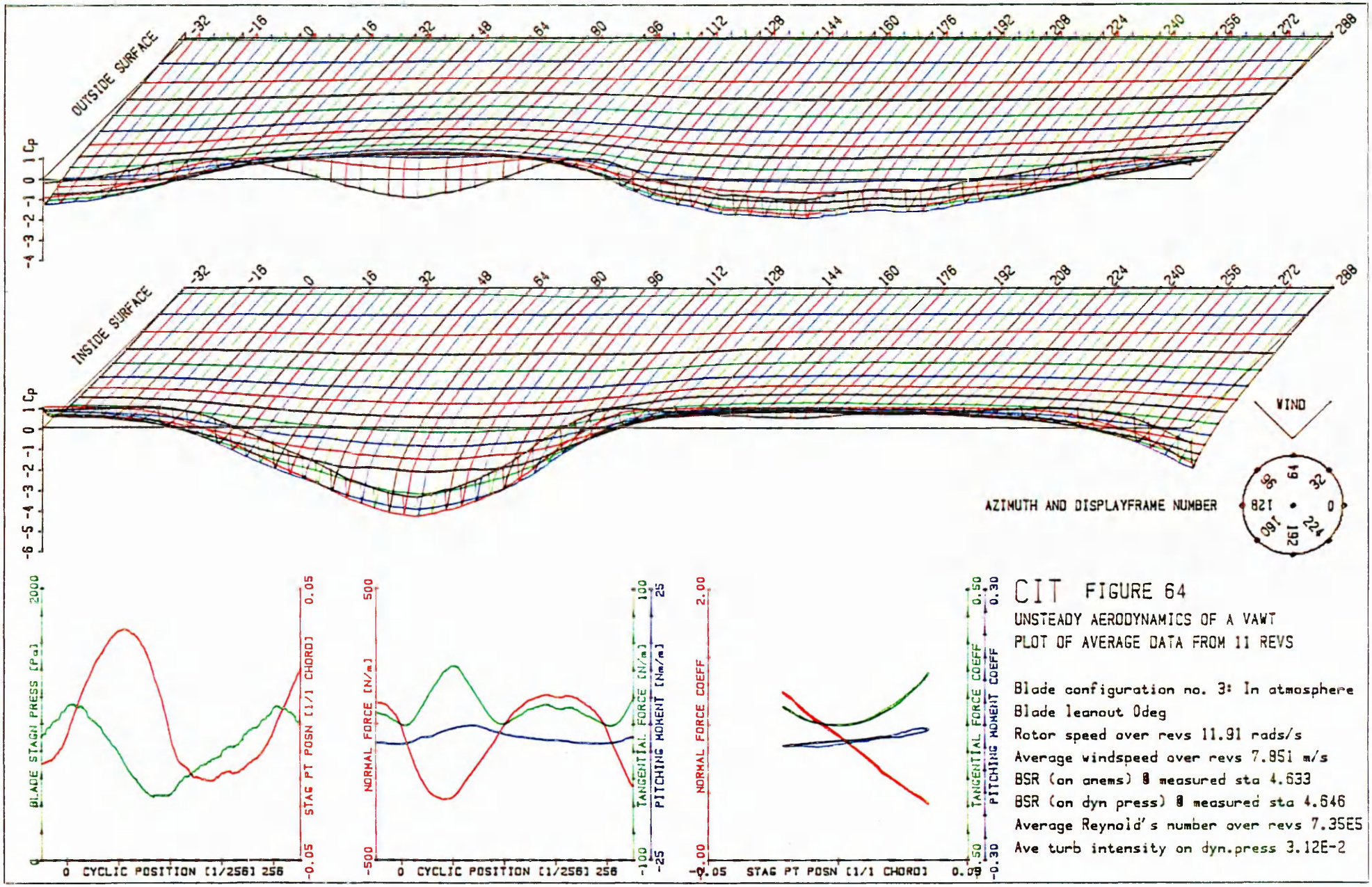

CIT FIGURE 64

UNSTEADY AERODYNAMICS OF A VAWT
PLOT OF AVERAGE DATA FROM 11 REVS

Blade configuration no. 3: In atmosphere
Blade leanout 0deg
Rotor speed over revs 11.91 rads/s
Average windspeed over revs 7.851 m/s
BSR (on anems) @ measured sta 4.633
BSR (on dyn press) @ measured sta 4.646
Average Reynold's number over revs 7.35E5
Ave turb intensity on dyn.press 3.12E-2

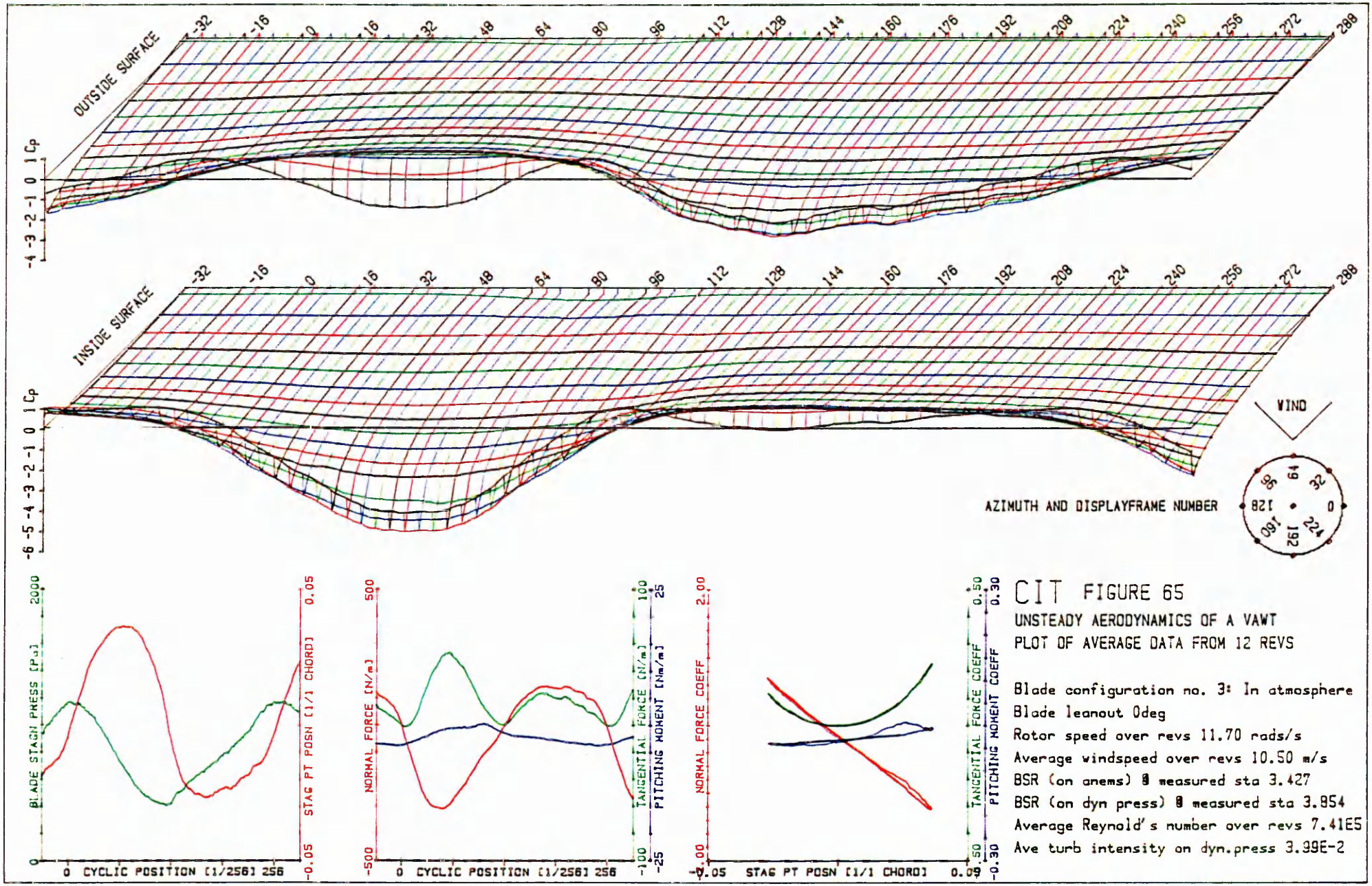

CIT FIGURE 65

UNSTEADY AERODYNAMICS OF A VAWT

PLOT OF AVERAGE DATA FROM 12 REVS

Blade configuration no. 3: In atmosphere

Blade leanout 0deg

Rotor speed over revs 11.70 rads/s

Average windspeed over revs 10.50 m/s

BSR (on anems) @ measured sta 3.427

BSR (on dyn press) @ measured sta 3.854

Average Reynold's number over revs 7.41E5

Ave turb intensity on dyn.press 3.99E-2

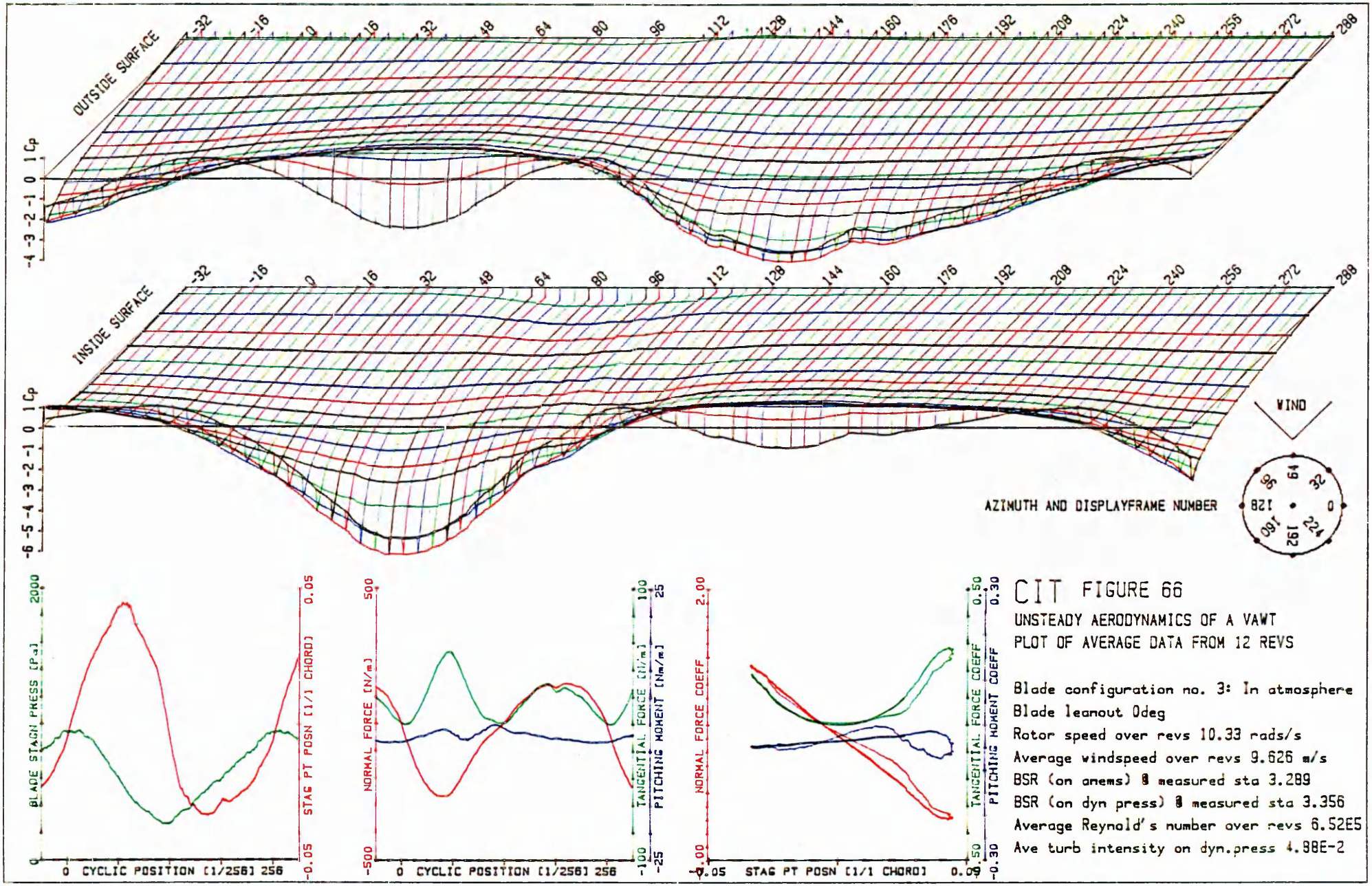

CIT FIGURE 66

UNSTEADY AERODYNAMICS OF A VAWT
PLOT OF AVERAGE DATA FROM 12 REVS

Blade configuration no. 3: In atmosphere
Blade leanout 0deg
Rotor speed over revs 10.33 rads/s
Average windspeed over revs 9.626 m/s
BSR (on anems) @ measured sta 3.289
BSR (on dyn press) @ measured sta 3.356
Average Reynold's number over revs 6.52E5
Ave turb intensity on dyn.press 4.88E-2

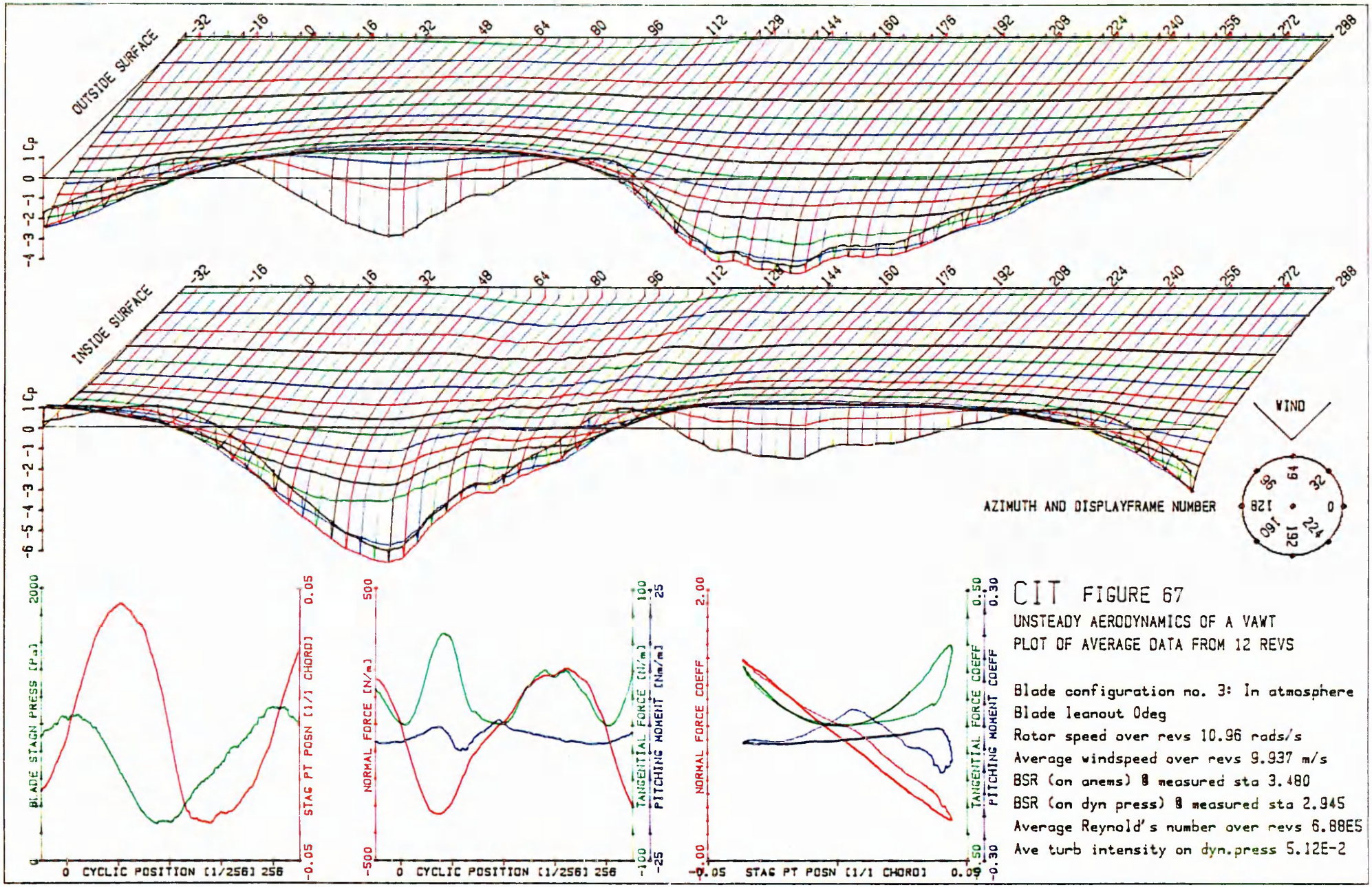

CIT FIGURE 67

UNSTEADY AERODYNAMICS OF A VAWT

PLOT OF AVERAGE DATA FROM 12 REVS

Blade configuration no. 3: In atmosphere
Blade leanout 0deg
Rotor speed over revs 10.96 rads/s
Average windspeed over revs 9.937 m/s
BSR (on anems) @ measured sta 3.480
BSR (on dyn press) @ measured sta 2.945
Average Reynold's number over revs 6.88E5
Ave turb intensity on dyn.press 5.12E-2

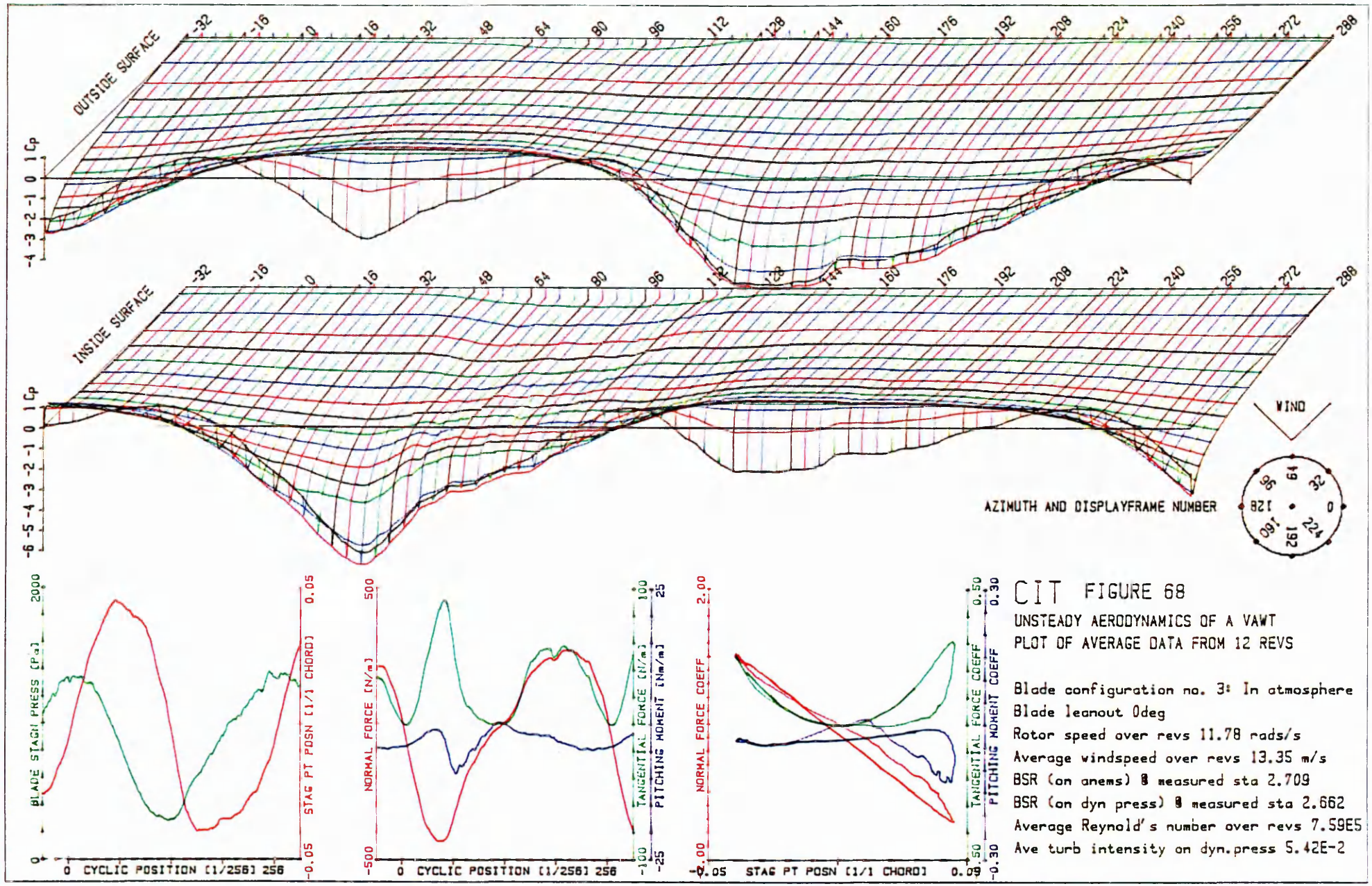

CIT FIGURE 68

UNSTEADY AERODYNAMICS OF A VAWT
PLOT OF AVERAGE DATA FROM 12 REVS

Blade configuration no. 3: In atmosphere
Blade leanout 0deg
Rotor speed over revs 11.78 rads/s
Average windspeed over revs 13.35 m/s
BSR (on anems) @ measured sta 2.709
BSR (on dyn press) @ measured sta 2.662
Average Reynold's number over revs 7.59E5
Ave turb intensity on dyn.press 5.42E-2

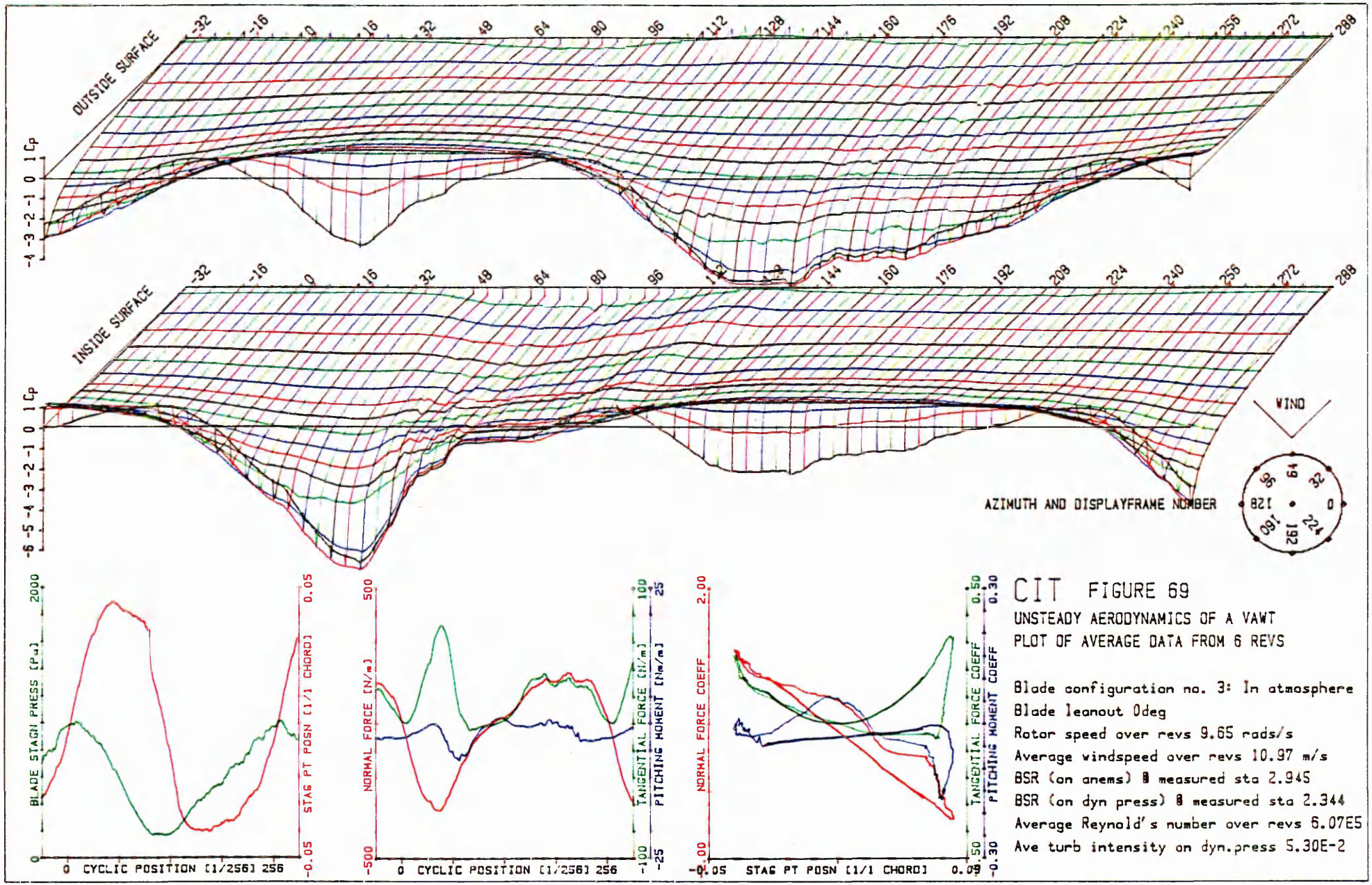

CIT FIGURE 69

UNSTEADY AERODYNAMICS OF A VAWT

PLOT OF AVERAGE DATA FROM 6 REVS

Blade configuration no. 3: In atmosphere
Blade leanout 0deg
Rotor speed over revs 9.65 rads/s
Average windspeed over revs 10.97 m/s
BSR (on anems) @ measured sta 2.945
BSR (on dyn press) @ measured sta 2.344
Average Reynold's number over revs 6.07E5
Ave turb intensity on dyn.press 5.30E-2

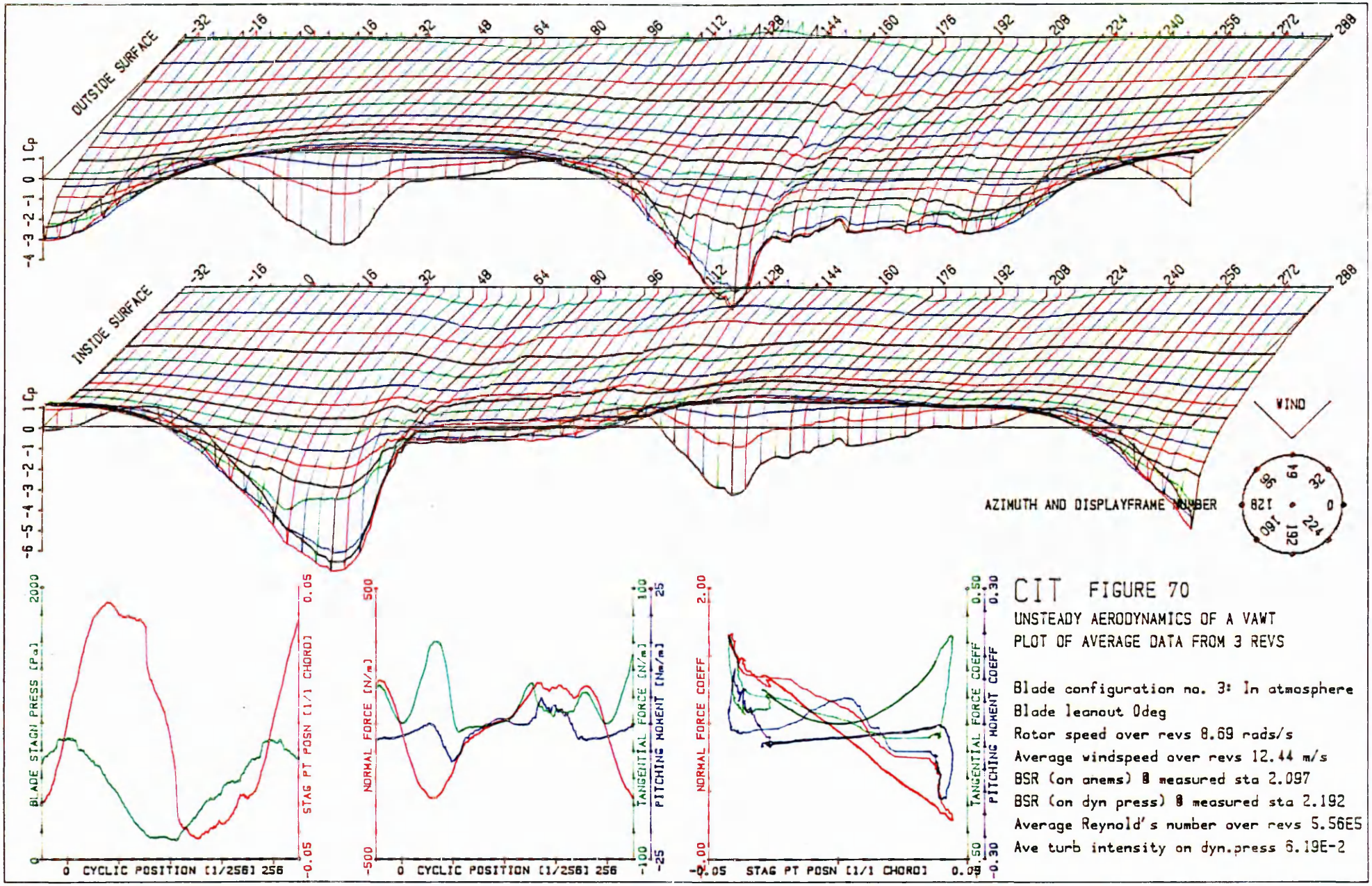

CIT FIGURE 70

UNSTEADY AERODYNAMICS OF A VAWT
PLOT OF AVERAGE DATA FROM 3 REVS

Blade configuration no. 3: In atmosphere
Blade leanout 0deg
Rotor speed over revs 8.69 rads/s
Average windspeed over revs 12.44 m/s
BSR (on anems) @ measured sta 2.097
BSR (on dyn press) @ measured sta 2.192
Average Reynold's number over revs 5.56E5
Ave turb intensity on dyn.press 6.19E-2

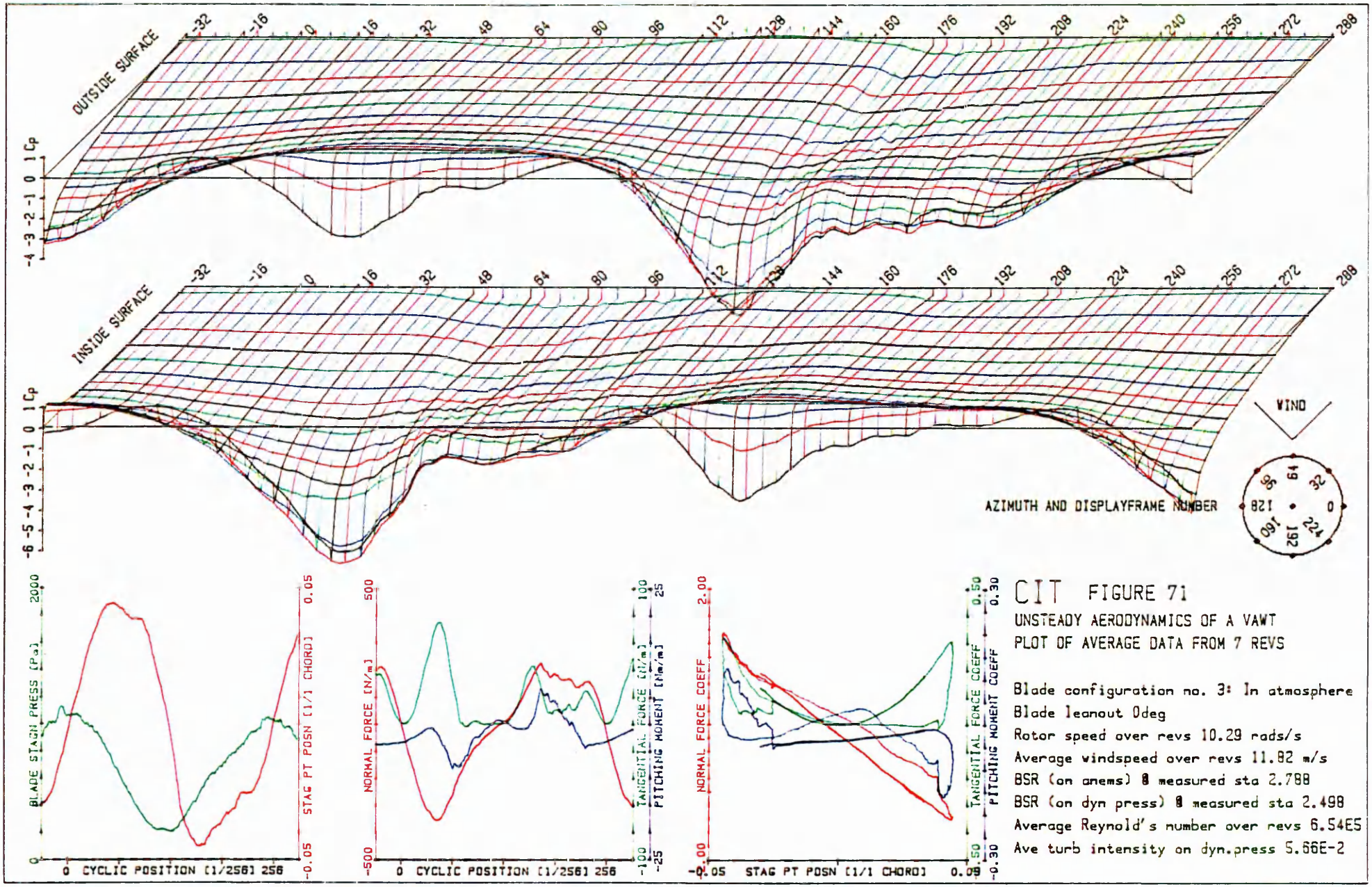

CIT FIGURE 71

UNSTEADY AERODYNAMICS OF A VAWT

PLOT OF AVERAGE DATA FROM 7 REVS

Blade configuration no. 3: In atmosphere

Blade leanout 0deg

Rotor speed over revs 10.29 rads/s

Average windspeed over revs 11.82 m/s

BSR (on anems) @ measured sta 2.788

BSR (on dyn press) @ measured sta 2.498

Average Reynold's number over revs 6.54E5

Ave turb intensity on dyn.press 5.66E-2

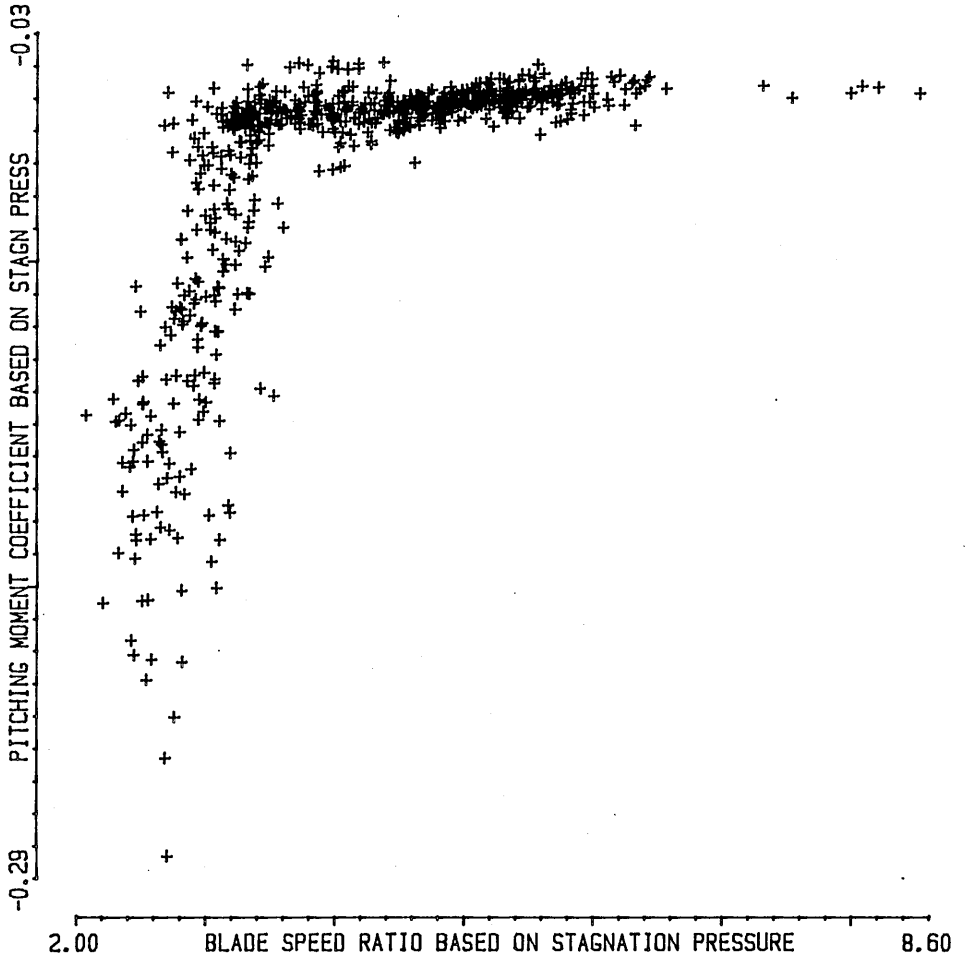

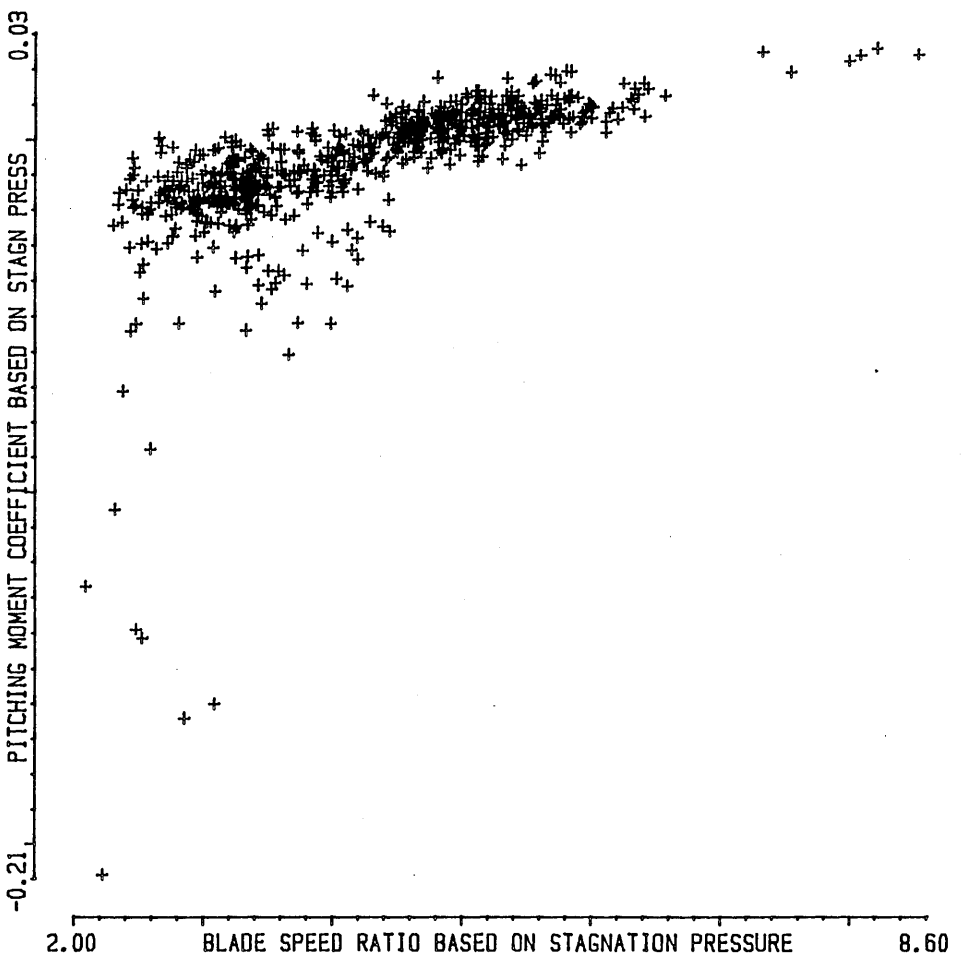

CIT

UNSTEADY AERODYNAMICS OF A VAWT

FIGURE 72

BLADE PITCHING MOMENT COEFFICIENTS FOR THE UPSTREAM AND DOWNSTREAM BLADE PASSES. 0 DEGREE BLADE LEANOUT DATA. COEFFICIENTS AND BLADE SPEED RATIO BASED ON STAGNATION PRESSURE.

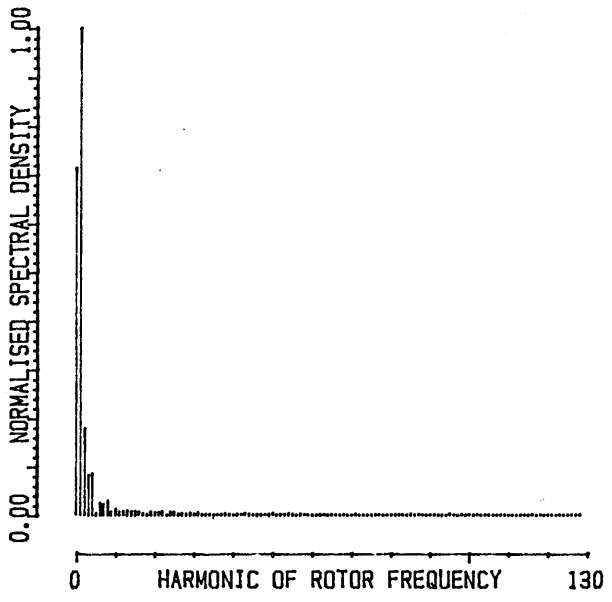

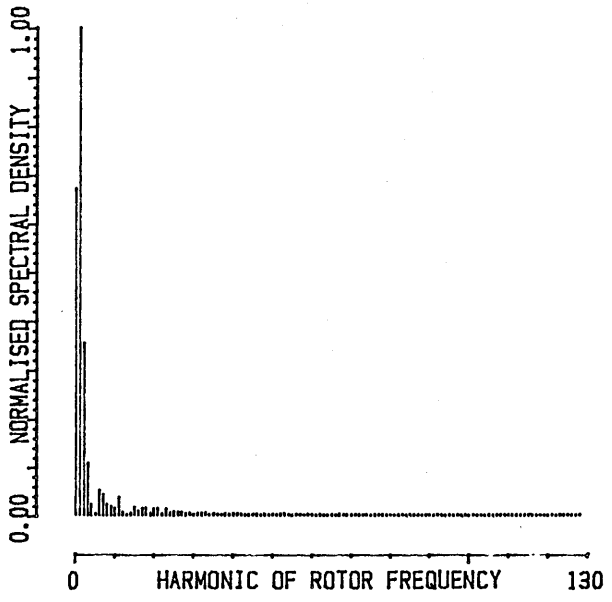

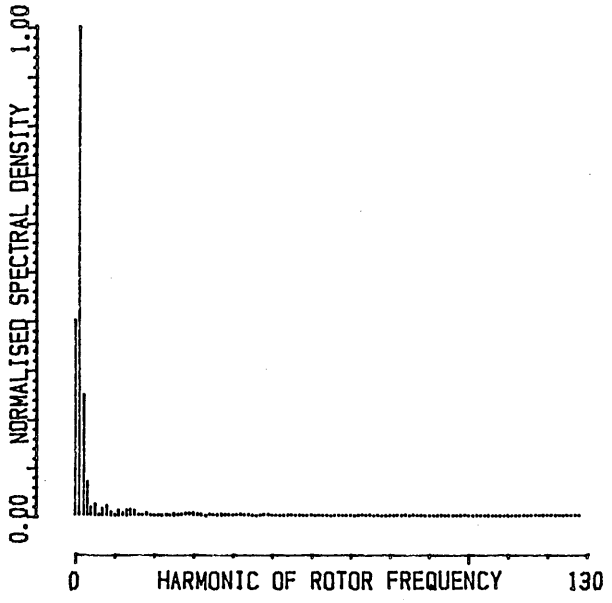

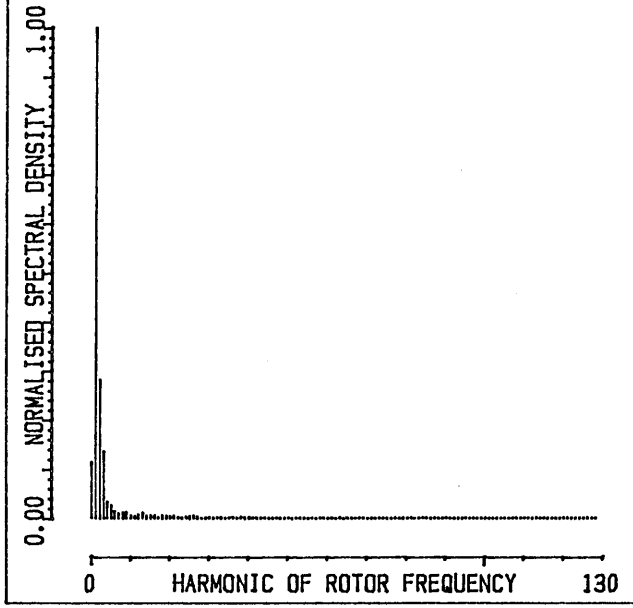

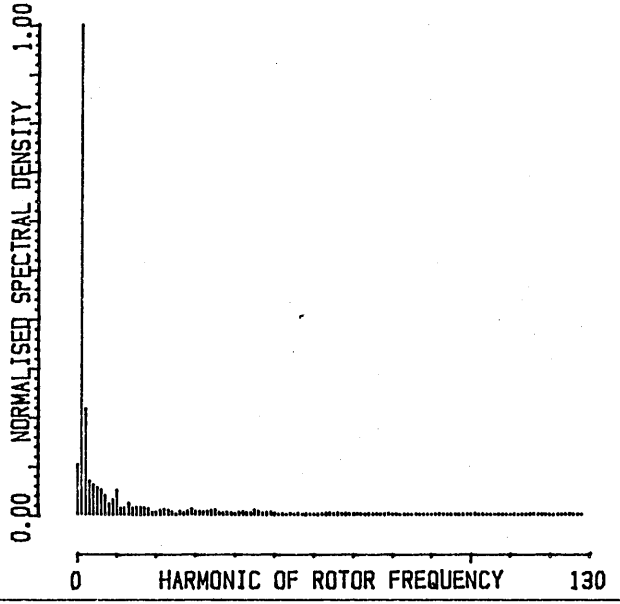

CIT

UNSTEADY AERODYNAMICS OF A VAWT

FIGURE 73

FOURIER TRANSFORMS OF BLADE NORMAL FORCE FROM SINGLE REVS. BLADE SPEED RATIOS ON STAGN PRESS FROM LEFT TO RIGHT AND TOP TO BOTTOM: 6.6, 5.2, 4.1, 3.1, 2.5 TURBULENCE LEVELS ON STAGN PRESS: 3%, 3%, 4%, 4%, 6% RESPECTIVELY. 0deg BLADE LEANOUT DATA.

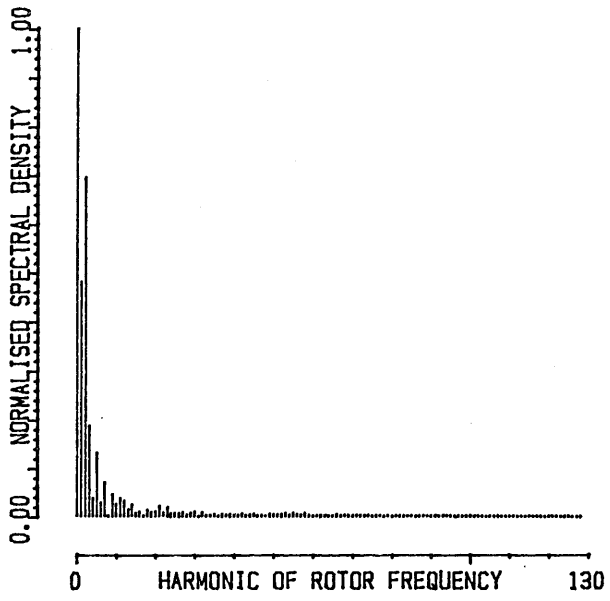

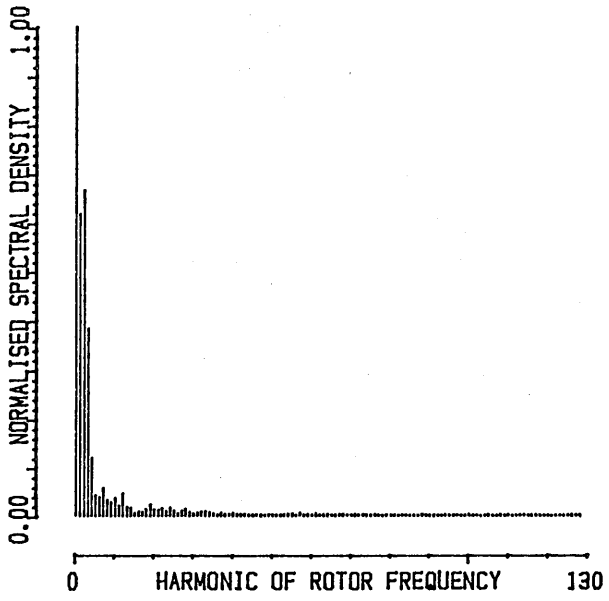

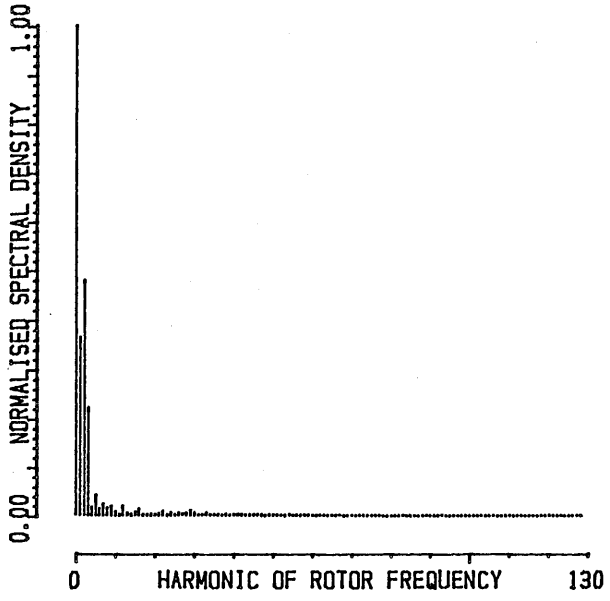

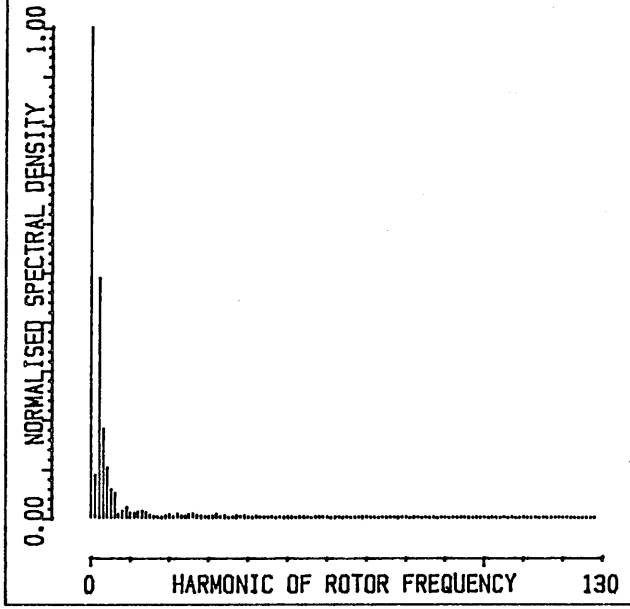

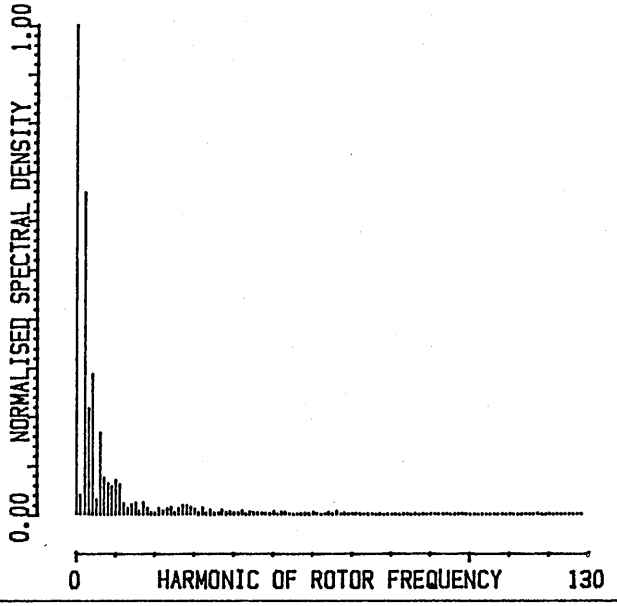

CIT

UNSTEADY AERODYNAMICS OF A VAWT

FIGURE 74

FOURIER TRANSFORMS OF BLADE TANGENTIAL FORCE FROM SINGLE REVS. BLADE SPEED RATIOS ON STAGN PRESS FROM LEFT TO RIGHT AND TOP TO BOTTOM: 6.6, 5.2, 4.1, 3.1, 2.5 TURBULENCE LEVELS ON STAGN PRESS: 3%, 3%, 4%, 4%, 6% RESPECTIVELY. 0deg BLADE LEANOUT DATA.

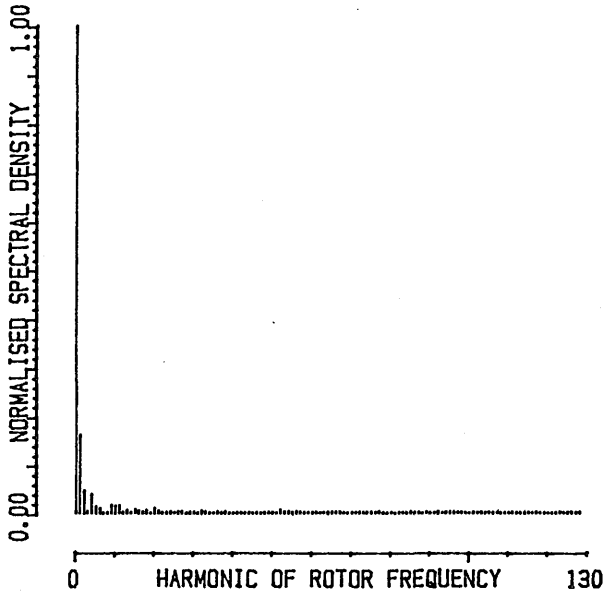

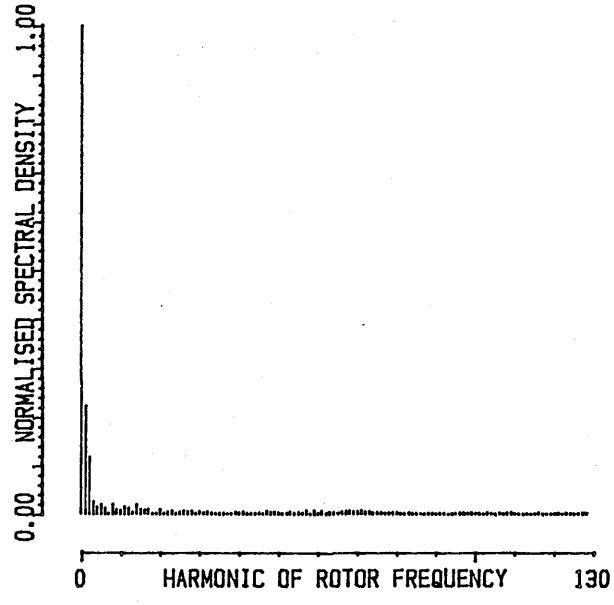

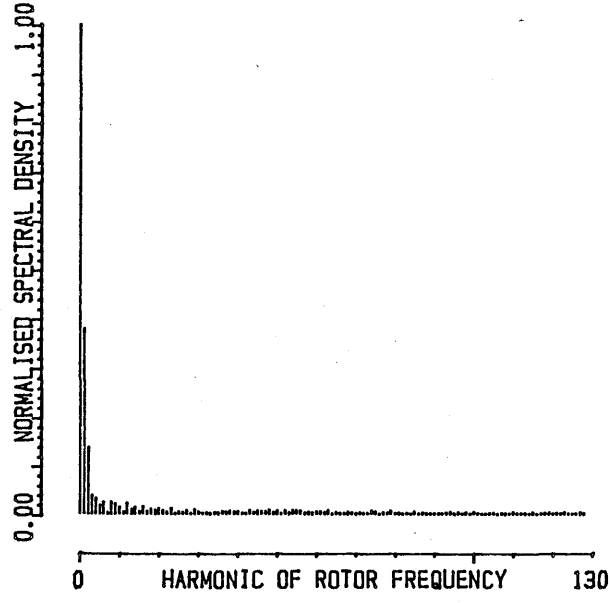

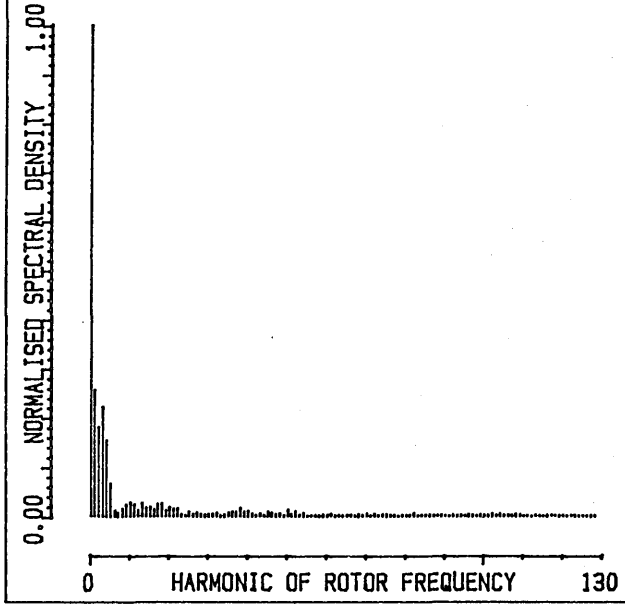

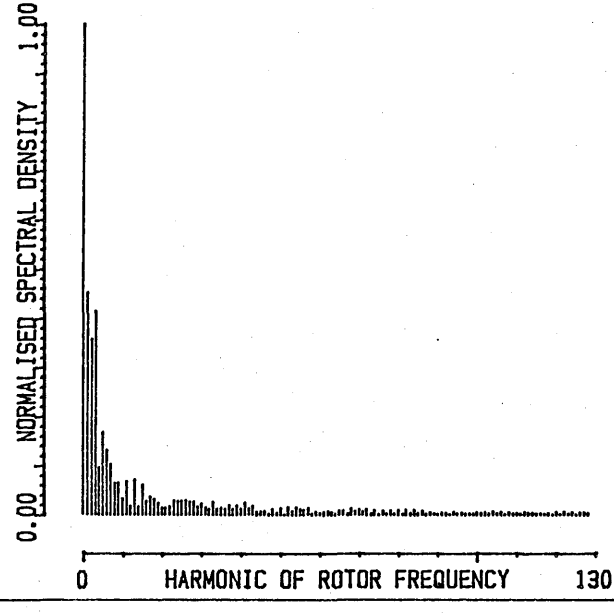

CIT

UNSTEADY AERODYNAMICS OF A VAWT

FIGURE 75

FOURIER TRANSFORMS OF BLADE PITCHING MOMENT FROM SINGLE REVS. BLADE SPEED RATIOS ON STAGN PRESS FROM LEFT TO RIGHT AND TOP TO BOTTOM: 6.6, 5.2, 4.1, 3.1, 2.5 TURBULENCE LEVELS ON STAGN PRESS: 3%, 3%, 4%, 4%, 6% RESPECTIVELY. 0deg BLADE LEANOUT DATA.

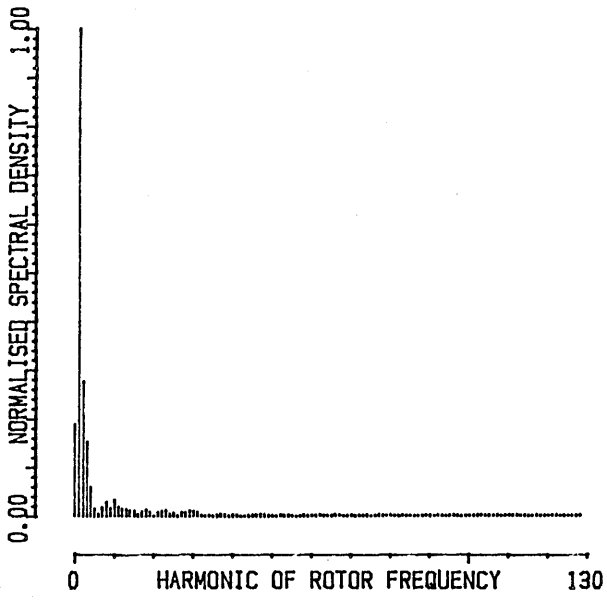

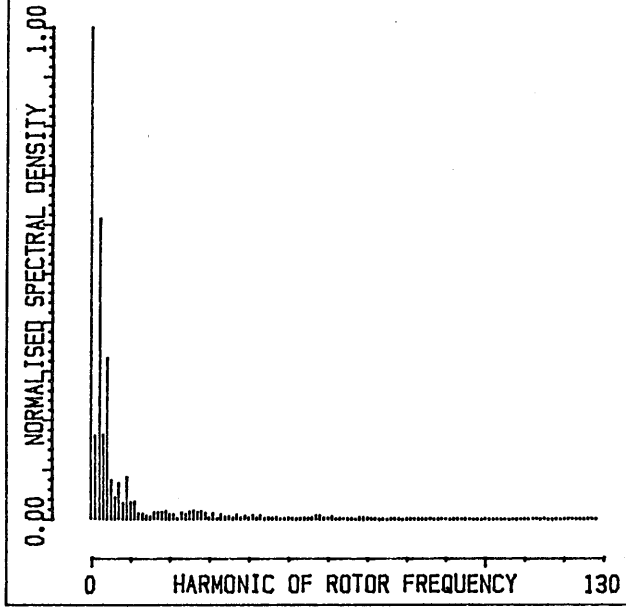

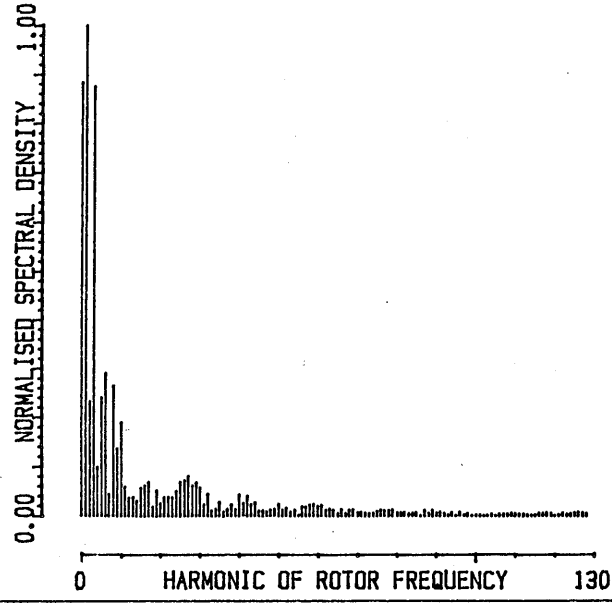

CIT

UNSTEADY AERODYNAMICS OF A VAWT

FIGURE 76

FOURIER TRANSFORMS OF BLADE NORMAL AND TANGENTIAL FORCE AND PITCHING MOMENT FOR REV 201.16

ROTOR FREQUENCY 1.99 Hz.

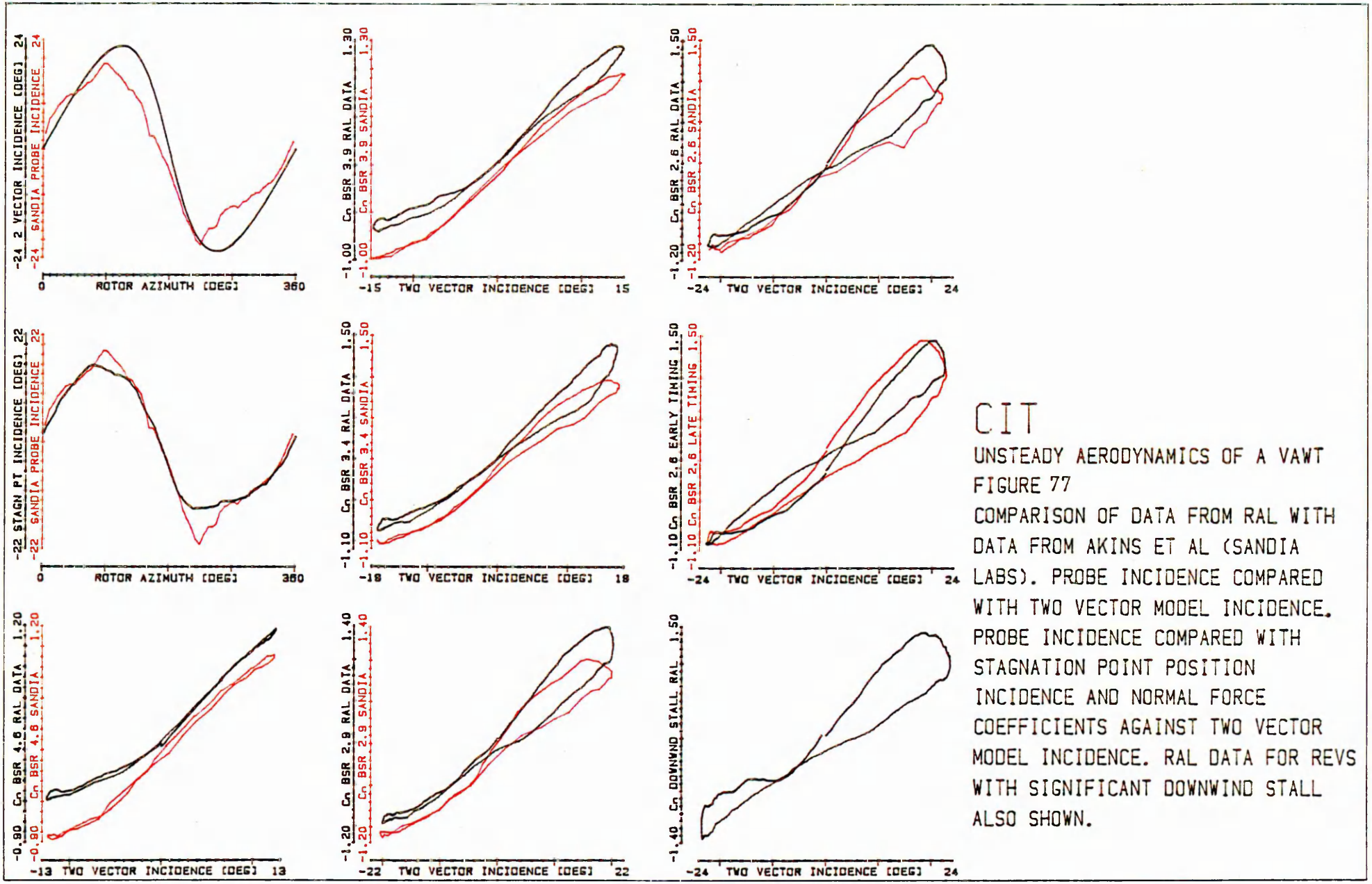

CIT

UNSTEADY AERODYNAMICS OF A VAWT

FIGURE 77

COMPARISON OF DATA FROM RAL WITH DATA FROM AKINS ET AL (SANDIA LABS). PROBE INCIDENCE COMPARED WITH TWO VECTOR MODEL INCIDENCE. PROBE INCIDENCE COMPARED WITH STAGNATION POINT POSITION INCIDENCE AND NORMAL FORCE COEFFICIENTS AGAINST TWO VECTOR MODEL INCIDENCE. RAL DATA FOR REVS WITH SIGNIFICANT DOWNWIND STALL ALSO SHOWN.

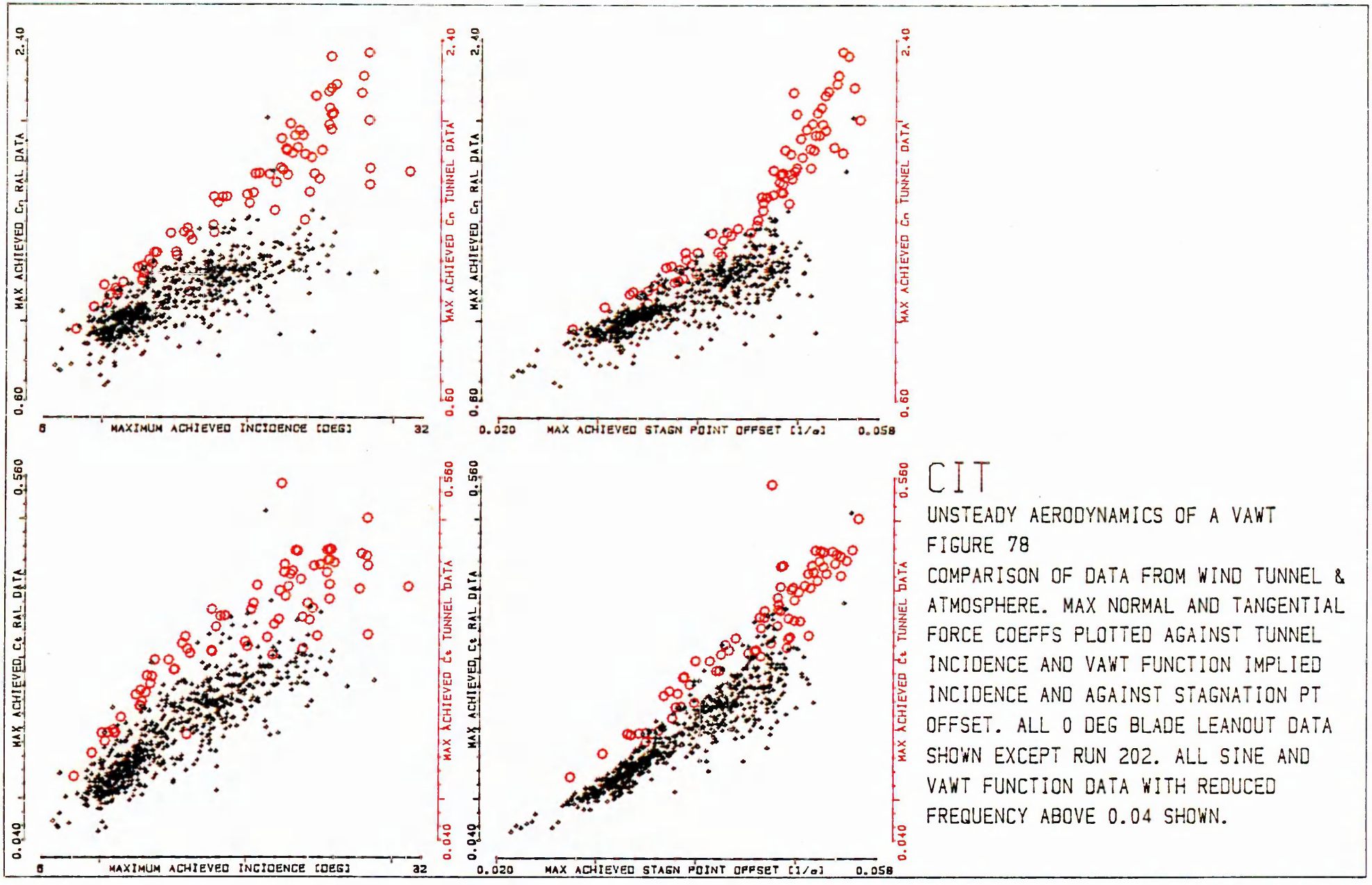

CIT

UNSTEADY AERODYNAMICS OF A VAWT

FIGURE 78

COMPARISON OF DATA FROM WIND TUNNEL & ATMOSPHERE. MAX NORMAL AND TANGENTIAL FORCE COEFFS PLOTTED AGAINST TUNNEL INCIDENCE AND VAWT FUNCTION IMPLIED INCIDENCE AND AGAINST STAGNATION PT OFFSET. ALL 0 DEG BLADE LEANOUT DATA SHOWN EXCEPT RUN 202. ALL SINE AND VAWT FUNCTION DATA WITH REDUCED FREQUENCY ABOVE 0.04 SHOWN.

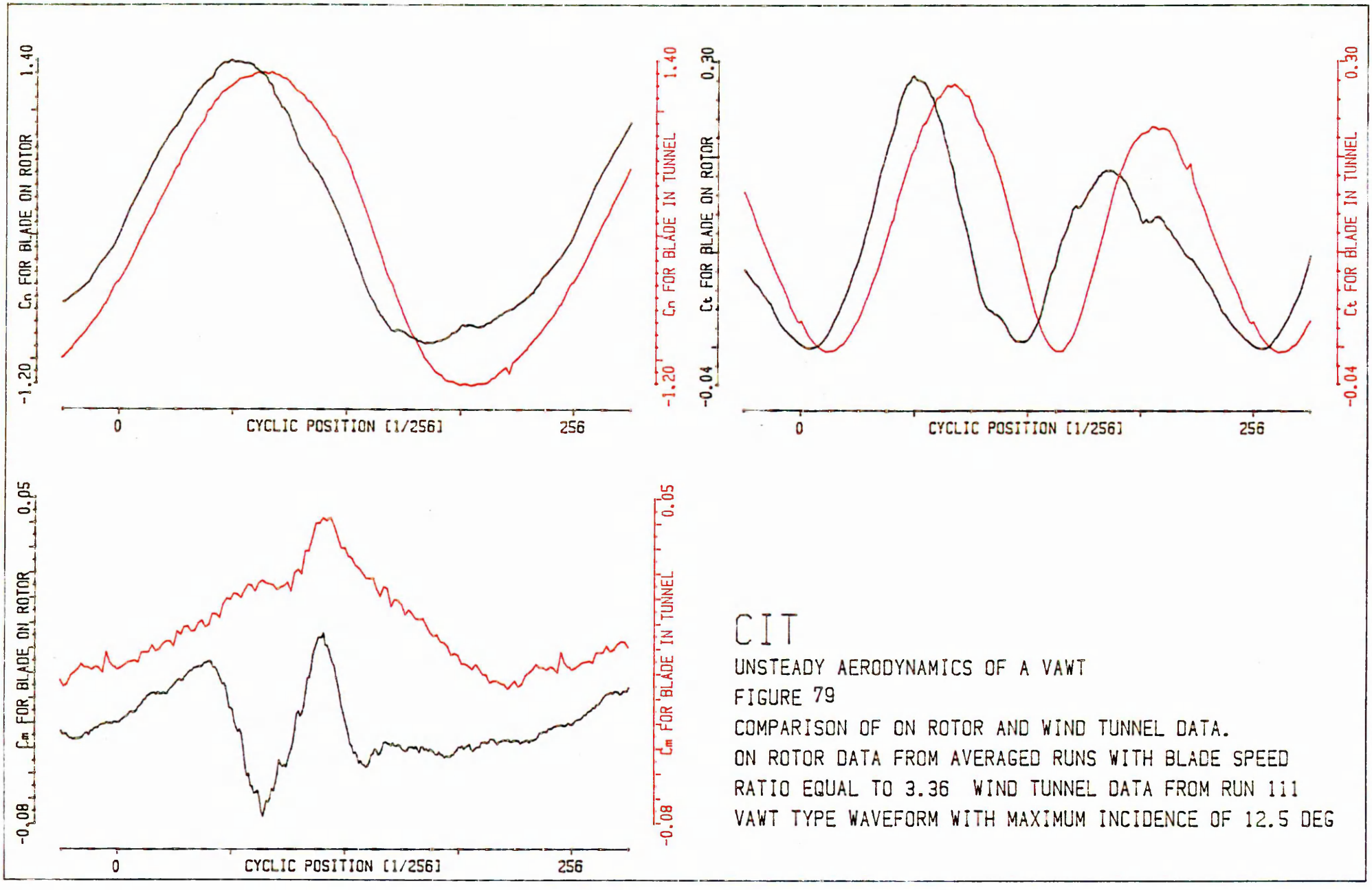

CIT

UNSTEADY AERODYNAMICS OF A VAWT

FIGURE 79

COMPARISON OF ON ROTOR AND WIND TUNNEL DATA.
ON ROTOR DATA FROM AVERAGED RUNS WITH BLADE SPEED RATIO EQUAL TO 3.36 WIND TUNNEL DATA FROM RUN 111
VAWT TYPE WAVEFORM WITH MAXIMUM INCIDENCE OF 12.5 DEG

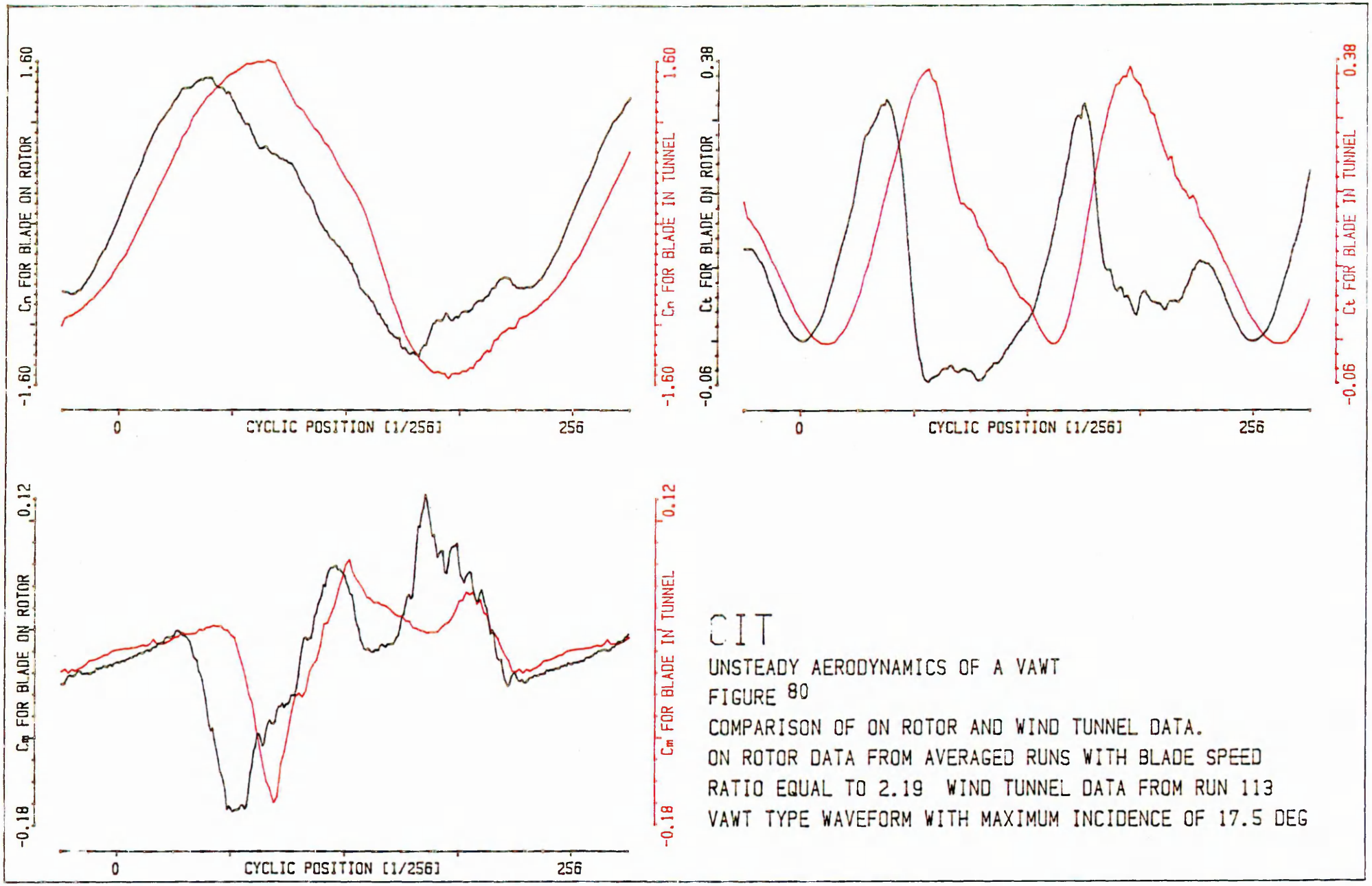
1.60
Cn FOR BLADE ON ROTOR
-1.60
0
CYCLIC POSITION [1/256]
256
Cn FOR BLADE IN TUNNEL
1.60
-1.60
0.38
Ct FOR BLADE ON ROTOR
-0.06
Ct FOR BLADE IN TUNNEL
0.38
-0.06
0.12
Cm FOR BLADE ON ROTOR
-0.18
Cm FOR BLADE IN TUNNEL
0.12
-0.18
CIT
UNSTEADY AERODYNAMICS OF A VAWT
FIGURE 80
COMPARISON OF ON ROTOR AND WIND TUNNEL DATA.
ON ROTOR DATA FROM AVERAGED RUNS WITH BLADE SPEED
RATIO EQUAL TO 2.19 WIND TUNNEL DATA FROM RUN 113
VAWT TYPE WAVEFORM WITH MAXIMUM INCIDENCE OF 17.5 DEG

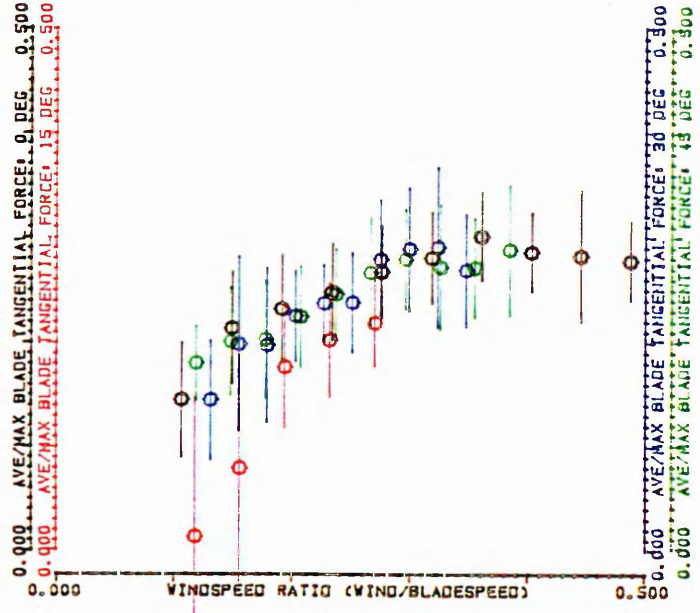

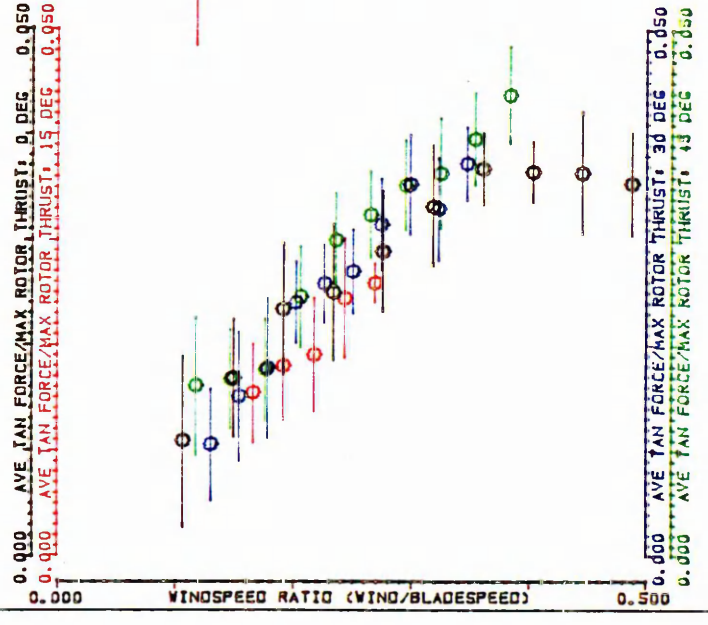

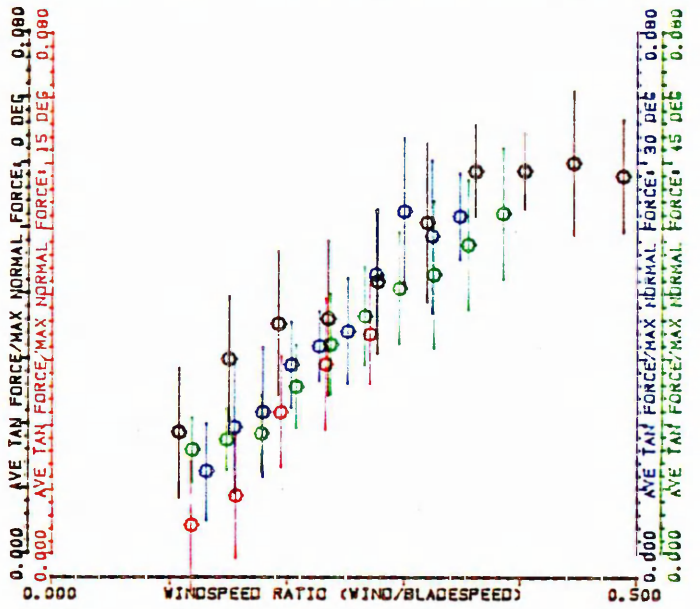

CIT

UNSTEADY AERODYNAMICS OF A VAWT

FIGURE 81

COMPARISON OF BLADE AVERAGE TANGENTIAL FORCE WITH MAXIMUM TANGENTIAL FORCE. MAXIMUM NORMAL FORCE AND MAXIMUM ROTOR THRUST FOR FOUR BLADE LEANOUT ANGLES. ALL ATMOSPHERIC DATA SHOWN. WINDSPEED BASED ON ANEMOMETER READINGS

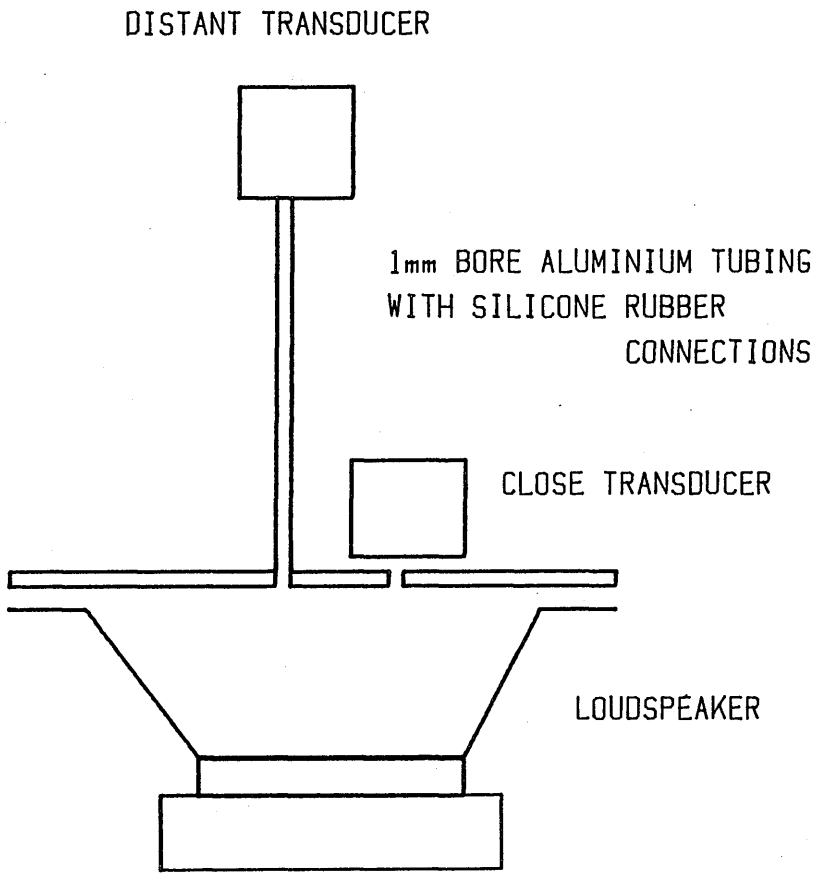

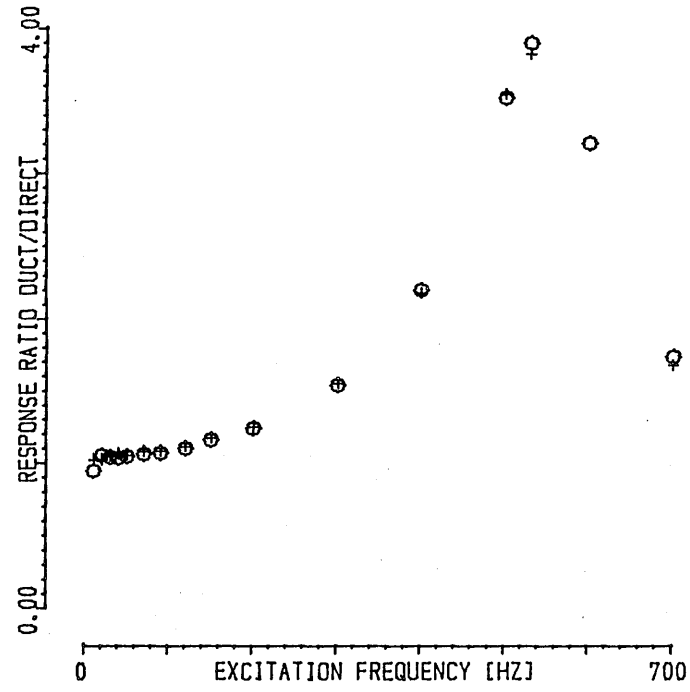

CIT

UNSTEADY AERODYNAMICS OF A VAWT

FIGURE 82

DUCT EXPERIMENTS WITH PLAIN AND SHARP 90 DEGREE BEND. SCHEMATIC OF EQUIPMENT SET UP ALSO SHOWN.

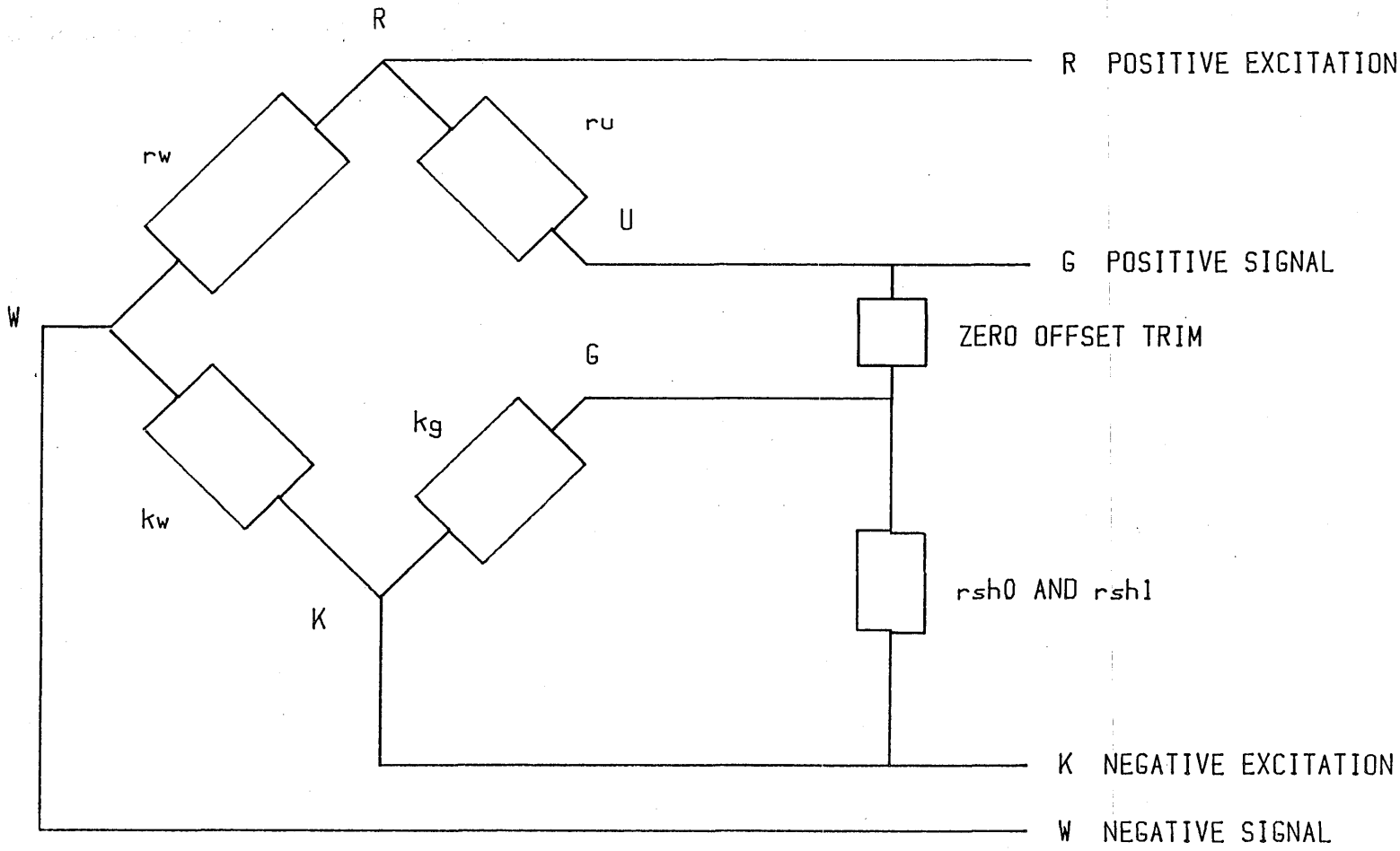

CIT

UNSTEADY AERODYNAMICS OF A VAWT

FIGURE 83

PRESSURE TRANSDUCER AND PASSIVE TEMPERATURE COMPENSATION MODULE CONNECTIONS AND NOMENCLATURE

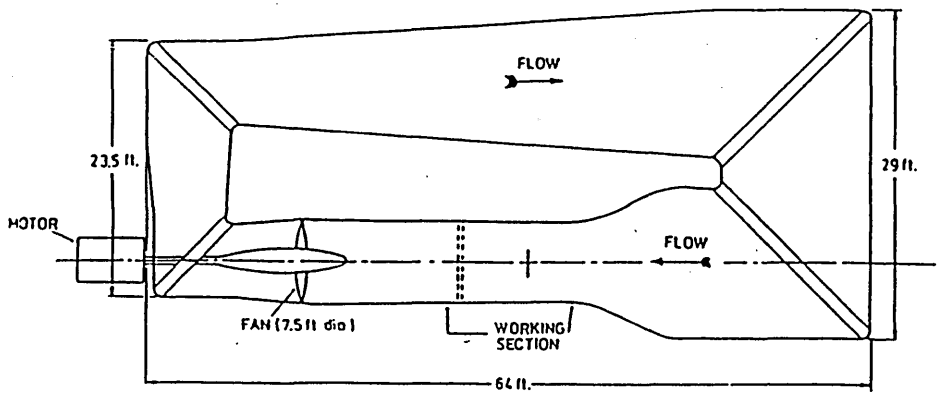

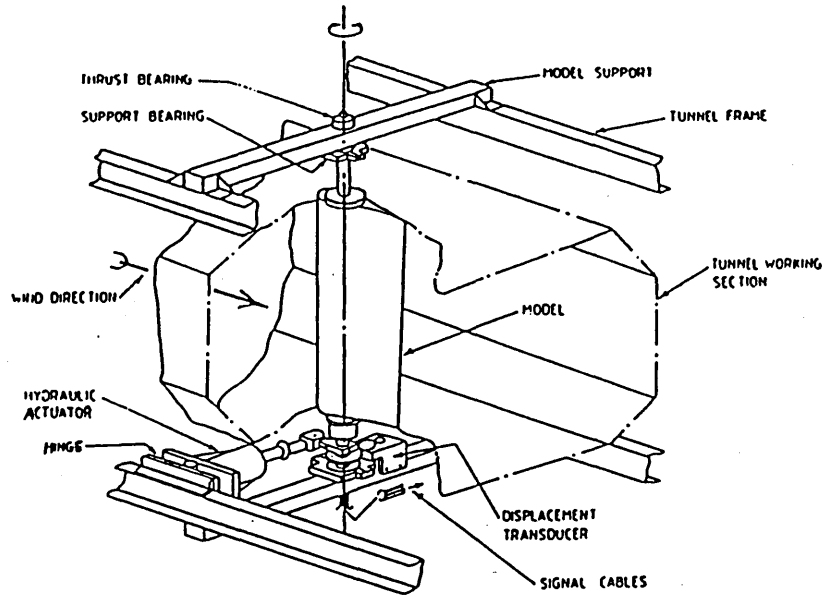

CIT

UNSTEADY AERODYNAMICS OF A VAWT

FIGURE 84

DETAILS OF THE UNIVERSITY OF GLASGOW HANDLEY PAGE WIND TUNNEL AND DYNAMIC STALL RIG.